



PHD

Synthetic Approaches to Protein Functionalisation and Sensing

Tilden, James

Award date:
2023

Awarding institution:
University of Bath

[Link to publication](#)

Alternative formats

If you require this document in an alternative format, please contact:
openaccess@bath.ac.uk

Copyright of this thesis rests with the author. Access is subject to the above licence, if given. If no licence is specified above, original content in this thesis is licensed under the terms of the Creative Commons Attribution-NonCommercial 4.0 International (CC BY-NC-ND 4.0) Licence (<https://creativecommons.org/licenses/by-nc-nd/4.0/>). Any third-party copyright material present remains the property of its respective owner(s) and is licensed under its existing terms.

Take down policy

If you consider content within Bath's Research Portal to be in breach of UK law, please contact: openaccess@bath.ac.uk with the details. Your claim will be investigated and, where appropriate, the item will be removed from public view as soon as possible.

Synthetic Approaches to Protein Functionalisation and Sensing

James Andrew Richard Tilden

Thesis Submitted for the Degree of Doctor of Philosophy

University of Bath
Department of Chemistry

April 2023

COPYRIGHT

Attention is drawn to the fact that copyright of this thesis/ portfolio rests with the author and copyright of any previously published materials included may rest with third parties. A copy of this thesis/ portfolio has been supplied on condition that anyone who consults it understands that they must not copy it or use material from it except as licenced, permitted by law or with the consent of the author or other copyright owners, as applicable.

We want to make good time, but for us now this is measured with emphasis on "good" rather than "time" and when you make that shift in emphasis the whole approach changes.

ROBERT M. PIRSIG – *Zen and the Art of Motorcycle Maintenance*

Acknowledgements

I would like to extend my thanks and appreciation to the three members of my supervisory team: Professor Christopher Frost, Dr Anneke Lubben and Dr James Taylor. Thank you to Chris for giving me the opportunity to spend the last few years doing research, for your seemingly endless enthusiasm, for convincing me that no idea is a bad idea (except for the ones that are), and for always fully supporting anything I could do to supplement my PhD. Thank you to Anneke for all your kind words of encouragement over coffee, they have helped me enormously over the years. Your technical assistance and patience teaching an organic chemist mass spectrometry has also been invaluable. James, thank you for encouraging me to keep on pushing – *you can walk but don't stop!* I will certainly miss you bursting into the office for a quick (hour long) chat, where we come up with solutions to many of the world's problems. Thank you all for the guidance and effort you have given me with writing this thesis, and your lightning-fast proof reading. On to the next adventure!

Thank you to Professor Alex Spokoyny for generously hosting me at UCLA and enabling such an engaging and fulfilling three months doing exciting science. Thanks are extended to Dr Evan Doud for helping me get to grips with life at UCLA and the group's chemistry in such a short time. Thanks also to Dr Manuel Müller at KCL for hosting a short visit, and to Ruqaiya Alam for your enthusiasm towards research.

Further thanks to Dr Shaun Reeksting and Dr Kathryn Proctor for mass spectrometry help, Dr Catherine Lyall and Dr John Lowe for NMR assistance, and to Dr Gabriele Kociok-Kohn for running and solving my X-ray crystal structures.

I would like to thank the members of the Frost/Taylor lab: Jess Hine, Emily Babcock, Sam Spring, Mark Shuttleworth, and Dr Shafiq Rahman, as well as all the project students I have had the pleasure of working with or supervising: Ffion Platt, Lewis Harper, Lucy Anderson, Henry Jee, James Wood, and Ross Bennett. I will surely miss subjecting you all to my often-questionable music taste, and the blindingly high standard of baking present in the office. Thanks also to all members of the Spokoyny lab for making my short time at UCLA such an enjoyable one.

Enormous thanks to my friends and family that have supported me for the last few years. Thanks to my oldest and dearest friend Ben Joynson for all the years of support and patience, to Charlie Ash for driving all our many past (and future) adventures, and to James Handley for sending it without fail. To Aleta – thank you, it's finally over. Finally, thank you to my parents and sister for your belief in me.

Abstract

Synthetic approaches to protein functionalisation and sensing, in particular the *S*-arylation of cysteine residues mediated by organometallic complexes of palladium and gold, have been investigated.

Firstly, the arylation of canonical amino acids using transition metals in biologically compatible conditions is reviewed. Despite transition metal catalysis being the obvious choice for the arylation of small molecules in modern organic chemistry, its application in bioconjugation chemistry is limited. This has led to the rapidly growing number of organometallic strategies for the arylation of canonical amino acids in biomolecules.

The synthesis and application of Pd(II) complexes prepared *via* C-H activation towards cysteine *S*-arylation is then described. It was found that synthesis of organometallic Pd(II) complexes *via* a C-H activation approach offers usability advantages compared to the oxidative addition approach currently prevalent in the literature. Isolated C-H activation complexes showed excellent bioconjugation efficiency and cysteine selectivity, and their generation *in situ* enabled cysteine functionalisation with aryl groups adorned with a wide range of functionalities with a rapid and user-friendly protocol. Further application of C-H activation complexes revealed their high selectivity towards exposed cysteine when arylating intact proteins.

Further investigation applied Pd(II) C-H activation complexes of amino acids bearing aromatic side chains towards the formation of cysteine-amino acid side chain-side chain linkages. Synthesis of Pd(II)-amino acid complexes from ammonium salts was found to be affected by the nature of the anion, and their subsequent ability to *S*-arylate cysteine was dependant on the phosphine ligand. The methodology was scaled up, allowing full characterisation of a bioconjugate, and exposed cysteine on an intact protein was functionalised. Initial investigations revealed potential applications of the chemistry towards the formation of macrocyclic peptides.

Finally, the *S*-arylation kinetics of organometallic Au(III) complexes in biologically relevant conditions were studied. Using a combination of competition experiments and stopped-flow kinetics experiments, the effect of the environment around Au(III) on the bioconjugation kinetics was probed. It was found that ligand and substrate both significantly affect the kinetics and revealed information about the mechanism of the process. Insights gained were then used to synthesise a bimetallic Au(III) reagent which enabled the synthesis of cross-coupled biomolecules.

Abbreviations

3-MPA	3-mercaptopropionic acid
Ac	acetyl
Ad	adamantyl
ADC	antibody-drug conjugate
amu	atomic mass unit
aq	aqueous
Ar	aryl
Boc	<i>tert</i> -butyloxycarbonyl
°C	degrees Celsius
CuAAC	copper-catalysed azide–alkyne cycloaddition
CV	column volumes
CyHex	cyclohexane
δ	chemical shift
d	doublet
Da	Daltons
DCE	1,2-dichloroethane
DIPEA	<i>N,N</i> -diisopropylethylamine
DM-ADHP	<i>N,N</i> -dimethyl-2-amino-4,6-dihydropyrimidine
dmba	<i>N,N</i> -dimethylbenzylamine
DMF	<i>N,N</i> -dimethylformamide
DMSO	dimethyl sulfoxide
dppe	1,2-bis(diphenylphosphino)ethane
EDC	1-ethyl-3-(3-dimethylaminopropyl)carbodiimide
EIC	extracted ion chromatogram
Equiv.	equivalents
ESI	electrospray ionisation
Et	ethyl
Fc	ferrocene
FA	formic acid
Fmoc	fluorenylmethoxycarbonyl
g	grams
GSH	glutathione
h	hours
HATU	hexafluorophosphate azabenzotriazole tetramethyl uronium
HBTU	hexafluorophosphate benzotriazole tetramethyl uronium
HFIP	hexafluoro-2-propanol
HOAt	1-hydroxy-7-azabenzotriazole
HOBt	hydroxybenzotriazole
HPLC	high-performance liquid chromatography

Hz	hertz
<i>J</i>	coupling constant
L	litre
LC	liquid chromatography
<i>m/z</i>	mass-to-charge
Me	methyl
MGS	mannosylglycerate
M	molar
MMAE	monomethyl auristatin E
Mol	mole
MS	mass spectrometry
MS/MS	tandem mass spectrometry
Ms	methanesulfonyl
MTBE	methyl <i>tert</i> -butyl ether
NAC	<i>N</i> -acetylcysteine
NHS	<i>N</i> -hydroxy succinimide
NMR	nuclear magnetic resonance
OAC	oxidative addition complex
PBS	phosphate buffered saline
PEG	(poly)ethylene glycol
Ph	phenyl
ppm	parts per million
PTM	post-translational modification
<i>p</i> TSA	<i>para</i> -toluenesulfonic acid
q	quartet
rt	room temperature
s	singlet
sat	saturated
t	triplet
TBAB	tetrabutyl ammonium bromide
TFA	trifluoroacetic acid
Tf	trifluoromethanesulfonyl
THF	tetrahydrofuran
TIC	total ion chromatogram
TMS	trimethylsilyl
Tris	tris(hydroxymethyl)aminomethane
Trt	trityl
Ts	<i>para</i> -toluenesulfonyl
VWD	variable wavelength detector
Z	molecular charge

Contents

1. Metal-Mediated Arylation of Canonical Amino Acid Residues	1
1.1. Bioconjugation.....	1
1.2. Arylation of Biomolecules.....	3
1.2.1. Metal-Catalysed Arylation.....	6
1.2.1.1. Palladium.....	6
1.2.1.2. Copper.....	10
1.2.1.3. Nickel.....	12
1.2.2. Arylation of Biomolecules <i>via</i> Transition Metal-Containing Reagents.....	14
1.2.2.1. Palladium.....	15
1.2.2.2. Gold.....	23
1.2.2.3. Platinum.....	27
1.3. Outlook.....	28
2. Pd(II)-Mediated C-H Activation for Cysteine Bioconjugation.....	29
2.1. Context.....	29
2.1.1. Pd(II) Oxidative Addition Complexes.....	29
2.1.2. Cyclopalladation.....	32
2.2. Results and Discussion.....	33
2.2.1. Synthesis of Pd(II)-dmba Complexes.....	33
2.2.2. Ligand Screen.....	36
2.2.3. Method Validation.....	38
2.2.4. Scope of Isolated Pd(II) Complexes.....	39
2.2.5. Competition Experiments.....	43
2.2.6. <i>In situ</i> Generated Pd(II) Complexes.....	45
2.2.7. Intact Protein Bioconjugation.....	51
2.3. Conclusions.....	55
3. Pd(II)-Mediated Amino Acid Side Chain-Side Chain Bioconjugation	56
3.1. Context.....	56
3.1.1. Cyclopalladation of Amino Acids.....	56
3.2. Aims.....	57
3.3. Results and Discussion.....	58
3.3.1. Bioconjugation with Pd(II)-Amino Acid Complexes.....	58
3.3.1.1. Preparation from Mesylate Salts.....	64
3.3.1.2. Validation of Reaction Conversions.....	67
3.3.2. Isolation of Bioconjugate.....	69
3.3.3. Protein Arylation.....	71
3.3.4. Macrocycle formation.....	72
3.4. Conclusions and Outlook.....	74
4. Applications of Organometallic Au(III) Complexes for Bioconjugation	76
4.1. Context: Cysteine Bioconjugation Kinetics.....	76
4.2. Aims.....	80
4.3. Results and Discussion.....	80
4.3.1. Studying Kinetics <i>via</i> Competition Experiments.....	80

4.3.2.	Stopped-Flow Kinetics	85
4.3.2.1.	Maleimide Cysteine Bioconjugation Kinetics	86
4.3.2.2.	Metal-Mediated C-S Arylation	88
4.3.3.	Synthesis of Biomolecule Heterostructures	96
4.3.3.1.	Synthesis of Bimetallic Au(III) Species	96
4.3.3.2.	Stopped-Flow Spectroscopy.....	97
4.3.3.3.	Biomolecule Cross-Coupling.....	98
4.4.	Conclusions	99
5.	Experimental.....	101
5.1.	General Synthetic Experimental for Chapters 2 and 3.....	101
5.2.	LC-MS Experimental for Chapters 2 and 3	103
5.3.	Pd(II)-Mediated C-H Activation for Cysteine Bioconjugation.....	105
5.3.1.	Synthesis of Isolated Pd(II) Complexes	105
5.3.2.	Synthesis of Compounds for <i>in situ</i> Arylation	131
5.3.3.	Bioconjugation Reactions	139
5.3.3.1.	Initial Ligand Screen	139
5.3.3.2.	Residue Selectivity of Pd(<i>dmba</i>)(<i>Xantphos</i>)Cl (70)	142
5.3.3.3.	Glutathione Calibration Curve.....	142
5.3.3.4.	Acetanilide and 2-Phenylpyridine Pd(II) Complexes	143
5.3.3.5.	Pd(II)- <i>dmba</i> Substrate Scope.....	144
5.3.3.6.	Competition Experiments.....	146
5.3.3.7.	<i>In situ</i> Protocols	148
5.3.3.8.	Optimisation of <i>In Situ</i> Pd(II)- <i>dmba</i> Generation.....	150
5.3.3.9.	<i>In situ</i> Generated Pd(II)- <i>dmba</i> Substrate Scope.....	150
5.3.3.9.	Intact Protein Bioconjugation With Complex 85.....	157
5.3.3.10.	Intact Protein Bioconjugation with <i>In Situ</i> Generated Complexes	157
5.3.4.	Crystallographic Data.....	171
5.4.	Pd(II)-Mediated Amino Acid Side Chain-Side Chain Bioconjugation	175
5.4.1.	Synthesis of Pd(II)-Amino Acid Complexes	175
5.4.2.	Isolation of Glutathione Bioconjugate	186
5.4.3.	Bioconjugation Reactions	188
5.4.3.1.	Glutathione Arylation.....	188
5.4.3.2.	BSA Arylation	191
5.4.3.3.	Macrocycle formation.....	191
5.5.	General Synthetic Experimental for Chapter 4	196
5.6.	HPLC and LC-MS Experimental for Chapter 4.....	198
5.7.	Applications of Organometallic Au(III) Complexes for Bioconjugation	199
5.7.1.	Preparation of Novel Organometallic Compounds	199
5.7.2.	Preparation of H-DRKCAT-NH ₂ (175).....	205
5.7.3.	Competition Experiments.....	208
5.7.4.	Stopped-Flow Kinetic Analysis	215
5.7.4.1.	Collection of Full UV/ <i>vis</i> Spectra.....	216
5.7.4.2.	Collection of Single Wavelength Absorbance Measurements.....	226
5.7.5.	Biomolecule Cross-Coupling	234
6.	References.....	236

1. Metal-Mediated Arylation of Canonical Amino Acid Residues

1.1. Bioconjugation

The ability to tag biomolecules, more commonly known as bioconjugation, is of significant interest to synthetic chemists, biochemists, and biologists alike. This process consists of forming a covalent or characterizable non-covalent interaction between a specific biomolecule and another chemical entity.¹ In nature, post-translational modifications (PTMs) such as methylation, acylation, or phosphorylation contribute to the vast diversity found in the proteome. The ability to mimic nature and modify biomolecules has in turn facilitated progress in other areas. Perhaps the most notable of these in recent research is the development of novel drugs, specifically antibody-drug conjugates (ADCs).² Since 2011, eight of these drugs have received approval for use in the field of oncology, and many more are being trialled. One of the first examples of an ADC marketed was Brentuximab vedotin (**1**) (Figure 1),³ which was approved for the treatment of non-Hodgkin lymphomas.

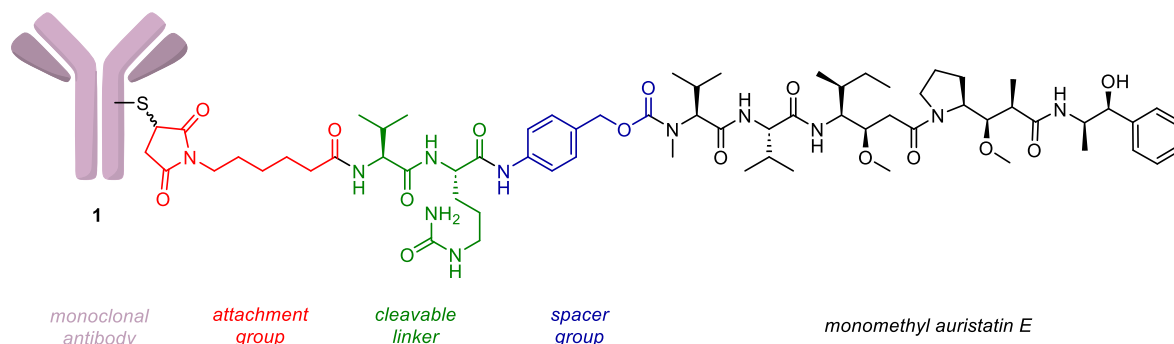


Figure 1: Schematic representation of Brentuximab vedotin, showing the small-molecule component of the ADC.

Brentuximab vedotin consists of a monoclonal antibody that specifically targets lymphoma cells, linked to a species known as vedotin. The primary activity of vedotin comes from monomethyl auristatin E (MMAE), which inhibits cell division.³ Due to its inherent toxicity, MMAE is not appropriate for therapeutic use by itself. However, in conjugation with a monoclonal antibody, targeted delivery of MMAE to cancer cells leads to specificity towards these cells, while minimal toxicity towards non-cancerous cells is observed. As shown in Figure 1, the preparation of this ADC is enabled by direct bioconjugation to one of the cysteine residues naturally present on the surface of brentuximab. Bioconjugation also has further applications in covalent inhibitors,⁴ probing complex biological processes,⁵ creating new biomaterials,^{6,7} and the development of novel diagnostic tools.⁸

Due to their nature, synthetic processes involving biomolecules require milder reaction conditions compared to traditional small molecule synthesis. Specifically,

temperatures under 37 °C, a pH close to 7, and the use of buffered aqueous solutions must be employed, as biomolecules are often sensitive to these factors. For example, high temperatures could cause proteins to unfold, deviation from neutral pH will change the protonation states of key residues, and many biomolecules simply may not dissolve in organic solvent systems. In some cases, simpler biomolecules may tolerate higher temperatures, and more basic or acidic pH. Along with the stringent reaction conditions these biomolecules require, reactions to tag them must be chemoselective and have favourable kinetics.

Bioconjugation reactions on amino acid-based biomolecules have typically relied on nucleophilic residues,⁹ and a single such biomolecule could contain hundreds of these: the hydroxyl group on serine, the thiol on cysteine, and the amine on lysine, to name a few. Selective targeting of these functional groups is well established in small-molecule organic chemistry; however, achieving this chemoselectivity under the restraints of bioconjugation chemistry represents a considerable synthetic challenge. As well as chemoselectivity, regioselectivity of this chemistry must be considered. For example, can a single cysteine on a protein be targeted over others? Fast kinetics of bioconjugation reactions are also important as many reactions involving proteins are performed at very low concentrations, often to prevent precipitation.

Traditional bioconjugation techniques take advantage of natural nucleophilic residues within proteins, most commonly the side chains on either lysine or cysteine (Figure 2). Lysine may be targeted¹⁰ using *N*-hydroxy succinimide (NHS) esters,^{11–13} isothiocyanates,¹⁴ sulfonyl fluorides,¹⁵ benzoyl fluorides,¹⁶ or *via* formation of iminoboronates.^{17,18} Although there exists many ways to target lysine, free cysteine is often seen as a more desirable target. Reduced cysteine is relatively scarce within proteins compared to lysine, as cysteine is most commonly found oxidised within disulfide linkages. Free thiols also possess uniquely soft nucleophilic characteristics, and therefore unique reactivity.¹⁹ Bioconjugates of cysteine may be formed using maleimides^{20,21} and iodoacetamides,²² most commonly. These techniques often demonstrate favourable kinetics, however large equivalents of bioconjugation reagent are frequently required, causing selectivity issues.²³ To overcome this problem, many approaches to the regioselective functionalisation of a single site is often accomplished *via* enzyme-mediated reactions.^{24–27}

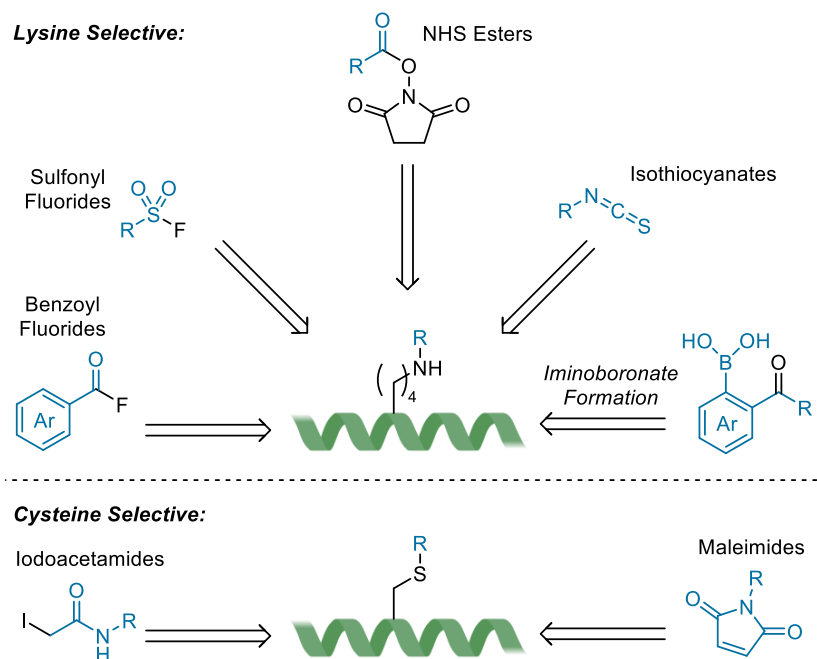


Figure 2: Traditional electrophilic bioconjugation strategies for functionalisation of lysine (top) and cysteine (bottom).

The chemoselectivity of more traditional bioconjugation techniques may be addressed by genetically encoding unnatural reactive sites into proteins such as alkynes or azides, which are considered bioorthogonal.²⁸ The Cu(I)-catalysed alkyne/azide cycloaddition (CuAAC) reaction²⁹ may be used to perform bioorthogonal chemistry on alkyne- or azide-containing proteins. This reaction represented the birth of ‘click’ chemistry³⁰ and enabled a broad range of substrates to be covalently attached to biomolecules *via* triazole linkers.

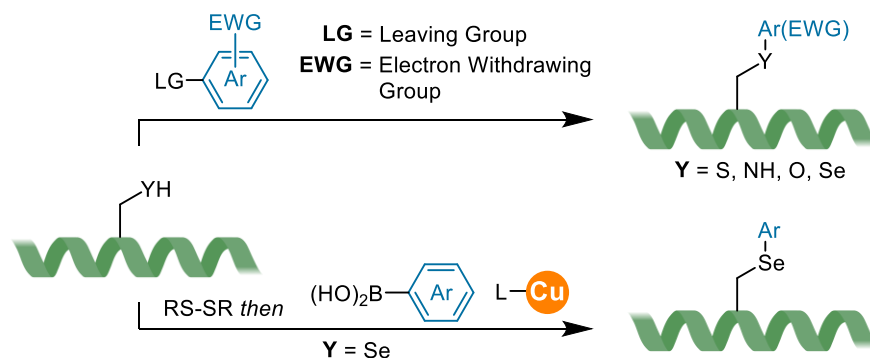
1.2. Arylation of Biomolecules

Despite incredible advances in bioconjugation chemistry since the discovery of the CuAAC reaction, there is still a desire to develop efficient and selective chemical processes that allow the functionalisation of natural amino acids, and recent years have seen a huge amount of progress in the area. In particular, arylation chemistry, the formation of X-C(sp²) bonds (where X is carbon or a heteroatom) to biomolecules, has become a thriving area of research. The relatively recent application of arylation chemistry may be surprising, given how ubiquitous it has become in small-molecule chemistry. However, the adaptation of chemical reactions to conditions favoured by biomolecules is not trivial. For example, the CuAAC reaction had to overcome many hurdles when applied to bioconjugation, one of which being deleterious cellular effects, which were mitigated by modifying the Cu(I) ligand system.^{31,32}

Arylation chemistry for bioconjugation can be divided into four main sections. Firstly, metal-catalysed arylation, using cross-coupling or C-H activation processes. Secondly, using (super)stoichiometric organometallic complexes that react with

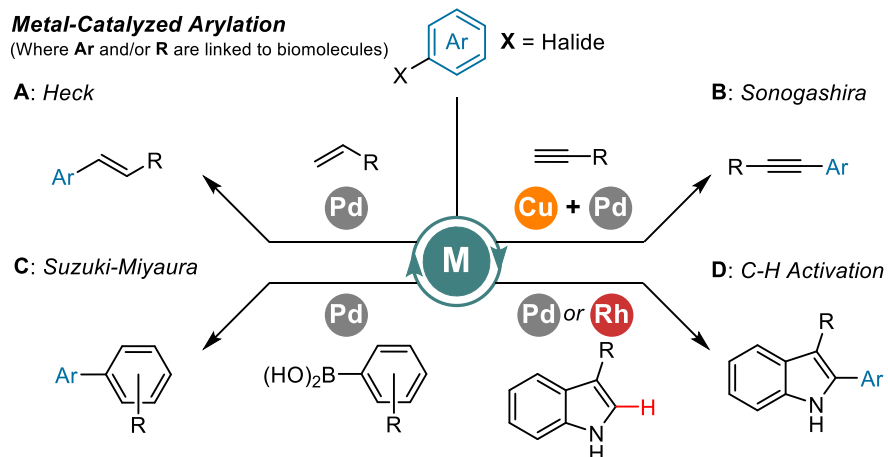
nucleophilic residues or pre-installed reactive groups to achieve bioconjugation. Thirdly, using electron-deficient aryl halides as electrophiles that undergo nucleophilic aromatic substitution (S_NAr) reactions with residues containing nucleophilic functionality, such as thiols, primary amines, alcohols, and selenols. Finally, umpolung chemistry can be employed, turning selenols into electrophiles *via* oxidation with disulfides to form Se-S species which can then be arylated with copper chemistry in a reductive process. Of these four areas, this introduction will discuss the fields of metal-catalysed arylation and organometallic complexes for bioconjugation, specifically focussing on methodology which facilitates the arylation of canonical amino acid residues in biocompatible conditions (Figure 3).

Previous Reviews:
Nucleophilic Aromatic Substitution + Umpolung Chemistry



Metal-Catalyzed Arylation

(Where Ar and/or R are linked to biomolecules)



This Overview:

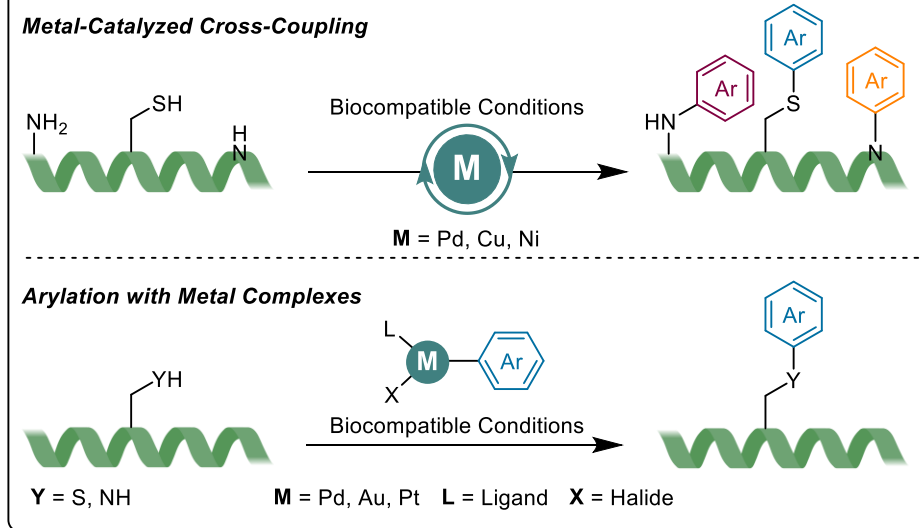


Figure 3: General strategies towards the arylation of biomolecules, outlining the focus of this overview.

1.2.1. Metal-Catalysed Arylation

1.2.1.1. Palladium

The discovery of palladium cross-coupling reactions in the 1970s marked the beginning of a revolution in the synthetic chemist's ability to form carbon-carbon bonds.³³ Extensive work in the field of transition metal-catalysed chemistry means that carbon-carbon and carbon-heteroatom bonds can be formed quickly and efficiently with high selectivity. Consequently, transition metal-based chemistry has become an invaluable tool for the synthesis of many commercially produced pharmaceuticals, drug candidates, and agrochemicals³⁴ over the last fifty years. As a result, the recent interest in adapting this chemistry to be compatible with the strict reaction conditions required to label biomolecules has risen. This focus includes techniques for bonding a sp^2 carbon centre with a protein, peptide, or antibody of interest.

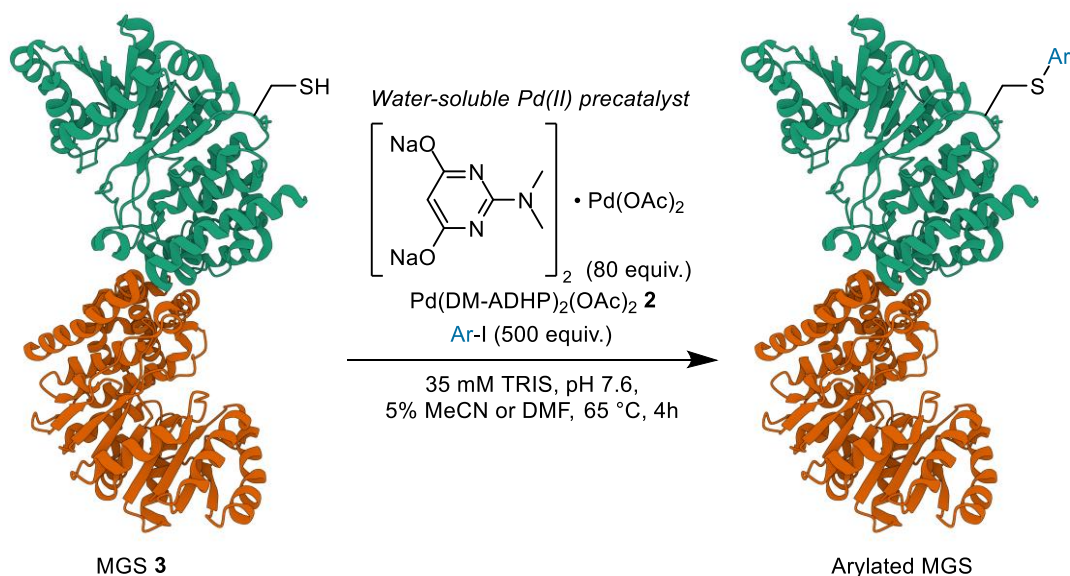
Generally, palladium-catalysed arylation of biomolecules uses one of three classes of palladium chemistry, the first being C-C bond forming reactions based on Pd(0) systems: Heck, Sonogashira, and Suzuki-Miyaura cross-couplings. The importance of these processes in synthetic chemistry cannot be overstated, and analysis of the most widely used reactions in medicinal chemistry showed that Suzuki-Miyaura couplings were the second most common chemical transformations in 2014.³⁵ Typically, the Heck, Sonogashira, and Suzuki-Miyaura involve the cross-coupling of aryl halides with alkenes, alkynes, or aryl boronic acids, respectively. Despite their incredible synthetic utility, these processes present challenges in bioconjugation reactions; most notably, the required functional groups (aryl-halides, alkenes, alkynes, and aryl-boronic acids) are not found naturally in biomolecules. Thus, biomolecules must be pre-functionalised with one of the requisite groups prior to cross-coupling. The need for an additional step to prepare the biomolecule means that no further discussion of this methodology is included in this introduction.

The second class of palladium-catalysed arylation uses C-H activation chemistry. Palladium-catalysed C-H activation is an important tool in small molecule synthesis facilitating the formation of an array of C-C or C-heteroatom bonds.³⁶ Commonly, this uses a source of Pd(II) that inserts into a reactive C-H bond and, after coupling with a boronic acid or heteroatom, reductively eliminates to form Pd(0) and a new C-C or C-heteroatom bond. The catalytic Pd(II) is then regenerated using an external oxidant. Most relevant to bioconjugation, many palladium-mediated strategies towards indole functionalisation have been developed.^{37,38} Contrasting with Suzuki-Miyaura chemistry, these C-H activation processes allow functionalisation of amino acid residues found in nature, and many have

focussed on reactions of tryptophan due to its indole side-chain. However, as of the time of writing, there are currently no reports of Pd-catalysed arylation of biomolecules *via* C-H activation in the literature which adhere to biocompatible conditions.

Thirdly, Pd-mediated cross-coupling reactions forming C-N, C-O, and C-S bonds are extensively used in total synthesis, production of drug candidates, and process chemistry, among other areas.³⁹ The first of these carbon-heteroatom cross-couplings to be observed was an intramolecular coupling of an aryl bromide with an aryl amide to form a β -carboline motif towards the synthesis of lavendamycin.⁴⁰ Since, C-N bond forming processes have developed from being low-yielding and requiring the use of organotin compounds, to highly efficient reactions, which can be attributed to extensive work optimising phosphine-based ligands.⁴¹ The scope of these cross-coupling reactions has expanded to C-O⁴² and C-S⁴³ bond formation, again through tuning ligands. These carbon-heteroatom bond forming reactions allow direct functionalisation of natural nucleophilic residues within proteins without the need for pre-functionalisation. In particular, the arylation of cysteine has been a thriving area of research, and much of the literature discussed herein focusses primarily on cysteine functionalisation.

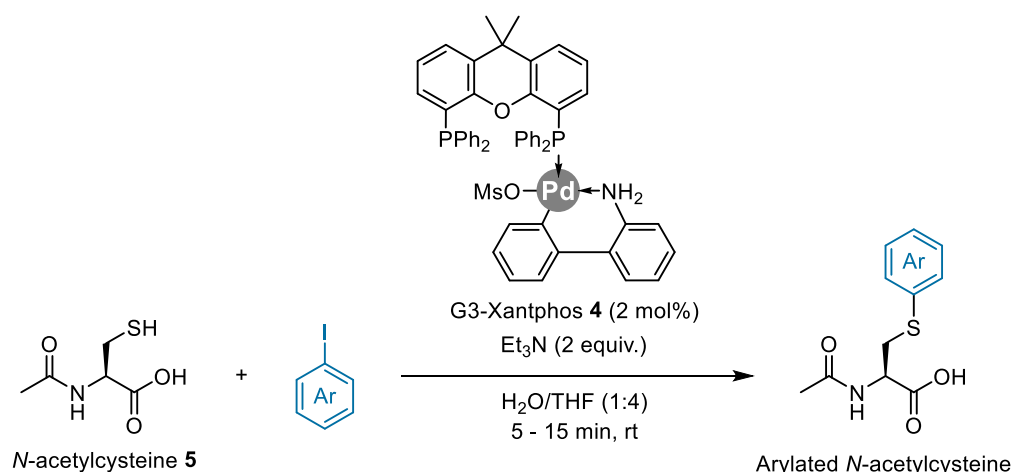
Building on previous aqueous palladium-catalysed methods, including Suzuki-Miyaura cross-coupling of biomolecules pre-functionalised with aryl iodides⁴⁴ and copper-free Sonogashira coupling of alkyne encoded biomolecules,⁴⁵ Davis and co-workers reported a seminal direct palladium-catalysed arylation of cysteine residues on a protein.⁴⁶ The work initially screened a range of water-soluble Pd precatalysts, finding $\text{Na}_2\text{Pd}(\text{DM-ADHP})_2(\text{OAc})_2$ (**2**) (DM-ADHP = *N,N*-dimethyl-2-amino-4,6-dihydropyrimidine) to be the most effective ligand using their standard conditions (Scheme 1). Under these optimised conditions, conversions of greater than 85% to arylated protein were achieved in four hours. The temperature required for this transformation (65 °C) is higher than what is usually accepted to be biocompatible and may not be tolerated by many proteins, which the authors acknowledge.



Scheme 1: Optimised conditions reached in the 2016 work of Davis *et al.* for the arylation of MGS (**3**) in aqueous media mediated by Pd(Oac)₂(DM-ADHP)₂ (**2**). Structure of MGS (**3**) (PDB entry 2BO6)⁴⁷ generated in Mol*.⁴⁸

Notably, the protein chosen for these studies, mannosylglycerate synthase (MGS, **3**), contained a poly-histidine site adjacent to a cysteine residue. It was hypothesised that this would direct arylation towards this single cysteine residue *via* coordination to Pd. After extensive labelling studies, it was proven that the three other solvent-exposed cysteine residues in MGS (**3**) were not arylated. This selectivity highlighted the importance of the adjacent histidine metal-binding site in MGS (**3**) in enabling arylation. After demonstrating selectivity, the group explored the substrate scope, showing good conversions with aryl groups functionalised with azides, nitriles, an affinity tag, and other common functionalities.

The 2016 work of Messaoudi *et al.* reported using a commercially available Pd-based precatalyst, G₃-XantPhos (**4**) as a way of selectively functionalising cysteine residues.⁴⁹ Previous work had shown that this precatalyst was effective for the rapid arylation of glycosyl thiols⁵⁰ under mild conditions. Applying the system to cysteine first enabled the quantitative arylation of *N*-acetyl cysteine (**5**) in ten minutes with 10% THF, or five minutes with 20% THF (Scheme 2). In fully aqueous conditions, the reaction took 90 minutes to achieve quantitative yield. The reaction only tolerated aryl iodides or alkynyl bromides, and optimised conditions were not buffered, limiting the use of the process for larger or more sensitive biomolecules. Isolated yields of labelled di- and tri- peptides of consistently greater than 97% were reported.

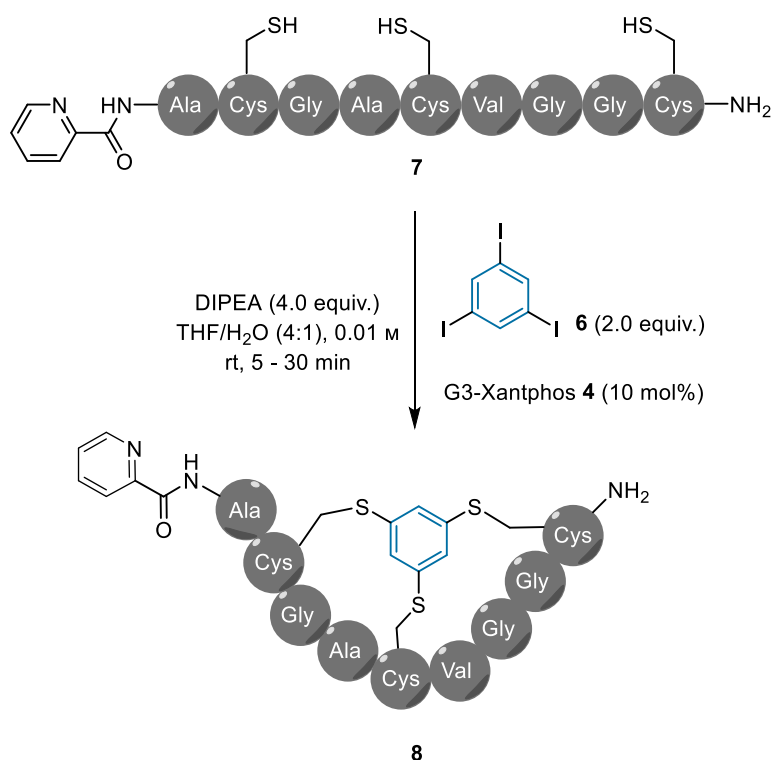


Scheme 2: Optimised conditions for arylation of di- and tri-peptides using G3-XantPhos.

Further application of this work allowed the tagging of the antibody trastuzumab with a rhodamine-derived fluorophore, requiring five equivalents of Pd-G₃ Xantphos (**4**). Conditions for the one-pot reduction of the disulfide linkage of oxytocin, followed by *S*-arylation of both resulting free cysteines used 50 mol% Pd-G₃ Xantphos (**4**). This high catalyst loading for more complex biomolecules produced a significant amount of a side-product resulting from arylation with 2-phenylaniline originating from the precatalyst.

The Messaoudi group has continued to develop this work utilising G3-Xantphos (**4**). In 2017,⁵¹ the precatalyst was used to facilitate the C-S cross coupling of halogenated oligonucleotides with thiosugars. Further application⁵² saw the cross coupling of thiosugars with haloarene-functionalised peptides toward the synthesis of aryl-thioglycopeptides. In 2021, Humpert *et al.* reported the use of G₃-Xantphos (**4**) for the rapid ¹⁸F labelling of cysteine residues in aqueous media using ¹⁸F-labelled aryl iodides.⁵³

In 2021, the Chen group further applied G3-Xantphos (**4**) in the formation of aryl-thioether-bridged peptide macrocycles. This chemistry required the installation of an aryl iodide onto a peptide, which then undergoes an intramolecular C-S cross-coupling with a cysteine residue to form a macrocycle.^{54,55} However, later the same year, the group successfully applied the chemistry towards peptides containing two or three cysteine residues, removing the requirement for pre-functionalisation of the peptide through use of a di- or tri-iodo (**6**) arene substrate to link the cysteine residues (Scheme 3).



Scheme 3: Optimised conditions for macrocyclization of PA-Ala-Cys-Gly-Ala-Cys-Val-Gly-Gly-Cys-NH₂ (7) using 1,3,5-triiodobenzene (6) and G3-Xantphos (4) to form peptide bicycle 8.

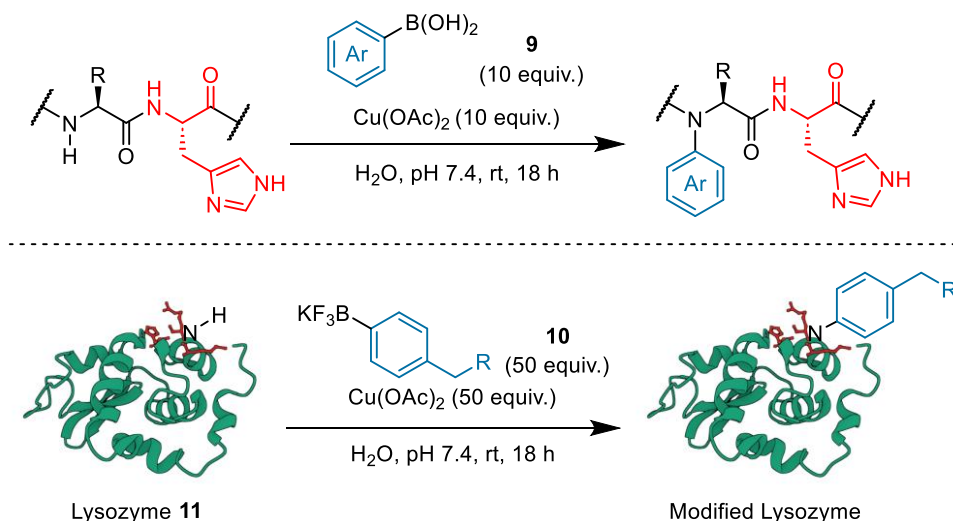
This process was optimised using a hexapeptide containing two cysteine residues, which was cyclised using 1,4-diiodobenzene. Optimised conditions for this reaction required two equivalents of aryl iodide, 20% catalyst loading, 20% water in THF and four equivalents of DIPEA. The authors noted that the addition of the base allowed the reaction time to be reduced from four hours to ten minutes, and that other bases such as triethylamine and K₂CO₃ achieved similar results. Other water-miscible solvents such as DMF, MeCN, MeOH and EtOH were well tolerated with yields between 76% and 81%. However, the yield dropped substantially when either HFIP or DMSO were used, giving 8% and 21% yield, respectively. A diverse range of di- and tri- halogenated linkers were trialled to cyclise a collection of peptides up to 15 amino acids in length containing one or two cysteine residues.

1.2.1.2. Copper

Examples of biocompatible copper-catalysed arylation are sparse, and the methodology currently reported does not result in arylated amino acid side chains, rather *N*-arylation of amide linkages. However, the examples below demonstrate an interesting transformation of natural biomolecules.

In 2016, *N*-arylation of amides was explored by Ball and co-workers utilising the directing effects of histidine residues (Scheme 4 top).⁵⁶ The histidine residues direct the coupling of aryl boronic acids (9) and boronates (10) to a neighbouring amide nitrogen *via*

a Chan-Lam-type coupling reaction. The process proceeded under mild conditions in HEPES-buffered water with organic solvent additives at ambient temperature. The amide nitrogen of an *N*-terminal proline with an adjacent histidine residue produced the best conversions, however the substrate scope extended to amide nitrogen atoms in the middle of amino acid sequences, albeit with significantly reduced conversions. The authors postulated that the reaction could be enabled by the formation of a four-coordinate copper(II) species ligated by the amino acid itself, which had been reported previously.^{57,58}

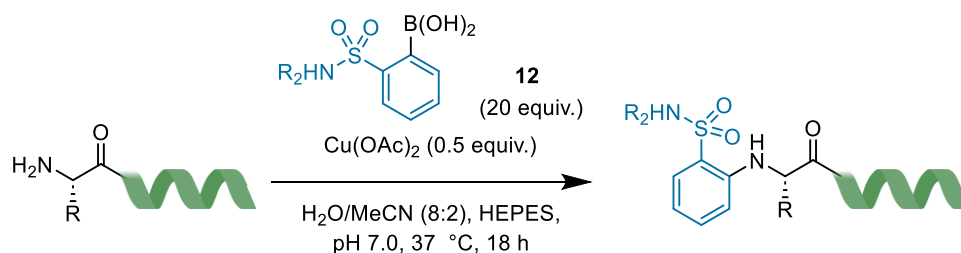


Scheme 4: **Top:** General scheme for the Chan-Lam-type *N*-arylation of backbone amide nitrogens. **Bottom:** *N*-Arylation of Arg14-Lys13 amide bond directed by His-15 (all shown in red). Structure of lysozyme (PDB entry 1HEL)⁵⁹ generated in Mol*.⁴⁸

This process was further applied to protein arylation using lysozyme (**11**) (Scheme 4 bottom), a 14 kDa protein, as the model substrate thanks to its native histidine residue (His-15). For the protein arylation, trifluoroborate salts (**10**) adorned with affinity handles such as an alkyne, azide, or desthiobiotin, were used. A modest conversion to modified protein was reported and analysis by mass spectrometry demonstrated that a single modification had occurred, confirming the selectivity of the process. Further development saw Ball and co-workers use Cu(II) and aryl boronic acids to facilitate arylation of *C*-terminal pyroglutamate-histidine.⁶⁰

In 2020, the Ball group expanded the versatility of copper-catalysed arylation for bioconjugation through development of a strategy for *N*-terminus-selective arylation (Scheme 5).⁶¹ They discovered that aryl boronic acids bearing *ortho*-sulfonamides (**12**) enabled efficient arylation of the *N*-terminus of peptides. Optimisation of the reaction showed twenty equivalents of boronic acid, 50 mol% of Cu(OAc)₂, HEPES buffer, with 20% MeCN additive, at 37 °C and pH 7.0 for 18 hours to be the most effective conditions for the process. Despite this optimisation, the authors chose a separate set of conditions for their

aryl boronic acid substrate scope, the results of which found that it was essential that the aryl boronic acid bore an *ortho*-sulfonamide. This requirement was not commented on by the authors. The process was specific for the *N*-terminal nitrogen even when the peptide contained lysine, and the authors suggested that binding of the copper specifically to the *N*-terminus is responsible for the selectivity. *N*-terminal proline or homoalanine were not tolerated.

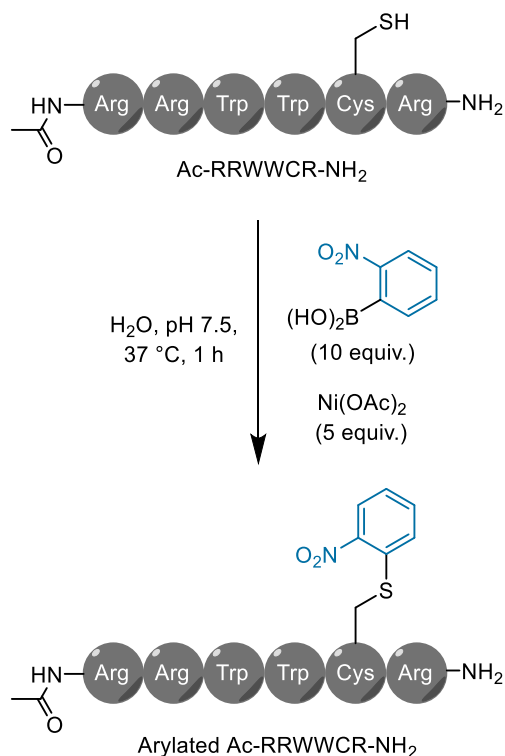


Scheme 5: Optimised reaction conditions for Cu(II)-catalysed *N*-terminal arylation.

1.2.1.3. Nickel

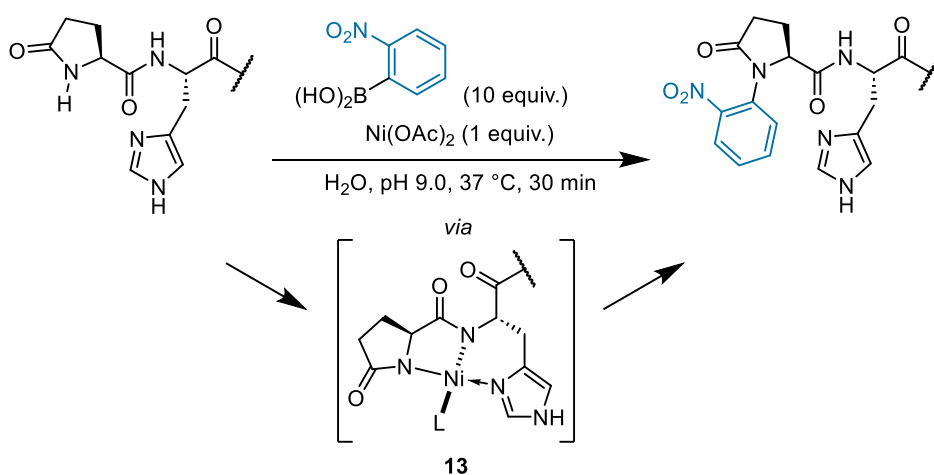
Homogeneous nickel catalysis has proven its utility in recent years, and has earned its place in the chemists arsenal of arylation chemistry.⁶² Compared to Cu(II), Ni(II) exhibits significantly less cellular toxicity,⁶³ and is therefore an area of interest for many bioconjugation chemists.

The 2019 work of Ball documented the discovery of a nickel-catalysed cysteine *S*-arylation using *ortho*-nitrophenylboronic acids in aqueous media.⁶⁴ Initial screening of ten different metals showed excellent conversions for Ni(OAc)₂, Cu(OAc)₂ and Co(OAc)₂. The authors justified continuing to optimise using Ni(II) by citing Cu(II)'s ability to oxidise cysteine residues,⁶⁵ but did not offer an explanation for choosing Ni(II) over Co(II). Optimised conditions of five equivalents of Ni(OAc)₂ and ten equivalents of boronic acid to cysteine-containing biomolecules were reported (Scheme 6). Reactions proceeded in water at pH 7.5 and, after thirty minutes at 37 °C, conversions of up to 99% were reported. However, it was paramount that the aryl boronic acid was substituted with a strong electron withdrawing group *ortho*-, and the reaction did not tolerate any other substituted aryl boronic acids.



Scheme 6: Optimised conditions of Ni(II)-catalysed cysteine S-arylation using phenylboronic acids, showing arylation of Ac-RRWWCR-NH₂ with *o*-nitrophenylboronic acid mediated by Ni(OAc)₂.

The Ball group subsequently reported nickel-catalysed methodology towards *N*-arylation of *N*-terminal proline with an adjacent histidine residue.⁶⁶ Much like their previously reported Cu(II)-mediated process, the reaction was postulated to proceed *via* a four-coordinate metal species (**13**) which directs *N*-arylation of the amide nitrogen (Scheme 7). A handful of drawbacks of this transformation were noted: the reaction only proceeds in basic conditions and reactivity dropped significantly below pH 8.5, it was essential for the aryl boronic acids to be adorned with an *ortho*-nitro group, and *N*-terminal pyroglutamate was also essential. However, with the tolerated substrates conversions were excellent, and biomolecules could be decorated with reactive handles such as aryl alkynes or azides. Conversions fell to moderate when the aryl ring contained an electron-donating group *para*- to the boronic acid.



Scheme 7: Optimised conditions for *N*-terminal pyroglutamate *N*-arylation of NH_2 -Pro-His-peptides using *ortho*-nitrophenylboronic acid and $\text{Ni}(\text{OAc})_2$. Reaction is theorised to proceed through Chan-Lam-type intermediate (**13**).

Ball and co-workers further applied their nickel-mediated chemistry to the formation of protein-polymer conjugates by functionalising the 2-nitrophenylboronic acid with a polymer.⁶⁷ Combining their nickel-mediated cysteine arylation chemistry with their copper-mediated histidine-directed *N*-terminal proline arylation chemistry, the group were able to synthesis complex macrocycles and protein-protein conjugates.⁶⁸ Most recently, Ball's nickel methodology was used to functionalise biomolecules using bis-boronic acids, which formed dynamic bioconjugates with salicylhydroxamic acids.⁶⁹

1.2.2. Arylation of Biomolecules *via* Transition Metal-Containing Reagents

It is interesting to note that despite its ubiquity in modern organic chemistry, application of metal catalysis in the bioconjugation field has been a largely unsuccessful one, with a few notable exceptions as discussed above. Existing methodologies all suffer from at least one of the following caveats: high catalyst loading, high loading of aryl substrate, aryl substrates requiring highly specific functionalisation, poor substrate scope, poor chemoselectivity, slow reaction rate, or the need for conditions that may not be tolerated by most biomolecules. Thus, the development of stoichiometric organometallic reagents towards the arylation of canonical residues has become a major focus of bioconjugation research. Despite stoichiometric transition metal reagents being a rare sight in modern organic chemistry, they often do not suffer from the same limitations as catalysis when applied in the context of bioconjugation.

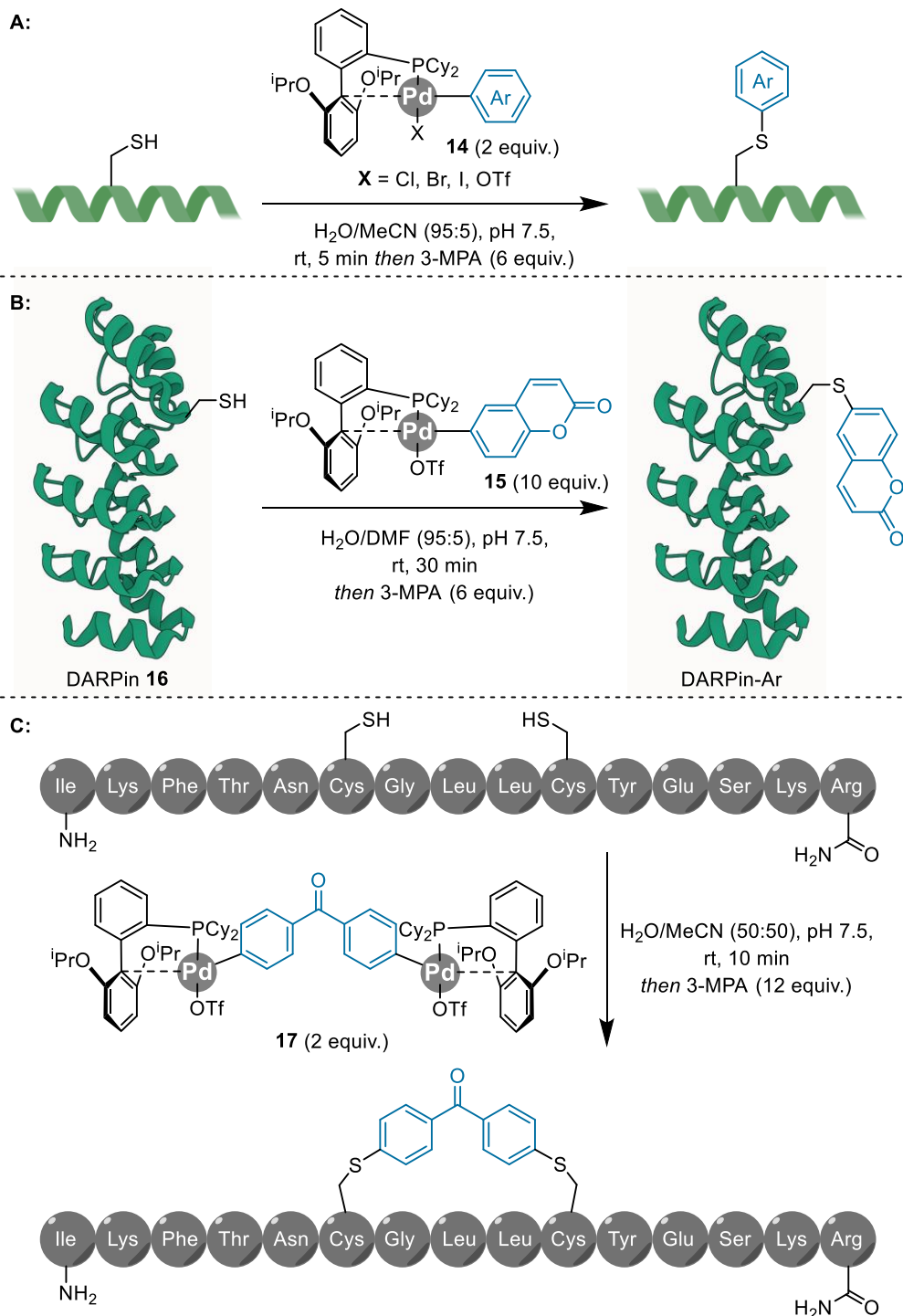
Some of the most important recent discoveries in the field of bioconjugation chemistry using metal complexes are outlined below.

1.2.2.1. Palladium

The first example of a stoichiometric palladium species being used for bioconjugation was the work of Francis and Tilley,⁷⁰ who reported selective functionalisation of tyrosine using stoichiometric π -allylpalladium complexes. The work involved taking the well-established chemistry of π -allylpalladium complexes and adapting it to the stringent aqueous conditions required by biomolecules. Although not describing arylation chemistry, this seminal work showed the potential of palladium complexes to offer selective and biocompatible bioconjugation.

There have been a handful of reports describing the arylation of non-canonical amino acids with palladium complexes: 2011 saw Simmons *et al.* demonstrate the ability of Pd(II) complexes to arylate biomolecules labelled with alkenes,⁷¹ and in 2013, Lin *et al.* developed a protocol for using palladacycles in bioconjugation reactions with biomolecules tagged with a terminal alkyne⁷² which was built upon by subsequent work in 2014.⁷³

In 2015, the landmark work by Buchwald and Pentelute reported using organometallic complexes of palladium to arylate cysteine residues with high selectivity and efficiency (Scheme 8).⁷⁴ This was achieved by pre-forming an organometallic Pd(II)-Ar species (**14**), which was ligated by a bulky biaryl phosphine ligand, RuPhos. The use of a stoichiometric Pd reagent, rather than Pd-mediated catalysis is advantageous as the presence of thiols has been demonstrated to deactivate Pd catalysts.⁷⁵



*Scheme 8: Organometallic palladium reagents for cysteine bioconjugation. A: Standard conditions for arylation of peptides with Pd(II) complexes ligated with RuPhos (**14**). B: Standard conditions for arylation of proteins, showing arylation of DARPin (**16**) to with Pd-coumarin complex (**15**). Depicted protein DARPin (PDB entry 50OU). Protein structure generated in mol*. C: Conditions for stapling of dicysteine peptide using bimetallic palladium complex (**17**) to form stapled peptide.*

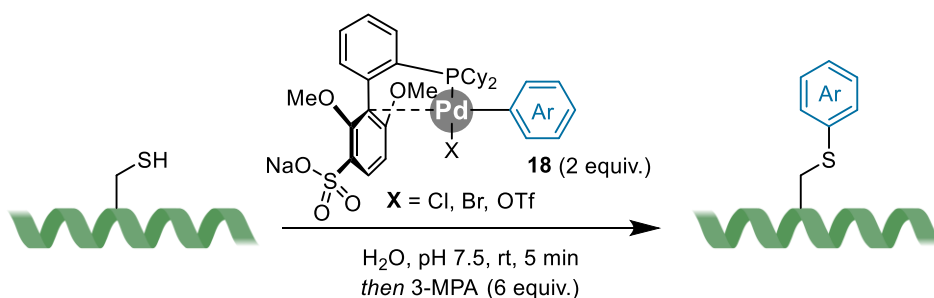
The reaction proceeded to quantitative conversions of peptides in five minutes at low micromolar concentrations, required no heating, and 5% of organic co-solvent such as MeCN, DMF, or DMSO (Scheme 8 A). Only two equivalents of palladium reagent were required, and the reaction was quenched with 3-mercaptopropionic acid (3-MPA) upon

completion, reacting with excess palladium reagent. The reaction also proceeded at a pH range of between two and ten, which allowed the labelling of cysteine in water even with 0.1% trifluoroacetic acid (TFA) added, albeit with much longer reaction times at lower pH.

Importantly, the complexes were bench-stable and storable, and could be accessed in a single step from commercially available aryl halide or triflate precursors. This allowed application of this procedure to achieve cysteine labelled with a wide variety of aryl species including fluorophores, bioconjugation handles, and an affinity tag. Intact protein experiments showed the chemoselective arylation of a handful of model protein substrates containing a single surface cysteine residue, maintaining biocompatible conditions using ten equivalents of palladium complex (Scheme 8 B). The methodology was successfully applied to peptide stapling (Scheme 8 C) and enabled the formation of a linker-free ADC.

The peptide stapling ability of this methodology was further expanded on in 2017,⁷⁶ where the authors measured the physicochemical properties and change in binding affinities of their stapled peptides to proteins of interest. Also in 2017, Buchwald and co-workers used their methodology to enable the radiochemical labelling of peptides with aryl ¹¹CN.⁷⁷

A drawback identified in the 2015 work of Buchwald and Pentelute was the need for 5% organic co-solvent in the reaction media, which could potentially disrupt the structure of more sensitive biomolecules. This was addressed in 2017, where follow-up work described the generation of water-soluble palladium reagents (**18**) for the arylation of cysteine.⁷⁸ This was achieved by replacing the initially used biaryl phosphine ligand, RuPhos, with a water-soluble ligand, sSPhos (Scheme 9). This increased the yields from 18% for RuPhos-ligated complexes, to 99% for sSPhos when in fully aqueous conditions.

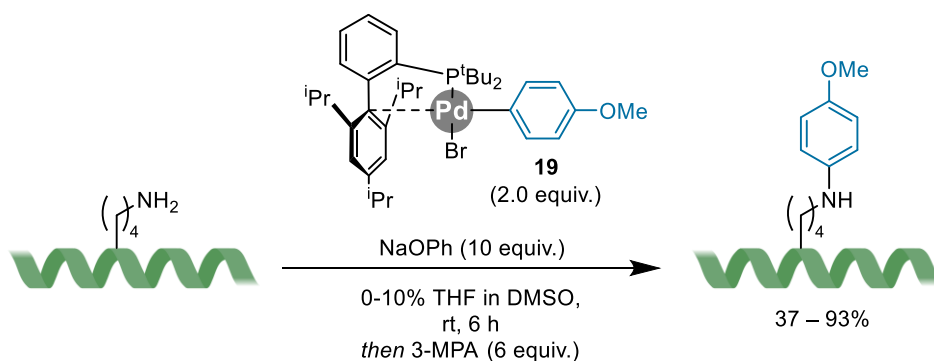


Scheme 9: Cysteine bioconjugation using Pd(II) oxidative addition complexes ligated with sSPhos, eliminating the need for organic co-solvents.

Changing the properties of the phosphine ligand successfully eliminated the need for any organic co-solvent, and the utility of these reagents was again demonstrated with a variety of aryl groups. The LC-MS yields from these reactions remained high, ranging from 82 – 99%. Bifunctional analogues of these reagents were also used to generate macrocyclic peptides. However, in approximately half of the examples given, 15% MeCN was required

to reach full conversion. Switching the ligand system to sSPhos did not alter the stability of the complexes to ambient moisture and air.

Work in 2017 by Buchwald and Pentelute shifted the focus from targeting cysteine to targeting lysine.⁷⁹ Targeting lysine with palladium complexes was seen to be more challenging due to the amine group being less nucleophilic than a thiol, and the lower acidity of the palladium-amido complex necessitating a stronger base. Sodium phenoxide was found to be a suitable base for lysine arylation, and the work mostly focussed on ligand optimisation.

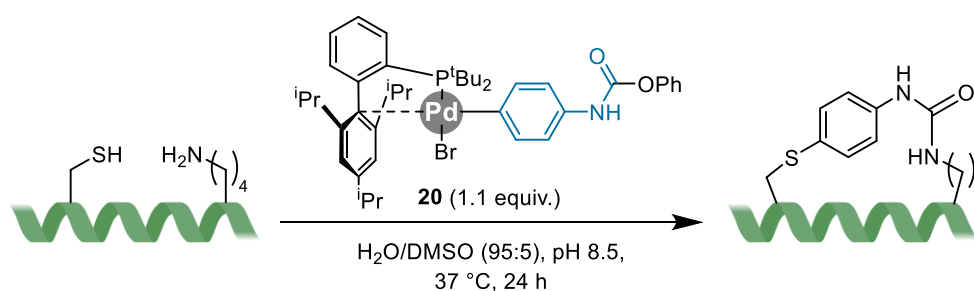


Scheme 10: Lysine bionconjugation using pre-formed Pd(II) oxidative addition complexes in optimised conditions.

A variety of ligands were screened, with the most effective being *t*BuBrettPhos, giving yields of up to 93%. These high yields were dependant on the characteristics of the aryl ring, with electron donating groups giving high yields, but yields were significantly lower for electron withdrawing groups. This was clearly demonstrated with *para*-OMe and CO₂Me groups giving 94%, and 18% yields, respectively. Subsequently, **19** was chosen to optimise the procedure and assess selectivity (Scheme 10). The selectivity towards lysine was very high, with no competing arylation observed in the presence of serine, tyrosine, methionine, histidine, or tryptophan residues. However, the presence of cystines, primary amides, and guanidines caused selectivity issues and were not tolerated. The reaction also was not performed in aqueous media and required DMSO with up to 10% THF as the solvent. Lack of aqueous conditions and the requirement for a strong base means that this protocol is unlikely to be compatible with many biomolecules.

The utility of this protocol was demonstrated by tagging a tumour-suppressing peptide with a variety of groups. These included natural product derivatives, affinity tags, chromophores, and pharmaceuticals. A variety of yields were obtained, ranging from 38% to 88%. Bifunctional palladium reagents were again used to successfully form macrocyclic peptides *via* coupling of two lysine residues.

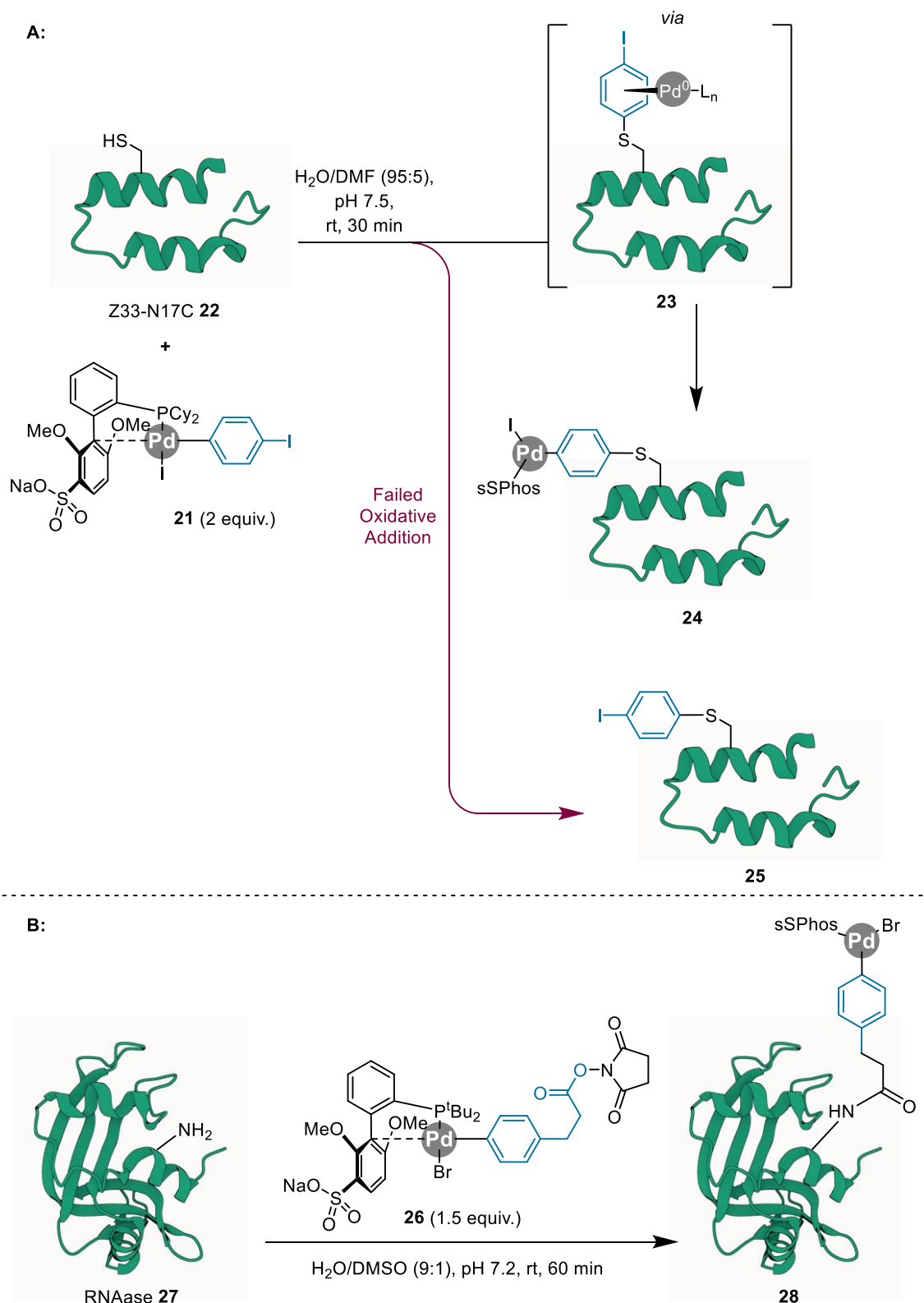
Cross-linking of peptides and proteins, whether intra- or intermolecularly, is a useful strategy for controlling their conformation, and studying protein-protein interactions, among other utilities. As an example, the formation of disulfide bonds in nature is key to protein structure and function. In 2018, the work of Buchwald and Pentelute looked to apply their already well-established methodology for bioconjugation using palladium complexes to the cross-linking of biomolecules.⁸⁰ The new bifunctional reagents (**20**) looked to combine the cysteine-selective palladium complexes with a lysine-selective phenyl carbamate reagent (Scheme 11).



Scheme 11: Peptide stapling employing bifunctional reagents containing Pd(II)-Ar and carbamate warheads.

This optimised strategy successfully produced stapled peptides in high yield. The protocol supported a wide range of macrocycle sizes, ranging from the lysine and cysteine residues being adjacent, to having ten residues between them, all giving LC-MS yields upwards of 70%. Once formed, these macrocycles were demonstrated to be stable to a variety of conditions, and no degradation was observed after 24 hours in basic, acidic, or oxidative conditions. The methodology was also applied to intermolecular crosslinking of mouse double minute 2 homolog (MDM2), a protein involved in tumour-suppressing pathways, and two peptides with different affinities toward MDM2. As expected, the peptide with a lower affinity toward MDM2 showed a lower degree of cross-linking after ten hours.

Further application of organometallic palladium complexes in bioconjugation saw the development of methodology towards the synthesis of palladium-protein complexes (Scheme 12).^{81,82} The Buchwald lab published two approaches to this. The first, published in 2020, used Pd-aryl halides (**21**) as bioconjugation substrates. The authors proposed that after C-S bond formation had occurred, the Pd(0) generated undergoes oxidative addition into the carbon-halide bond *via* a ring walking mechanism (**23**) to generate Pd-protein complex **24** (Scheme 12 A). The second approach, published later the same year, used bifunctional reagents (**26**) functionalised at one end with a lysine-selective *N*-hydroxysuccinimide (NHS) ester, and at the other with cysteine-selective Pd(II) (Scheme 12 B).



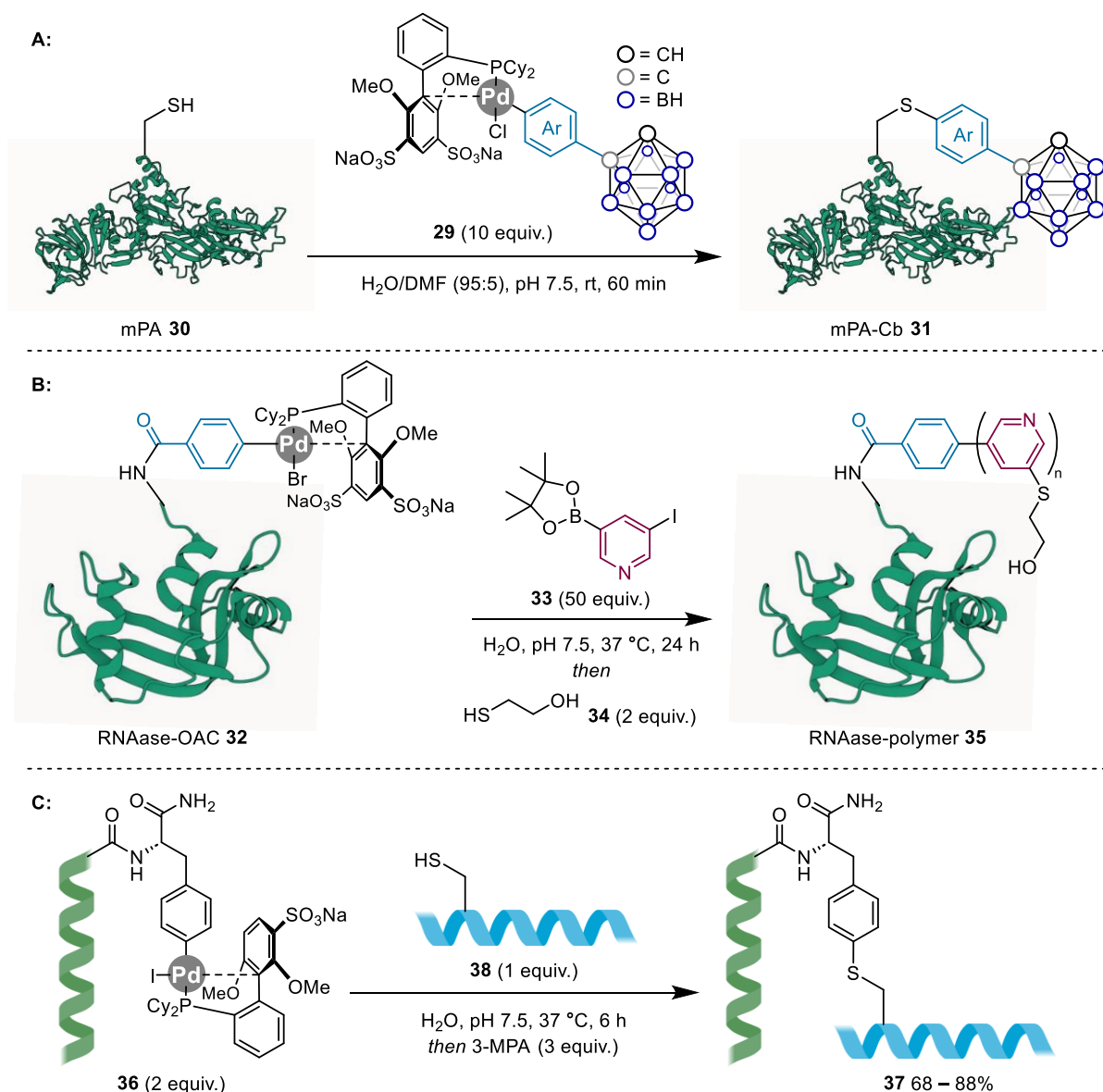
Scheme 12: Approaches towards the formation of active Pd(II)-protein oxidative addition complexes. **A:** Using Pd-aryl halide complex **21** to functionalise Z33-N17C (**22**) (PDB entry 1ZDA)⁸³. **B:** Using bifunctional reagent **26** to functionalise RNAase (**27**) (PDB entry 2AAS).⁸⁴

Optimisation of the strategy published first showed that the ligand system, aryl halide, and additive were all crucial in maximising the conversion to Pd-protein complex **24**, whilst minimising the conversion to **26**. Screening of BrettPhos, SPhos and sSPhos showed

sSPhos to be the most effective ligand, and it was crucial that the Pd complex was an aryl iodide, as this maximised the efficiency of the intramolecular oxidative addition. Finally, changing the solvent additive from 10% DMSO to 5% DMF produced isolable protein-Pd complexes with LC-MS yields of up to 87% after purification *via* desalting column. Notably, following storage in aqueous buffer (20 mM Tris, 150 mM NaCl, pH 7.5) for 24 h, the Pd-protein complexes showed no loss of activity. After initial formation of these complexes, they were treated with a different cysteine-containing protein, producing cross-coupled proteins which could be isolated *via* HisTrap™ affinity chromatography followed by size-exclusion chromatography. The isolated yield of cross-coupled protein was determined to be 28%.

The second strategy used well-established NHS ester chemistry, reacting bifunctional reagent **26** with lysine-containing protein (RNAase, **27**) to produce Pd-protein complex **28**, which was obtained in 30% yield after RP-HPLC purification. This work takes advantage of the high selectivity of palladium-aryl complexes toward thiols, which facilitates the formation of Pd-protein complexes. In this work, the Pd-protein complexes were used to form protein homodimers, conjugate proteins or peptides to an antibody, and competition experiments showed them to be at least ten times as reactive as protein-maleimide complexes at pH 7.5 and under.

In 2022, the Buchwald lab further applied their methodology in three ways (Scheme 13): the palladium-mediated incorporation of carboranes into biomolecules,⁸⁵ the synthesis of protein-polyarene conjugates,⁸⁶ and the synthesis of palladium-peptide oxidative addition complexes.⁸⁷



Scheme 13: 2022 work from the Buchwald lab using organometallic palladium complexes in bioconjugation chemistry. **A:** Palladium-mediated incorporation of carboranes into biomolecules, showing the functionalisation of mPA (**30**) (PDB entry 1ACC)⁸⁸ with carborane-palladium complex (**29**). **B:** Palladium-mediated synthesis of protein-polyarene complexes, showing the reaction of palladium-protein complex RNAase-OAC (**32**) with monomer **33** to form RNAase-polymer **35** following quench with 2-mercaptoethanol (**34**). Structure of RNAase adapted from PDB entry 2AAS.⁸⁴ **C:** Reaction of palladium-peptide complex **36** with cysteine-containing peptides (**38**) to form peptide-peptide conjugates (**37**).

Carboranes have attracted significant interest in the drug discovery field,⁸⁹ however there are few ways to enable their incorporation into biological molecules. In 2022, the functionalisation of biomolecules with carborane (Scheme 13 A) was achieved using Pd(II)-carborane complexes with an aryl linker (**29**). These complexes were ligated with bsSPhos, a recently reported⁹⁰ water-soluble bis-sulfonated bulky biaryl phosphine ligand. This aryl linker allowed the isolation of the reactive palladium complexes, as the authors were unable to isolate linker-free Pd-carborane complexes. The reaction of these carborane-containing complexes was optimised using mutant protective antigen K563C protein

(mPA, **30**), producing yields of greater than 95% to bioconjugate **31** at room temperature in one hour buffered to pH 7.4. The nature of the bis-sulfonated bulky biaryl phosphine ligand allowed the reaction to be run in aqueous conditions, requiring just 5% of DMF as an additive despite the extremely hydrophobic nature of the carborane.

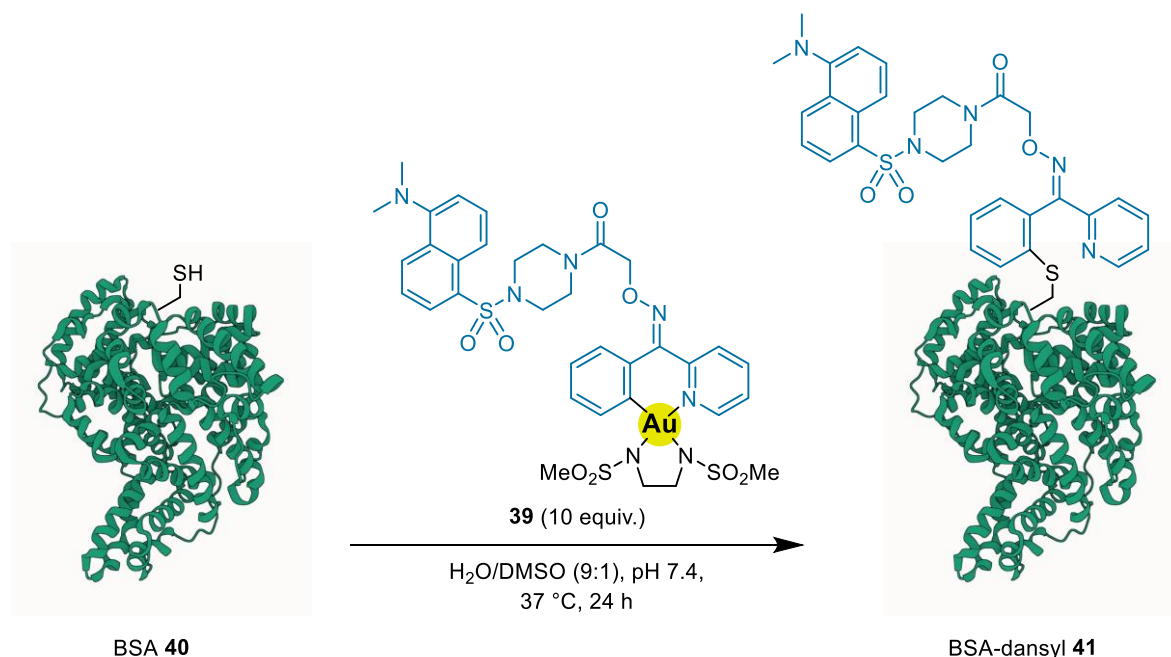
The palladium-synthesis of protein-polyarene complexes (Scheme 13 B) used Catalyst Transfer Polymerisation (CTP) to grow polymers from isolated palladium-protein complexes. The work was demonstrated using isolated RNAase-OAC complex **32**, reacting with a large excess of 3-BPin-5-iodopyridine (**33**) as the monomer. The polymers, with palladium still bound to their termini, were then quenched with 2-mercaptoethanol (**34**) to form RNAase-polymer conjugate **35** capped with 2-mercaptoethanol. The polymerisation could also be terminated with thiol-containing protein to form protein-polymer-protein complexes. This methodology employed bsSPhos as the ligand, and polymerisations proceeded at 37 °C over 24 h.

The most recent application of palladium chemistry in bioconjugation was the report of palladium-peptide complexes for bioconjugation (Scheme 13 C). Palladium-peptide complexes were generated from peptides that contained an unnatural C-terminal 4-iodophenylalanine. The optimised reaction conditions, 37 °C for six hours in water at pH 7.4, facilitated the reaction of palladium-peptide complexes (**36**) with cysteine-containing peptides, forming peptide-peptide conjugates (**37**). When the cysteine of peptide **38** was internal or at the C-terminus, the reaction produced conversions of 88% and 86%, respectively. However, this fell to 68% for *N*-terminal cysteine-containing peptides. The authors subsequently applied this methodology towards the synthesis of peptide-protein conjugates, achieving 90% conversion.

1.2.2.2. Gold

The first example of using stoichiometric gold complexes for protein arylation was work by Leung and Wong in 2014, which demonstrated the utility of cyclometallated Au(III) complexes for bioconjugation.⁹¹ Prior work had demonstrated the formation of Au-S interactions in biomolecules,^{92,93} however the reductive elimination to form C-S bonds had not been observed. Leung and Wong discovered that ligating their gold complexes with *N,N'*-bis(methanesulfonyl) ethylenediamine (msen) allowed chemoselective cysteine arylation. Peptide-gold complexes could be isolated with a defined Au-S bond, which would then reductively eliminate to form arylated cysteine when heated to 40 °C, provided the

organometallic complex was a six-membered metallocycle. Modification of model peptides afforded LC-MS yields of up to 99%.



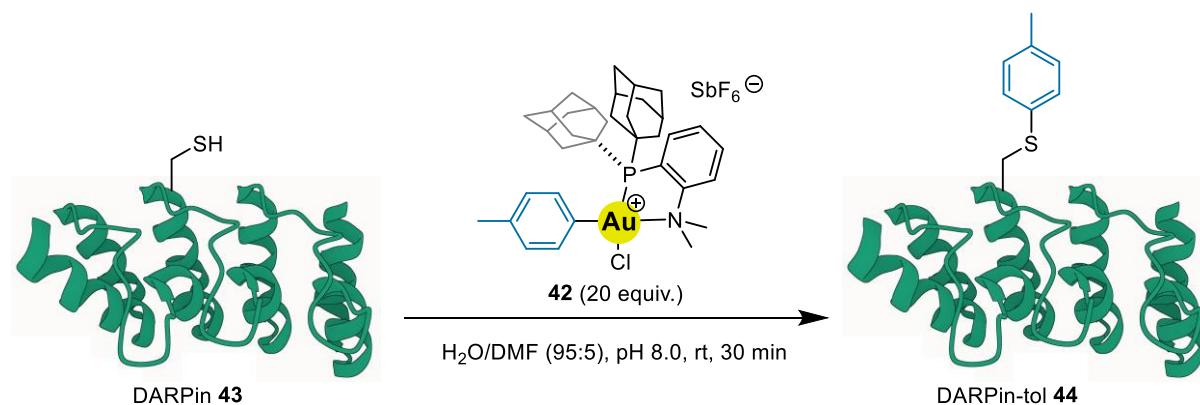
Scheme 14: Functionalisation of BSA (40) with cyclometallated Au-dansyl complex (39) to form BSA-dansyl bioconjugate (41).

The utility of this protocol was demonstrated by labelling the surface cysteine of bovine serum albumin (BSA, 40) (Scheme 14) and human serum albumin (HSA) using Au-dansyl complex 39. LC-MS analysis after 24h showed successful modification of both proteins. Conversely, attempted labelling of lysozyme, which has no free cysteine residue, was unsuccessful.

Three further studies have been carried out on the cyclometallated gold complexes for bioconjugation. Wenzel *et al.* applied these complexes towards selective cysteine arylation in zinc finger protein domains in 2019.⁹⁴ In 2020, Thomas *et al.* further explored the reactivity and chemoselectivity through a combination of mass spectrometry experiments and DFT studies, and in 2021 Gukathasan *et al.* demonstrated the effect of ligand on the rate of cysteine arylation.⁹⁵

In 2018, the Spokoyny lab made a significant breakthrough in gold-mediated bioconjugation chemistry. By utilising Au(III) complexes prepared *via* oxidative addition into a C-I bond, they described a highly efficient and selective cysteine *S*-arylation procedure in biocompatible conditions (Scheme 15).⁹⁶ Using the Au(III)(Me-DalPhos) system, optimisation of the bioconjugation procedure using cysteine-containing tripeptide glutathione resulted in quantitative conversions after five minutes at room temperature with three equivalents of Au(III) complex. Many substitutions of the aryl group were tolerated,

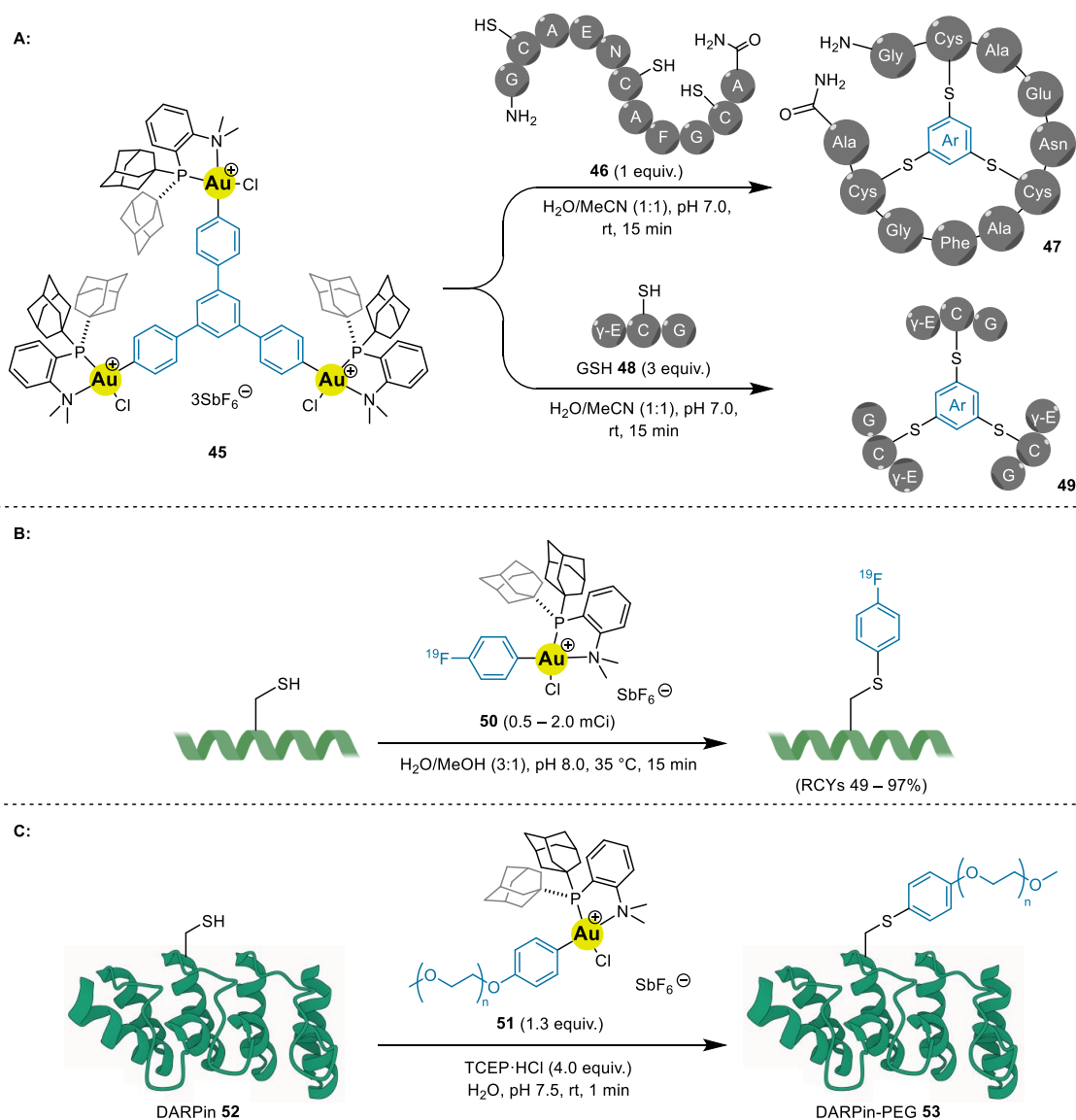
including polymers, fluorescent dyes, affinity tags, and drug-like molecules. A wide range of buffers and solvent conditions were trialled including 10% trifluoroacetic acid (TFA) as an additive. Remarkably, the reaction maintained 99% conversion after five minutes even in such harsh conditions.



*Scheme 15: Optimised conditions for Au(III)-mediated bioconjugation, showing arylation of DARPin (**43**) with Au(III) complex (**42**) to produce bioconjugate **44**.*

Arylation of the antibody mimetic DARPin (**43**) with (4-MePh)AuCl(Me-DalPhos) (**42**) furnished arylated DARPin (**44**) in just thirty minutes at room temperature. Further experiments saw bimetallic Au(III) species facilitating the preparation of stapled peptides. In a competition experiment against the Pd(II) complexes of Buchwald, the product arising from the Au(III)(Me-DalPhos) complex outweighed the Pd(II)(RuPhos) product in a 92:8 ratio. As a result, the authors postulated that the kinetics of the Au(III)-mediated bioconjugation could be an order of magnitude faster than those of the Pd(II)-mediated process. This is possibly a result of faster reductive elimination from Au(III) to Au(I) compared to Pd(II) to Pd(0). In 2019, Zhang and Dong published an analysis of the mechanism and chemoselectivity of these Au(III)(Me-DalPhos) reagents in cysteine bioconjugation, finding the reductive elimination to be the rate limiting step in the process.⁹⁷

The Spokoyny lab have since expanded their Au(III)-mediated bioconjugation chemistry (Scheme 16) to facilitate the preparation of hybrid peptide-based assemblies,⁹⁸ rapid ¹⁸F radiolabelling of biomolecules, and PEGylation of biomolecules.⁹⁹



Scheme 16: Recent work from the Spokoyny lab expanding the scope of their Au(III)-mediated bioconjugation chemistry. **A:** Preparation of bicyclic peptide **47** from tri-cysteine peptide **46** and preparation of tri-peptide conjugate **49** from glutathione (**48**), both facilitated by tri-aurated compound **45**. **B:** Au(III)-mediated radio fluorination of cysteine-containing peptide(s) using ^{19}F -labelled Au(III) complex **50** to produce radiolabelled peptide. **C:** Functionalisation of cysteine-containing DARPin (**52**) with Au-PEG complex **51** to form PEGylated DARPin (**53**).

The group's work describing the preparation of hybrid peptide-based assemblies initially expanded on previous work on peptide stapling, using bimetallic Au(III) complexes to produce stapled peptides with excellent efficiency. Trimetallic Au(III) complex **45** was then synthesised and reacted with peptide **46**, which contains three cysteine residues, to form peptide bicycle **47** (Scheme 16 A). Using trimetallic Au(III) complexes to form bicycles was further investigated by Bicycle Therapeutics in 2022.¹⁰⁰ In Spokoyny's paper, the trimetallic Au(III) complex was also reacted with glutathione (**48**) to form trimeric structure **49**, and glutathione (**48**) was later reacted with a B₁₂ boron cluster core that had been functionalised with Au(III) to form highly complex peptide assemblies.

In 2022, Au(III)-mediated cysteine bioconjugation was applied to the rapid radiolabelling of cysteine-containing biomolecules with ^{18}F (Scheme 16 B). Preparation of the ^{19}F -labelled gold complex **50** was enabled by the rapid oxidative addition of Au(I) into C-I bonds. Cysteine *S*-arylation using radiolabelled Au(III) complex **50** proceeded at neutral pH with 25% added methanol in 15 minutes at 35 °C. The authors noted radiochemical yields (RCYs) in excess of 97% for certain substrates.

Later in 2022, the Spokoyny group, in collaboration with the Maynard group, published a protocol enabling the Au(III)-mediated PEGylation of cysteine-containing biomolecules (Scheme 16 C). Treatment of cysteine-containing protein DARPIn (**52**) with 1.3 equivalents of PEGylated Au(III) complex **51** produced DARPIn-PEG (**53**) quantitatively in one minute. Notably, this process was tolerant to the presence of (tris(2-carboxyethyl)phosphine), a commonly-used biological reducing agent, and also tolerated acidic pH (4.0), low temperature (4 °C), and low concentration (7 μM).

1.2.2.3. Platinum

Most recently, organometallic platinum complexes have been applied to the field (Scheme 17). The first example of this was published by the Spokoyny group in 2021 (Scheme 17 A).¹⁰¹ Their work described the reaction of Pt(II)-carborane complex **54** with cysteine to form borylated cysteine residues, ultimately facilitating the borylation of cysteine-containing protein DARPIn (**52**). The reaction required 85% DMF co-solvent, limiting its application to more sensitive biomolecules.

To date, there has been just one example of arylation chemistry using platinum complexes: in 2022, the Vigalok group described the selective arylation of natural amino acid residues with Pt(IV) complexes (**55**) (Scheme 17 B).¹⁰² The work reported a clear hierarchy in selectivity of these complexes, with arylations occurring in the following order: cysteine *S*-arylation > *N*-terminal *N*-arylation > lysine *N*-arylation > tryptophan *N*-arylation. However, reactions using the reported Pt(IV) complexes were carried out in organic solvent such as acetonitrile and DMSO, severely limiting their application to more complicated biomolecules. The authors note that they are currently focussing on applying this methodology to bioconjugation in aqueous conditions.

2. Pd(II)-Mediated C-H Activation for Cysteine Bioconjugation

2.1. Context

As discussed in 1.2.2.1, palladium oxidative addition complexes (OACs) have emerged as excellent reagents for the functionalisation of free cysteine on complex biological systems. However, their synthetic tractability, especially for potential users of the technology, namely biologists and chemical biologists, may present a significant barrier towards their widespread adoption. The synthetic route toward Buchwald's OACs, combined with their continued push towards more complex and cost-prohibitive ligand systems, may help to explain why no other research group has published work using them despite their initial report emerging over seven years ago. In view of the excellent utility of OACs in bioconjugation processes, investigation into an alternative system with a more facile preparation was launched.

2.1.1. Pd(II) Oxidative Addition Complexes

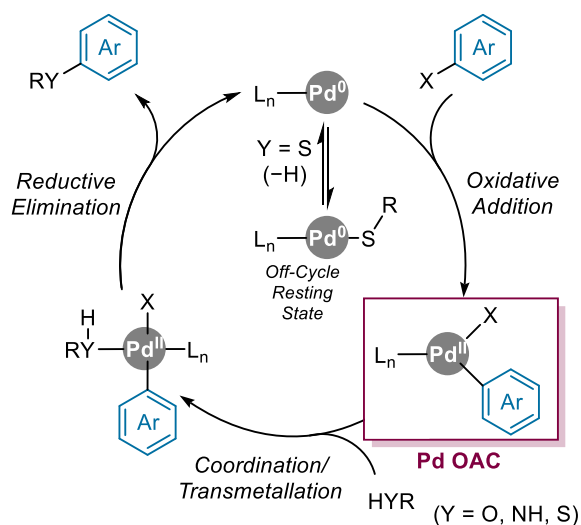
For quite some time, palladium OACs have found significant use in mechanistic studies of palladium-catalysed processes.^{103–105} They have also found applications as pre-catalysts for a variety of palladium-catalysed transformations,^{106,107} and most recently Buchwald's sixth-generation pre-catalyst is built around an OAC.¹⁰⁸ Thus, their application in bioconjugation chemistry was a rather logical one, despite the obvious sustainability and financial drawbacks of employing super-stoichiometric palladium for a chemical transformation.

The widely agreed-upon mechanism for palladium-catalysed cross-coupling reactions consists of three elemental steps (Figure 4 top): oxidative addition, nucleophile coordination or transmetalation, and reductive elimination, with all three steps essential for catalyst turnover. However, the requirement for catalyst turnover presents a significant challenge in the application of catalysis to bioconjugation chemistry, which was briefly touched upon in 1.2.1. The problem arises due to cysteine-containing biological substrates poisoning palladium catalysts, which was studied in detail by the Hartwig lab in 2009.⁷⁵ This mechanistic study noted that each elemental step of the palladium-catalysed cross coupling between aryl halides and thiophenol occurs at or below room temperature. Despite this, the reaction requires several hours at 110 °C to reach completion. Their study discovered the presence of several off-cycle resting states which act to siphon the palladium away from the desired pathway, necessitating such a high reaction temperature to return the 'poisoned' palladium back to a catalytically active species. As these forcing conditions are incompatible

with biomolecules, it is difficult to apply palladium catalysis to biological systems, and all the existing methodologies have significant drawbacks.

The use of palladium OACs for cysteine bioconjugation completely circumvents this issue. By isolating the OAC of interest, the reaction pathway is reduced to two steps: coordination and reductive elimination (Figure 4 bottom). Thus, the formation of product is completely independent of catalyst turnover. This technique of reacting isolated OACs has been applied to the diversification of pharmaceuticals to great effect, where the authors quote that despite using one equivalent of palladium, the reactions are still cost effective at approximately \$1 per 25 mg reaction.¹⁰⁹ This cost is far less than that of many highly functionalized drug-like substrates. The cost-effectiveness of using OACs in bioconjugation reactions is yet more apparent due to the low scale that many of these reactions are performed on, alongside the comparatively high monetary and labour cost of manufacturing peptides, proteins, and antibodies.

Pd(II)-Catalysed C-Y Arylation:



Pd(II)-Mediated Cysteine Bioconjugation:

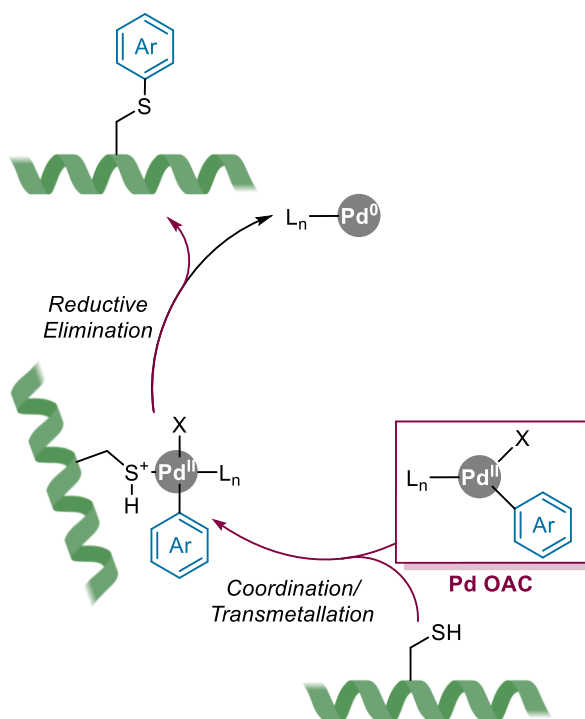
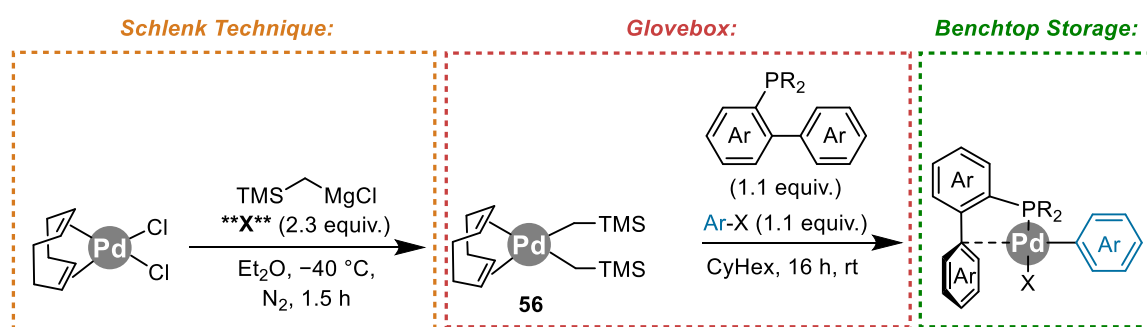


Figure 4: Difference in traditional catalytic cycle for palladium catalysed C-Y cross coupling ($Y = O, NH, S$) (top) versus organometallic palladium complexes for cysteine bioconjugation (bottom).

Despite the triumph of applying OACs to the field of bioconjugation chemistry, there exists an “elephant in the room” regarding their synthesis (Scheme 18). The synthetic route requires a highly active palladium source, $(COD)Pd[(CH_2)TMS]_2$ (**56**), which must be prepared using specialist techniques and stored at $-20\text{ }^\circ\text{C}$ in a glovebox. This palladium source is key, as it allows the preparation of OACs with any phosphine ligand, rather than using pre-ligated palladium sources where the phosphine ligand cannot be exchanged. Although commonplace in well-equipped modern synthetic chemistry laboratories, the

equipment and expertise required to synthesise **56** may not be found in many of the laboratories interested in applying bioconjugation chemistry. This is clearly demonstrated by the commercial availability of protein labelling kits that require little synthetic expertise from the user, such as those available from Thermo Fisher Scientific, which tag cysteine residues with maleimides. The Buchwald lab even acknowledge this significant limitation of their OAC chemistry, and in 2021 they reported an air- and thermally-stable alternative to **56**.¹¹⁰ Regardless, the synthesis of this alternative is significantly lower yielding, and all reports from the Buchwald lab since still use **56** in the synthesis of their OACs.^{85–87}



Scheme 18: Synthesis of palladium OACs for bioconjugation.

Another noteworthy barrier to the widespread adoption of this methodology is the ligand cost. When the investigations detailed later in this chapter were commenced, the patent on bulky biaryl phosphine ligand RuPhos had not yet expired, and the cost was around £80 per gram. Since, the Buchwald lab have moved forward to using more complex and expensive ligands: *t*BuBrettPhos (£370 per gram), sSPhos (£270 per gram), and bsSPhos, which is not commercially available, and must be synthesised using highly corrosive fuming sulfuric acid.

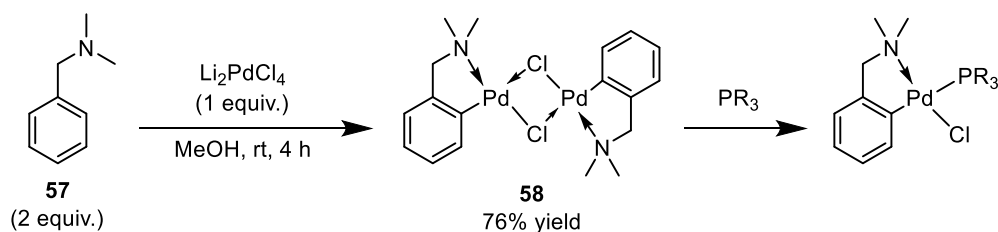
Evidently, the current methods for palladium-mediated bioconjugation have limitations that hinder their widespread adoption, such as complex synthetic routes and the use of expensive ligands. To overcome these issues, there is a need for a more streamlined and cost-effective approach to increase the accessibility of the technology. If these needs are met, it is entirely conceivable that this methodology could see more widespread adoption in academia and industry, placing another arrow in the quiver of rapid and reliable biomolecule functionalisation reactions.

2.1.2. Cyclopalladation

The birth of C-H activation chemistry is regarded to be around six decades ago, when Kleiman and Dubeck reported the preparation of cyclopentadienyl [*o*-(phenylazo)phenyl]nickel *via* the reaction of azobenzene with Cp₂Ni.¹¹¹ Since, development

has seen metal complexes prepared *via* C-H activation change from reagents that facilitate functional group transformations to precatalysts, facilitating efficient cross-coupling processes.^{112,113}

The ability of palladium to insert into C-H bonds was reported by Cope and Siekman in 1965, where Pd(II) (in the form of PdCl₂) was found to react with azobenzene to form the corresponding palladacycle as a dimer with two bridging chloride ligands.¹¹⁴ This work was later expanded on, with the reaction of *N,N*-dimethylbenzylamine (dmba, **57**) with lithium tetrachloropalladate to produce [Pd(dmba)(μ-Cl)]₂ (**58**).¹¹⁵ **58** can then be cleaved into the corresponding monomer using phosphine ligands (Scheme 19).¹¹⁶ The full scope of compounds accessed using cyclopalladation chemistry is far too extensive to warrant its full discussion here.¹¹³



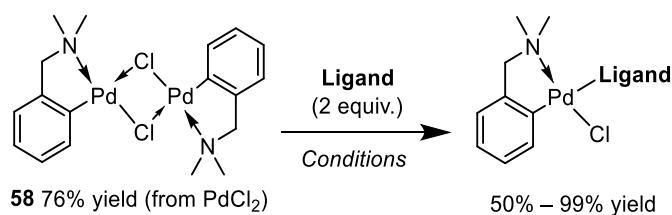
Scheme 19: Synthesis of dimeric [Pd(dmba)(μ-Cl)]₂ (**58**) from *N,N*-dimethylbenzylamine (**57**) and subsequent reaction with phosphines to form monomeric Pd species.

Importantly, the above synthesis proceeds in methanol at room temperature and requires no exclusion of air or moisture. Because of this, dmba-derived Pd(II) complexes were identified as excellent potential alternatives to OACs for bioconjugation.

2.2. Results and Discussion

2.2.1. Synthesis of Pd(II)-dmba Complexes

Investigations began with the synthesis of [Pd(dmba)(μ-Cl)]₂ (**58**). Using a slightly modified literature procedure, stirring dmba (**57**) in methanol with PdCl₂ for six hours at room temperature gave **58** in 73% yield after recrystallisation. Compound **58** was then treated with phosphine ligands (Scheme 20): PPh₃ (**59**) and dppe (**60**) due to their ubiquity in palladium catalysis, CyJohnPhos (**61**) and XPhos (**62**) as alternative bulky biaryl phosphine systems, Xantphos (**64**) due to its precedent in catalysing C-S bond forming reactions,¹¹⁷ and RuPhos (**63**) being an obvious choice for method validation. Moderate to quantitative yields were obtained for compounds **65** – **70** following crystallisation from methyl *tert*-butyl ether (MTBE)/pentane (Table 1).



Scheme 20: Reaction of **58** with phosphine ligands.

Entry	Ligand	Conditions	Product
1	PPh ₃ 59	CH ₂ Cl ₂ , rt, 15 min	<p>65 50% yield</p>
2	<p>dppe 60</p>	CH ₂ Cl ₂ , rt, 15 min	<p>66 55% yield</p>
3	<p>CyJohnPhos 61</p>	CH ₂ Cl ₂ , reflux, N ₂ , 2 h	<p>67 69% yield</p>
4	<p>XPhos 62</p>	CH ₂ Cl ₂ , reflux, N ₂ , 2 h	<p>68 81% yield</p>
5	<p>RuPhos 63</p>	CH ₂ Cl ₂ , rt, 1 h	<p>69 99% yield</p>
6	<p>Xantphos 64</p>	CH ₂ Cl ₂ , rt, 1 h	<p>70 99% yield</p>

Table 1: Synthesis of Pd(II) C-H activation complexes ligated with phosphine ligands.

The structure of **69** was confirmed with X-ray crystallography, revealing an interesting difference compared to the structure of RuPhos-ligated OAC **71** (Figure 5). In **71**, RuPhos acts as a bidentate ligand, coordinating through C-1', resulting in a significant deflection of C-1, C-1' and C-4' from linearity. This interaction has been extensively

studied, and it is believed that it plays a key role in facilitating facile reductive elimination from Pd(II).¹¹⁸ Conversely, **69** shows no such effect, and the dimethylamino moiety is instead coordinated to the palladium. This observation is likely to result from the counterion: weakly coordinating TfO⁻ in **71** *versus* Cl⁻ in **69** which coordinates more strongly. Yet, whilst chloride analogues of Pd(II) precatalysts are reported to possess lower reactivity compared to their mesylate-ligated counterparts,¹¹⁹ chloride-ligated OACs still produce quantitative yields in bioconjugation reactions.⁷⁴ Furthermore, the structures in Figure 5 show a snapshot in the solid state, which are likely unrepresentative of their structures in solution.

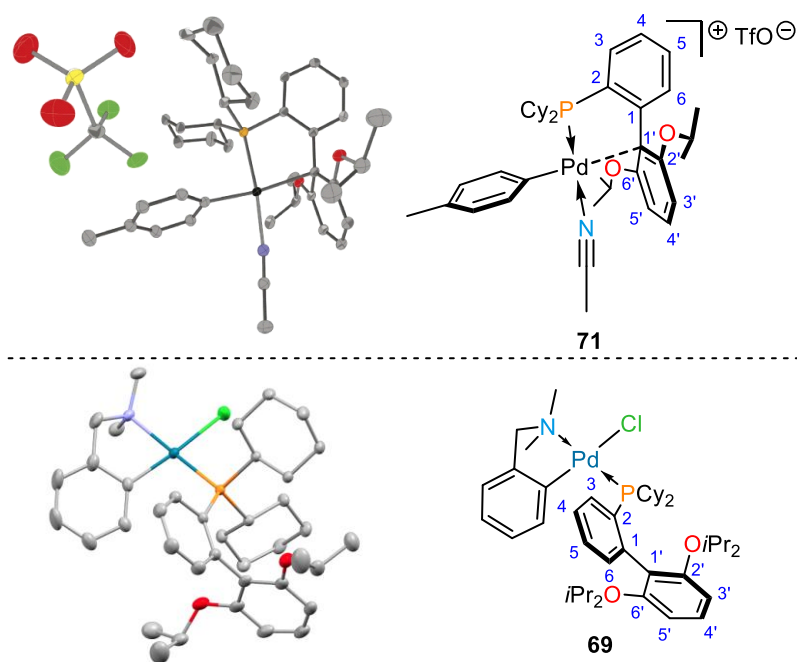


Figure 5: Top: X-ray structure of OAC acetonitrile adduct **71** alongside ChemDraw view. Thermal ellipsoid plots are drawn at 50% probability, hydrogen atoms are omitted for clarity. X-ray structure (left) reproduced from DOI: 10.1038/nature15739 with permission from SNCSC. Bottom: X-ray structure of C-H activation complex **69** alongside ChemDraw view. Solvent (MeOH) and hydrogen atoms omitted for clarity, and thermal ellipsoids drawn at 50 % probability.

The structure of **70** was also confirmed by X-ray crystallography (Figure 6), showing Xantphos bound in a monodentate manner.

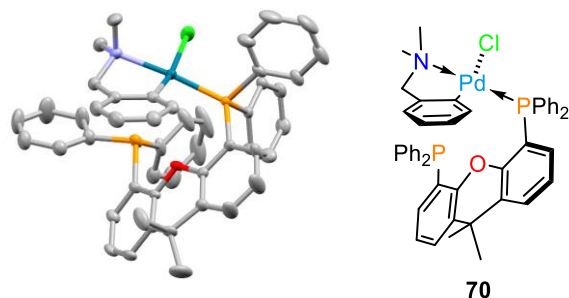
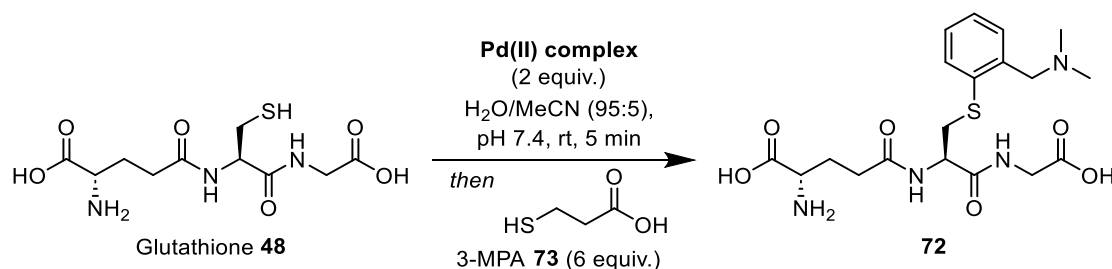


Figure 6: X-ray structure of C-H activation complex **70** alongside ChemDraw view. Solvent (CHCl₃) and hydrogen atoms omitted for clarity, and thermal ellipsoids drawn at 50 % probability.

2.2.2. Ligand Screen

With phosphine-ligated Pd(II)(dmba) complexes in hand, the next stage was to assess their ability to arylate cysteine residues under biocompatible conditions. Using cysteine arylation conditions adapted from the literature⁷⁴ of two equivalents of Pd(II) complex per cysteine thiol, 10 mM phosphate buffer at pH 7.5, and 5% MeCN or DMF additive at room temperature for five minutes, followed by quenching the Pd(II) complexes with six equivalents of 3-mercaptopropionic acid (**73**), the bioconjugation efficiency of the synthesised Pd(II) complexes was assessed (Scheme 21). Glutathione (**48**) was chosen as the model peptide substrate owing to literature precedent,⁹⁶ and conversions were assessed by LC-MS of the crude reaction mixtures, integrating the Extracted Ion Chromatogram (EIC) of unmodified and modified glutathione (Table 2).



Scheme 21: Cysteine arylation conditions using Pd(II)-dmba complexes.

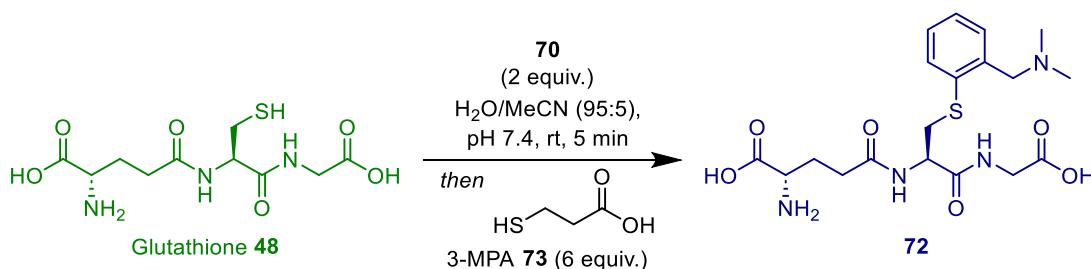
Entry	Pd(II) Complex	LC-MS Yield ^[a]
1	65	2%
2	66	0%
3	67	33%
4	68	93%
5	69	98%
6	70	93%

Table 2: Arylation of glutathione with Pd(II)(dmba) complexes. ^[a] Obtained by dividing the EIC peak area of **72** by the sum of the EIC peak area for **48** and **72**. See 5.3.3.1 for LC-MS conditions.

Perhaps unsurprisingly, compounds **65** and **66** were not suitable to be carried forward owing to lack of product formation. CyJohnPhos-ligated complex **67** produced a 44% yield, and XPhos-ligated complex **68** improved the yield drastically to 93%. Reaction efficiency of the RuPhos-ligated complex **69** was in-line with analogous OACs, and Xantphos-ligated complex **70** gave an excellent yield of 93%. As such, RuPhos **69** and Xantphos **70** were chosen as the two ligands to continue investigation of C-H activation complexes for bioconjugation. Although XPhos (**62**) gave a similar conversion, the attractiveness of

Xantphos (**64**) as an alternative to Buchwald's bulkybiaryl phosphine ligands warranted its investigation. Despite their poor yields, **65** and **67** did produce product in the five minute reaction time, suggesting that higher yields could be achieved if the reaction was allowed to progress for longer. However, it was desirable to offer an alternative to OACs that were able to arylate cysteine in the same short timescale and so the arylation with **65** and **67** was not optimised.

As there was no literature precedent for Xantphos-ligated Pd(II)-aryl compounds in bioconjugation chemistry, experiments to investigate the cysteine-selectivity of **70** were carried out, as it was possible **70** could have been arylating the free primary amine present in glutathione (**48**). **70** showed no reaction with lysine methyl ester in the standard reaction conditions. Submitting the crude reaction mixture of the reaction with glutathione to tandem mass spectrometry (MS/MS) analysis revealed clear fragmentation of **72**. After fragmentation, the dmba moiety was only present on the cysteine-containing fragment, proving the cysteine-selectivity of **70**. Finally, inspection of the total ion chromatogram (TIC) of the reaction in Table 2 (Scheme 22) revealed no significant levels of ionisable side-products, and clearly revealed the quench product (**74**) resulting from the reaction of **70** with 3-MPA (**73**) (Figure 7).



Scheme 22: Reaction of **70** with glutathione under standard conditions.

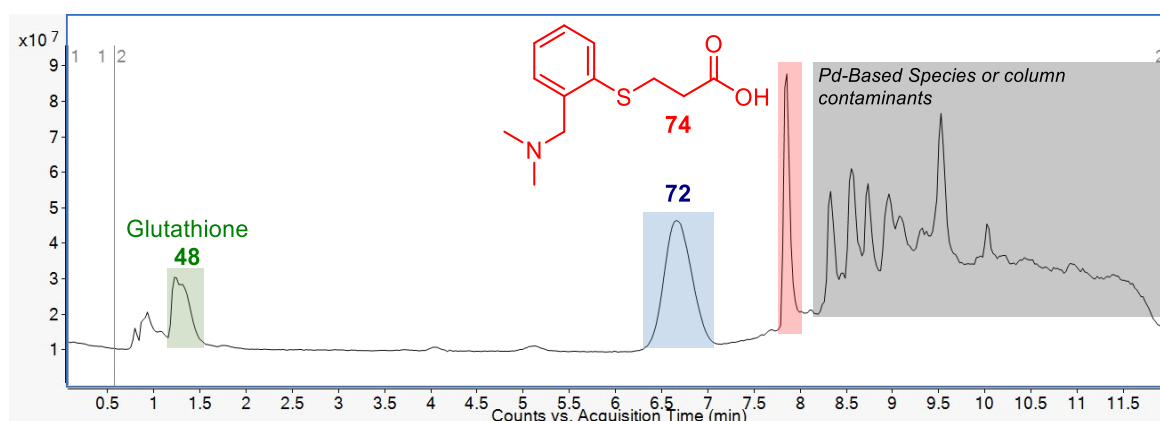
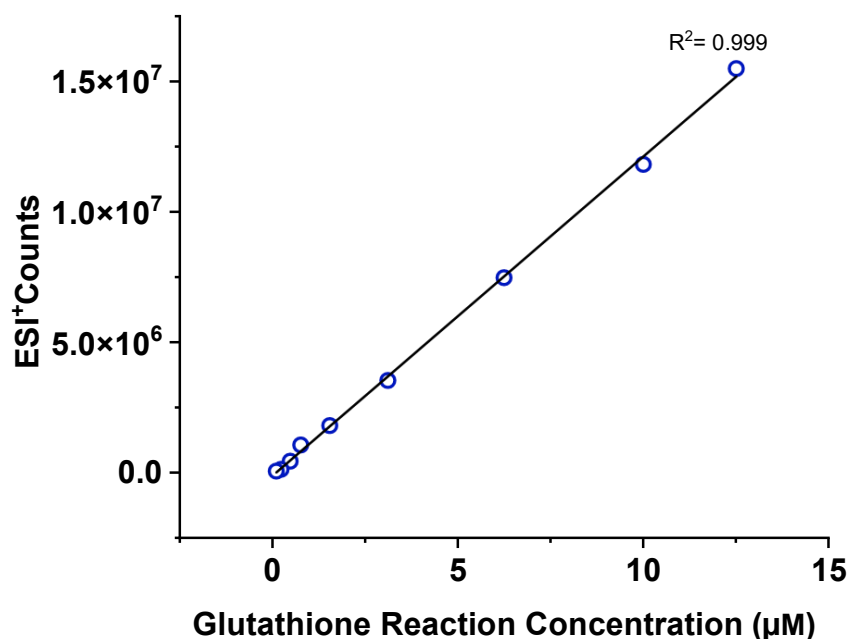


Figure 7: TIC from LC-MS analysis of glutathione with **70**. See 5.3.3.2 for LC-MS conditions.

2.2.3. Method Validation

With RuPhos (**63**) and Xantphos (**64**) confirmed as suitable ligands to continue the investigation of Pd(II) complexes prepared *via* C-H activation for bioconjugation, it was of high importance to confirm the LC-MS-based assay being used to assess yields was appropriate. Literature precedent uses the integration of TIC peaks from LC-MS to confirm yields by comparing unreacted peptide to C-S arylated peptide. However, this is not an accurate method for studying the bioconjugation of glutathione in this case, as this assumes an equal intensity response for starting material and product at any given concentration. It is well documented that Electrospray Ionization (ESI) intensity is very often non-linear,¹²⁰ and affected by a multitude of factors, the most relevant being analyte concentration, the matrix, the solvent, and analyte basicity.^{121,122} The difference in basicity between glutathione and the dmba conjugate **72** due to the added tertiary amine makes the likelihood of both analytes producing an equal ESI⁺ response at the same concentration very small. Another drawback of using the TIC to calculate yields is the peaks may have a larger intensity due to the matrix and contaminants present within the instrument. In fact, the peak corresponding to glutathione in Figure 7 also contained a considerable intensity of triethylamine as a contaminant due to co-elution.

Due to the issues with calculating reaction yields using TIC spectra, it was necessary to evaluate conversions based on the amount of remaining glutathione using a validated quantitative method. This was achieved by generating integrated EIC spectra of LC-MS runs, integrating the EICs of unreacted glutathione and arylated glutathione, and comparing the peak area of glutathione to a calibration curve. A solution of palladium complex **69** in reaction media was quenched with 3-MPA (**73**), and then the reaction doped with concentrations of glutathione descending from 12.5 μ M. LC-MS analysis (following dilution with 1000 μ L H₂O to prevent buffer salt build up in the instrument) gave the peak area of glutathione at each concentration. A calibration curve was then produced from this data, which demonstrated a clear linear relationship between concentration and ESI⁺ response within concentrations relevant to the standard bioconjugation conditions (Graph 1). Using this validated method, RuPhos-ligated complex **69** and Xantphos-ligated complex **70** produced conversions of 94% and 95%, respectively.



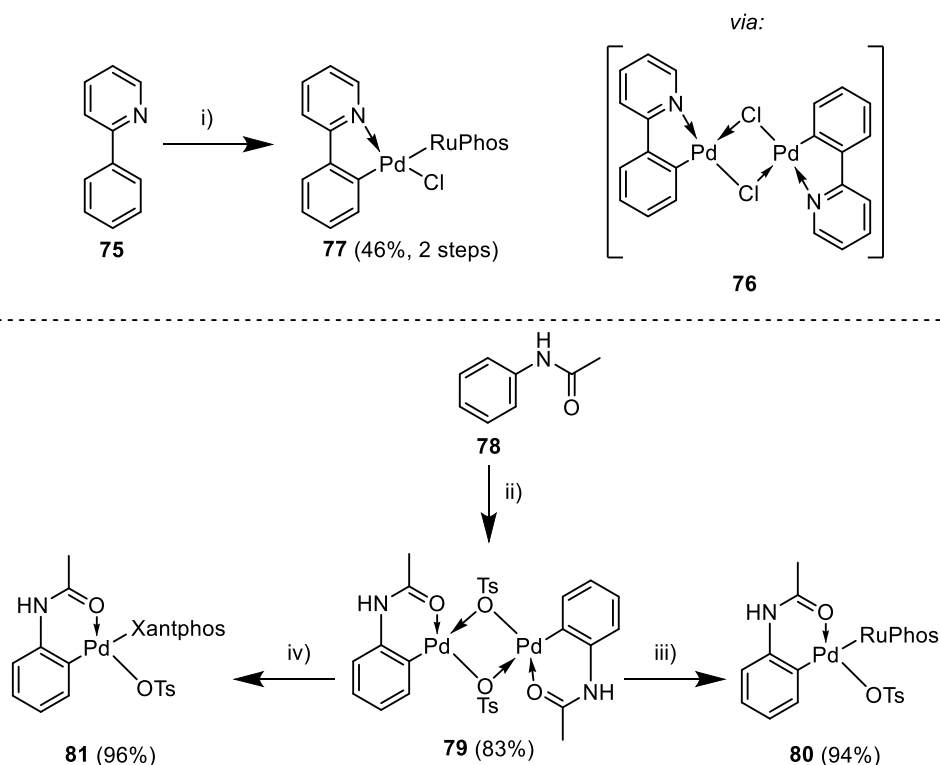
Graph 1: Glutathione calibration curve up to 12.5 μM .

This method was also used to validate the bioconjugation of ‘aged’ **70**. The Buchwald lab celebrated the stability of their RuPhos-ligated Pd(II) OACs reporting no loss in bioconjugation efficiency following storage for nine months at 4 °C.⁷⁴ As the stability of RuPhos-ligated complexes is well reported, compound **70** should possess adequate stability to justify the use of Xantphos as an alternative ligand. Pleasingly, negligible degradation was seen after eight months of benchtop storage, as assessed by ¹H and ³¹P{¹H} NMR. Glutathione conversion of 92% was demonstrated when the same ‘aged’ complex was reacted with glutathione, representing a modest drop from 95% for freshly synthesised complex, which is within experimental error.

2.2.4. Scope of Isolated Pd(II) Complexes

With preliminary experiments confirming Pd(II) C-H activation complexes as potential alternatives to OACs for bioconjugation and a validated LC-MS based assay to assess their bioconjugation efficiency developed, the next course of investigation was to expand the scope of Pd(II) complexes by modifying the directing group. The cyclopalladation of 2-phenylpyridine (**75**) was first described in 1968 by reaction with Na₂PdCl₄ in EtOH,¹²³ and the analogous complex synthesised from acetanilide (**78**) is prepared by heating at reflux in toluene with Pd(OAc)₂.¹²⁴ For this investigation, [Pd(2-phenylpyridine)(μ-Cl)]₂ **76** was synthesised by stirring 2-phenylpyridine (**75**) with PdCl₂ in methanol for three days at room temperature, and [Pd(acetanilide)(μ-OTs)]₂ (**79**) was synthesised by heating acetanilide (**78**) with *para*-toluenesulfonic acid (*p*TSA) and Pd(OAc)₂ at reflux in CH₂Cl₂ for one minute.

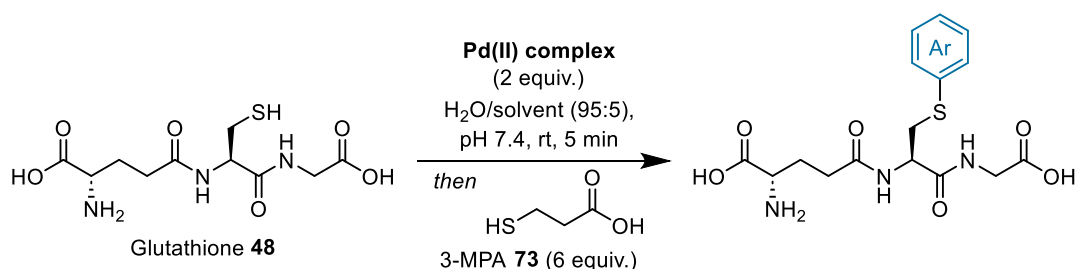
Although 2-phenylpyridine-derived complex **76** was not characterised by NMR spectroscopy owing to low solubility,¹²⁵ stirring **76** with RuPhos in CH₂Cl₂ gave Pd(2-phenylpyridine)(RuPhos)Cl (**77**) in 43% yield over two steps which was fully characterised (Scheme 23 top). Phosphine ligated complexes of acetanilide were obtained in a similar fashion. Treating isolated **79** with RuPhos or Xantphos yielded Pd(acetanilide)(RuPhos)Cl (**80**) and Pd(acetanilide)(Xantphos)Cl (**81**), both in 80% yield over two steps (Scheme 23 bottom).



Scheme 23: Synthesis of Pd(II) complexes prepared via C-H activation. **Top:** Synthesis of **77**. **Reagents and conditions:** i) PdCl₂ (0.5 equiv.), MeOH, rt, 72 h then RuPhos (1.0 equiv.), CH₂Cl₂, reflux, 2 h. **Bottom:** Synthesis of **80** and **81**. **Reagents and conditions:** ii) Pd(OAc)₂ (1.0 equiv.), p-TSA·H₂O (1.0 equiv.), CH₂Cl₂, reflux, 1 min. iii) RuPhos (2.0 equiv.), CH₂Cl₂, rt, 1 h. iv) Xantphos (2.0 equiv.), CH₂Cl₂, rt, 1 h.

Attempted arylation of glutathione using compound **77** in standard conditions was unsuccessful (Scheme 24). It is possible that this result is due to the very low solubility of **77**, as it was not sufficiently soluble in MeCN or DMF for the bioconjugation reaction, requiring THF as the co-solvent (Table 3 entry 1). However, another explanation could be the nature of the 2-phenylpyridine bound to palladium. The aryl group in this case is rather bulky and could be preventing cysteine thiol from binding to the Pd(II) centre. This lack of reactivity is demonstrated by the absence of literature studies on the reaction scope of 2-phenylpyridine-based Pd(II) complexes, with reactivity only being observed once ligated with azide.¹²⁶ Because of this, investigation into 2-phenylpyridine-based complexes was abandoned, and the next step was to assess the ability of acetanilide complexes to arylate

cysteine (Scheme 24). Using slightly modified standard conditions, with DMF as the co-solvent due to low solubility in MeCN, compounds **80** and **81** produced excellent conversions to arylated glutathione (Table 3 entries 2 and 3).



Scheme 24: Arylation of glutathione with 2-phenylpyridine or acetanilide-based Pd(II) complexes.

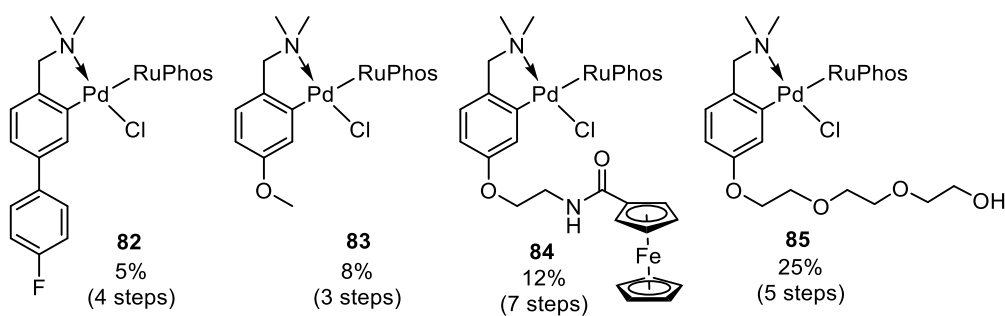
Entry	Pd(II) Complex	Co-solvent	LC-MS Conversion ^[a]
1	 77	THF	0%
2	 80	DMF	98%
3	 81	DMF	97%

Table 3: Assessment of acetanilide and 2-phenylpyridine-based Pd(II) complexes for cysteine bioconjugation.^[a] See 5.3.3.4 for LC-MS conditions.

Another way to diversify the scope of the methodology was to investigate modifying the palladium-bound aryl ring to add functionality (Figure 8). Thus, analogues of Pd(dmba)(RuPhos)Cl (**69**) were synthesised from their corresponding dmba derivatives. The synthesis of these compounds was relatively straightforward and is outlined in 5.3.1, which involved either reductively aminating commercially available benzaldehydes with dimethylamine, or synthesising *para*-functionalised benzaldehydes by alkylation of 4-hydroxybenzaldehyde followed by reductive amination. Pd(II) complexes were prepared by reaction with Na₂PdCl₄ or PdCl₂ to produce Pd(II) dimers, which were then treated with RuPhos to produce the corresponding monomeric Pd(II) complexes. All reactions proceeded under air and produced bench stable, crystalline solids.

Using the preparations described above, a handful of derivatives were successfully synthesised bearing a fluorinated aromatic ring (**82**), electron-donating methoxy group (**83**), ferrocene attached with a short linker (**84**), and a PEG chain (**85**). However, synthesis of **86**, **87**, and **88** was unsuccessful. Functionalisation with a TMS-alkyne prevented the cyclopalladation reaction, producing Pd(II) nanoparticles and no desired product. This observation is consistent with literature reports describing the reaction of cyclopalladated complexes with alkynes.⁷³ *Para*-nitro was not tolerated, consistent with Ryabov *et al.* who previously reported that the cyclopalladation of *N,N*-dimethyl-4-nitrobenzylamine does not proceed using Na₂PdCl₄.¹²⁷ Despite Tollari *et al.* reporting successful cyclopalladation of *N*-methylgramine in 1997,¹²⁸ attempts to repeat their procedure did not produce product of sufficient purity, preventing the preparation of **88**.

Prepared compounds:



Preparation unsuccessful:

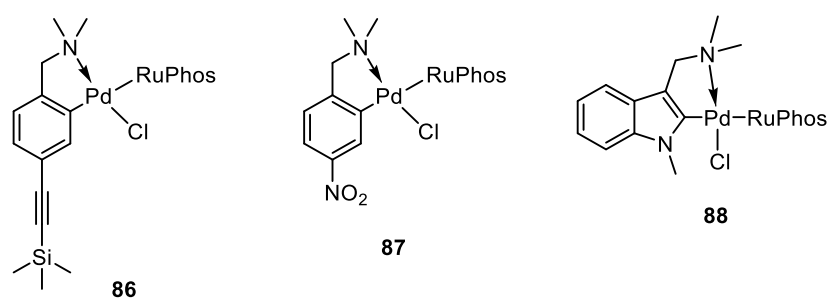
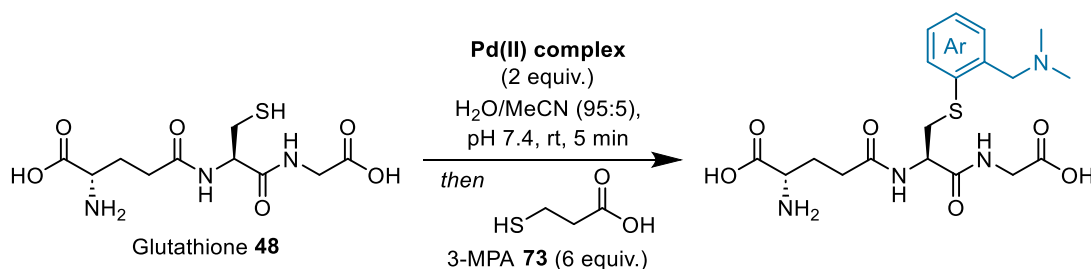


Figure 8: Isolated Pd(II)dmbs derivatives.

Glutathione arylation with successfully isolated complexes (**82 – 85**) produced conversions ranging from 67% to 93%, demonstrating successful expansion of reaction scope with *para*-substituted Pd(II)-dmbs derivatives (Scheme 25). However, conversions were certainly lower than desired (Table 4), and this could arise from the presence of impurities. Due to difficulties in purification, these complexes were only successfully characterised by ³¹P{¹H} NMR and high-resolution mass spectrometry (HRMS). Whilst not obtaining full NMR characterisation data for organometallic complexes used in the literature is commonplace,⁹⁶ any impurities lacking phosphorous will not have been identified.

Certainly, any Pd-based impurities could bind to cysteine thiol, preventing the desired reaction.



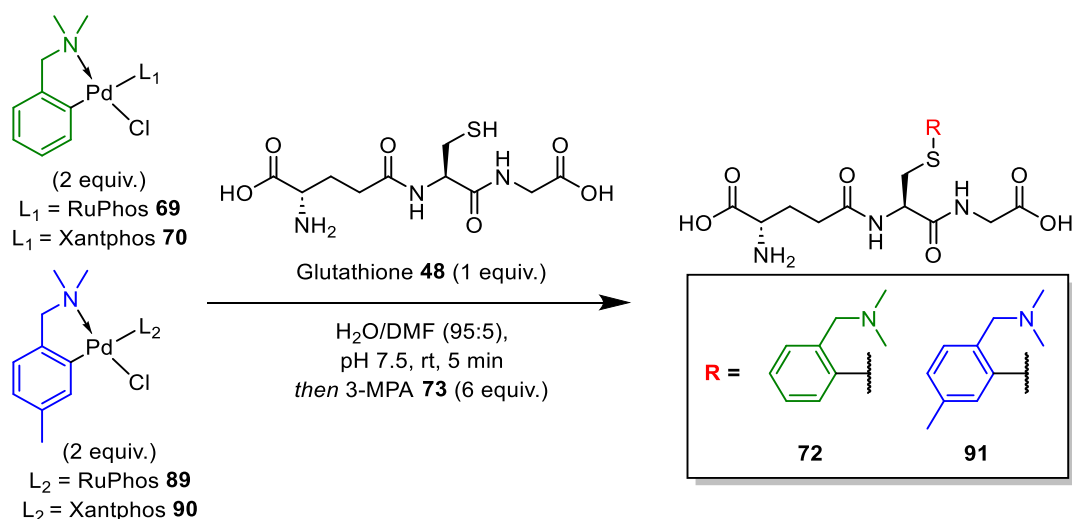
Scheme 25: Glutathione S-arylation using functionalised Pd(II)dmba derivatives.

Entry	Pd(II) Complex	LC-MS Conversion ^[a]
1	82	82%
2	83	93%
3	84	90%
4	85	67%

Table 4: Conversions for glutathione C-S arylation. ^[a] See 5.3.3.5 for LC-MS conditions.

2.2.5. Competition Experiments

Competition experiments have been used by the Buchwald⁷⁴ and Spokoyny⁹⁶ labs for qualitative evaluation of kinetics between bioconjugation reagents. As RuPhos and Xantphos were chosen as the two phosphine ligands to conduct bioconjugation studies with, assessment of their relative kinetics may be of interest to future users of the technology. Thus, Pd(II) complexes **89** and **90** were synthesised from *N,N*-dimethyl-4-methylbenzylamine, and used in competition experiments against **69** and **70** (Scheme 26). Both complexes also produced conversions to arylated glutathione of greater than 97% in control experiments (section 5.3.3.6).



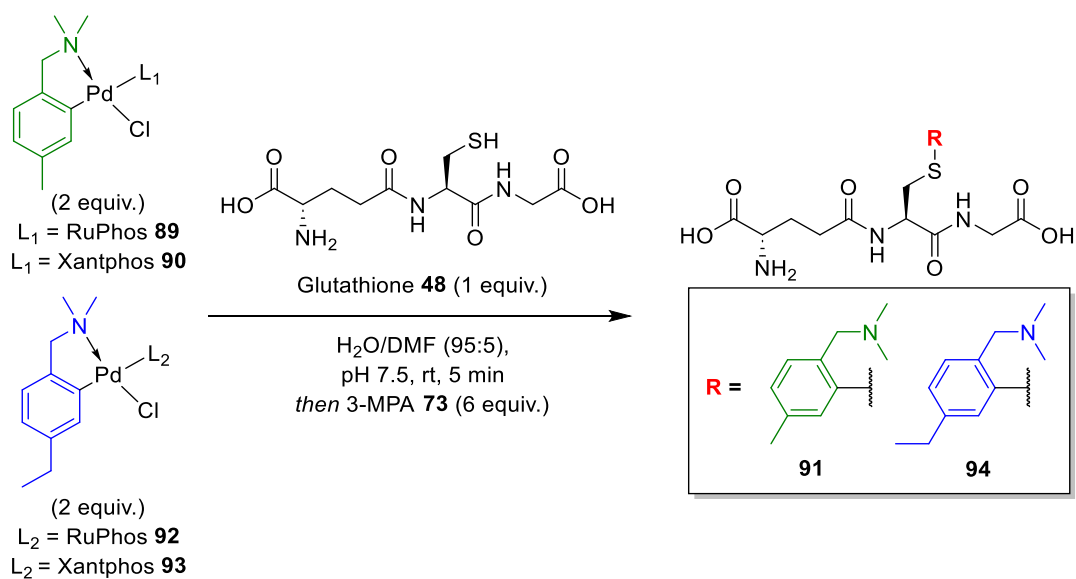
Scheme 26: Initial competition experiments comparing RuPhos and Xantphos-ligated Pd(II)dmba complexes.

Entry	$L_1 =$	$L_2 =$	72 ^[a]	91 ^[a]
1	RuPhos	Xantphos	8%	92%
2	Xantphos	RuPhos	63%	37%
3	Xantphos	Xantphos	51%	49%
4	RuPhos	RuPhos	21%	79%

Table 5: Data for initial ligand competition experiments. ^[a] Determined by LC-MS. See section 5.3.3.6 for conditions.

The first experiments (Table 5 entries 1 and 2), showed a significant skew towards Xantphos-ligated complexes, however the data strongly suggested an electronic effect of *para*-methyl versus *para*-H. If there were no electronic effects, the ratio of **72** to **91** should be reversed when comparing Table 5 entries 1 and 2. This was confirmed (Table 5 entries 3 and 4) for RuPhos-ligated complexes **69** and **89**; yet the same effect was not demonstrated for the Xantphos-ligated complexes **70** and **90**. This suggests that RuPhos-ligated complexes are more sensitive to the electron density of the Pd(II)-bound aryl ring than Xantphos-ligated compounds. However, as these reactions were not repeated, the unusually large difference in reactivity observed could also be attributed to experimental error.

To control for substrate electronic effects, Pd(II) complexes **92** and **93** were synthesised from *N,N*-dimethyl-4-ethylbenzylamine and used in competition experiments versus **89** and **90** (Scheme 27). **92** and **93** also produced conversions to arylated glutathione of greater than 96% in control experiments (section 5.3.3.6).



Scheme 27: Competition experiments between RuPhos- and Xantphos-ligated Pd(II)dmba complexes, controlling for electronic effects.

Entry	$L_1 =$	$L_2 =$	91 ^[a]	94 ^[a]
1	RuPhos	Xantphos	35%	65%
2	Xantphos	RuPhos	62%	38%
3	Xantphos	Xantphos	52%	48%
4	RuPhos	RuPhos	47%	53%

Table 6: Data for competition experiments controlled for electronic effects. ^[a] Determined by LC-MS. See 5.3.3.6 for conditions.

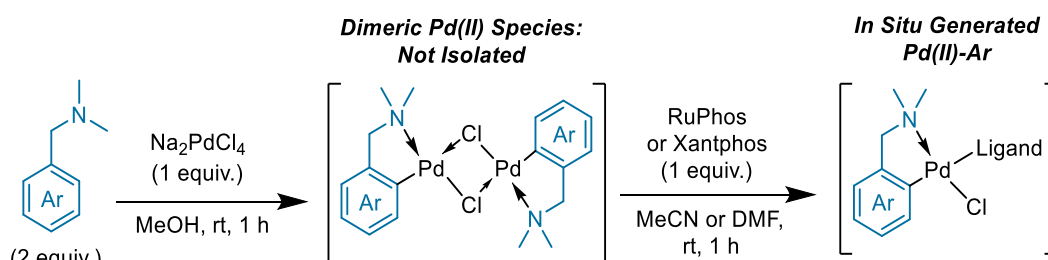
The results of ligand competition experiments showed that Xantphos-ligated complexes could possess kinetics up to twice as fast as their RuPhos-ligated counterparts (Table 6 entries 1 and 2). Pleasingly, these experiments also showed very little ($\pm 3\%$) deviation between the two different ring substitutions, which was corroborated when both Pd(II) complexes were ligated with the same ligand (Table 6 entries 3 and 4). This is likely due to the similar electronic properties of *para*-tolyl versus *para*-ethyl, meaning there is no electronic effect on the ratio of **91** to **94**.

2.2.6. *In situ* Generated Pd(II) Complexes

Thus far, the application of Pd(II) C-H activation complexes towards cysteine C-S arylation has revealed significant advantages in their preparation compared to previously reported OACs. No air-free chemistry is required, stable and commercially available palladium sources are used, and Xantphos was identified as a more cost-effective and kinetically superior ligand to RuPhos. However, the process of purifying, isolating and fully characterising these organometallic species remains non-trivial, and may still present a

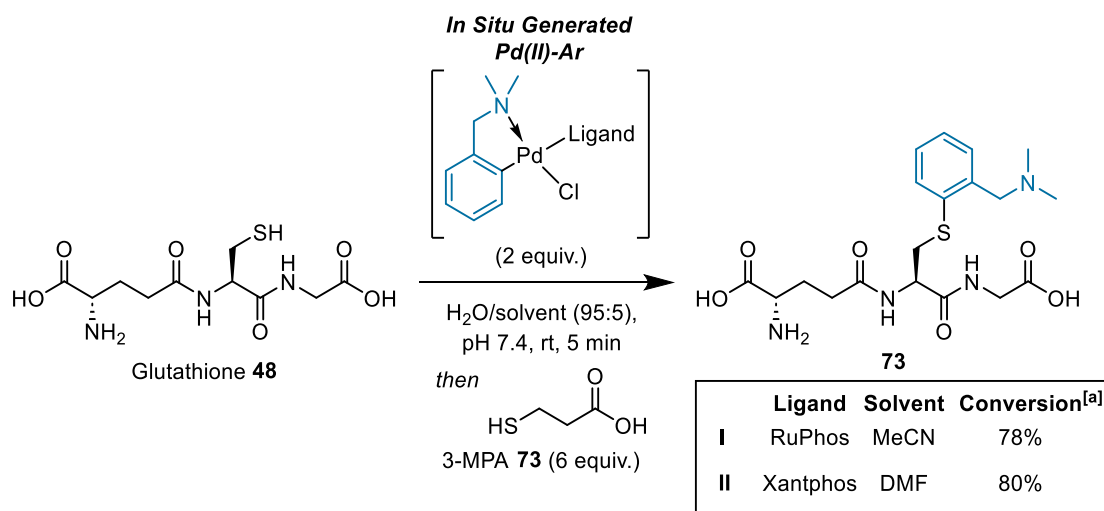
significant barrier to the chemistry being adopted by the wider field. As such, a procedure that generates the desired reactive Pd(II) species *in situ* was identified as the logical next step for the project.

The aims for this investigation were as follows: to generate Pd(II) complexes for bioconjugation within a few hours, to keep the equipment required as close as possible to what may be found in a biology laboratory setting and, most importantly, maintain bioconjugation efficiency comparable to that of isolated reagents. The nature of the palladium source was identified as being important for efficient cyclopalladation, thus Na₂PdCl₄ was chosen over PdCl₂ as its higher solubility results in more rapid cyclopalladation. Initial experiments reacted two equivalents of dmba with one equivalent of Na₂PdCl₄ for one hour in MeOH in an Eppendorf tube, resulting in precipitation of the cyclometallated dimer. A solution of phosphine ligand was then added and the resulting mixture was allowed to stand for a further hour, resulting in redissolution of the Pd(II) species, and therefore a stock solution of active Pd(II) complex that could potentially be used for cysteine *S*-arylation (Scheme 28). Notably, it was important that the Pd(II) source and phosphine ligand were added sequentially, as the presence of phosphine ligands prevents the initial cyclopalladation step.¹²⁹ The low solubility of Xantphos in MeCN also necessitated the use of DMF as a solvent for the second step.



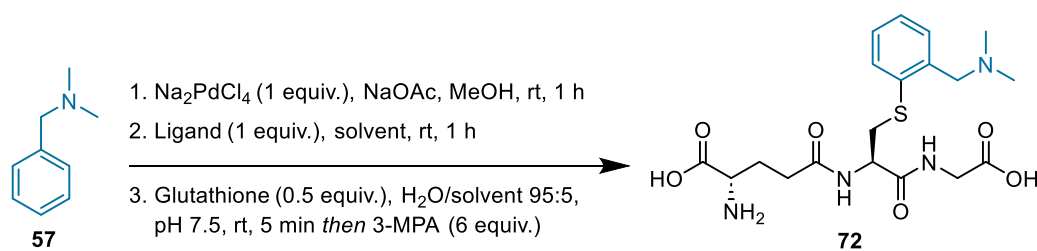
Scheme 28: Initial conditions for *in situ* generation of Pd(II)dmba analogues.

The *in situ* generated Pd(II)-Ar stock solutions was then tested for their ability to arylate cysteine with dmba **57** as the aryl species. Conversions showed a modest drop compared with the isolated complexes, with the *in situ* generated RuPhos and Xantphos-ligated species producing conversions of 78% and 80%, respectively (Scheme 29), as determined by LC-MS .



Scheme 29: Initial experiments for glutathione S arylation using in situ generated Pd(II)dmba. ^[a] Determined by LC-MS. See section 5.3.3.9 for conditions.

A substrate scope with various aryl compounds gave lower-than-desired conversions, and thus the *in situ* method required optimisation to bring conversions in line with isolated reagents. The bottleneck was likely the initial cyclopalladation not proceeding to completion in one hour before adding phosphine ligand, as the phosphine ligation step is likely quantitative, as shown for many isolated compounds (section 5.3.1). Initial conditions (Scheme 28) used two equivalents of dmba derivative, one to undergo the cyclopalladation, and another to sequester the proton liberated in the cyclopalladation step. Alternative literature procedures use one equivalent of the aryl reagent alongside one equivalent of sodium acetate as a base and catalyst. The catalytic effects of the acetate arise from activation of a concerted metalation deprotonation (CMD) pathway for cyclometallation, lowering the energy of the transition state, and therefore increasing the rate of reaction.¹³⁰ A screen of the effect of sodium acetate in the *in situ* protocol (Scheme 30) for the RuPhos and Xantphos complexes revealed that one equivalent of both dmba and sodium acetate to Na₂PdCl₄ was optimum, producing conversions greater than 93% for both ligands (Table 7).

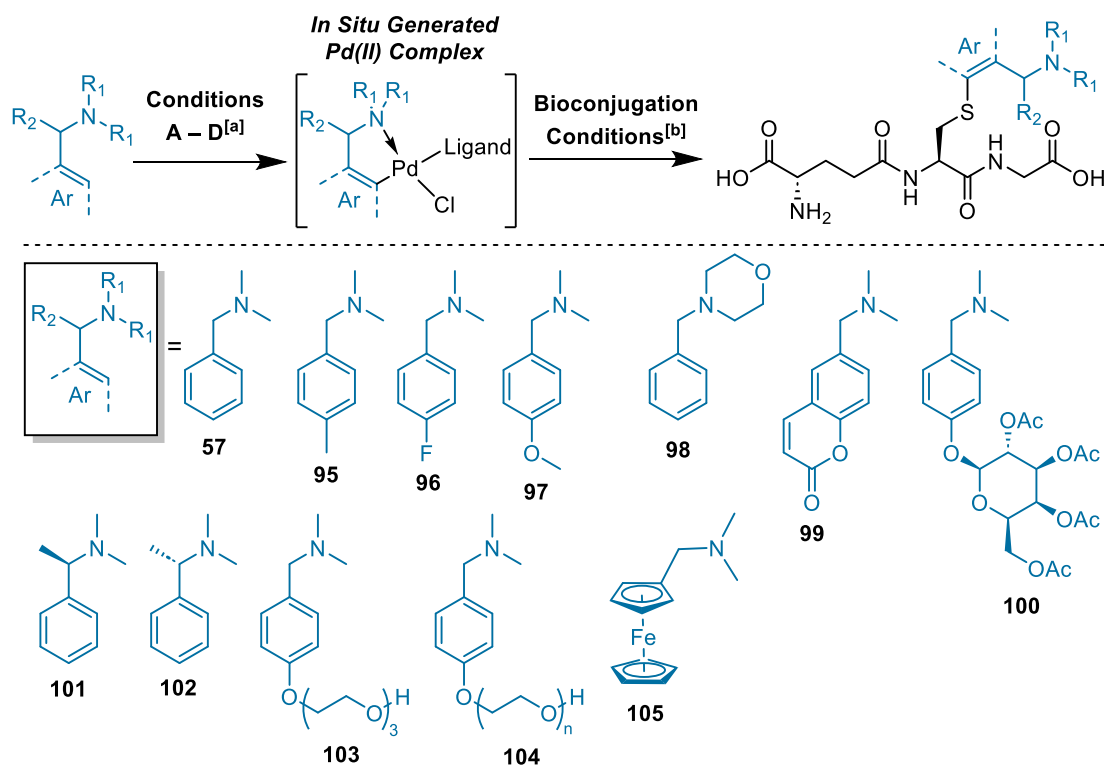


Scheme 30: Effect of sodium acetate on glutathione S-arylation using in situ generated Pd(II)dmba.

Entry	Equivalents of 57	Equivalents of NaOAc	Ligand	Solvent	Glutathione conversion ^[a]
1	2	0	RuPhos	MeCN	78%
2	2	0	Xantphos	DMF	80%
3	2	2	RuPhos	MeCN	89%
4	2	2	Xantphos	DMF	88%
5	1	1	RuPhos	MeCN	93%
6	1	1	Xantphos	DMF	98%

Table 7: Conditions trialed for glutathione S-arylation with in situ generated Pd(II)dmba. ^[a] Determined by LC-MS. See 5.3.3.7 for conditions.

With these optimised conditions producing conversions comparable to isolated reagents, the next step was to assess the scope of the protocol (Scheme 31). Most substrates were evaluated using the original conditions (**A** and **B**: Table 7 entries 1 and 2), alongside optimised conditions (**C** and **D**: Table 7 entries 5 and 6). Pleasingly, most substrates saw a significant increase in conversion with the addition of sodium acetate, showing the key step in this process is likely the cyclopalladation. High purity of the dmba derivative was critical, due to the synthesis of many of these substrates involving a reductive amination using NaBH(OAc)₃ as the last step. If any residual boron-containing species were present, the cyclopalladation was completely shut down, rapidly reducing the Pd(II) to nanoparticles. As a result, column chromatography was required for all substrates prior to cyclopalladation even if the ¹H NMR showed high purity post-workup. Full syntheses of all substrates are outlined in 5.3.2.



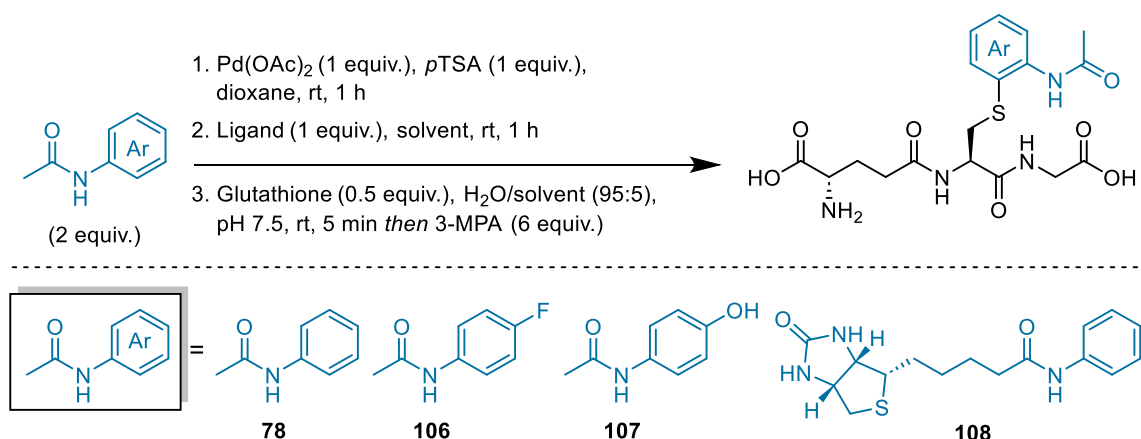
Scheme 31: In situ method substrate scope. ^[a] Pd(II)-Ar complex forming conditions: **A**: Ar (2 equiv.), Na₂PdCl₄ (1 equiv.), MeOH, rt, 1 h then RuPhos (1 equiv.), MeCN, rt, 1 h; **B**: Ar (2 equiv.), Na₂PdCl₄ (1 equiv.), MeOH, rt, 1 h then Xantphos (1 equiv.), DMF, rt, 1 h; **C**: Ar-H (1 equiv.), Na₂PdCl₄ (1 equiv.), NaOAc (1 equiv.) MeOH, rt, 1 h then RuPhos (1 equiv.), MeCN, rt, 1 h; **D**: Ar (1 equiv.), Na₂PdCl₄ (1 equiv.), NaOAc (1 equiv.) MeOH, rt, 1 h then Xantphos (1 equiv.), DMF, rt, 1 h. ^[b] Bioconjugation conditions: glutathione (1 equiv.), in situ generated Pd(II) complex (2 equiv.), H₂O/solvent (95:5), pH 7.4, rt, 5 min, then 3-MPA (6 equiv.).

Entry	Ar =	Conversion to arylated glutathione ^[a]			
		A	B	C	D
1	57	78%	80%	93%	98%
2	95	—	—	96%	96%
3	96	51%	21%	87%	71%
4	97	62%	74%	97%	89%
5	98	72%	66%	—	—
6	99	74%	45%	71%	67%
7	100	—	—	84%	93%
8	101	72%	63%	47%	61%
9	102	54%	79%	58%	56%
10	103	87% ^[b]	94% ^[b]	—	—
11	104	87% ^[a]	79% ^[b]	—	—
12	105	22%	29%	66%	77%

Table 8: Conversions for in situ glutathione C-S arylation substrate scope with dmbs derivatives. ^[a] Using conditions from Scheme 31. Conversions determined by LC-MS. See 5.3.3.9 for LC-MS conditions. ^[b] Deviation from conditions: **103** and **104** combined with Na₂PdCl₄ in MeOH for 18 h instead of 1 h.

The scope revealed excellent tolerance of this procedure for electron rich (**95** and **97**) and electron deficient (**96**) aryl systems. The dimethylaminomethyl moiety tolerated modification to a morpholine (**98**), and the addition of a stereocentre adjacent to the nitrogen atom showed no evidence of any matched or mis-matched stereochemical effects upon reaction with the chiral peptide with enantiomeric substrates, with **101** and **102** giving comparable conversions. However, the overall lower conversions for **101** and **102** compared with other substrates may be due to increased steric hinderance of the α -methyl slowing the initial cyclopalladation step. Pleasingly, the protocol facilitated the functionalisation of cysteine with biologically relevant PEG chains (**103** and **104**), a coumarin dye (**99**), and protected galactose derivative (**100**). Most notably, direct cysteine conjugation to ferrocene was achieved (**105**) which, prior to this work, had not been previously reported. Overall, it is possible that greater conversions could be achieved for many substrates provided that this step was optimised for each substrate, however this was out of the scope of the study. This would likely involve increasing the reaction time for many substrates, as the cyclopalladations of PEG-containing substrates **103** and **104** required 18 h, producing very low conversions using standard conditions.

Generation of acetanilide-based Pd(II) complexes was also achieved *in situ*, requiring slightly modified conditions for the initial cyclopalladation step, as the conditions used for dmba derivatives were unsuccessful when acetanilide was the substrate. The synthesis of cyclopalladated acetanilide has been previously reported in dioxane at room temperature.⁷² This is more desirable for an *in situ* method than heating to reflux in dichloromethane, which was the method used for synthesis of **79** in **2.2.4**, due to the water miscibility of dioxane, alongside no requirement for heating. Thus, cyclopalladation for the *in situ* preparation of acetanilides was performed in dioxane at room temperature for one hour with *p*TSA and Pd(OAc)₂ instead of Na₂PdCl₄, before phosphine ligand was added (Scheme 32).



Scheme 32: *In situ* method using acetanilide derivatives.

Conversion to Arylated Glutathione			
Entry	Ar =	Ligand/Solvent = RuPhos/MeCN	Ligand/Solvent = Xantphos/DMF
1	78	87%	92%
2	106	90%	78%
3	107	96%	83%
4	108	<i>No conjugate found</i>	<i>No conjugate found</i>

Table 9: Conversions for *in situ* glutathione C-S arylation substrate scope with acetanilide derivatives.

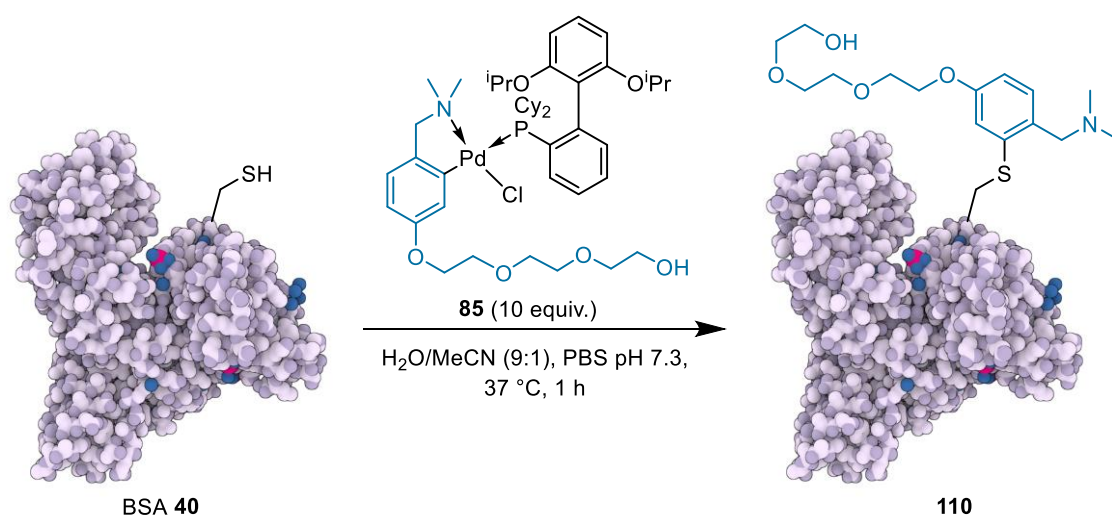
Pleasingly, this method for generation of Pd(II)acetanilide complexes *in situ* facilitated glutathione C-S arylation with acetanilide (**78**), 4-fluoroacetanilide (**106**) and paracetamol (**107**) in good to excellent conversions (Table 9). Unfortunately, biotin analogue (**108**) was too insoluble to be used in this protocol, even when the concentration of the process was significantly reduced, and no bioconjugation was observed.

2.2.7. Intact Protein Bioconjugation

Following the successful C-S arylation of glutathione with isolated and *in situ* generated Pd(II) complexes prepared *via* C-H activation, investigations next turned to C-S arylation of intact proteins. To achieve this, Bovine Serum Albumin (BSA) was selected as the model protein substrate. BSA is commercially available and prevalent in the literature for validation of bioconjugation reactions due to its single surface-exposed cysteine residue (Cys-34).^{91,131}

Initial experiments involved treating 100 μM BSA in phosphate-buffered saline (PBS)/MeCN at pH 7.3 with ten equivalents of isolated PEGylated Pd(II) complex **85**. The mixture was then left to stand at 37 °C for one hour and analysed by LC-MS (Scheme 33). The deconvoluted mass spectrum of the reaction mixture clearly showed a shift in mass of +281 Da, indicating that a single-site modification had occurred. The control sample

containing no Pd(II) complex showed two well-defined peaks at 66430.55 Da and 66531.25 Da, which were shifted +281 Da in the reaction sample to 66711.95 Da and 66812.30 Da, respectively (Figure 9). BSA is a mixture of proteins rather than one species, known as isoforms, which explains the lack of a single well-defined peak in the mass spectra. In this case, both isoforms represented by the peaks in the deconvoluted mass spectrum underwent modification. Conjugation of BSA using *in situ* generated Pd(II) complex suggested Xantphos was a more effective ligand for the conjugation, as the reaction using *in situ* generated RuPhos-ligated complex displayed unreacted BSA (section 5.3.3.10).



Scheme 33: C-S arylation of BSA (**40**) using isolated Pd(II) complex **85**.

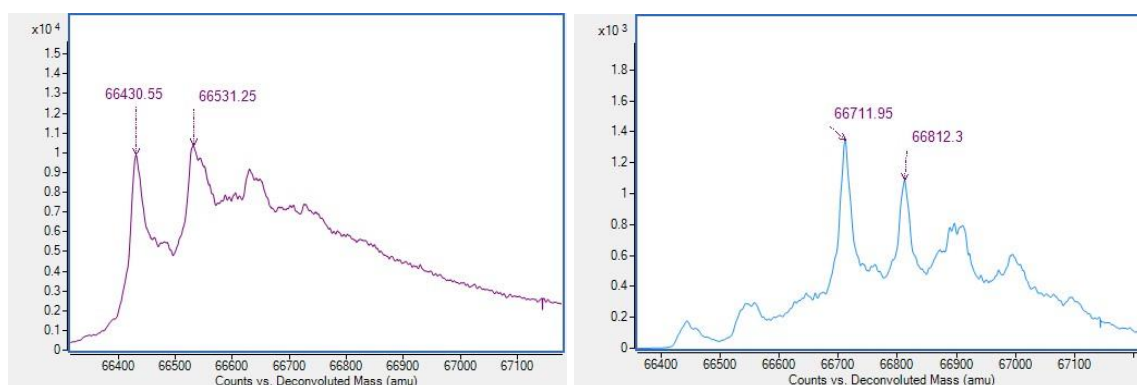
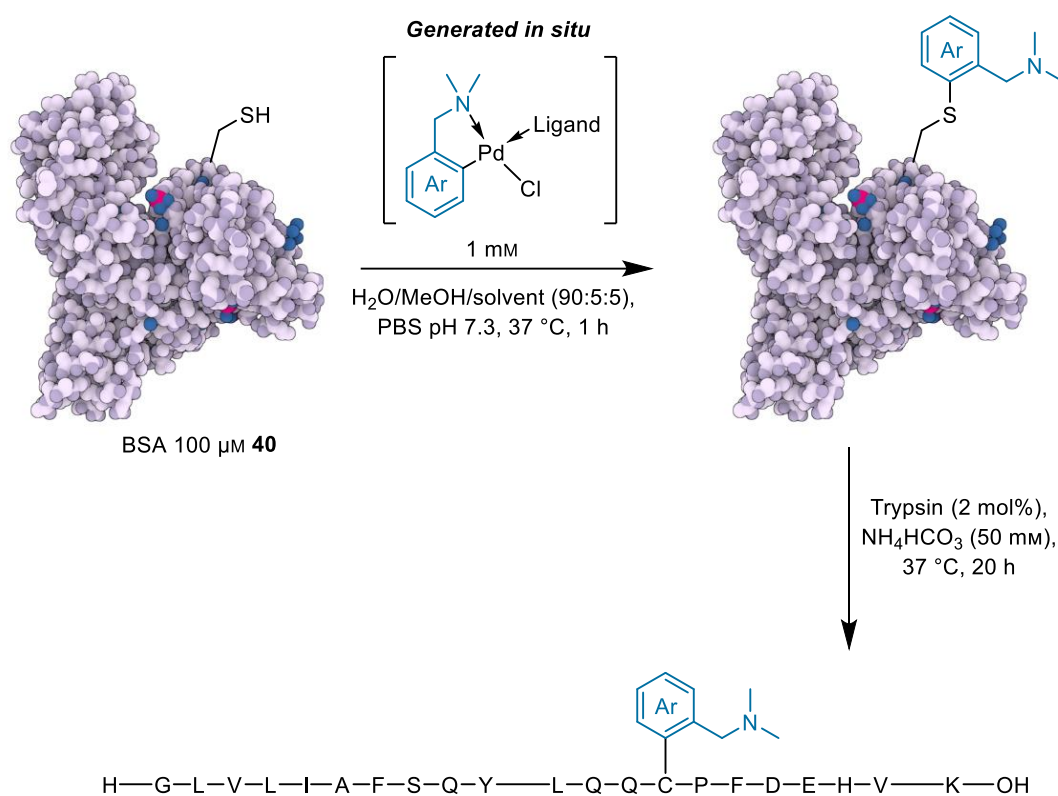


Figure 9: **Left:** Deconvoluted mass spectra of BSA (**40**) **Right:** Deconvoluted mass spectra of the reaction of BSA (**40**) with **85**. Annotated peaks correspond to product (**110**). See section 5.3.3.9 for LC-MS conditions.

To verify that only Cys-34 had been arylated, the protein products from reaction with *in situ* generated complexes from dmbsa analogues **100** and **103** were subjected to a trypsin digest. Trypsin is a protease which cleaves the backbone of proteins on the C-terminal side of arginine and lysine residues.¹³² Thus, proteins of interest are cleaved into predictable, smaller peptides which may then be identified by MS/MS, a method which selectively fragments ions to aid analysis, giving information relating to the protein's

structure and sequence. In this case, BSA could be digested using trypsin, and then the shorter peptide containing Cys-34 could be selectively fragmented with MS/MS. Peptides will commonly fragment in two ways along amide C-N bonds: b- ions describe fragments extending from the *N*-terminus, and y- ions from the *C*-terminus. Thus, if Cys-34 has selectively been modified, then only the b- and y- ions containing the residue should show a mass difference corresponding to modification.



Scheme 34: Modification of BSA (**40**) with *in situ* generated Pd(II) complexes followed by trypsin digest.

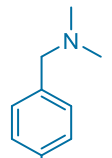
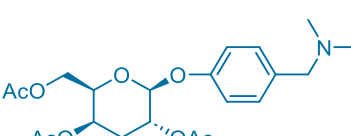
Entry	Ar =	Ligand/ Solvent	Estimated Conversion ^[a]	Cys-34 Selectivity
1		RuPhos/ MeCN	98%	>99%
2	103 	Xantphos/ DMF	99%	>99%
3		RuPhos/ MeCN	93%	>99%
4	100 	Xantphos/ DMF	91%	>99%

Table 10: Conversions to arylated BSA using *in situ* generated Pd(II) complexes, as estimated by LC-MS. ^[a] Conversions determined by dividing the EIC peak area of the peptide product by the unmodified H-GLVLIAFSQYLQQCPFDEHVK-OH. See section 5.3.3.10 for LC-MS conditions.

For protein functionalisation, **100** and **103** were chosen due to their biologically relevant functionalities, and their corresponding Pd(II) complexes were generated *in situ* using a modified version of the method discussed in **2.2.6**. This method resulted in the Pd(II) complex solution being an equal mixture of methanol and DMF or MeCN. For each substrate and ligand combination, ten equivalents of *in situ* generated Pd(II) complex was added to a 100 μM solution of BSA in PBS, resulting in 10% organic co-solvent, and the reaction was held at 37 $^{\circ}\text{C}$ for one hour. An aliquot of this reaction mixture was then treated with 2 mol% of trypsin and held for twenty hours at 37 $^{\circ}\text{C}$ to ensure complete digestion. LC-MS analysis of the trypsin digest confirmed that the correct peptide had been successfully functionalised with triethylene glycol and protected galactose (Scheme 34). Conversions to arylated BSA could be very crudely estimated by comparing the EIC peak area of the unmodified cysteine-containing BSA fragment to the modified product after trypsin digest. These conversions were estimated to be between 91% and 99% (Table 10). Site selectivity was then assessed using LC-MS/MS, and this confirmed the successful functionalisation of Cys-34 (Figure 10) with all four reaction conditions described in Table 10. Importantly, no other digestion products exhibited any evidence of functionalisation. Complete MS/MS spectra (section **5.3.3.10**) for $Z = 2, 3$, and 4 showed excellent coverage of cysteine-containing y -ions for all conditions.

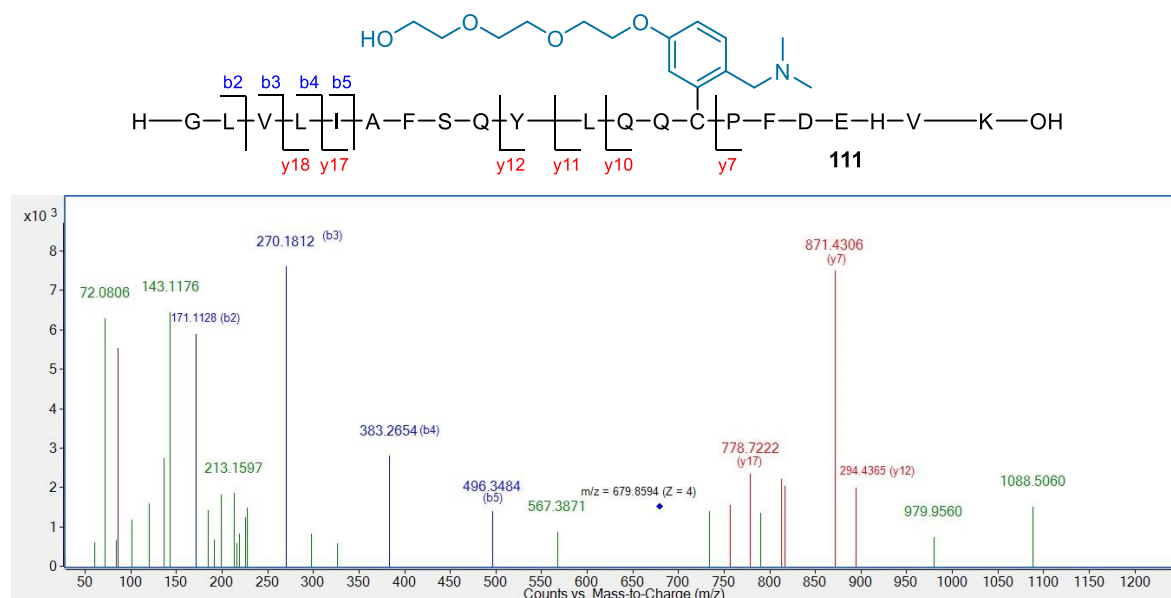


Figure 10: LC-MS/MS spectrum of peptide **111** obtained by selecting for $m/z = 680.1098 [M+4H]^{4+}$ as the precursor ion. Reaction conditions: Table 10 Entry 1. See section **5.3.3.10** for a detailed breakdown of b - and y -ions.

2.3. Conclusions

The work described within the chapter demonstrated the use of Pd(II) complexes prepared *via* C-H activation for C-S arylation of cysteine residues in biocompatible conditions. Initially, isolated complexes prepared from *N,N*-dimethylbenzylamine ligated with RuPhos or Xantphos were confirmed to have similar selectivity to OACs reported in the literature, whilst also offering a more facile synthesis. A scope of functionalised derivatives allowed the diversification of cysteine with a range of aryl substituents, including a short polymer chain and ferrocene-containing moiety. A much larger substrate scope was enabled by the development of an *in situ* preparation of Pd(II)-Ar complexes, producing high conversions to arylated peptide in just under two hours from commercially available compounds. Both isolated and *in situ* generated compounds were able to arylate a surface cysteine residue on intact BSA, which was confirmed using intact protein LC-MS, and LC-MS/MS of a trypsin digest. Overall, this work has resulted in a facile methodology for cysteine *S*-arylation using Pd(II) complexes which may be completed without the use of specialist equipment or air-free techniques.

3. Pd(II)-Mediated Amino Acid Side Chain-Side Chain

Bioconjugation

3.1. Context

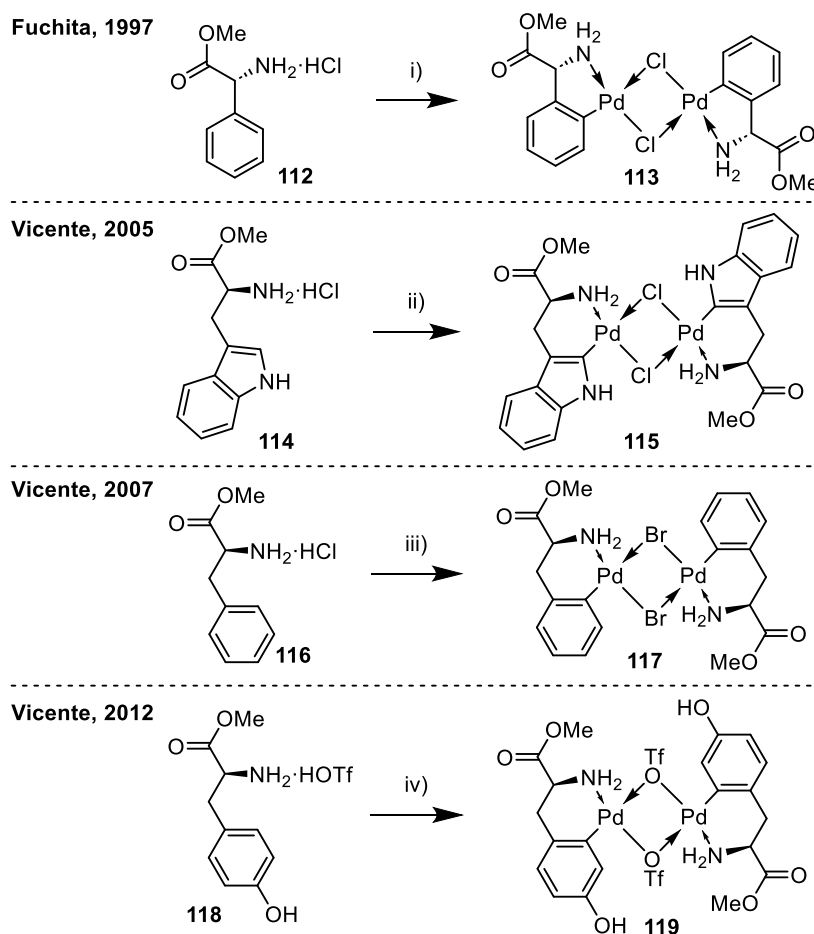
Section 2.2 outlined the development of Pd(II)-Ar complexes prepared *via* C-H activation for bioconjugation of cysteine as an alternative to OACs. Although these compounds were able to successfully arylate cysteine in peptides and proteins with comparable efficiency to existing technology, the requirement for dmbs or acetanilide cores to direct the cyclopalladation limits their scope. Thus, investigation into compounds that undergo cyclopalladation which would result in more complex and versatile C-S arylation products was the next avenue for the methodology.

3.1.1. Cyclopalladation of Amino Acids

In 1984, Ryabov *et al.* reported the synthesis of optically active Pd(II) complexes produced by cyclopalladation of (*R*)-*N,N*-dimethylphenylglycine ethyl ester, a derivative of dmbs.¹³³ However, the authors were unable to form the corresponding Pd(II) complex starting from (*R*)-phenylglycine methyl ester, likely due to the primary amine. Until the mid-1990s, it was generally accepted that the activation of sp² C-H bonds directed by primary and secondary amines was not possible, owing to the stronger coordination of nitrogen to Pd(II) preventing electrophilic attack of Pd(II) on the aromatic ring.¹³⁴ The only reported exception to this was cyclopalladation of compounds bearing very bulky functionality α - to a secondary amine.¹³⁵ However, in 1993 Fuchita *et al.* reported the synthesis of cyclopalladated complexes of *N*-methylbenzylamine as the first example of *ortho*-palladation of an α -unsubstituted secondary benzylamine.¹³⁶ Later that same year, Fuchita *et al.* published the first successful *ortho*-palladation of benzylamine.¹³⁷ The key to both of these processes was the use of Pd(OAc)₂ as the source of Pd(II), due to its higher reactivity compared to the more traditionally used tetrachloropalladates. Although the Pd(II) complexes of free benzylamines had been previously reported, their synthesis was more complex,^{138,139} and Fuchita's use of Pd(OAc)₂ resulted in a far more general method.¹⁴⁰

The successful formation of carbon-Pd(II) bonds directed by primary amines paved the way for the synthesis of optically active Pd(II) complexes synthesised from *N*-unprotected amino acids (Scheme 35). The first of these was the cyclopalladation of (*R*)-(-)-2-phenylglycine methyl ester (**113**) reported by Fuchita *et al.* in 1997.¹⁴¹ Further work by the Vicente lab produced cyclopalladated complexes of L-tryptophan methyl ester (**115**),¹⁴²

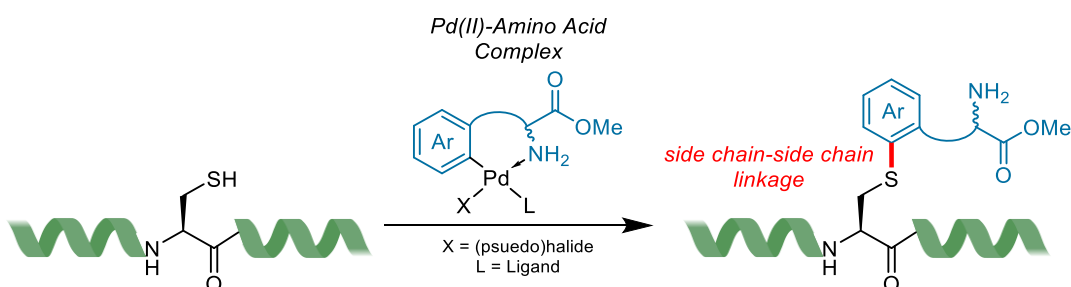
L-phenylalanine methyl ester (**117**),¹⁴³ and L-tyrosine methyl ester (**119**).¹⁴⁴ All of these methods used ammonium chloride or ammonium triflate salts of amino acid methyl esters.



Scheme 35: Cyclopalladation of amino acids. **Reagents and conditions:** i) $\text{Pd}(\text{OAc})_2$ (1 equiv.), acetone, reflux, 20 h, 58%; ii) $\text{Pd}(\text{OAc})_2$ (1 equiv.), MeCN, rt, 48 h, 84%; iii) $\text{Pd}(\text{OAc})_2$ (1 equiv.), MeCN, rt, 6 days then NaBr (5 equiv.), acetone, rt, 12 h, 49% over two steps; iv) $\text{Pd}(\text{OAc})_2$ (1 equiv.), MeCN, 60 °C – 70 °C, 5 h, 73%.

3.2. Aims

The reactivity of *ortho*-cyclopalladated amino acids has been used to synthesise many *ortho*-functionalised derivatives of amino acids, such as the reaction with carbon monoxide to produce lactams,^{143,144} or treatment with isocyanides and isothiocyanates.¹⁴⁵ However, cyclopalladated amino acids have not yet been applied to the synthesis of novel peptide- or protein-derived structures. In this project, it was envisioned that the reactivity of cyclopalladated amino acids towards cysteine would be similar to those synthesised from dmbs and acetanilide discussed in section 2.2, provided a suitable phosphine ligand was employed to promote C-S reductive elimination. The products of these reactions would possess a unique sidechain-sidechain linkage between cysteine and the aromatic ring of suitable amino acids (Scheme 36).



Scheme 36: General scheme for proposed side chain-side chain bioconjugation between cysteine-containing biomolecules and palladium complexes of amino acids.

To date, there is still significant interest in forming novel linkages between peptides for the synthesis of peptide-based therapeutics. Such therapeutics have gained traction in the pharmaceutical industry due to low toxicity combined with high selectivity and potency similar to biologics, but with the lower costs of small-molecule drugs.^{146,147} In particular, the formation of macrocycles *via* side chain-side chain conjugation has seen significant development using a variety of strategies such as oxidation of cysteine side chains to form disulfide bridges,¹⁴⁸ C-H activation stapling of tryptophan and phenylalanine/tyrosine residues,¹⁴⁹ among many others. As well as the formation of macrocycles, the ability to form bonds between amino acid side chains is being investigated to expand the toolbox in peptide synthesis. Native chemical ligation has been one of the most powerful advances in this field, offering a method to connect two peptide fragments.¹⁵⁰

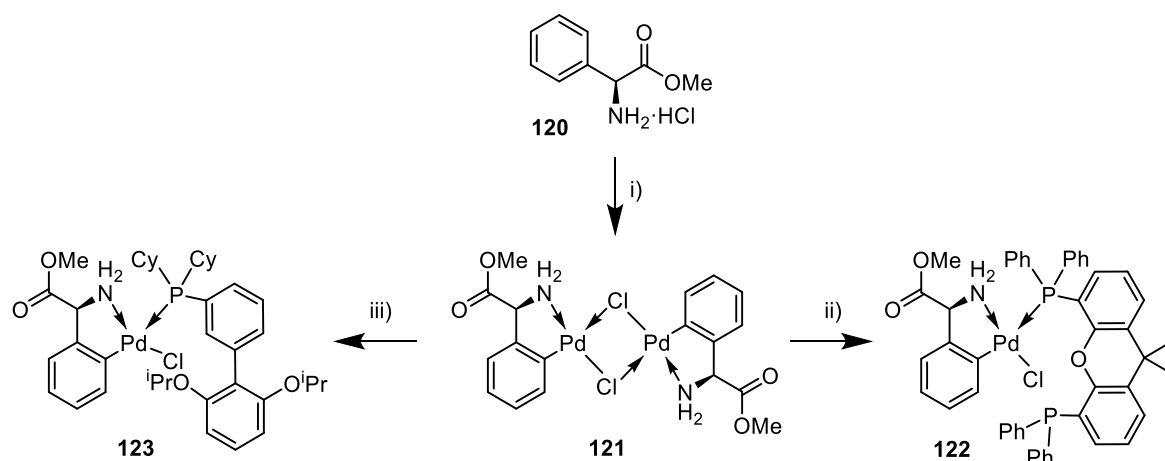
Due to the ongoing requirement for methodologies for the synthesis of novel peptide architectures, investigation into the use of cyclopalladated amino acids for side chain-side chain bioconjugation was initiated.

3.3. Results and Discussion

3.3.1. Bioconjugation with Pd(II)-Amino Acid

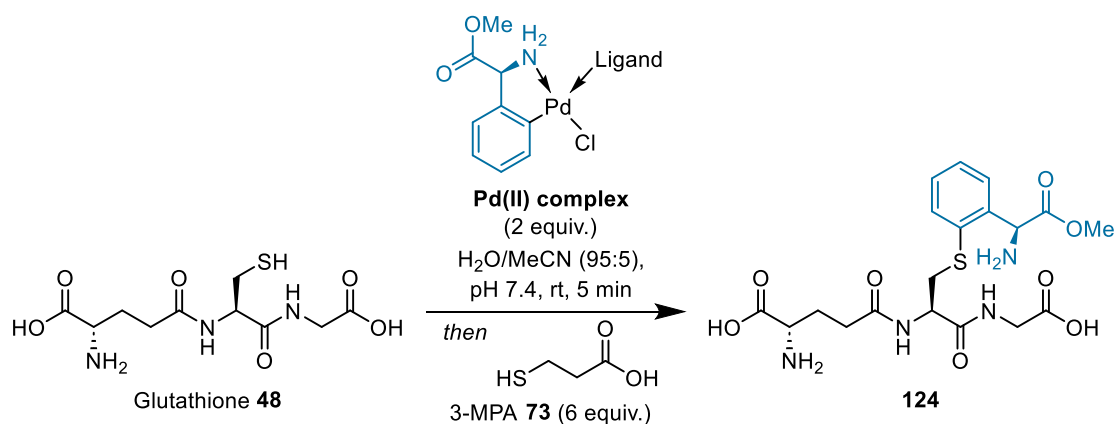
Complexes

Synthesis of cyclopalladated amino acids for bioconjugation began with phenylglycine (Scheme 37). Using a procedure adapted from the work of Fuchita,¹⁴¹ but from L-phenylglycine methyl ester hydrochloride (**120**) instead of the *dextro*- isomer (**112**), **121** was synthesised in excellent yield after purification by flash column chromatography. Treatment of **121** with Xantphos or RuPhos then gave **122** and **123** respectively, which could also be purified by flash column chromatography.



Scheme 37: Synthesis of Xantphos and RuPhos ligated Pd(II) complexes of L-phenylglycine. **Reagents and conditions:** i) Pd(OAc)₂ (1.0 equiv.), acetone, reflux, N₂, 48 h, 82%; ii) Xantphos (2.0 equiv.), CH₂Cl₂, rt, 1 h, 48%; iii) RuPhos (2.0 equiv.), CH₂Cl₂, rt, 1 h, 72%.

With these two compounds in hand, the next step was to assess their ability to arylate cysteine. Glutathione was used as the model peptide substrate, assessing conversions using LC-MS conditions outlined in section 2.2.3. Xantphos-ligated compound **122** produced an excellent 94% conversion to arylated glutathione (Table 11 entry 1). Surprisingly, RuPhos-ligated **123** showed no evidence of cysteine reactivity, with neither **124** nor the quench product observed in the LC-MS spectrum (Table 11 entry 2).



Scheme 38: Arylation of glutathione with Pd(II) complexes of L-phenylglycine.

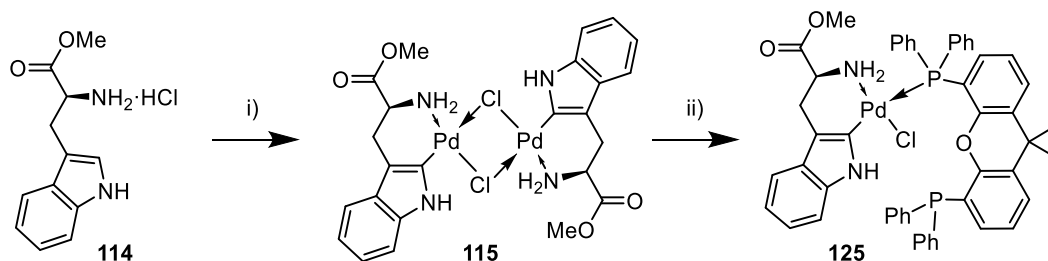
Entry	Ligand	LC-MS Conversion ^[a]
1	Xantphos (122)	94%
2	RuPhos (123)	No 124 found

Table 11: Conversions to arylated glutathione with Pd(II) complexes of L-phenylglycine. ^[a] Conversions determined by LC-MS (Section 5.4.3.1).

Notably, the glutathione-**123** coordination complex was observed by LC-MS, indicating the lack reactivity arises from the reductive elimination step. It is possible that the strongly donating primary amine was not sufficiently labile to allow the RuPhos to

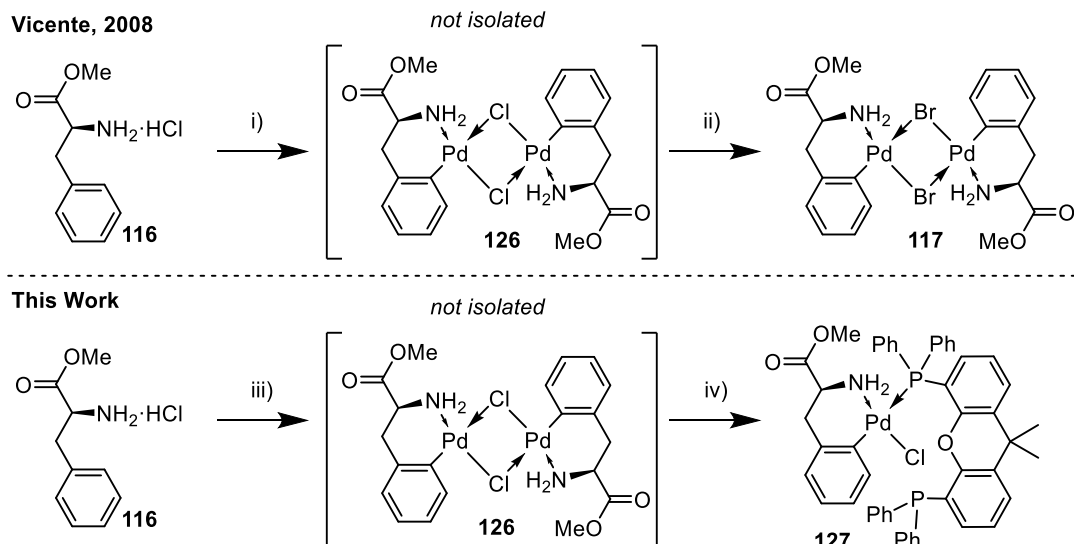
coordinate in the bidentate manner that is reportedly required for reductive elimination, as discussed in section 2.2.1.¹¹⁸ Due to this, Xantphos was chosen as the preferred ligand for bioconjugation with Pd(II)-amino acid complexes moving forward.

With the successful Pd(II)-mediated cysteine-phenylglycine side chain-side chain bioconjugation achieved, the next step was to expand the scope to other amino acids. The three canonical amino acids with aromatic side chains were chosen, namely L-tryptophan, L-phenylalanine, and L-tyrosine, with the initial cyclopalladated complexes of each previously reported in the literature.^{142–144} Thus, combining L-tryptophan methyl ester hydrochloride (**114**) with Pd(OAc)₂ in MeCN at 30 °C for two days gave **115** in a 49% yield after filtration through MgSO₄. Two equivalents of Xantphos were then combined with one equivalent of **115** in CH₂Cl₂ to produce **125** in 99% yield, with no chromatographic purification being necessary.



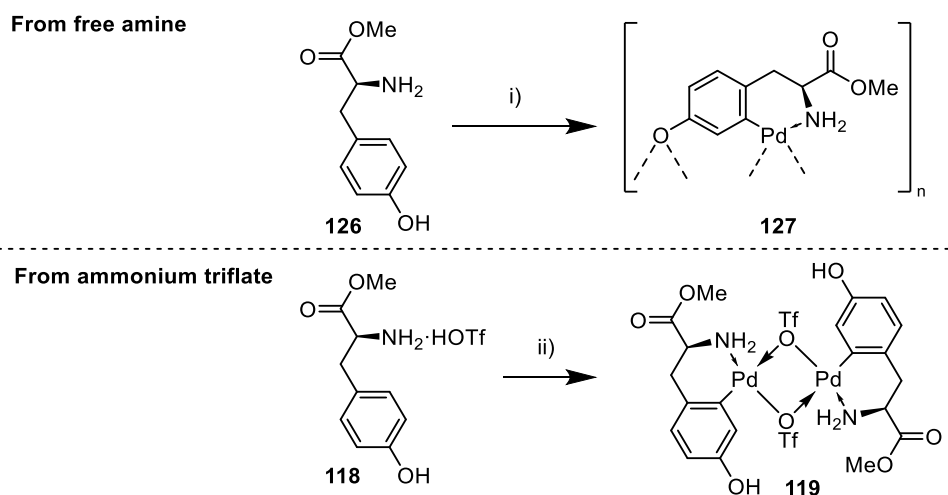
Scheme 39: Synthesis of Xantphos-ligated Pd(II) complex of L-tryptophan. **Reagents and conditions:** i) Pd(OAc)₂ (1 equiv.), MeCN, 30 °C, 48 h, 49%; ii) Xantphos (2.0 equiv.), CH₂Cl₂, rt, 1 h, 99%.

The 2007 work of Vicente *et al.* describes challenges in the synthesis of the cyclopalladation of L-phenylalanine, primarily due to purification. Treatment of L-phenylalanine methyl ester hydrochloride (**116**) with Pd(OAc)₂ gave the cyclopalladated complex with bridging chloride ligands, as evidenced by NMR, but a sample of sufficient purity for full spectroscopic characterisation could not be obtained. The authors instead had to treat their impure sample with sodium bromide in acetone to exchange the bridging chloride ligands for bromides, which could then be recrystallised to form **117** (Scheme 40 top). This approach was not adopted here, as it was desirable to keep the halide consistent across all cyclopalladated complexes for bioconjugation conversion comparisons. Instead, the crude sample of **126** was treated directly with Xantphos, and the resulting complex (**127**) was purified by flash column chromatography, giving a good yield of 42% over two steps (Scheme 40 bottom). Conditions for the formation of **126** also deviated from the literature, with the reaction being performed at 40 °C for 24 hours instead of room temperature for six days, significantly shortening the reaction time.



Scheme 40: Synthesis of cyclopalladated L-phenylalanine. **Top:** Route used by Vicente *et al.* **Bottom:** This work. **Reagents and conditions:** i) $\text{Pd}(\text{OAc})_2$ (1 equiv.), MeCN, rt, 6 days; ii) NaBr (5 equiv.), acetone, rt, 12 h, 49% (2 steps); iii) $\text{Pd}(\text{OAc})_2$ (1 equiv.), MeCN, 40 °C, 24 h; iv) Xantphos (2 equiv.), CH_2Cl_2 , rt, 1 h; 42% (2 steps).

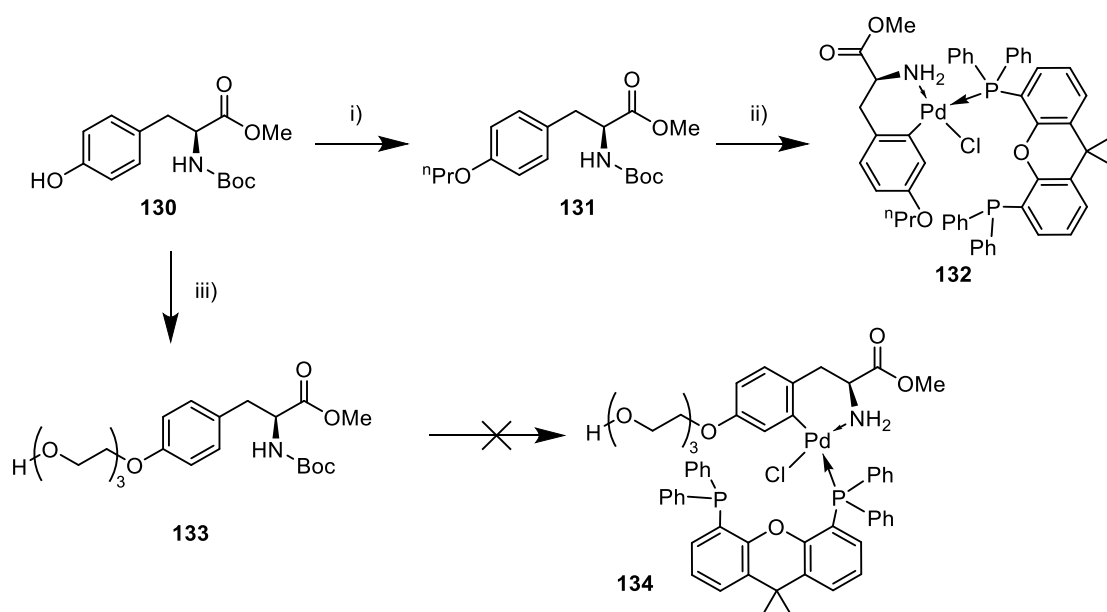
The cyclopalladation of L-tyrosine methyl ester hydrochloride proved to be more challenging than that of **114** and **116**. As reported by Vicente *et al.*, if the hydrochloride salt or free amine (**128**) is used, the reaction forms an insoluble polymeric species (**129**) binding through the free tyrosine oxygen upon drying (Scheme 41 top).¹⁴⁴ Thus, the chloride-bridged Pd(II) dimer cannot be formed. Instead, Vicente *et al.* report using the ammonium triflate salt of L-tyrosine methyl ester (**118**) to prepare **119** (Scheme 41 bottom). The authors cite the charge density at Pd during the cyclopalladation reaction as being key to the observed differences in reactivity. When chloride is present, it is bound to Pd during the cyclopalladation process producing a neutral intermediate, whereas the weakly coordinating triflate anion does not coordinate to Pd, producing a cationic intermediate.¹⁵¹ This faster metalation process likely prevents the cyclometallated tyrosine from polymerising during its formation.



Scheme 41: Synthesis of Pd(II)-tyrosine species by Vicente *et al.* **Top:** Formation of Pd(II)-based polymer. **Bottom:** Synthesis from ammonium triflate salt. **Reagents and conditions:** i) Pd(OAc)₂ (1 equiv.), MeCN, 78 °C, 8 h; ii) Pd(OAc)₂ (1 equiv.), MeCN, 60 °C – 70 °C, 5 h, 73%.

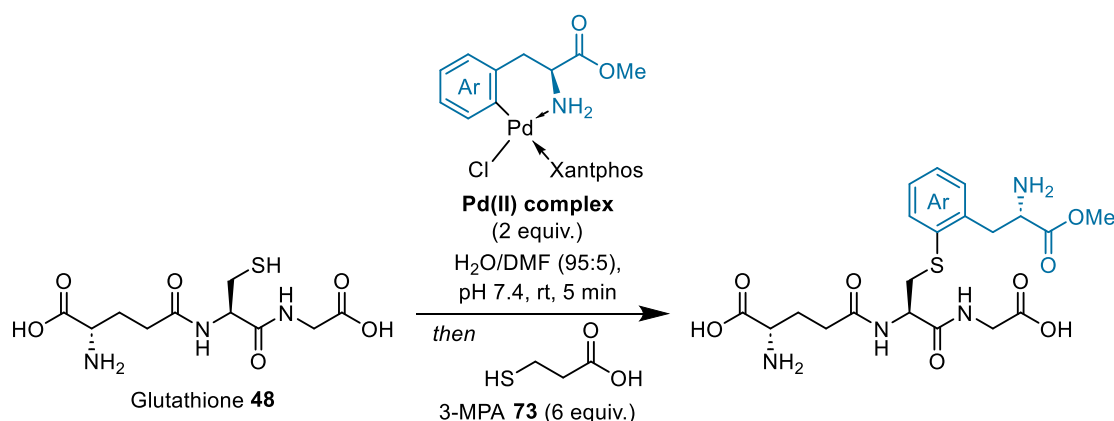
In this investigation, it was desirable to avoid the use of triflic acid to allow easy transfer of the methodology to biology or biochemistry laboratories. Thus, an initial strategy to protect the tyrosine hydroxyl was devised, which allowed synthesis of the Pd(II) complex from the *O*-protected tyrosine methyl ester hydrochloride salt (Scheme 42). Firstly, *N*-Boc-L-tyrosine (**130**) was *O*-alkylated using 1-bromopropane to produce **131** in 53% yield. Intermediate **131** was *N*-deprotected using 4 M HCl in dioxane, and concentrated to yield the hydrochloride salt, which was not purified or characterised. The hydrochloride salt was then treated with Pd(OAc)₂, followed by Xantphos in a manner similar to the preparation of **127**, producing **132** in 12% yield over three steps from the Boc-protected amino acid **131**. To *O*-protect with a group of more biological relevance than a simple propyl chain, functionalisation of **130** with tosylated triethylene glycol produced **133** in 27% yield. However, using the same telescoping conditions as previously did not give the desired complex **134**. This is likely due to the PEG chain or the free alcohol disrupting the cyclopalladation process by coordinating to Pd²⁺.

The successful telescoped procedure to convert **131** into complex **132** suggested this methodology had potential for an *in situ* formation of Pd(II) complexes for bioconjugation, analogous to the procedure developed in section 2.2.6. However, the increased reaction time for the preparation of cyclometallated amino acids, alongside the requirement for heating, makes the *in situ* preparation of these complexes comparatively impractical for use in biological labs. For the purposes of this project, it was also desirable to fully characterise the Pd(II) complexes due to their increased complexity.



Scheme 42: Synthesis of Xantphos ligated O-protected Pd(II) complex of L-tyrosine methyl ester. **Reagents and conditions:** i) 1-Bromopropane (4 equiv.), K₂CO₃ (2 equiv.), DMF, 70 °C, 21 h, 53%; ii) 4 M HCl in dioxane (15 equiv.), rt, 15 mins, then Pd(OAc)₂ (1 equiv.), 50 °C, 24 h, then Xantphos (1 equiv.), CH₂Cl₂, rt, 1h, 14% over three steps; iii) 2-(2-(2-Hydroxyethoxy)ethoxy)ethyl 4-methylbenzenesulfonate (1 equiv.), K₂CO₃ (1 equiv.), DMF, 80 °C, 18 h, 27%.

Following their successful synthesis, the ability of **125**, **127**, and **132** to arylate glutathione was assessed using the standard assay as detailed in section 2.2.6 (Scheme 43). All three compounds produced conversions of over 90%, with **125** and **127** being greater than 95% (Table 12). This positive result showed that six-membered palladacycles were no less reactive towards cysteine compared to the five-membered palladacycle produced by the metalation of phenylglycine.



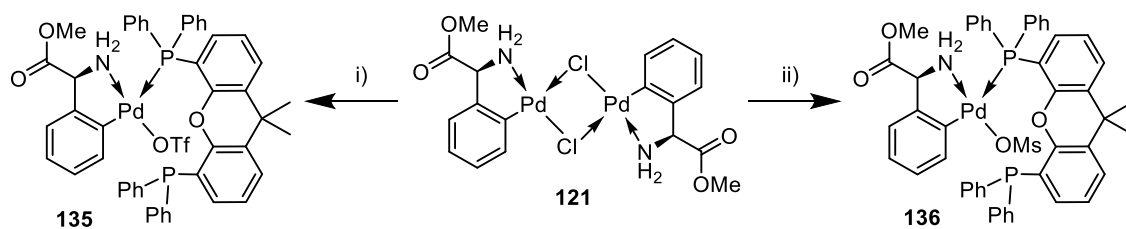
Scheme 43: Arylation of glutathione using Pd(II)-amino acid complexes synthesised from hydrochloride salts.

Entry	Pd(Ar)(Xantphos)Cl =	LC-MS Conversion ^[a]
1		96%
2		96%
3		91%

Table 12: Yields for arylation of glutathione using Pd(II)-amino acid complexes synthesised from hydrochloride salts.
^[a] Conversions determined by LC-MS (Section 5.4.3.1).

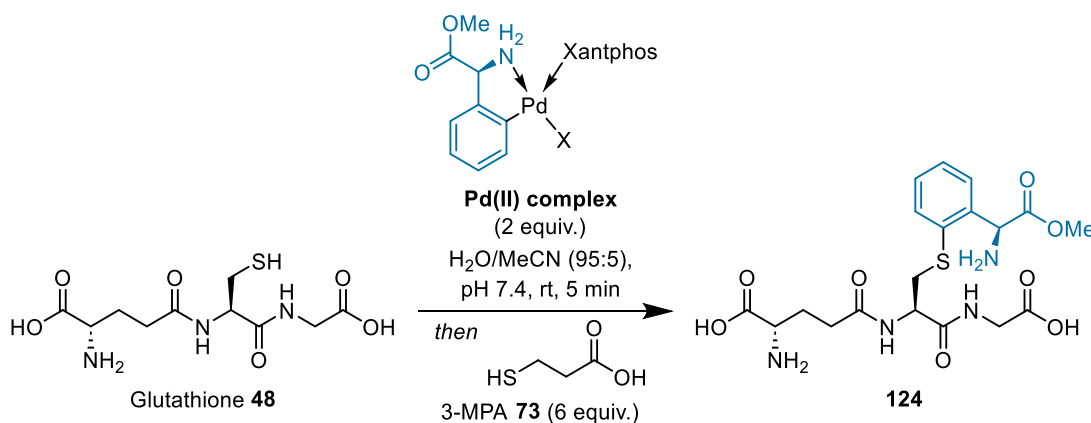
3.3.1.1. Preparation from Mesylate Salts

Despite the success of the Pd(II)-amino acid complexes synthesised from hydrochloride salts, the Pd complex of unprotected tyrosine still eluded this study. Thus, investigations next turned to the synthesis of cyclopalladated tyrosine without the use of triflic acid. Methane sulfonic acid was chosen as an alternative, being weakly coordinating like triflic acid, but much less acidic. To test whether a triflate or mesylate counterion would hinder the efficiency of cysteine S-arylation, cyclometallated L-phenylglycine **121** was subjected to a halide exchange by treatment with either silver mesylate or silver triflate, to produce the corresponding dimeric compounds which were not isolated. These compounds were then combined with Xantphos to yield either **135** or **136** in moderate yields over two steps following flash column chromatography (Scheme 44).



Scheme 44: Synthesis of halide-exchanged Pd(II)-L-phenylglycine complexes. **Reagents and conditions:** i) AgOTf (2 equiv.), CH₂Cl₂, rt, 1 h, then Xantphos (1 equiv.), CH₂Cl₂, rt, 1 h, 52%; ii) AgOMs (2 equiv.), CH₂Cl₂, rt, 1 h, then Xantphos (1 equiv.), CH₂Cl₂, rt, 1 h, 49%.

The ability of **135** and **136** to arylate glutathione was then assessed using the standard bioconjugation conditions. Both compounds produced greater than 90% conversion to arylated glutathione, but **136** produced a slightly higher conversion of 94%. This validated that exchanging the chloride for either mesylate or triflate would not significantly affect the bioconjugation chemistry.



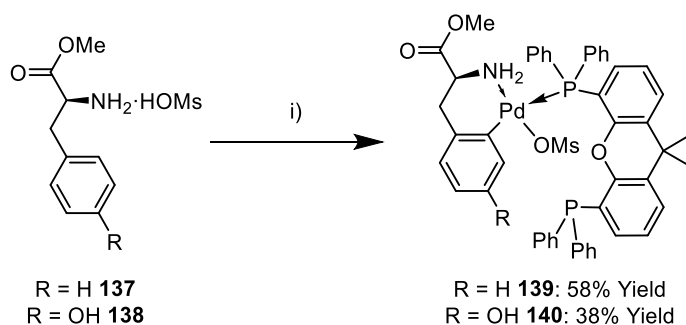
Scheme 45: Arylation of glutathione with halide-exchanged Pd(II)-L-phenylglycine complexes.

Entry	Pd(Ar)(Xantphos)X	LC-MS Conversion ^[a]
1	X = OMs (136)	94%
2	X = OTf (135)	90%

Table 13: Conversions to arylated glutathione using halide-exchanged Pd(II)-L-phenylglycine complexes. ^[a] Conversions determined by LC-MS (Section 5.4.3.1).

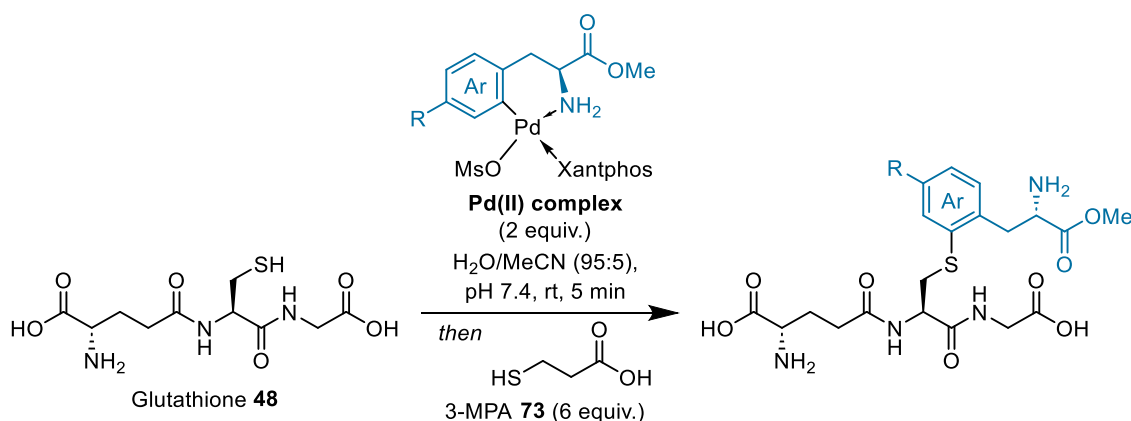
Cyclopalladation of the mesylate salt of 2-aminobiphenyl has been used in the literature for the preparation of the commercially available G₃ precatalysts.¹¹⁹ Thus, L-phenylalanine methyl ester mesylate (**137**) was synthesised *via* salt-exchange from its corresponding hydrochloride salts, and L-tyrosine methyl ester mesylate (**138**) was synthesised simply by treating L-tyrosine methyl ester with methanesulfonic acid. The two-step reaction of **137** and **138**, firstly with Pd(OAc)₂ in acetonitrile to produce the corresponding dimeric Pd(II) species which was not isolated, followed by reaction with Xantphos, produced **139** and **140** in moderate yields after purification by flash column

chromatography (Scheme 46). Notably, the synthesis of compound **139** from the mesylate salt offered a modest improvement in yield compared to the synthesis of **127** from the hydrochloride salt.



Scheme 46: Synthesis of Xantphos-ligated Pd(II)-amino acid complexes from mesylate salts. **Reagents and conditions:** i) Pd(OAc)₂ (1 equiv.), MeCN, 60 °C – 78 °C, 4 h, then Xantphos (2 equiv.), CH₂Cl₂, rt, 1 h.

Reactions of with **139** and **140** (Scheme 47) showed excellent conversions into the *S*-arylation products of greater than 97% (Table 14). With the Pd(II)-mediated cysteine-tyrosine side chain-side chain conjugation successful, it had been shown that most canonical amino acids with aromatic side chains plus L-phenylglycine are compatible with this methodology. The only absentee from this study is histidine, the Pd(II) complexes of which are not present in the literature. Pd(II)-catalysed C-H activation of histidine requires *N*-benzylation of the imidazole moiety, and *N*-acylation of the amino acid free amine,¹⁵² making these substrates of little interest to this work.



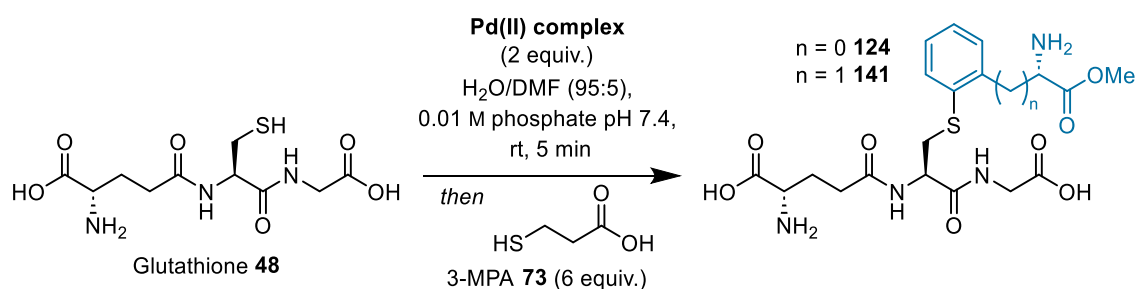
Scheme 47: Arylation of glutathione using Pd(II) complexes prepared from mesylate salts. *R* = H **139**; *R* = OH **140**.

Entry	Pd(II) Complex	LC-MS Conversion ^[a]
1	139	97%
2	140	98%

Table 14: Conversions to arylated glutathione using Pd(II) complexes prepared from mesylate salts. ^[a] Conversions determined by LC-MS (Section 5.4.3.1).

3.3.1.2. Validation of Reaction Conversions

With the efficiency of Pd(II)-mediated side chain-side chain conjugation of cysteine to aromatic amino acids determined by LC-MS conversions, further studies were conducted to confirm the validity of this method. Each reaction was performed once, as previous validation had shown very little variation between LC-MS runs between repeat analysis of the same sample and repeat experiments. This was prompted by the observation of a significant matrix effect for the product of glutathione arylation using **122** and **127**, with the ESI⁺ response varying significantly depending on co-solvent and buffer system. Varying the defined 'standard conditions' for the arylation of glutathione with either **122** or **127** (Scheme 48) generally gave a statistically insignificant variation in the final calculated glutathione conversion. However, the variation in absolute count for the ESI⁺ response of the reaction product was much larger. MeCN as the co-solvent in place of DMF saw the absolute ESI⁺ response of the product almost triple, whilst the glutathione response did not significantly change (Table 15 entries 1 and 2). Changing the percentage of DMF from 5% to 10% saw a drop in response (Table 15 entries 1 and 3; 9 and 10), but an increase when more than 10% DMF was used (Table 15 entries 3 and 4; 10 and 11), an effect that was demonstrated by both **122** and **127**. Changing the buffer system from phosphate to tris (Table 15 entries 3 and 7; 6 and 8) saw the ESI⁺ response halve for both DMF and DMSO co-solvent systems, whilst giving negligible change in glutathione conversion. With these results, it was clear that whilst the ESI⁺ response of glutathione was not significantly affected by the reaction conditions, the ESI⁺ response of the product was. The small observed effect of reaction conditions on glutathione ESI⁺ response further validated the use of a glutathione calibration curve to assess bioconjugation reaction conversions.

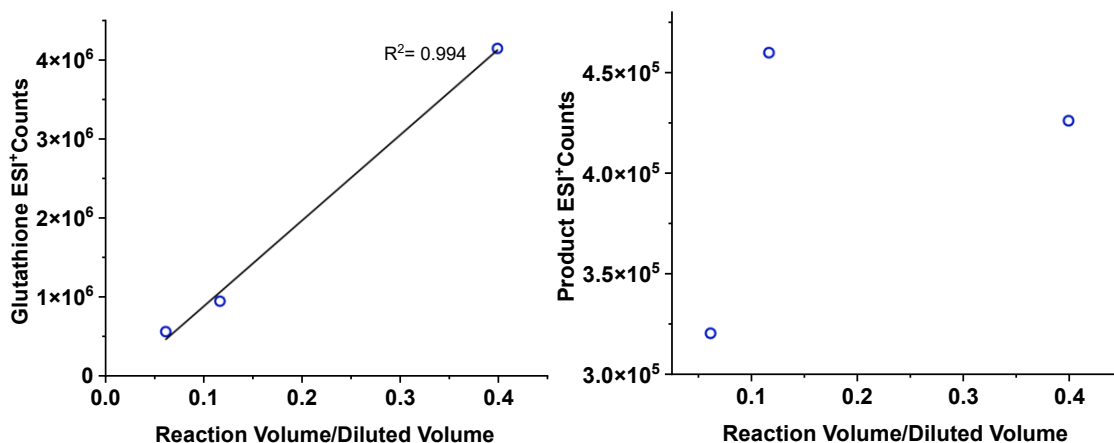


Scheme 48: 'Standard conditions' for the arylation of glutathione with 122 or 127.

Entry	Pd(II) Complex	Deviation from Standard Conditions	Glutathione Conversion ^[a]	Glutathione EIC Peak Area	Product EIC Peak Area
1	122	None	93.7%	604,030	110,267
2	122	5% MeCN	94.1%	563,135	320,490
3	122	10% DMF	92.5%	761,146	60,084
4	122	50% DMF	92.6%	749,181	97,374
5	122	5% DMSO	90.6%	990,546	92,485
6	122	10% DMSO	90.9%	951,540	84,717
7	122	0.01 M Tris, 10% DMF	92.5%	753,492	29,018
8	122	0.01 M Tris, 10% DMSO	91.3%	905,549	38,328
9	127	None	96.0%	319,561	1,033,969
10	127	10% DMF	94.7%	482,397	627,489
11	127	33% DMF	94.9%	464,655	756,300

Table 15: Effect of reaction conditions on the observed EIC peak area for the arylation of glutathione. ^[a] Conversions determined by LC-MS.

Furthermore, changing the dilution factor prior to analysis revealed more complexity with the ESI⁺ response of the product. Prior to LC-MS analysis, the reactions are diluted with 1000 μL of water, giving a total sample volume of 1066.3 μL. When the reaction of **122** with glutathione was instead diluted with either 100 μL or 500 μL of water, the glutathione ESI⁺ response showed a linear relationship (Graph 2 left), whereas the product (**124**) showed evidence of suppression at lower dilution (Graph 2 right).



Graph 2: *Left:* Dilution effect on ESI⁺ response of glutathione after reaction with **122**. *Right:* Dilution effect on ESI⁺ response of product **124** after reaction of glutathione with **122**.

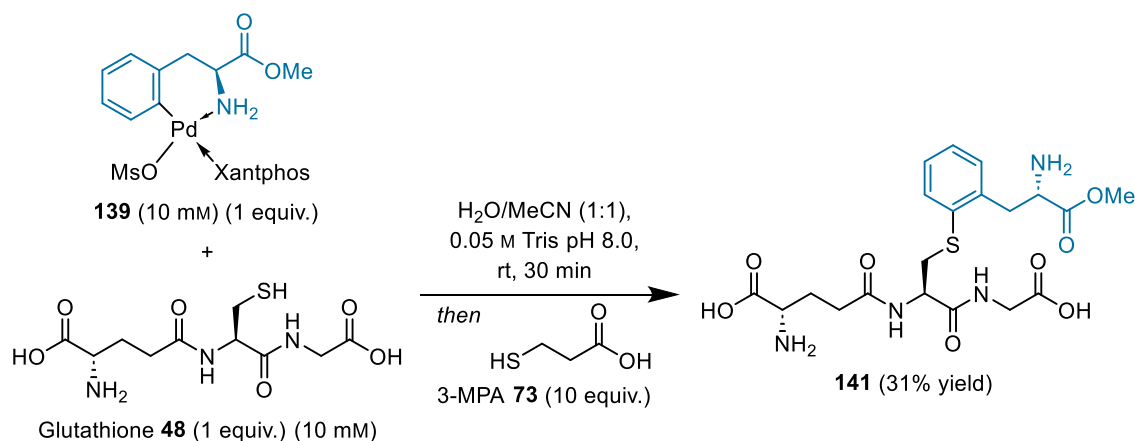
The nature of the (pseudo)halide bound to the Pd(II) complex also appeared to alter the ESI⁺ response of the product. No correlation between the glutathione conversion and product EIC peak area was observed for **122**, **135** and **136**, with the only difference being their counterions, Cl⁻, TfO⁻, and MsO⁻, respectively. This is likely due to the product eluting much closer to any Pd-based side-products in the chromatography, at around seven minutes into the run, whereas glutathione elutes at around one minute.

The data discussed above served to effectively validate the continued use of determining glutathione conversion by LC-MS. Whilst less desirable than isolating and fully characterising each bioconjugation product, the method used is satisfactory in the field of bioconjugation chemistry. Furthermore, the use of a starting material calibration curve and the lack of any observed ionisable side-products still is likely to give more accurate quantitative data compared to the methods used in the literature.⁷⁴

3.3.2. Isolation of Bioconjugate

As none of the bioconjugation products thus far had been isolated and fully characterised, it was desirable to significantly scale-up the reaction and isolate one of the glutathione arylation products. For this large-scale reaction, one equivalent of complex **139** was selected for the arylation, and the reaction was performed on a 100 μmol scale at 10 mM glutathione concentration (Scheme 49). Using one equivalent of **139** *verses* two that is standard for this methodology was simply due to the elevated cost of materials for such a large-scale reaction. The reaction was also performed using 50% MeCN due to the low solubility of **139** at higher concentrations in highly aqueous reaction media, and tris was chosen as the buffer system due to literature precedent.⁷⁴ A longer reaction time of thirty minutes was chosen to guarantee complete conversion, and quenching with ten equivalents of 3-MPA ensured that

all of the palladium-containing by-products precipitated and could be removed *via* filtration prior to further purification.



Scheme 49: Scaled-up reaction of glutathione with **139**.

The purification of peptides functionalised using organometallic reagents is most commonly performed using preparative HPLC. However, **141** was purified using an automated reverse-phase flash chromatography system equipped with a C-18 cartridge. Even at such a low scale, **141** was clearly visible on the UV trace (section 5.4.2). Following lyophilisation, **141** was obtained as the formic acid salt in 31% yield, which cannot be compared to literature isolated yields, as much of what is presently reported requires reaction concentrations 1000 times lower. Most of the losses likely came from the filtration step, with the product remaining associated with the Pd-based side products, causing them to precipitate. Importantly, **141** was isolated in sufficient purity to enable its full characterisation. The 500 MHz ^1H NMR spectrum of **141** (Figure 11) in D_2O unequivocally proved the selective *S*-modification. Most diagnostic were the alkyl protons α - to sulfur, which are shifted by approximately 0.5 ppm downfield compared to the NMR spectrum of unmodified glutathione,¹⁵³ as well as the disappearance of the free thiol proton. Both the 500 MHz ^1H NMR and the 126 MHz $^{13}\text{C}\{^1\text{H}\}$ NMR spectra were fully assigned (section 5.4.2) with the aid of 2D ^1H - ^1H COSY and ^1H - ^{13}C HSQC techniques.

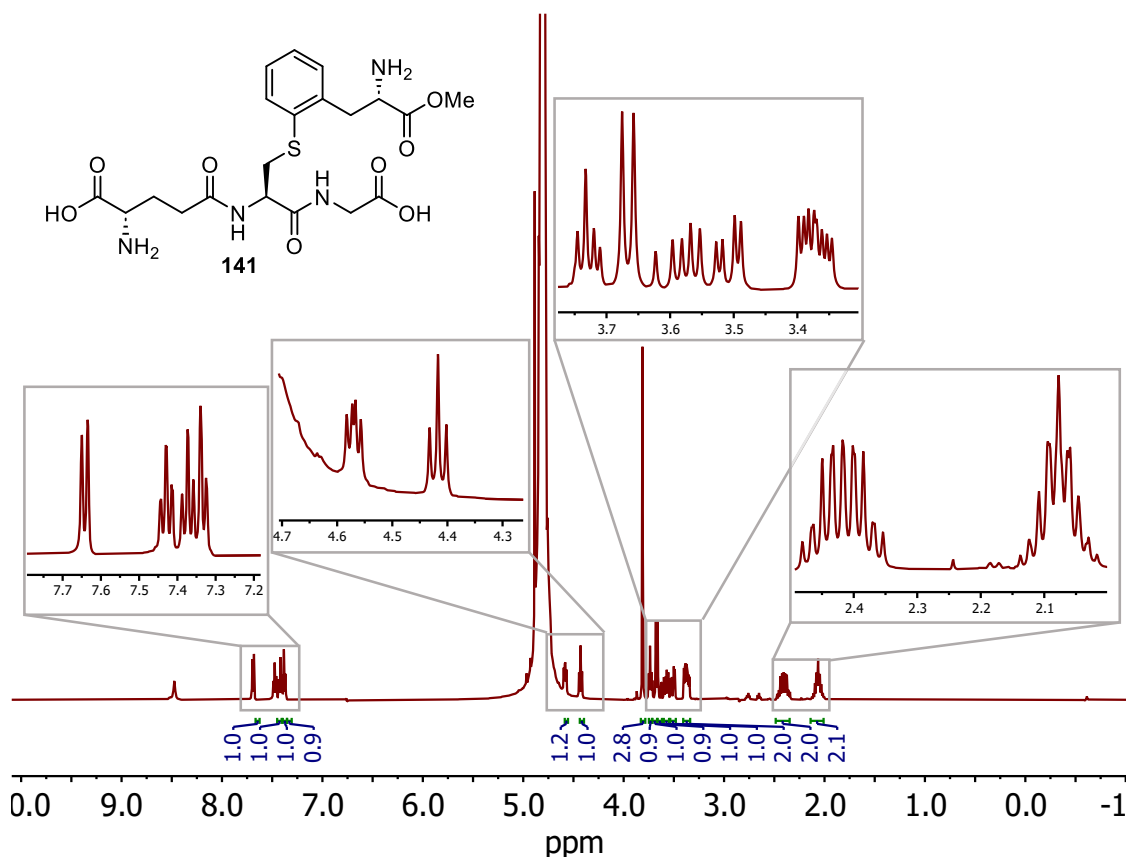
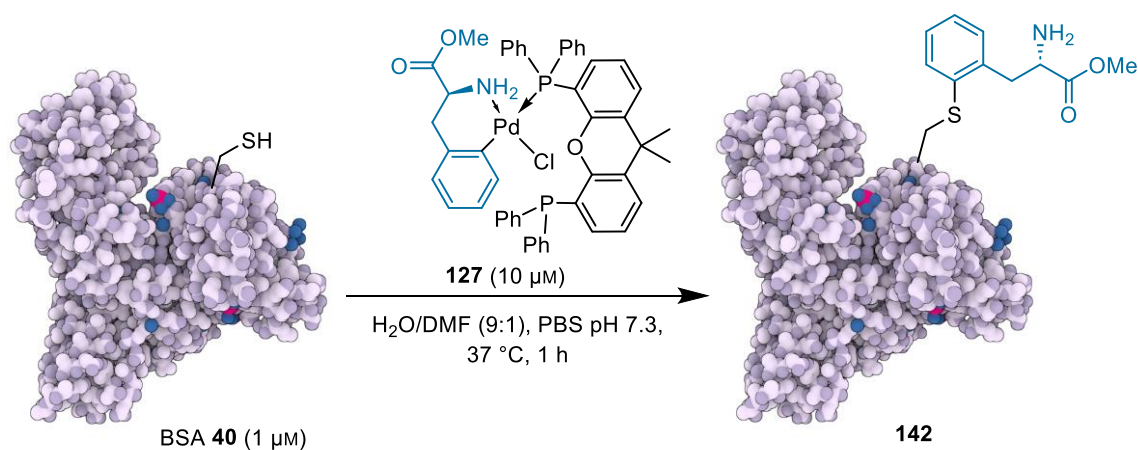


Figure 11: 500 MHz ^1H NMR spectrum of **141** in D_2O .

3.3.3. Protein Arylation

With peptide arylation using Pd(II)-amino acid complexes successfully validated, protein arylation was assessed using BSA as the model protein substrate, as in section 2.2.7. BSA (**40**) at $1\ \mu\text{M}$ was treated with L-phenylalanine-derived Pd(II) complex **127** at $10\ \mu\text{M}$ for one hour at $37\ ^\circ\text{C}$ in PBS buffer, with 10% DMF additive (Scheme 47). The reaction mixture was analysed by LC-MS and the deconvoluted mass spectrum showed a clear mass shift from unmodified BSA (**40**) (Figure 12 left) to modified BSA (Figure 12 right). This corresponded to a single-site modification with **127**.



*Scheme 50: Arylation of BSA (**40**) with Pd(II)-amino acid complex **127**.*

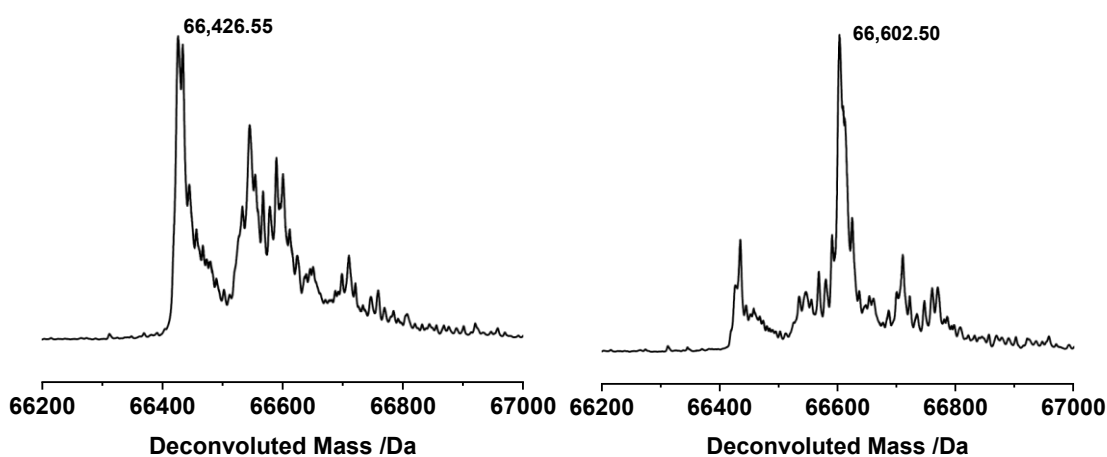
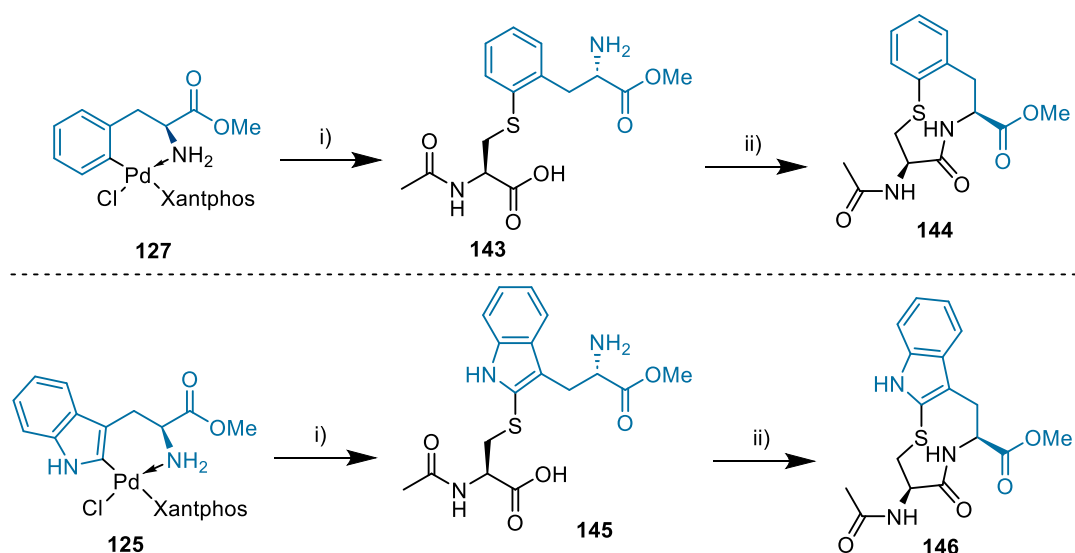


*Figure 12: Left: Deconvoluted mass spectrum of BSA (**40**). Right: Deconvoluted mass spectrum of BSA arylation with **127** showing peak arising from product (**142**). See section 5.4.3.2 for LC-MS methods.*

3.3.4. Macrocycle formation

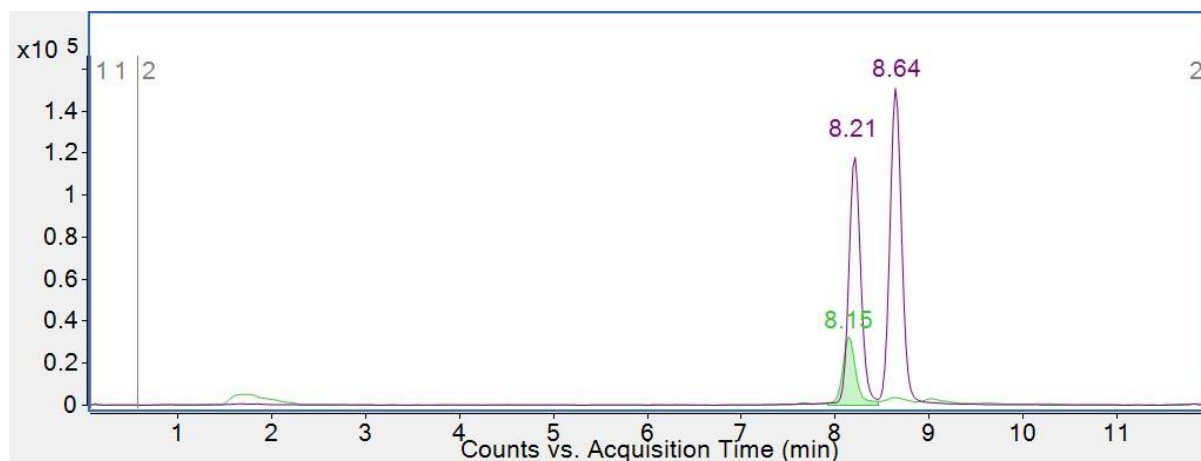
As one of the desirable uses of the chemistry discussed herein is the formation of peptide macrocycles with novel topology, exploratory experiments were undertaken to demonstrate the ability of this chemistry to contribute to the field of peptide macrocyclization. These initial studies were to model the formation of a macrocycle at C-terminal cysteine, by forming an amide bond between the free amine of the newly installed amino acid and the carboxylic acid of cysteine at the C-terminus. To do this, a one-pot bioconjugation-cyclisation method was devised, using *N*-acetylcysteine (**5**) as a simple model of a C-terminal cysteine, and either **127** (Scheme 51 top) or **125** (Scheme 51 bottom) as bioconjugation reagents. The proposed structures of **144** and **146** would be nine-membered lactams containing a thioether and two stereogenic centres.



*Scheme 51: Top: One pot bioconjugation-cyclisation of NAC using **127**. Bottom: One pot bioconjugation-cyclisation of NAC using **125**. Showing the two proposed products. Reagents and conditions: i) NAC (1 equiv.), DIPEA (1 equiv.), DMF, rt, 5 min; ii) DIPEA (1 equiv.), EDC·HCl (3 equiv.), HOBt (6 equiv.), rt, 4 h.*

N-Acetylcysteine (NAC, **5**) was treated with one equivalent of **127** or **125** in DMF with one equivalent of DIPEA at room temperature for five minutes to form the *S*-arylated NAC derivatives **143** and **145**. The reaction was performed in DMF to ensure the following macrocyclization would be compatible with the reaction solvent. To validate the success of the original bioconjugation, initially the reaction was quenched with 3-MPA, diluted with water, and analysed by LC-MS, clearly showing the successful formation of **143** and **145** (section 5.4.3.3). After the formation of bioconjugation products was validated, instead of quenching the reaction, another equivalent of DIPEA was added, alongside three equivalents of EDC·HCl and six equivalents of HOBt·H₂O. This reaction was performed at approximately 200 μM to minimise any undesirable side-reactions, as low concentrations are generally required for macrocyclizations.¹⁵⁴ Following standing at room temperature for four hours, the reaction mixture was diluted and then analysed by LC-MS (section 5.4.3.3).

The EIC for the cyclisation of **143** (section 5.4.3.3) clearly showed a single peak corresponding to the required mass loss of H₂O for cyclisation. However, the EIC for the cyclisation of **145** showed two peaks corresponding to identical masses (EIC 1). Whilst one can be attributed to **146**, **145** could have also cyclised through the indole nitrogen, producing **147** (Figure 13). Whilst it is not possible to ascertain which of the two peaks corresponds to which structure without additional methods of characterisation, it is possible that **147** is more polar due to its free amine and is therefore the peak that elutes earlier.



EIC 1: **145** (ESI⁺) *m/z* of [M+H]⁺ detected: 380.1270, expected for C₁₇H₂₁N₃O₅S: 380.1275. **145** peak area: 323,333 (rt = 8.15 min). **146/147** (ESI⁺) *m/z* of [M+H]⁺ detected: 363.1199, expected for C₁₇H₁₉N₃O₄S: 363.1199. **146/147** peak area: 1,051,984 (rt = 8.21 min), 1,353,131 (rt = 8.64 min).

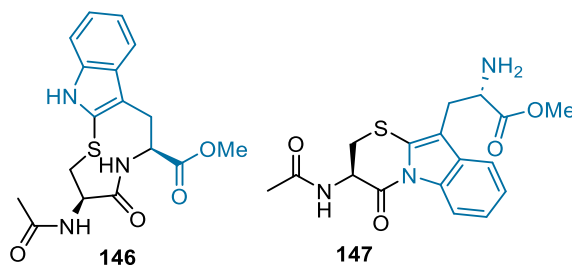


Figure 13: Proposed structures for the products of the cyclisation of **145**.

3.4. Conclusions and Outlook

This chapter described the application of palladium C-H activation complexes of aromatic amino acids towards cysteine *S*-arylation. Complexes were initially synthesised from hydrochloride salts, but it was later discovered that preparation from mesylate salts was more general, allowing the synthesis of a palladium complex from L-tyrosine methyl ester. It was found that unlike the results discussed in 2.2, RuPhos was not tolerated as the ligand for these complexes, and Xantphos was required. With these Xantphos ligated complexes, conversions to *S*-arylated glutathione were excellent, offering a novel methodology for forming side chain-side chain linkages in peptides. However, when performing cysteine *S*-arylation with palladium amino acid complexes, caution must be exercised when assessing conversion using LC-MS methods. In these systems, due to the significant effect of matrix on the ESI⁺ response of the product, conversion must be determined by ESI⁺ response of glutathione, which was validated over a wide range of conditions and concentrations. Furthermore, the methodology tolerated scale-up, allowing isolation and characterisation of a glutathione bioconjugate. The potential for bioconjugation followed by cyclisation was

explored, and preliminary LC-MS data suggested the formation of six- and nine-membered macrocycles had been formed.

There is much room for further investigation as a result of this exploratory work, firstly by expanding the scope of cyclometallated peptides to include di- and tripeptides, which would allow the formation of even more complex bioconjugates. Further work would also investigate purifying and characterising the products of the macrocyclization reactions, to fully confirm their structure.

4. Applications of Organometallic Au(III) Complexes for Bioconjugation

The work described herein was undertaken during a three-month institutional visit to the University of California, Los Angeles (UCLA), USA from September – December 2022. Work was supervised by Professor Alexander Spokoyny (Department of Chemistry and Biochemistry, UCLA), and some experimental data reported within this chapter was collected by Dr Evan Doud (Spokoyny lab, Department of Chemistry and Biochemistry, UCLA). Credit is given where this is the case. All computational experiments discussed were carried out by Billy Treacy (Houk/Maynard Labs, Department of Chemistry and Biochemistry, UCLA).

4.1. Context: Cysteine Bioconjugation Kinetics

Rapid kinetics are of paramount importance when performing bioconjugation chemistry. The primary reason for this is the low concentrations that a majority of bioconjugation reactions are performed at, meaning a low reaction rate would require a significant excess of coupling reagent, which can in turn cause issues with side reactions, purification, and chemoselectivity. In live cells, large excesses of reagent may also result in cytotoxicity, further justifying the demand for fast kinetics. For example, with a second order rate constant (k_2) of $10 \text{ M}^{-1} \text{ s}^{-1}$, a reaction between a biomolecule and a coupling reagent at $10 \text{ }\mu\text{M}$ and $100 \text{ }\mu\text{M}$ respectively would proceed to 97% completion within one hour. In a recent review, Chen and Gao define this k_2 value of greater than $10 \text{ M}^{-1}\text{s}^{-1}$ as ‘fast cysteine bioconjugation’.¹⁵⁵

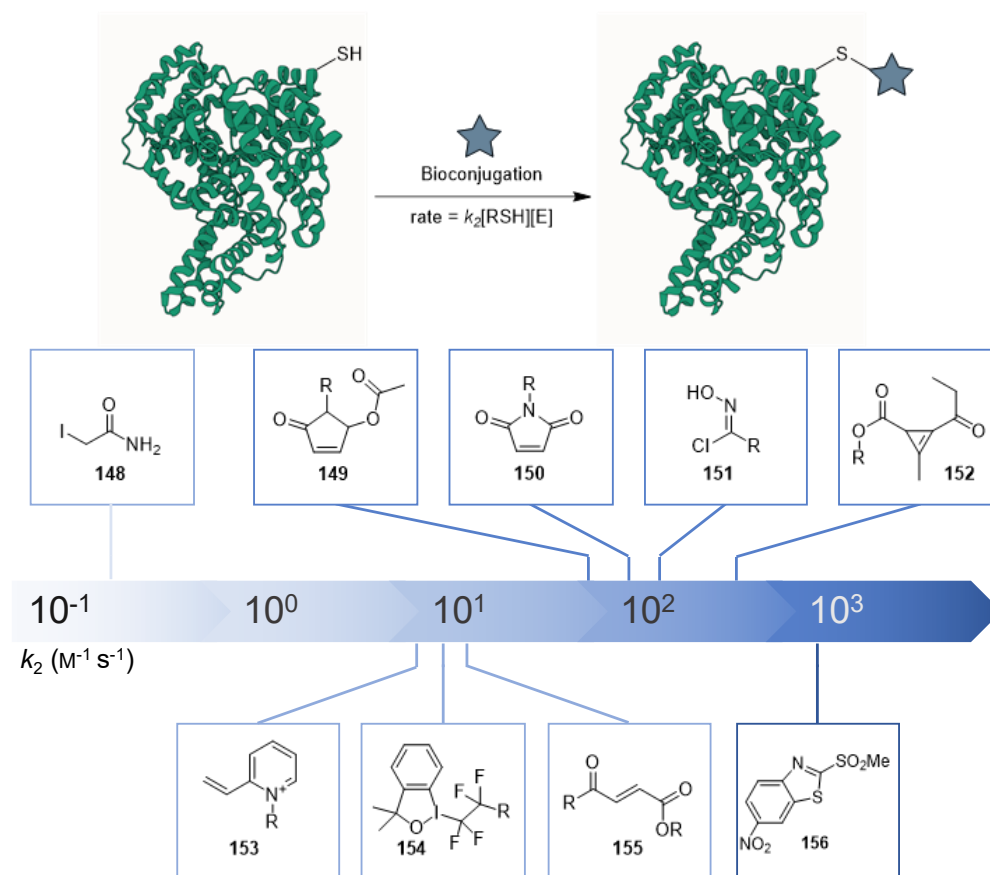
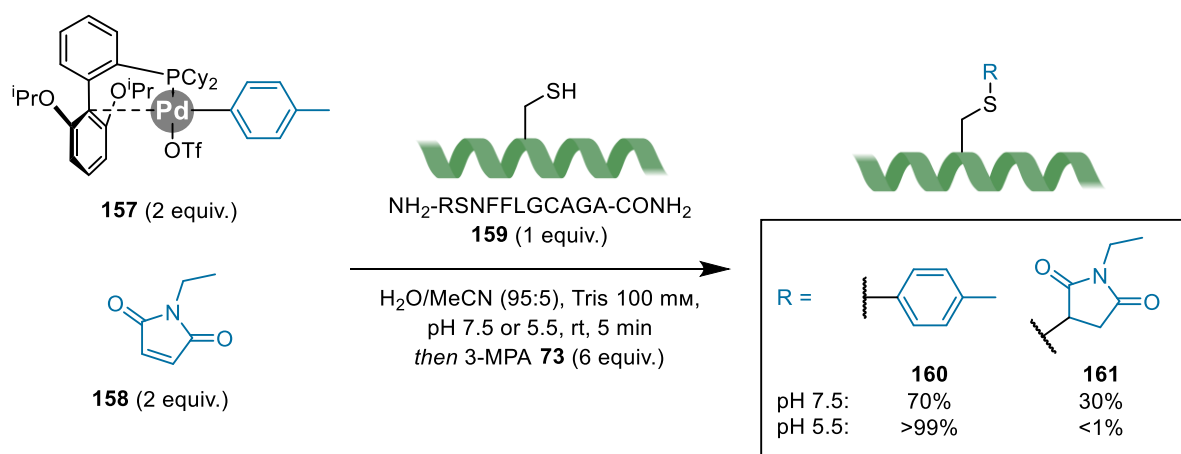


Figure 14: Overview of the second-order kinetics of recently published cysteine-selective reactive groups.

There have been a significant number of reagents developed which satisfy this definition of ‘fast’, whilst also complying to the stringent reaction conditions required by biomolecules: aqueous conditions, neutral pH, and a temperature below 37 °C (Figure 14). Of the popular internal cysteine-selective reactive groups, iodoacetamides (**148**) have the slowest kinetics ($k_2 \approx 0.6 \text{ M}^{-1} \text{ s}^{-1}$),¹⁵⁵ requiring long reaction times and a large excess of labelling reagent. Maleimides (**150**) ($k_2 \approx 10^2 \text{ M}^{-1} \text{ s}^{-1}$)²¹ are often used as the benchmark for comparing cysteine-selective bioconjugation techniques to, with the rate of bioconjugation being two to three orders of magnitude larger than iodoacetamides. Other reagents displaying favourable kinetics include *N*-alkylated vinylpyridines (**153**),¹⁵⁶ hypervalent iodine reagents (**154**),^{157,158} carbonylacrylic reagents (**155**),¹⁵⁹ 4-substituted cyclopentenones (**149**),^{160,161} chlorooximes (**151**),¹⁶² cyclopropenyl ketones (**152**),¹⁶³ and heteroaromatic sulfones (**156**).¹⁶⁴

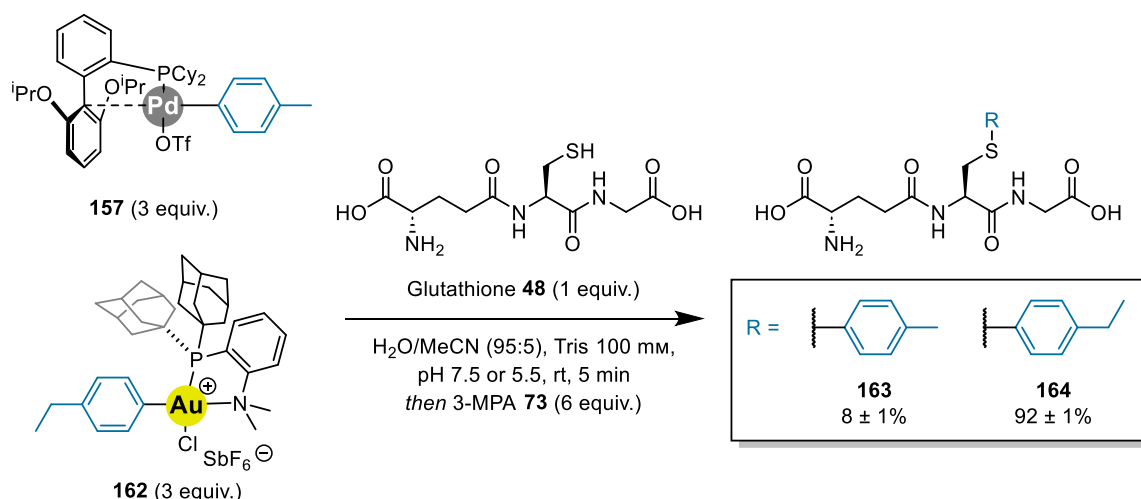
Despite the extensive work investigating the kinetics of cysteine-selective bioconjugation methodologies, the kinetics of recently reported transition-metal-mediated bioconjugation processes (namely the Pd(II) complexes from Buchwald⁷⁴ and Au(III) reagents from Spokoyny⁹⁶) are unknown. Both methodologies boast cysteine arylation that

proceeds to quantitative conversion in fewer than five minutes at micromolar concentrations. In the initial report of their Pd(II) methodology, the Buchwald lab report an estimate of the second order rate constant of their cysteine arylation process to be in the same order of magnitude as maleimide conjugation, which is generally reported around $10^2 \text{ M}^{-1} \text{ s}^{-1}$. They achieved this using a competition experiment (Scheme 52), showing the ratio of arylated cysteine (**160**) to maleimide-labelled cysteine (**161**) was 70:30 in favour of arylated cysteine, when an equal excess of *N*-ethyl maleimide (**158**) and Pd(II) complex (**157**) was used at pH 7.5. Conversely, at pH 5.5, >99% of the product was a result of bioconjugation with the Pd(II) reagent, resulting from the very low reaction rate of maleimides under acidic conditions. However, it is very difficult to form meaningful conclusions from this data, as the formation of the cysteine-maleimide conjugate is known to be reversible *via* a retro Michael addition,¹⁶⁵ whereas the arylation using OACs is irreversible. This could result in a ratio of products that is unrepresentative of the relative kinetics of the two systems.



Scheme 52: Competition experiment between *N*-ethylmaleimide **158** and Pd(II) complex **157** for cysteine bioconjugation. Yields determined by LC-MS.

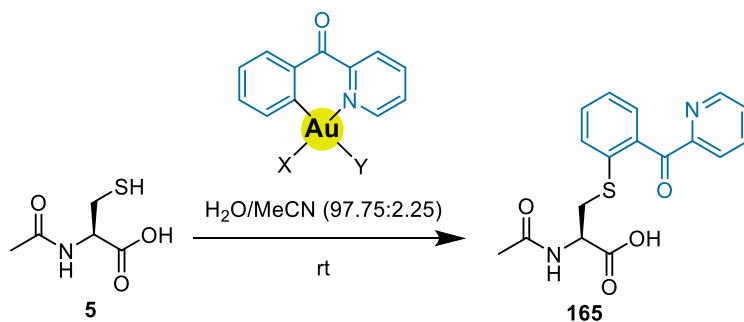
Previous work in the Spokoyny lab also employed the use of a competition experiment to estimate the second order rate constant of their bioconjugation methodology (Scheme 53). In a competition experiment of Au(III) complex **162** *versus* Pd(II) complex **157**, 92% of the arylation product of glutathione (**48**) was the result of reaction with Au(III) complex **162**, suggesting the value of the second order rate constant may be an order of magnitude larger than that of the Pd(II) reagents, around $10^3 - 10^4 \text{ M}^{-1} \text{ s}^{-1}$.



Scheme 53: Competition experiment between Au(III) complex and Pd(II) complex for cysteine bioconjugation. Yields determined by LC-MS.

The results of these two competition experiments clearly place Pd(II) and Au(III)-mediated cysteine *S*-arylation processes and being among the fastest, if not the fastest, bioconjugation reactions in the literature today. However, unlike the more traditional Michael-acceptor chemistry of maleimides and many of the other reagents depicted in Figure 14, there is likely a significant difference in mechanism (and therefore rate-limiting step) of organometallic reagents. A full assessment of a structure-activity relationship of these complexes coupled with accurate measurement of their rate constants is certainly necessary to allow meaningful conclusions to be drawn.

In 2021, Gukathasan *et al.* reported numerical values for the kinetics of cysteine *S*-arylation using cyclometallated Au(III) species (Scheme 54).⁹⁵ Using UV/vis spectroscopy, they assessed the reaction rate of cyclometallated complexes with *N*-acetylcysteine (**5**) in aqueous conditions with 2.25% added MeCN at room temperature. The limitations of their equipment meant that the fastest rate measured was that of complex **168** ($k_2 = 110 \text{ M}^{-1}\text{s}^{-1}$), which is roughly on par with the kinetics of the thiol-maleimide process (Table 16). Compound **173** showed kinetics that were too rapid to be measured using their UV/vis assay. Overall, the limited number of published studies show that a more detailed assessment of the kinetics of Au(III) and Pd(II)-based systems is necessary to further understand them, and could serve to guide their applications.



Scheme 54: Ligand effects of the rate of bioconjugation of cyclometallated Au(III) complexes.

Entry	X =	Y =	$k_2/\text{M}^{-1}\text{s}^{-1}$
1	Cl	Cl (168)	110
2	Br	Br (169)	68
3	I	I (170)	66
4	N ₃	N ₃ (171)	8
5	SCN	SCN (172)	47
6	Cl	acac (173)	“ultrafast”

Table 16: Second order rates of bioconjugation for cyclometallated Au(III) complexes determined with UV/vis spectroscopy.

4.2. Aims

The primary objective of this project was to interrogate the kinetics of Au(III)-based systems for bioconjugation and to gain further understanding into what affects the kinetics of these systems, including ligand electronics and steric demand, as well as the electronics and steric demand of the aryl group.

4.3. Results and Discussion

4.3.1. Studying Kinetics *via* Competition Experiments

With the goal of creating two Au(III)-based arylation complexes that had vastly different kinetics whilst still maintaining high cysteine selectivity in mind, the first avenue of investigation was to use competition experiments to compare the relative rates of Au(III) complexes. Despite competition experiments not producing quantitative kinetic data, qualitative comparisons between different cysteine-reactive compounds would allow a relative reactivity scale to be produced in a high-throughput manner.

Initial investigations began by varying the alkyl groups on the phosphorous ligands of the Au(III) complexes (Figure 15). Me-DalPhos (**172**) has been the standard ligand used for Au(III)-mediated cysteine *S*-arylation.⁹⁶ Previous work in the group used 2-(di(*tert*-

butyl)phosphino)-*N,N*-dimethylbenzenamine (**173**) as the optimal ligand for the construction of hybrid peptide-based assemblies,⁹⁸ thus this was chosen alongside 2-(dicyclohexylphosphino)-*N,N*-dimethylbenzenamine (**174**) for competition experiments *versus* complexes derived from Me-DalPhos (**172**). Varying the substitution at nitrogen was not explored in this instance due to the synthetic tractability of the ligands, as **172**, **173**, and **174** were all accessed from a single synthetic transformation from a common intermediate. Once the corresponding Au(III) complexes of **172**, and **173** are synthesised, they are reported to be storable for over six months,⁹⁸ and it is likely that the complex of ligand **174** exhibits the same stability.[†]

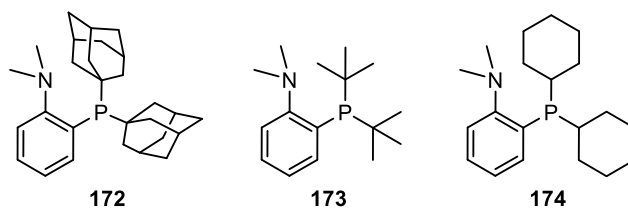
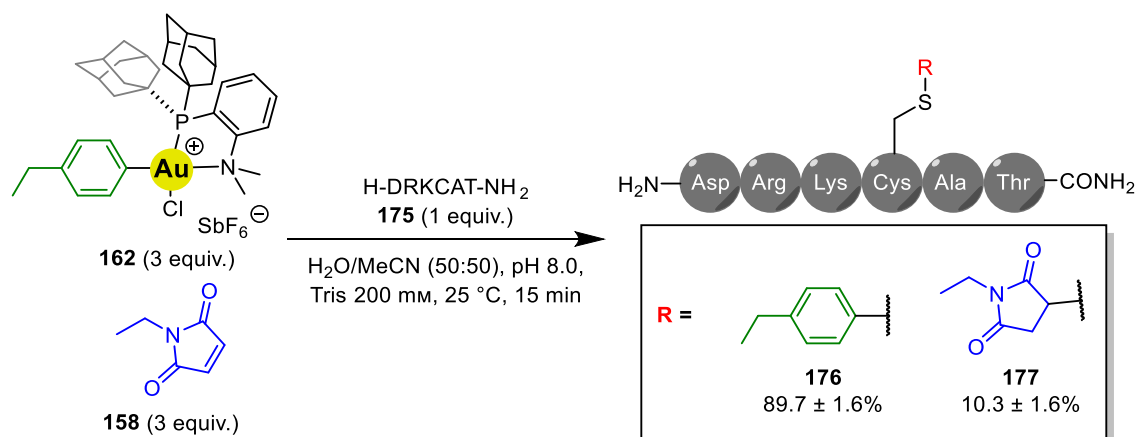


Figure 15: Ligands used for competition experiments: Me-DalPhos (**172**), 2-(di(*tert*-butyl)phosphino)-*N,N*-dimethylbenzenamine (**173**), and 2-(dicyclohexylphosphino)-*N,N*-dimethylbenzenamine (**174**).

The peptide chosen for the competition experiments, H-DRKCAT-NH₂ (**175**) has been previously used within the group for assessment of bioconjugation efficiency and selectivity,¹⁰¹ thanks to its nucleophilic cysteine, lysine, and threonine moieties, and was therefore used for all competition experiments detailed herein. The first competition experiment assessed the selectivity of Me-DalPhos-ligated Au(III) complex **162** compared to *N*-ethylmaleimide (**158**) to serve as a baseline. Experiments were performed in triplicate at pH 8.0 in H₂O/MeCN (50:50) at room temperature for 15 minutes before being diluted with 0.1% TFA in H₂O and analysed by LC-MS. Integration of the Total Ion Chromatogram (TIC) peaks corresponding to the product of each bioconjugation reagent was used to determine their relative ratios, which were averaged over three runs allowing calculation of the standard error of the mean (Scheme 55).[‡]

[†] Ligands **172** and **174** synthesised by Dr Evan Doud (UCLA).

[‡] All competition experiments in this chapter performed by Dr Evan Doud (UCLA).



Scheme 55: Competition experiment between Au(III) complex **162** and N-ethylmaleimide (**158**), labelling peptide **175**. Yields determined by LC-MS (Section 5.7.3).

The ratio of **176** to **177** was higher than the ratio of the product arising from Pd(II) complex (**160**) to maleimide product (**161**) in the similar competition experiment carried out by Buchwald (Scheme 53). This is consistent with the suggestion that the Au(III) systems exhibit faster kinetics of cysteine *S*-arylation than Pd(II) complexes. However, it is worth noting that these experiments were carried out at pH 8.0 instead of pH 7.5 as in Buchwald's experiments, and the maleimide-thiol reaction is known to exhibit a strong positive pH dependence on reaction rate.¹⁶⁶ Inspection of the TICs of all three experiments showed that the only significantly ionisable products formed from the reactions were **176** and **177** (Figure 16). From this point onwards, all TICs can be found in 5.7.3, except if their discussion is warranted.

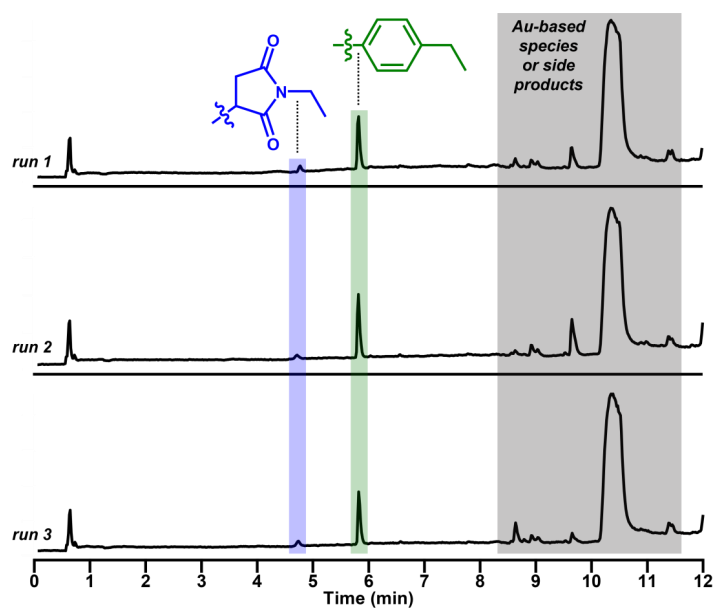
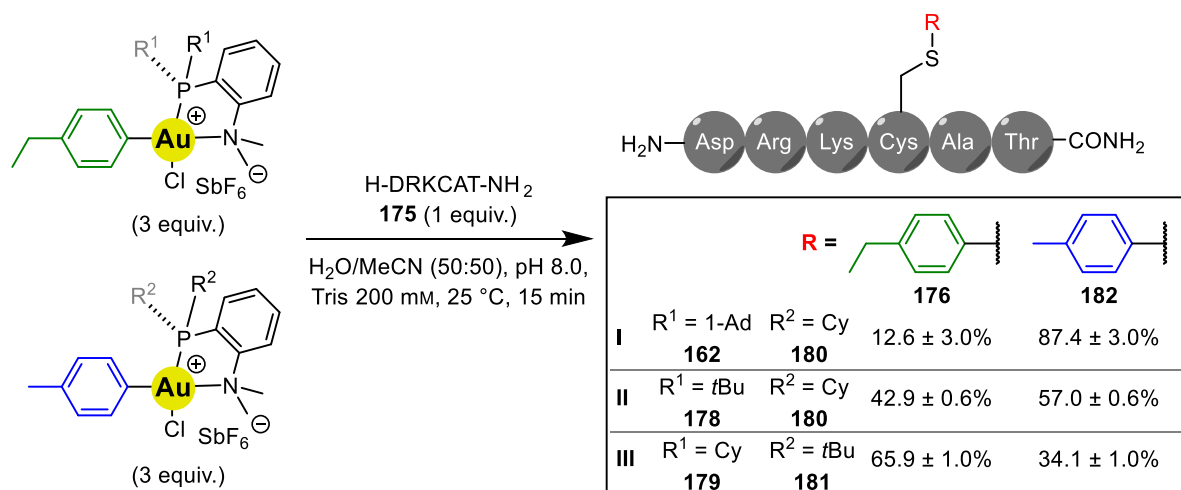


Figure 16: TICs of experiment from Scheme 55, run in triplicate.

Following this baseline experiment, the next step was the assessment of selectivity between Au(III) complexes ligated with the three ligand systems selected for this study, **172**,

173, or **174** (Scheme 56). Importantly, these experiments revealed a clear hierarchy between the arylation efficiency of the different *P*-substituted ligands: 1-adamantyl < *tert*-butyl < cyclohexyl, which likely mirrors the relative reaction kinetics for each complex. The largest difference in selectivity (13:87) was observed with competition experiments between **172**- and **174**-ligated systems (Scheme 56 entry I).

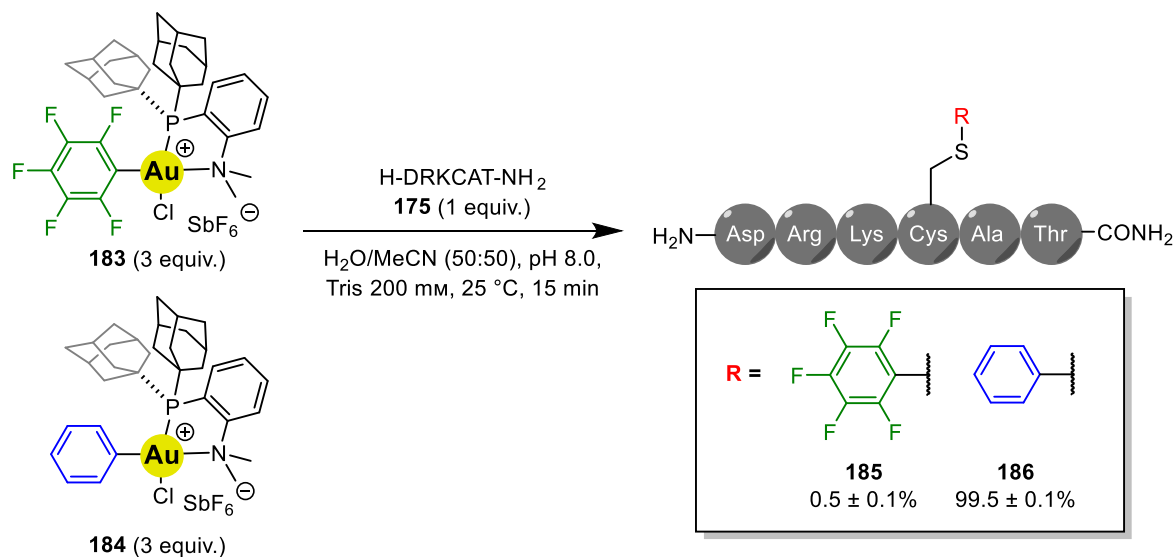


Scheme 56: Competition experiments between Au(III)-tolyl systems ligated with the three ligands shown in Figure 15. Yields determined by LC-MS (Section 5.7.3).

Despite the selectivity achieved in variation of the ligand bound to Au(III), work continued in order to gain sufficient control over bioconjugation rate to achieve >99% selectivity towards a single product in competition experiments. Therefore, the next step was to investigate the effect of aryl group substitution. This can be achieved in two ways: firstly, addition of steric bulk *ortho*- to Au(III) should slow the reaction rate by hindering the attack of the cysteine thiol, provided that nucleophilic attack is involved in the rate-limiting step for the bioconjugation process. Secondly, it was postulated that using a highly electron deficient aryl ring should affect the reaction rate. However there is little literature evidence¹⁶⁷ to support whether this may accelerate the reaction, as would be expected for reductive elimination from Pd(II)-Ar complexes,^{168,169} or retard the reaction.

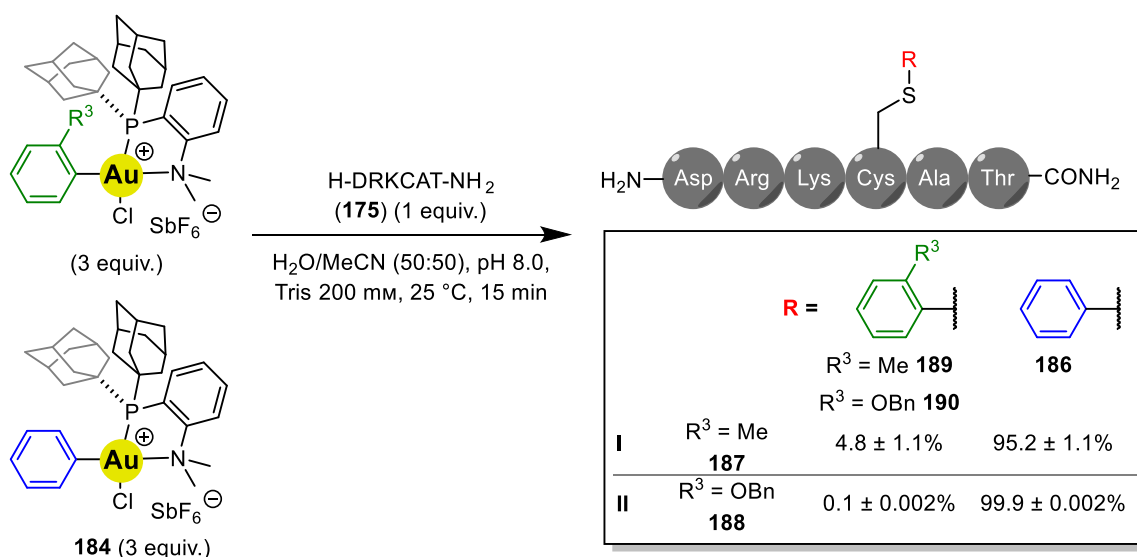
To assess the effect of electronics, pentafluoroaryl Au(III) complex **183** was synthesised from commercially available iodopentafluorobenzene. The competition experiment of **183** *versus* the corresponding phenyl Au(III) compound **184** showed remarkable selectivity in favour of the phenyl-labelled peptide **186**, suggesting the reaction rate is significantly slowed by electron-deficient arenes (Scheme 57). Pleasingly, despite the ability of perfluoroarenes to undergo S_NAr processes,¹⁷⁰ the LC-MS data for these competition experiments showed just product **185** and **186**, and no other ionisable side-products were detected. This is likely due to the S_NAr reaction between cysteine and

perfluoroaryl species likely being much slower than the Au(III)-mediated cysteine S-arylation.¹⁷¹



Scheme 57: Competition experiment between pentafluoro Au(III) complexes **183** and **184**.

The effect of steric hinderance on bioconjugation selectivity (Scheme 58) was then assessed. Reacting *ortho*-tolyl complex **187** in the presence of phenyl complex **184** gave a high degree of selectivity, with around a 95:5 ratio of **186** to **189**. An even larger difference was observed with *ortho*-oxybenzyl substituted compound **190**, which gave just 0.1% of the arylated product when used in competition with compound **184**. The more sterically demanding *ortho*-oxybenzyl can therefore be implied to have the slowest rate of bioconjugation of all the synthesised Au(III) ligands.



Scheme 58: Competition experiments assessing the effect of adding steric bulk to the aryl ring of Au(III) complexes for bioconjugation. Yields determined by LC-MS (Section 5.7.3).

Further competition experiments (section 5.7.3) enabled the elucidation of relative reactivity of the discussed Au(III) complexes, along with Pd(II) complex **157** (Figure 17).

As *N*-ethylmaleimide was used as a benchmark, compounds **157**, **184**, **42**, **163**, **181**, **178**, **180** and **179** likely possess second order rate constants of at least $10^2 \text{ M}^{-1} \text{ s}^{-1}$, with the rate constants of **183**, **187** and **188** being lower. However, it is not possible to use the ratios of products used in competition experiments to calculate numerical values for the rate constants for two reasons: firstly, this would assume similar mechanisms for the cysteine-maleimide and metal-mediated bioconjugation reactions, which is discussed in more detail below. Secondly, the competition experiments were not carried out in pseudo first-order conditions, making the rate equation for the consumption of peptide insoluble.

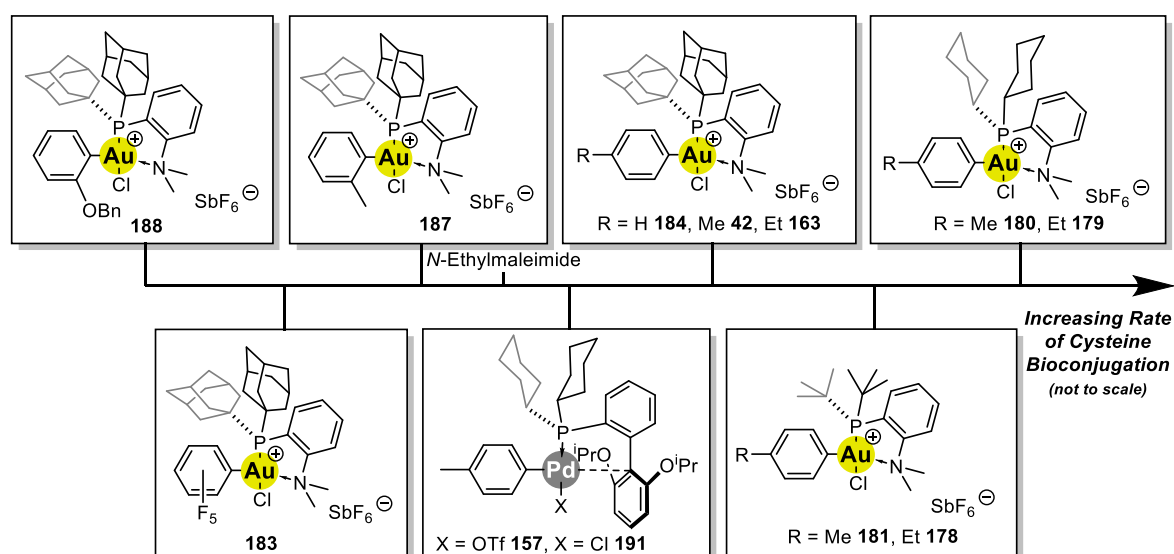


Figure 17: Relative rates of metal-mediated cysteine bioconjugation technologies.

4.3.2. Stopped-Flow Kinetics

With competition experiment data in hand implying a large range in second order rate constant of the various Au(III) arylation complexes, the next step was to collect quantitative data relating to the reaction rates. Examples in the literature popularly employ one of three methods to measure bioconjugation kinetics. The simplest from an experimental standpoint is to run repeats of reactions and quench at known timepoints, followed by LC-MS analysis to calculate yields and allow time *versus* conversion graphs to be constructed.¹⁷² Another common method is to monitor conversion over time using UV-vis or fluorescence experiments, where the bioconjugation reaction is often performed inside a cuvette.^{164,173,174} Whilst both of these techniques are effective for reactions that may take minutes to proceed to completion, they do not offer the data collection speed at a suitable signal-to-noise ratio for the fast metal-mediated processes being studied herein (which proceed to full conversion in less than one minute). These fast reactions cannot be performed in cuvettes, as the variable mixing time would cause significant error in measured reaction rate. Hence, for very fast

bioconjugation processes, examples in the literature^{163,164} use stopped-flow/UV-vis spectrometers owing to their extremely fast sampling rate, and ability to ensure rapid and complete mixing of stock solutions.

Since its inception in the early 1950s,^{175,176} stopped-flow has become a mainstay technique for studying chemical kinetics, finding particular use in enzyme-catalysed processes. Stopped-flow spectrometers (Figure 18) can rapidly mix two reactant solutions and transfer them to an optical cell within one millisecond. The instrument achieves this by simultaneously plunging syringes containing reaction solution with a drive piston. The two reaction solutions then enter a mixing cell designed to ensure complete mixing, before flowing to the observation point. Flow stops when the plunger of the stopping syringe hits the trigger, which also sends a signal to the computer to start collecting data from the detector. In this case, the light source and detector are set up for measurement of UV/vis data.

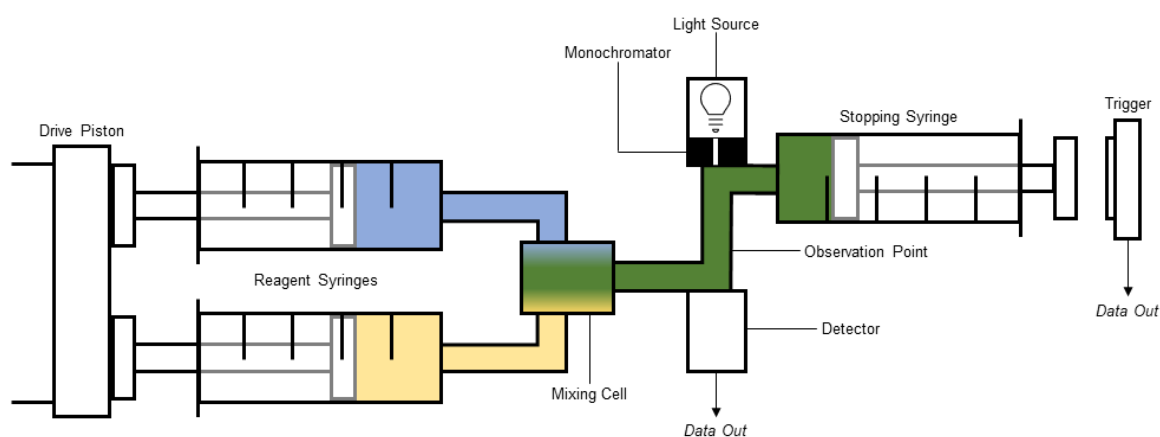
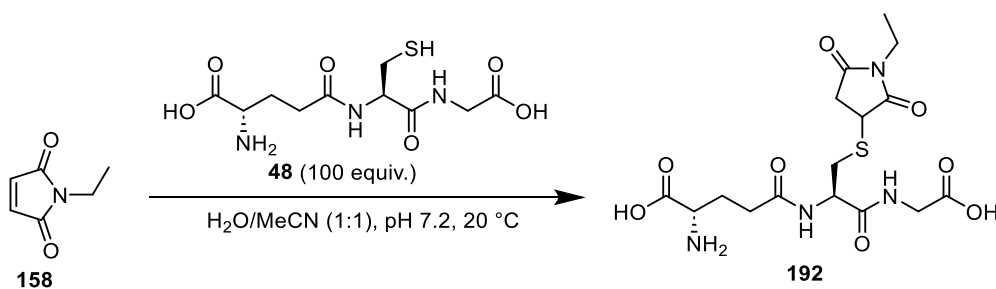


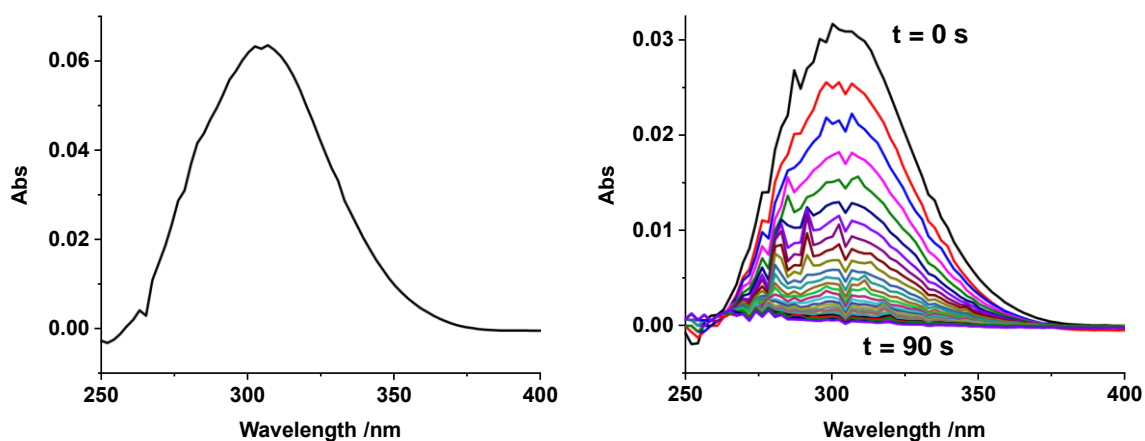
Figure 18: Schematic of a stopped-flow spectrometer.

4.3.2.1. Maleimide Cysteine Bioconjugation Kinetics

To validate that stopped-flow was a suitable method for the measurement of bioconjugation reactions with Pd(II) and Au(III) complexes, the method was validated with the reaction of *N*-ethylmaleimide (**158**) with glutathione (**48**). First, the photodiode array (PDA) was used to collect qualitative data of how the full UV/vis spectrum evolved over the course of the reaction, to ensure there was an appreciable change in absorbance of the sample at the concentrations used for bioconjugation reactions. One syringe was loaded with 10 μM *N*-ethylmaleimide (**158**) in reaction buffer ($\text{H}_2\text{O}/\text{MeCN}$ 50:50, 100 mM Tris pH 7.2), and the other syringe loaded with 1 mM glutathione (**48**) in reaction buffer (Scheme 59). This large excess of glutathione ensured pseudo first-order conditions.

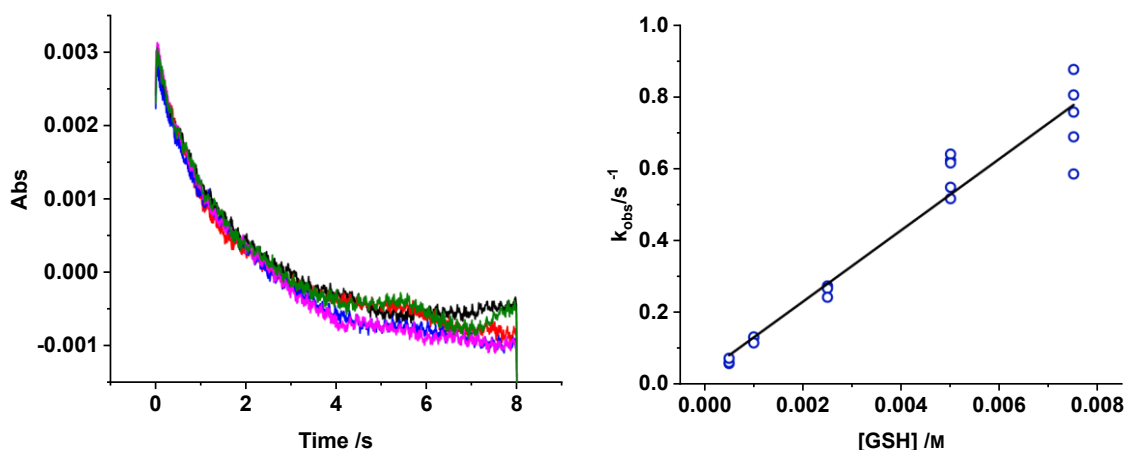


Scheme 59: Reaction of *N*-ethylmaleimide with glutathione in stopped-flow.



Graph 3: UV/vis spectra collected using Applied Photophysics SX-20 with PDA accessory. **Left:** 10 μM *N*-ethylmaleimide (**158**) in $\text{H}_2\text{O}/\text{MeCN}$ (50:50) buffered to pH 7.5 with 100 mM tris. Spectra: 1. Sample period: 1 ms. Samples per spectrum: 1000. **Right:** 10 μM *N*-ethylmaleimide (**158**) plus 1 mM GSH in $\text{H}_2\text{O}/\text{MeCN}$ (50:50) buffered to pH 7.4 with 100 mM tris. Reaction time: 90 s. Spectra: 30. Sample period: 1 ms. Samples per spectrum: 3000.

The spectrum of *N*-ethylmaleimide (**158**) in reaction buffer (Graph 3 left) showed a clear peak at around 300 nm arising from the conjugated alkene, consistent with literature reports.¹⁷⁷ When the reaction was performed with glutathione under stopped-flow conditions, this peak disappeared over the course of 90 seconds (Graph 3 right), indicating the loss of the maleimide double bond and the formation of **192**. Whilst effective as a qualitative confirmation of spectral change, the use of the PDA was not appropriate for collection of kinetic data, as the results did not have satisfactory signal-to-noise at the collection rate that would be required for faster reactions. To overcome this issue, kinetic data was collected using the Absorbance Photomultiplier accessory for the instrument, which samples eighty times faster than the PDA, but only at a single wavelength.



Graph 4: **Left:** Absorbance at 300 nm of reaction between 10 μ M *N*-ethylmaleimide (**158**) and 10 mM glutathione over 8 seconds with five repeats represented by separate colours. **Right:** Linear plot of pseudo first-order rate constants for the reaction of 10 μ M *N*-ethylmaleimide (**158**) with 1.0, 2.0, 5.0, 10, 15 mM glutathione. Measured second order rate constant: $k_2 = 99.3 \pm 6.1 \text{ M}^{-1}\text{s}^{-1}$.

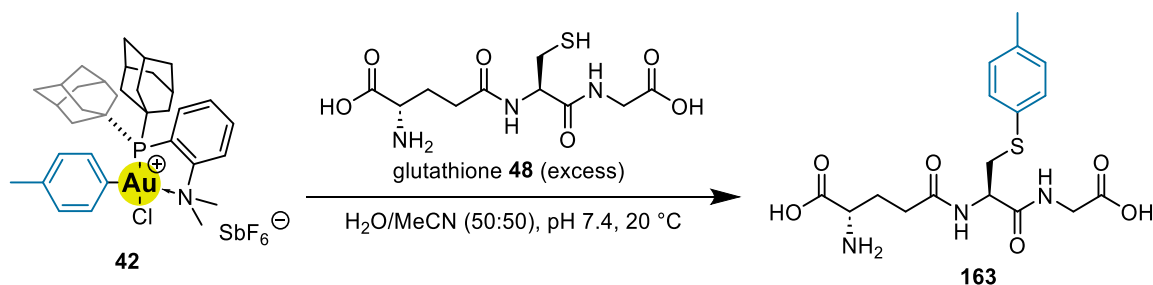
Monitoring the reaction of 10 μ M *N*-ethylmaleimide with concentrations of glutathione ranging from one mM to 15 mM revealed a decrease in absorbance at 300 nm over time (Graph 4 left), corresponding to the loss of the maleimide double bond. Fitting these curves to $e^{-k_{obs}t}$ produced pseudo first-order rate constants (k_{obs}) for the reaction at each concentration at glutathione, which could then be plotted according to $k_{obs} = k_2[\text{Glutathione}]$ (Graph 4 right) to obtain the second-order rate constant for the reaction (k_2), which was calculated as $99.3 \pm 6.1 \text{ M}^{-1}\text{s}^{-1}$. This is consistent with literature reports,²¹ and gave validation that monitoring bioconjugation processes with stopped flow would produce accurate rate constant values.

4.3.2.2. Metal-Mediated C-S Arylation

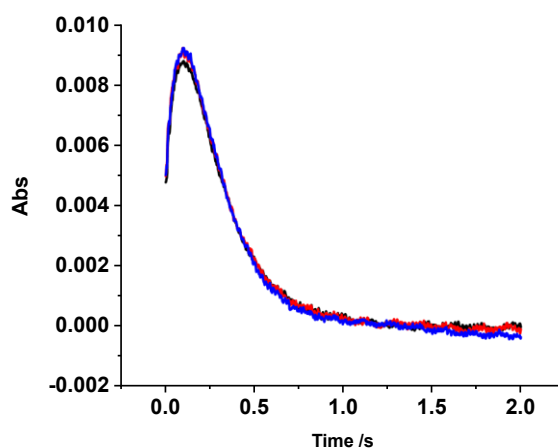
With stopped-flow identified as a suitable method for assessing the rate of glutathione bioconjugation with maleimide, the rates of *S*-arylation with metal complexes were investigated. The proposed mechanism for this process is as follows: first, the cysteine thiol coordinates to the metal centre, followed by deprotonation to form a metal-thiolate complex, and then reductive elimination to form a new C-S bond. For cysteine *S*-arylation with Au(III) complexes, this was corroborated by DFT studies in 2019 by Zhang and Dong.⁹⁷ These DFT studies report that the rate limiting step in the Au(III)-mediated bioconjugation is the reductive elimination.

Initial experiments involved collecting full absorption spectra of reactions between the various organometallic complexes and glutathione in stopped-flow to confirm there was an appreciable wavelength change, and these data can be found in **5.7.4.1**. Next, the reaction of organometallic complexes with glutathione monitored using the Absorbance Photomultiplier at a single wavelength. Compound **42** was the first to be studied

(Scheme 60), showing an exponential decrease in absorption over around three seconds was observed (Graph 5), and no further change was observed when the reaction was monitored for a further 15 minutes, suggesting full consumption of Au(III) complex. In general, stopped flow experiments were performed using at least three different concentrations of glutathione, with a minimum of three repeats at each concentration.

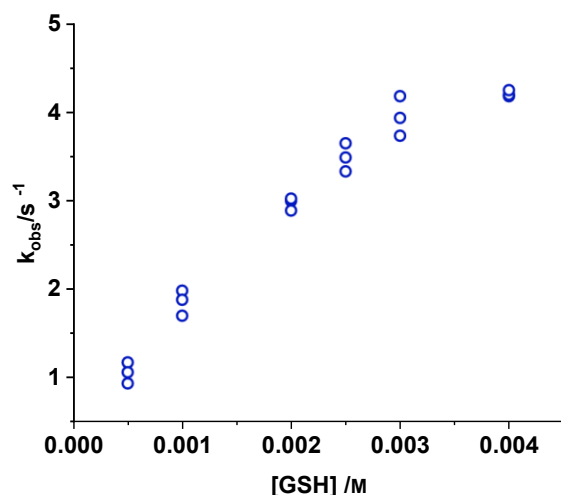


Scheme 60: Reaction of **42** with glutathione in stopped flow.



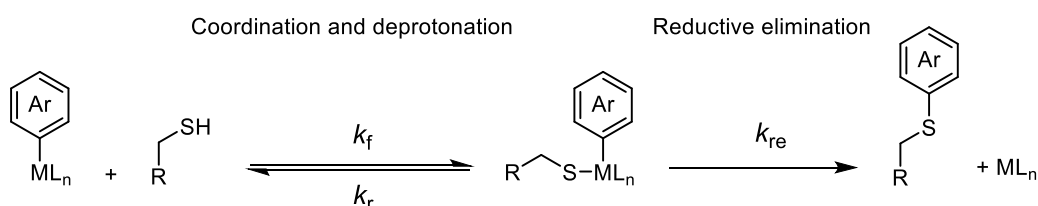
Graph 5: Absorbance at 330 nm of reaction between 10 μM **42** and 8 mM glutathione over three seconds with three repeats represented by separate colours.

Plotting the observed pseudo first-order rate constants (k_{obs}), which were obtained by fitting the absorbance data according to $e^{-k_{\text{obs}}t}$, against the concentration of glutathione showed a non-linear relationship (Graph 6), suggesting more complexity to the mechanism compared with the maleimide-thiol reaction.



Graph 6: Plot of k_{obs} against glutathione concentration for the observed wavelength change for the reaction in Scheme 60.

Based on kinetic analysis for reactions with rapid pre-equilibria,¹⁷⁸ a slightly simplified mechanism for Au(III)-mediated arylation was considered, in which coordination and deprotonation are treated as one reversible pre-equilibrium (Scheme 61).



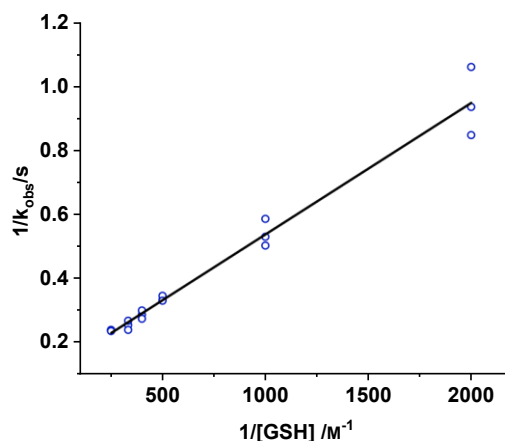
Scheme 61: Proposed mechanism for bioconjugation with metal complexes. $R-SH = \text{Glutathione}$.

Using the mechanism from Scheme 61, it is possible to solve the rate equation and obtain values for the first-order rate constant corresponding to reductive elimination, as well as the equilibrium constant for the formation of the metal-thiolate complex (Equation 1). The key assumption of Equation 1 is that the rate of equilibrium formation, $k_{eq} (= k_f + k_r)$ is much larger than the rate of reductive elimination.

$$\frac{1}{k_{obs}} = \frac{1}{k_{re}} + \frac{1}{k_{re}K[\text{Glutathione}]}$$

Equation 1: Calculation of k_1 for a reaction with pre-equilibrium. k_{obs} = observed pseudo first order rate constant, $K = k_f/k_r$.

Plotting k_{obs} for the reaction of **42** with glutathione according to Equation 1 demonstrated a linear relationship (Graph 7). It can therefore be concluded that the change in absorbance observed (Graph 5) is likely result of reductive elimination.



Graph 7: Plot of observed kinetic data for the reaction of **42** with glutathione according to Equation 1.

From Graph 7, the values for equilibrium constant, K , and rate of reductive elimination, k_1 , for the reaction of **42** with glutathione were calculated as $306 \pm 50 \text{ M}^{-1}$ and $7.92 \pm 0.98 \text{ s}^{-1}$, respectively. The stopped-flow kinetics experiments were then performed in an analogous fashion for glutathione bioconjugation with all the complexes discussed in **5.7.3**, and the pre-equilibrium constants (K) and rate constant for reductive elimination (k_1) estimated in each case (Figure 19).

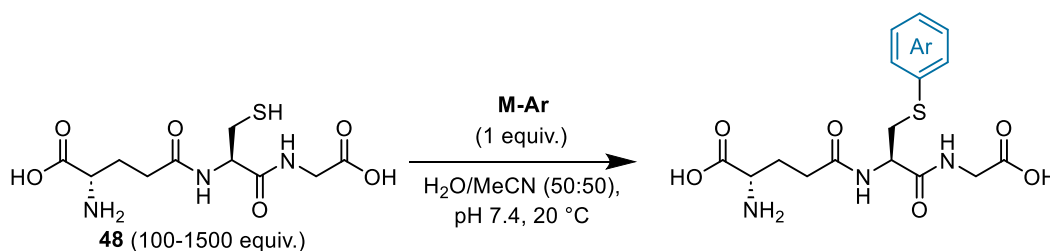


Figure 19: Reactions for assessing reductive elimination kinetics in stopped flow.

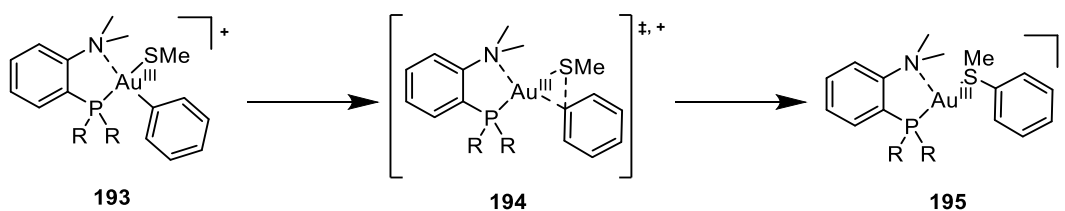
Entry	M-Ar =	K / M^{-1}	k_{re} / s^{-1}
1	191	701 ± 27	0.122 ± 0.0027
2	42	306 ± 50	7.92 ± 0.98
3	181	1260 ± 78	4.32 ± 0.98
4	180	401 ± 55	1.28 ± 0.084
5	183	172 ± 38	0.0473 ± 0.0088
6	187	290 ± 14	0.0208 ± 0.00074
7	188	<i>Not measured</i>	<i>Not measured</i>

Table 17: Rates of reductive elimination for C-S arylation with Au(III) and Pd(II) complexes measured by stopped-flow.

The calculated rate of reductive elimination of the Pd(II)-RuPhos system **191** (Table 17 entry 1) was around sixty times slower than that of the Au-(Me-DalPhos) system **42**.

Varying the ligand on Au(III) showed a clear dependence on steric bulk, with Me-DalPhos (Table 17 entry 2) having the fastest rate of reductive elimination, followed by the *tert*-butyl derivative (Table 17 entry 3), and then the cyclohexyl (Table 17 entry 4).

This selectivity is consistent with the mechanism computed by Zhang and Dong⁹⁷ (Scheme 62), as transition state **194** will offer relief in the steric interactions between the ligand and substrate, resulting in a lower activation energy for the reductive elimination pathway.



Scheme 62: Calculated mechanism for reductive elimination from Au(III)-thiolate complexes.

Pentafluoroaryl Au(III) species **183** demonstrated a rate of reductive elimination two orders of magnitude lower than **42**, suggesting reductive elimination from Au(III)-aryl complexes is significantly retarded by electron deficient aryl groups. This appears to be contrary to reductive elimination from Pd(II) to form carbon-heteroatom bonds, where general consensus is that a more electron deficient aryl substrate will accelerate rate.¹⁶⁸ There have been no studies on substituent effects in Au(III) C-S bond forming reactions, however, DFT calculations[‡] suggested a larger change in Gibbs free energy between the Au(III)-thiolate complex and transition state for the reductive elimination of **183** compared to **184** (Figure 20).

[‡] ωB97X-D/6-311+G(d,p), SDD, CPCM(Water)//B3LYP-D3/6-31G(d), lanl2dz, CPCM(Water). Unpublished work. DFT calculations performed by Billy Treacy (UCLA).

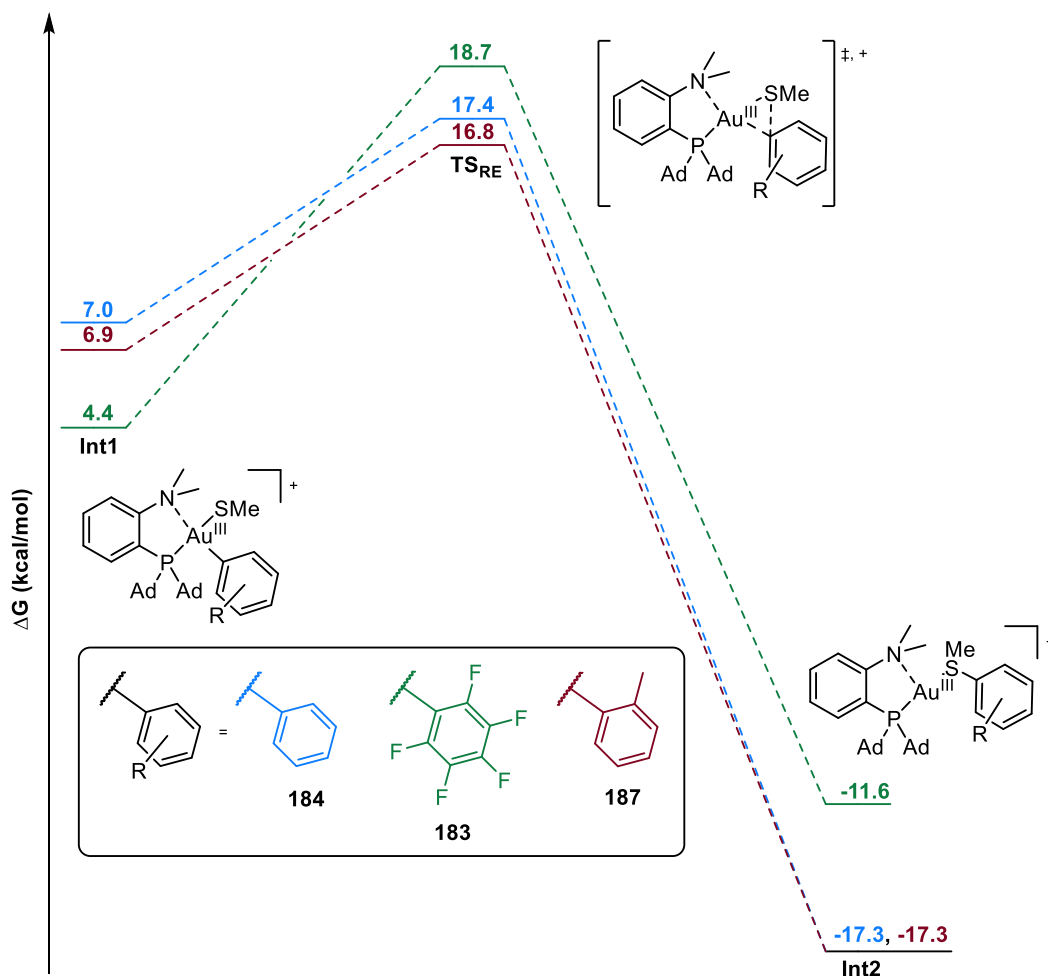


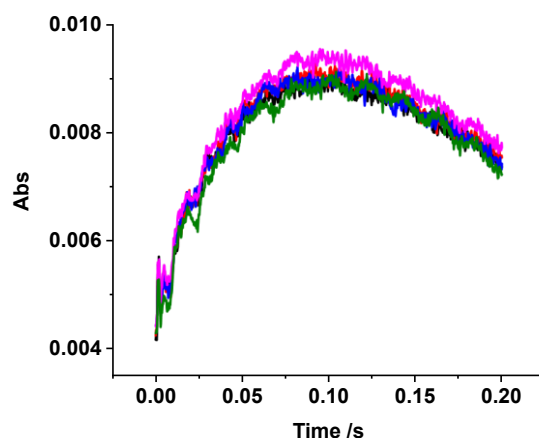
Figure 20: Energy diagram for the reductive elimination pathway from Au(III)-thiolate complexes, varying substituent.

The very slow reductive elimination for the reaction with **187** (Table 17 entry 6) is surprising, as the observed slow rate of **187** in competition experiments was postulated to arise from the additional steric bulk preventing the initial coordination of the thiol to the Au(III) centre. The calculated Gibbs free energy difference between **Int1** and **TS_{RE}** for **187** also does not explain the slower rate of reductive elimination compared to **183**. The most likely explanation for this is that the kinetic model used to obtain k_{re} is not valid in this case, as the reductive elimination may no longer be the rate-limiting step.

With the rates of reductive elimination of Pd(II) and Au(III) complexes determined *via* stopped flow, it was noted that there was a disagreement with the results of the competition experiments. Notably, in the competition experiments, **180** had the highest relative reactivity, yet the rate of C-S reductive elimination was measured to be slower than **42** and **181**. Thus, the next course of investigation was to measure the rate of thiol coordination to these metal complexes.

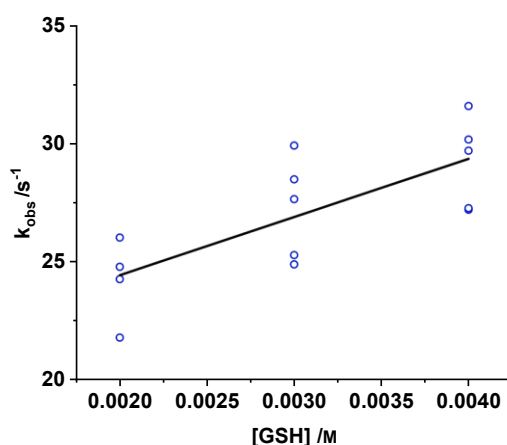
For the reaction of **42** with glutathione, a clear change in absorbance was noted between zero and 0.2 seconds (Graph 8). Stopped-flow experiments run at such short

timescales required a pressure hold in the instrument, where the pressure of the drive piston is not released for the duration of the run to prevent cavitation within the observation cell. As the change in absorbance was relatively small compared to the change observed for the reductive elimination, and the process occurs over a much shorter timescale, the signal-to-noise was much greater for these data.



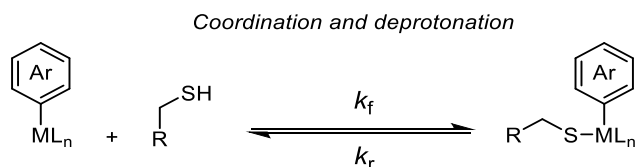
Graph 8: Absorbance at 330 nm of reaction between 10 μM **42** and 4 mM glutathione over 0.2 seconds with five repeats represented by separate colours.

The initial change from the absorbance data was then fitted to $e^{-k_{obs}t}$, producing the observed rate constant (k_{obs}) for the initial coordination step. As the initial coordination/deprotonation step is being treated as an equilibrium, this means that the initial increase in absorbance observed in Graph 8 corresponds to the pseudo-first order system reaching equilibrium, where $k_{obs} = [\text{Glutathione}]k_{eq}$, and $k_{eq} = k_f + k_r$. Therefore, plotting the concentration of glutathione *versus* the observed rate constant will yield k_{eq} (Graph 9).



Graph 9: Plot of k_{obs} against glutathione concentration for the observed wavelength change for the initial step of the reaction of **42** with glutathione.

Using k_{eq} determined from the gradient of Graph 9, the forward rate of the coordination/deprotonation equilibrium (Scheme 63) for each Au(III) complex could be calculated using $k_f = \frac{k_{eq}}{(1+\frac{1}{K})}$ (Table 18).

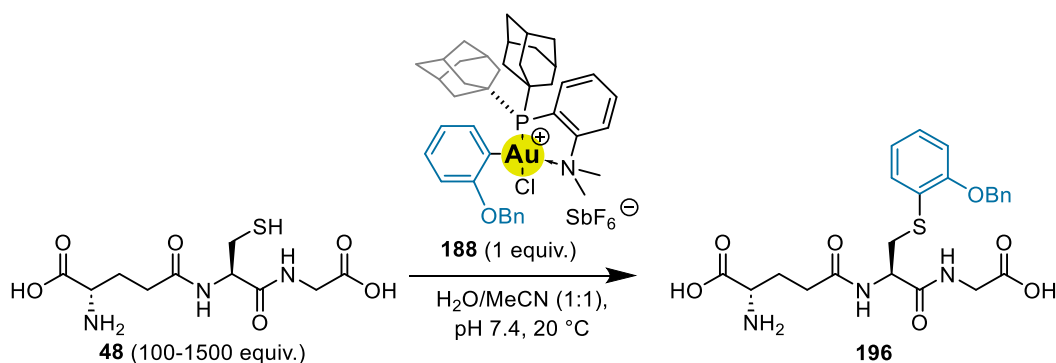


Scheme 63: Equilibrium for the coordination of cysteine thiol to metal complexes.

Entry	M-Ar =	$k_f / \text{M}^{-1}\text{s}^{-1}$	k_r / s^{-1}
1	191	2160 ± 260	3.08 ± 0.26
2	42	2460 ± 1300	8.33 ± 2.8
3	181	4220 ± 1100	2.99 ± 0.65
4	180	16600 ± 4900	41.3 ± 6.7
5	183	<i>Not measured</i>	<i>Not measured</i>
6	187	8950 ± 890	30.3 ± 3.0

Table 18: Rates of coordination of cysteine thiol to Au(III) and Pd(II) complexes measured by stopped-flow.

The rates of coordination, k_f , for compounds **42**, **180** and **181** explain the selectivity observed using competition experiments. Despite the rate of reductive elimination, k_1 , for **180** being approximately six times slower than for **42**, thiol coordination occurs almost seven times faster, resulting in the selectivity observed. The coordination event for **183** was not measured, it is possible that the highly electron deficient Au(III) leads to k_f being too large to be measured *via* stopped flow. The most interesting result of these experiments is **187** (Table 18 entry 6), the steric bulk from the *ortho*-tolyl should hinder the coordination of thiol to the Au(III) centre. Despite this, the coordination rate appears to be over four times larger than coordination to **42**. It is possible that the increased steric bulk from the aryl group causes the halide to dissociate, resulting in a far more electrophilic Au centre, and accelerating the rate of thiol coordination. However, this observation combined with the slow observed rate of reductive elimination is yet to be explained.



Scheme 64: Arylation of glutathione with 188.

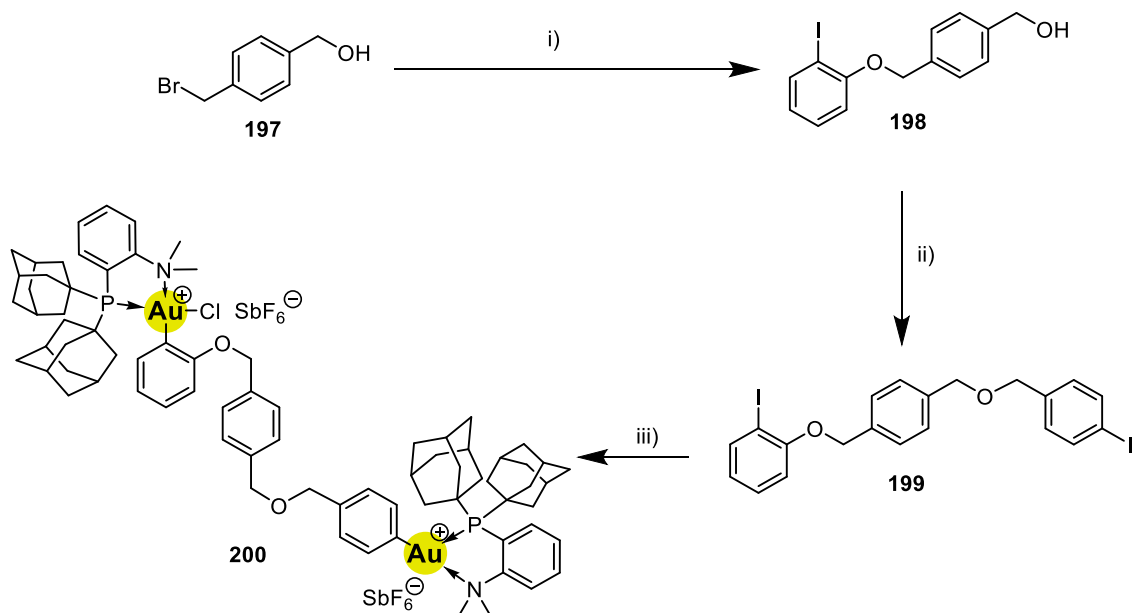
Thus far, the stopped-flow data for the discussed compounds has strongly supported a mechanism involving coordination followed by reductive elimination, which is rate-limiting. However, for the arylation with **188**, a single second order rate constant of $k_2 = 1.97 \pm 0.11 \text{ M}^{-1} \text{ s}^{-1}$ was obtained. This is likely a result of the extreme steric hinderance of the *ortho*-oxybenzyl group causing the rate-limiting step of this process to become the coordination, rather than the reductive elimination.

4.3.3. Synthesis of Biomolecule Heterostructures

4.3.3.1. Synthesis of Bimetallic Au(III) Species

With quantitative kinetic data covering a range of bioconjugation rates achieved through modification of the Au(III)-Ar species, the next course of investigation was to synthesise cross-coupled biomolecules to fully demonstrate rate control. To achieve this, a bimetallic Au(III) reagent was synthesised with Au(III)-Ar bearing an *ortho*-oxybenzyl moiety that was linked to a *para*-substituted Au(III)-Ar species which would, in theory, react more rapidly at the less hindered Au(III) centre. To this end, **200** was prepared in a three-step synthesis first by an $\text{S}_{\text{N}}2$ reaction between 4-(bromomethyl)benzyl alcohol (**197**) and 2-iodophenol to form **198**, then a second $\text{S}_{\text{N}}2$ between **198** and 4-iodobenzyl bromide to form **199**. **199** was then treated with 2.2 equivalents of silver hexafluoroantimonate and (Me-DalPhos)AuCl to yield bimetallic Au(III) species **200**.[‡]

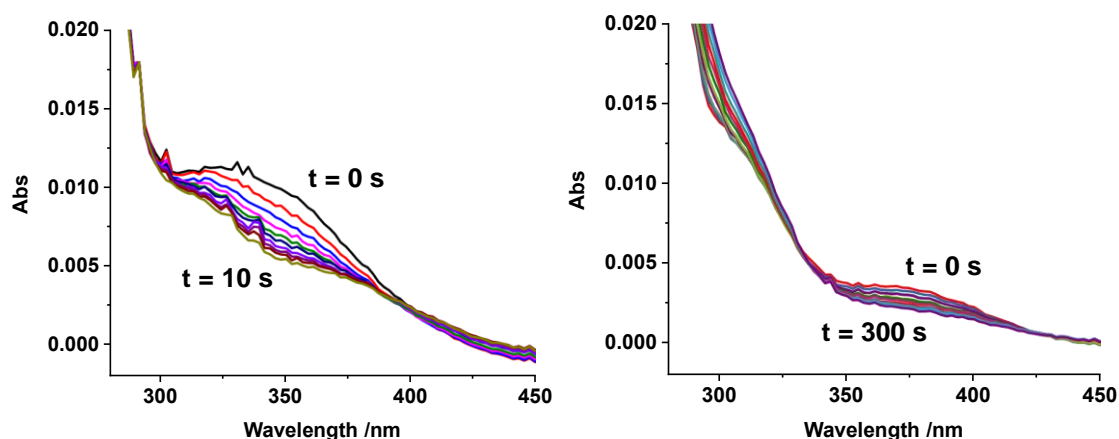
[‡] **198** and **199** prepared by Billy Treacy (UCLA), **200** prepared by Dr Evan Doud (UCLA).



Scheme 65: Three-step synthesis of bimetallic Au(III) species **200**. **Reagents and conditions:** i) 2-Iodophenol (1.1 equiv.), K_2CO_3 (1.2 equiv.), acetone, reflux, 20 h, 88%; ii) TBAB (0.3 equiv.), KOH (3 equiv.), 4-iodobenzyl bromide (2 equiv.), CH_2Cl_2/H_2O (3:1), 0 °C – rt, 20 h, 66%; iii) $AgSbF_6$ (2.2 equiv.), (Me-DalPhos)AuCl (2.2 equiv.), CH_2Cl_2 , -20 °C – rt, protection from light, 16 h, 79%.

4.3.3.2. Stopped-Flow Spectroscopy

Following the synthesis of **200**, its reactivity was initially qualitatively assessed by stopped-flow spectroscopy. One reagent syringe was loaded with a 10 μM solution of **200**, and the other was loaded with 1 mM glutathione, both in $H_2O/MeCN$ (50:50) buffered to pH 7.5 with 100 mM tris. Over a time period of ten seconds (Graph 10 left), a clear decrease in absorption around 250 nm was observed, whilst monitoring over a long time period of 300 seconds revealed a further decrease in absorption around 375 nm (Graph 10 right). This is consistent with two sequential conjugation reactions of complex **200**, which would be predicted to occur in order as dictated by steric demand around the Au(III) centre, as shown by the previous kinetic measurements of compounds **42** and **188**. This also assumes that the two centres do not interact with one another and are reacting independently.

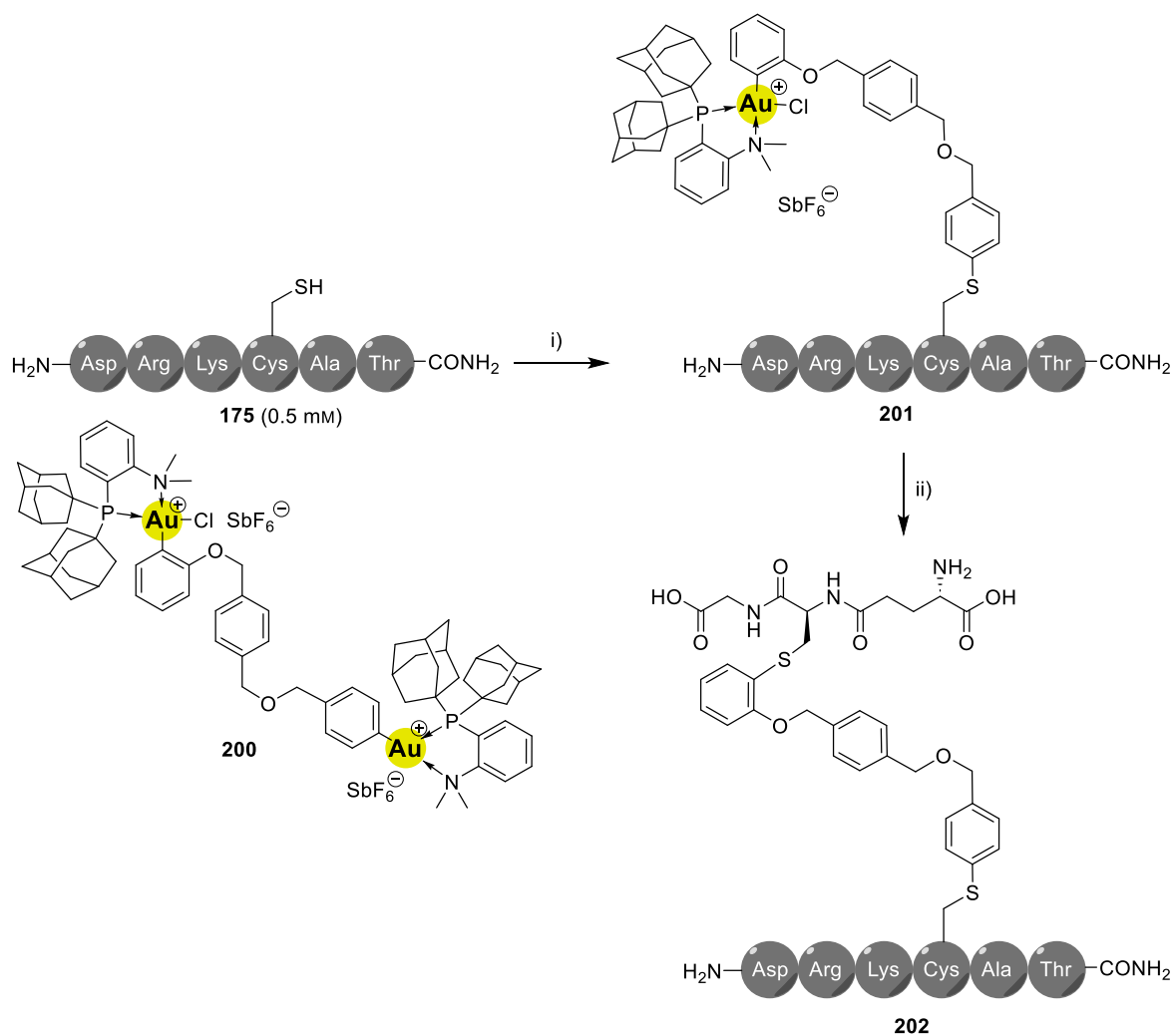


Graph 10: **Left:** Stopped-flow UV/vis spectrum of $10\ \mu\text{M}$ **200** plus $1\ \text{mM}$ GSH in $\text{H}_2\text{O}/\text{MeCN}$ (50:50) buffered to pH 7.5 with $100\ \text{mM}$ tris. Reaction time: $1\ \text{s}$. Spectra: 10. Sample period: $1\ \text{ms}$. Samples per spectrum: 100. **Right:** Stopped-flow UV/vis spectrum of $10\ \mu\text{M}$ **200** plus $1\ \text{mM}$ GSH in $\text{H}_2\text{O}/\text{MeCN}$ (50:50) buffered to pH 7.5 with $100\ \text{mM}$ tris. Reaction time: $300\ \text{s}$. Spectra: 100. Sample period: $1\ \text{ms}$. Samples per spectrum: 3000.

4.3.3.3. Biomolecule Cross-Coupling

A potential use of compound **200** is the preparation of cross-coupled biomolecules, many examples of which have recently gained significant interest as therapeutic agents.^{179–181} To test this concept, H-DRKCAT-NH₂ (**175**) was treated with one equivalent of **200** in a one-to-one mixture of MeCN and $200\ \text{mM}$ tris buffer at pH 8, and held at $35\ ^\circ\text{C}$ for 15 minutes to produce a stock solution of peptide-Au(III) species **201** which was confirmed with LC-MS analysis (section 5.7.5). The solution of **201** was then treated with one equivalent of glutathione in the same buffer system and held at $35\ ^\circ\text{C}$ for thirty minutes (Scheme 66). LC-MS analysis revealed the successful formation of **202**, thus confirming the ability of **200** to cross couple two thiol-containing biomolecules. As **202** has only been characterised using MS data there is not full certainty that the Au(III) centres have reacted in the order shown in Scheme 66. However, study of the reaction rates of the two relevant Au(III) compounds, **42** and **188**, make it very likely that **202** is the major product.[‡]

[‡] Preparation of cross-coupled H-DRKCAT-NH₂ glutathione (Scheme 66) performed by Dr Evan Doud (UCLA).



Scheme 66: Formation of cross-coupled glutathione-175 using bimetallic Au(III) reagent 200. **Reagents and conditions:** i) MeCN/H₂O (50:50), 200 mM tris, pH 8.0, 35 °C, 15 minutes; ii) glutathione (1.0 equiv.) MeCN/H₂O (50:50), 200 mM tris, pH 8.0, 35 °C, 30 minutes.

4.4. Conclusions

The work described within this chapter focussed on the kinetic control of organometallic Au(III) complexes for cysteine arylation in biomolecules. Initial studies worked on qualitatively assessing the cysteine C-S arylation kinetics of Au(III) complexes by varying the nature of the ligand system, as well as the electronics and steric demand of the aryl ring. Varying the ligand environment showed significant rate increases from less sterically bulky substitution at phosphorous, with almost 90% selectivity achieved. However, the highest selectivity was achieved by slowing the reaction rate using *ortho*-substitution of the Au(III)-bound aryl ring with an oxybenzyl moiety. Results of these competition experiments were used to estimate the second-order rate constants of the studied Au(III) compounds, as well as one of Buchwald's RuPhos-ligated Pd(II) compounds. To collect quantitative data for the bioconjugation reactions, stopped-flow spectroscopy was used. Using this data, a two-step

mechanism of the Au(III) and Pd(II) complexes was suggested, with an initial fast coordination/deprotonation step to form a metal-thiolate complex, followed by a slower reductive elimination step. Whilst the proposed mechanism held true for most complexes studied, the relative rates of these two steps depended on the ligand system and nature of the aryl group. This lack of correlation between theory and experiment for some complexes requires further investigation to elucidate their mechanisms. Quantitative rates showed the fastest Au(III) complex to coordinate to thiols with the fastest measured rate of any non-enzymatic biomolecule modification to-date. Using this kinetic data, a bimetallic Au(III) species with varying rates of reaction at each Au(III) centre was synthesised. Stopped-flow spectroscopy revealed two separate rates corresponding to the reaction at each Au(III) centre, and the bimetallic compound subsequently enabled the preparation of a simple cross-coupled peptide species. Overall, this work has revealed much information about the kinetics of Au(III)-mediated bioconjugation and has demonstrated how this could be applied in the synthesis of complex biomolecular species.

5. Experimental

5.1. General Synthetic Experimental for Chapters 2 and 3

All reactions were performed without the exclusion of air and moisture unless otherwise stated.

Chemicals and solvents were purchased from Sigma-Aldrich, Merck, Lancaster Synthesis Ltd., Fisher Scientific Ltd., Strem Chemicals UK, Fluorochem, or VWR International and used without further purification unless otherwise stated. Anhydrous acetonitrile (MeCN), anhydrous dichloromethane, anhydrous tetrahydrofuran (THF) and anhydrous toluene were dried and degassed by passing through anhydrous alumina columns using an Innovative Technology Inc. PS-400-7 solvent purification system and stored under an atmosphere of argon prior to use. Anhydrous ethyl acetate (EtOAc), anhydrous *N,N*-dimethylformamide (DMF), and anhydrous 1,4-dioxane were purchased from Sigma-Aldrich or Fisher Scientific and used as received.

NMR spectra were recorded on an Agilent Technologies 500 MHz spectrometer (^1H NMR at 500 MHz, $^{13}\text{C}\{^1\text{H}\}$ NMR at 126 MHz, ^{19}F NMR at 470 MHz and $^{31}\text{P}\{^1\text{H}\}$ NMR at 202.5 MHz), a Bruker 300 MHz spectrometer (^1H NMR at 300 MHz and $^{13}\text{C}\{^1\text{H}\}$ NMR at 75.5 MHz) or a Bruker 400 MHz spectrometer (^1H NMR at 400 MHz and $^{13}\text{C}\{^1\text{H}\}$ NMR at 101 MHz). Proton chemical shifts are reported in parts per million downfield from tetramethylsilane and are referenced to residual protium in the solvent. Carbon chemical shifts are reported in parts per million downfield from tetramethylsilane and are referenced to the carbon resonances of the solvent peak. Fluorine chemical shifts are reported in parts per million downfield from trichlorofluoromethane. Phosphorous chemical shifts are reported in parts per million downfield from 85% H_3PO_4 . NMR data are represented as follows: chemical shift, integration, multiplicity (s = singlet, d = doublet, dd = doublet of doublets, ddd = doublet of doublet of doublets, t = triplet, q = quartet, m = multiplet), coupling constants (Hz). All spectra were recorded at 298 K, unless otherwise stated.

High resolution mass spectra were obtained using an Agilent QTOF 6545 with Jetstream ESI spray source coupled to an Agilent 1260 Infinity II Quat pump HPLC with 1260 autosampler, column oven compartment and variable wavelength detector (VWD). The MS was operated in either positive or negative ionization mode with the gas temperature at 250°C, the drying gas at 12 L/min and the nebulizer gas at 45 psi (3.10 bar). The sheath gas temperature and flow were set to 350°C and 12 L/min,

respectively. The MS was calibrated using reference calibrant introduced from the independent ESI reference sprayer. The VCap, Fragmentor and Skimmer was set to 3500 V, 125 V and 45 V respectively. Data processing was in Qual B 07.00 with a Find by formula matching tolerance of 5 ppm.

Single crystal X-ray diffraction data was collected at 150 K using either an Agilent Xcalibur or Agilent SuperNova Dual diffractometer with either Mo-K α ($\lambda = 0.71073 \text{ \AA}$) or Cu-K α ($\lambda = 1.5418 \text{ \AA}$) radiation. The data collected by the diffractometer was processed using the proprietary Agilent software. Structures were solved by full-matrix least squares refinement using either the WinGX-170 suite of programs or the programme suite X-SEED. All structural data was obtained and refined by Dr Gabriele Kociok-Köhn.

Analytical thin layer chromatography (TLC) was performed using aluminium-backed plates coated with Alugram® SIL G/UV254 purchased from Macherey-Nagel and visualised by UV light (254 nm), vanillin, ninhydrin or potassium permanganate staining.

Silica gel column chromatography was carried out using 60 \AA , 200-400 mesh particle size silica gel purchased from Sigma-Aldrich.

Automated chromatography was performed on a Teledyne ISCO CombiFlash® NextGen 300+ with a UV/Vis detector and an ELS detector using the method stated and RediSep® Gold, Silver, Gold C18 reversed phase, or Silver C18 reversed phase columns.

IR spectra were recorded on a Perkin-Elmer 1600 FT IR spectrophotometer, with absorbencies quoted as ν in cm^{-1} . Strength of the peaks is defined as strong (s), medium (m), or weak (w). Broad (br) peaks are reported as such.

Melting points were obtained on an OptiMelt MPA100 automated melting point system.

5.2. LC-MS Experimental for Chapters 2 and 3

Peptide LC-MS analyses were performed using an Agilent QTOF 6545 with Jetstream ESI spray source coupled to an Agilent 1260 Infinity II Quat pump HPLC with 1260 autosampler, column oven compartment and variable wavelength detector (VWD). The MS was operated in positive ionization mode with the gas temperature at 250°C, the drying gas at 12 L/min and the nebulizer gas at 45 psi (3.10 bar). The sheath gas temperature and flow were set to 350°C and 12 L/min, respectively. The MS was calibrated using reference calibrant introduced from the independent ESI reference sprayer. The VCap, Fragmentor and Skimmer was set to 3500 V, 100 V and 45 V respectively. Chromatographic separation of a 5 μ L sample injection was performed on an InfinityLab Poroshell 120 EC-C18 (3.0 \times 50 mm, 2.7 μ m) column using H₂O (Merck, LC-MS grade) with 0.1 % formic acid (FA, Fluka) *v/v* and methanol (MeOH, VWR, HiPerSolv) with 0.1 % FA *v/v* as mobile phase A and B, respectively. The column was operated at flow rate of 0.3 mL/min at 40°C starting with 1 % mobile phase B for 3 min, thereafter the gradient was initiated and ran for 2 min to a final 100% B, held at 100% B for 3 min then returned to 1% B, held for re-equilibration for 3.9 min in a total 12 min run time. The VWD was set to collect 254 and 320 nm wavelengths at 2.5 Hz. Data processing was in Qual B 07.00 with a Find by formula matching tolerance of 5 ppm.

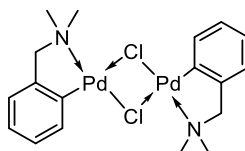
Intact protein LC-MS analyses were performed using an Agilent QTOF 6545 with Jetstream ESI spray source coupled to an Agilent 1260 Infinity II Quat pump HPLC with 1260 autosampler, column oven compartment and variable wavelength detector (VWD). For intact analysis the MS was operated in positive ionization mode with the gas temperature at 350°C, drying gas flow at 11 L/min and nebulizer gas flow at 50 psi (3.44 bar). The sheath gas temperature and flow were set to 400°C and 12 L/min, respectively. The MS was calibrated using reference calibrant introduced from the independent ESI reference sprayer. The VCap, Nozzle, Fragmentor and Skimmer voltages were set to 4000, 1000, 200 and 65 V respectively. The chromatographic separation (2 μ L sample injection) was performed on an Agilent polymeric reversed phase column (PLRP-S, 2.1 \times 50 mm, 3 μ m, 300 Å) at a flow rate of 0.2 mL/min. Mobile phase A was H₂O with 0.1% formic acid, and mobile phase B consisted of MeCN with 0.1% formic acid. Gradient elution started at 5% B, changed to 50% B at 8 min, then to 90% B at 9 min, held at 90% B until 10 min, thereafter returned to 5% B for re-equilibration in a total 13 min run. Data analyses were performed in MassHunter BioConfirm 10.0.

Peptide MS/MS analyses were performed using an Agilent QTOF 6545 with Jetstream ESI spray source coupled to an Agilent 1260 Infinity II Quat pump HPLC with 1260 autosampler, column oven compartment and variable wavelength detector (VWD). The MS was operated in positive ionization mode with the gas temperature at 325°C, the drying gas at 13 L/min and the nebulizer gas at 35 psi (2.41 bar) in the 100 – 2000 m/z ranges collecting 5 spectra/sec. The sheath gas temperature and flow were set to 300°C and 12 L/min, respectively. For MS/MS the selected precursor ion mass range was 50 – 2000 m/z collecting 3 spectra/sec with an isolation width set to medium (4 amu). Ions with charge states of 2, 3 or more were selected for fragmentation. For 2⁺ the slope was 3.1 with an offset of 1, 3⁺ the slope was 3.6 with an offset of –4.8, and more than 3 the slope was 3.6 with an offset of –4.8. Ten precursors were selected per cycle, actively excluded after 3 spectra for 0.2 min. The MS was calibrated using reference calibrant introduced from the independent ESI reference sprayer. Chromatographic separation was performed on a Water Acquity BEH C18 2.1 × 50 mm, 1.7 μm using H₂O (Merck, LC-MS grade) with 0.1% formic acid (FA, Fluka) *v/v* and acetonitrile (MeCN, VWR, HiPerSolv) with 0.1% FA *v/v* as mobile phase A and B, respectively. The column was operated at flow rate of 0.3 mL/min at 50°C starting with 1 % mobile phase B for 0.5 min, thereafter the was gradient set to 5 min at 40% B, then 100% B at 7 min, held at 100% B for 2 min then returned to 1% B at 9.1 min in a total 12 min run time. The VWD was set to collect 280 and 320 nm wavelengths at 2.5 Hz (unless specified differently by user). Ten microliter injections of the samples were made. Data processing was automated in BioConfirm v 10 (Build 10.01.10136) or Qual B 07.00.

5.3. Pd(II)-Mediated C-H Activation for Cysteine Bioconjugation

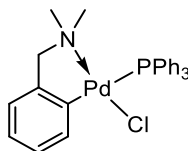
5.3.1. Synthesis of Isolated Pd(II) Complexes

[Pd(dmba)(μ -Cl)]₂ (58)



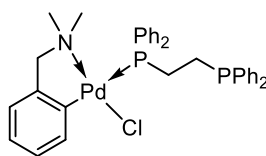
N,N-dimethylbenzylamine (7.35 g, 55 mmol, 2.0 equiv.) and PdCl₂ (4.82 g, 27 mmol, 1.0 equiv.) were combined in MeOH (270 mL) and stirred at rt for 6 h. The resulting solid was isolated *via* gravity filtration and purified by recrystallisation from benzene-*n*-hexane to yield the title compound (5.44 g, 73%) as a green solid: m.p. 174 °C [lit.¹⁸² 184-186 °C from benzene/hexane]; ¹H NMR (400 MHz, CDCl₃) δ 7.24 – 7.15 (m, 1H), 7.05 – 6.95 (m, 1H), 6.94 – 6.85 (m, 2H), 3.96 (s, 2H), 2.89 (s, 3H), 2.87 (s, 3H). The spectral data are in agreement with reported literature values.¹⁸³

Pd(dmba)(PPh₃)Cl (65)



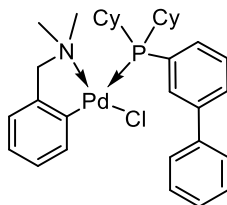
[Pd(dmba)(μ -Cl)]₂ (66 mg, 130 μ mol, 1.0 equiv.) was combined with PPh₃ (66 mg, 250 μ mol, 2.0 equiv.) in CH₂Cl₂ (10 mL) and stirred at rt for 15 min. The solvent was evaporated, and the remaining solid was washed with Et₂O (5 mL) and pentane (2 \times 5 mL) to yield the **title compound** (95 mg, 50 %) as a colourless solid: m.p. decomposes at 173 °C [lit.⁹ 158 – 160 °C] ¹H NMR (400 MHz, CDCl₃) δ 7.77 – 7.67 (m, 6H), 7.46 – 7.37 (m, 3H), 7.37 – 7.30 (m, 6H), 7.00 (dd, *J* = 7.4, 1.5 Hz, 1H), 6.82 (td, *J* = 7.3, 1.2 Hz, 1H), 6.40 – 6.35 (m, 1H), 6.34 – 6.29 (m, 1H), 4.07 (s, 2H), 2.86 (s, 6H); ³¹P{¹H} NMR (162 MHz, CDCl₃) δ 42.37. The spectral data are in agreement with reported literature values.¹⁸⁴

Pd(dmba)(dppe)Cl (66)



[Pd(dmba)(μ -Cl)]₂ (66 mg, 130 μ mol, 1.0 equiv.) was combined with dppe (100 mg, 250 μ mol, 2.0 equiv.) in CH₂Cl₂ (10 mL) and stirred at rt for 15 min. The solvent was evaporated, and the remaining solid was washed with Et₂O (5 mL) and pentane (2 \times 5 mL) to yield the **title compound** (90 mg, 55 %) as a colourless solid: m.p. decomposes at 216 °C; ¹H NMR (400 MHz, CDCl₃) δ 7.89 (dd, J = 12.2, 7.5 Hz, 4H), 7.73 (t, J = 8.6 Hz, 4H), 7.63 – 7.47 (m, 12H), 7.17 – 7.09 (m, 1H), 6.96 (t, J = 7.3 Hz, 1H), 6.69 (q, J = 7.0 Hz, 1H), 6.63 – 6.47 (m, 1H), 4.23 (s, 2H), 2.58 (s, 6H), 1.78 (s, 4H); ³¹P{¹H} NMR (162 MHz, CDCl₃) δ 60.77 (d, J = 24.8 Hz), 40.87 (d, J = 24.8 Hz); ¹³C{¹H} NMR (101 MHz, CDCl₃) δ 134.4, 134.3, 133.7, 133.6, 132.7, 132.5, 130.2, 130.1, 129.8, 129.7, 123.5, 74.7, 52.2, 27.1; (ESI⁺) of [M-Cl]⁺ detected: 813.1875, expected for C₄₈H₄₃NOP₂Pd: 813.7876; ν_{max} (thin film)/cm⁻¹ 1435 (s), 1101 (s), 741 (s), 693 (s).

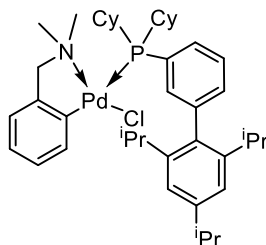
Pd(dmba)(CyJohnPhos)Cl (67)



[Pd(dmba)(μ -Cl)]₂ (26 mg, 50 μ mol, 1.0 equiv.) and CyJohnPhos (35 mg, 100 μ mol, 2.0 equiv.) were combined in CH₂Cl₂ (2.5 mL) under N₂ and heated to reflux. After 2 h, the mixture was allowed to cool, and concentrated *in vacuo*. MTBE (200 μ L) and pentane (800 μ L) were added, and the mixture was placed in a -20 °C freezer for 5 min. After removal from the freezer, the solvent was pipetted off, and the resulting solid was washed with pentane (2 \times 1 mL) to yield the **title compound** (42 mg, 69%) as a colourless solid: m.p. decomposes at 172 °C; ¹H NMR (400 MHz, CDCl₃, 323 K) δ 7.86 – 7.77 (m, 1H), 7.51 – 7.27 (m, 6H), 7.21 – 7.03 (m, 2H), 6.89 (d, J = 7.4 Hz, 1H), 6.79 (td, J = 7.1, 1.4 Hz, 1H), 6.57 – 6.35 (m, 2H), 3.90 (s, 2H), 2.73 (s, 6H), 2.26 (d, J = 11.6 Hz, 2H), 2.06 (s, 2H), 1.93 (d, J = 13.0 Hz, 2H), 1.73 (d, J = 12.0 Hz, 2H), 1.63 – 1.51 (m, 5H), 1.40 – 1.24 (m, 2H), 1.22 – 0.95 (m, 5H); ³¹P{¹H} NMR (162 MHz, CDCl₃, 323 K) δ 59.94; (ESI⁺) m/z of

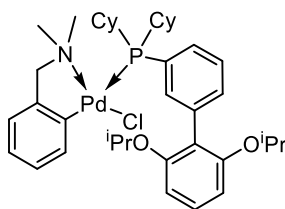
[M-Cl]⁺ detected: 586.2175, expected for C₃₃H₄₃NCIPPd: 586.2184; ν_{\max} (thin film)/cm⁻¹ 2925 (C-H, s), 2849 (C-H, s), 1581 (w), 1445 (s), 1111 (s), 999 (s), 848 (s), 764 (s), 740 (s).

Pd(dmba)(XPhos)Cl (68)



[Pd(dmba)(μ -Cl)]₂ (26 mg, 50 μ mol, 1.0 equiv.) and XPhos (48 mg, 100 μ mol, 2.0 equiv.) were combined in CH₂Cl₂ (2.5 mL) under N₂ and heated to reflux. After 2 h, the mixture was allowed to cool, and concentrated *in vacuo*. MTBE (200 μ L) and pentane (800 μ L) were added, and the mixture was placed in a -20 °C freezer for 5 min. After removal from the freezer, the solvent was pipetted off, and the resulting solid was washed with pentane (2 \times 1 mL) to yield the **title compound** (61 mg, 81%) as a colourless solid: m.p. decomposes at 210 °C; ¹H NMR (400 MHz, CDCl₃, 328 K) δ 8.27 (dd, J = 15.3, 8.0 Hz, 1H), 7.39 – 7.29 (m, 1H), 7.20 (t, J = 7.6 Hz, 1H), 7.14 – 7.02 (m, 3H), 6.92 (d, J = 7.4 Hz, 1H), 6.80 (t, J = 7.2 Hz, 1H), 6.54 (t, J = 7.0 Hz, 1H), 6.45 (t, J = 7.4 Hz, 1H), 3.93 (s, 2H), 2.99 – 2.88 (m, 1H), 2.72 (s, 4H), 2.04 – 1.69 (m, 6H), 1.47 (s, 4H), 1.34 – 0.86 (m, 18H); (ESI⁺) of [M+H]⁺ detected: 752.3337, expected for C₄₂H₆₁ClNPPd: 752.3350]; ν_{\max} (thin film)/cm⁻¹ 2925 (C-H, m), 1581 (w), 1455 (s), 1112 (s), 1056 (s), 848 (s), 740 (s).

Pd(dmba)(RuPhos)Cl (69)

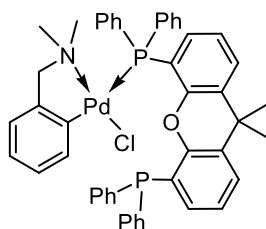


[Pd(dmba)(μ -Cl)]₂ (28 mg, 50 μ mol, 1.0 equiv.) and RuPhos (47 mg, 100 μ mol, 2.0 equiv.) were combined in CH₂Cl₂ (2 mL). After 1 h, the mixture was concentrated *in vacuo*. MTBE (200 μ L) and pentane (800 μ L) were added, and the mixture was left to stand for 15 min. After which, the solvent was pipetted off, and the resulting solid was washed with pentane (2 \times 1 mL) to yield the **title compound** (74 mg, 99%) as a colourless solid: m.p. decomposes at 202 °C; ¹H NMR (400 MHz, CDCl₃) δ 7.67 (ddd, J = 14.8, 8.0, 1.4 Hz, 1H), 7.29 (d, J = 8.5 Hz, 1H), 7.20 (tt, J = 7.5, 1.8 Hz, 1H), 6.92 (ddd, J = 7.9, 3.1, 1.4 Hz, 1H), 6.90 – 6.82

(m, 2H), 6.75 (td, $J = 7.3, 1.1$ Hz, 1H), 6.67 – 6.54 (m, 3H), 6.46 (td, $J = 7.5, 1.6$ Hz, 1H), 4.48 (s, 2H, H-1'), 2.73 (s, 6H, H-2'), 1.71 (s, 2H), 1.26 (s, 5H), 1.11 (s, 8H); $^{31}\text{P}\{^1\text{H}\}$ NMR (162 MHz, CDCl_3) δ 70.64; $^{13}\text{C}\{^1\text{H}\}$ NMR (101 MHz, CDCl_3) δ 153.1, 147.5, 140.6, 140.2, 140.1, 140.0, 139.8, 133.2, 133.1, 128.9, 128.6, 128.2, 127.8, 124.8, 124.7, 124.5, 124.4, 123.0, 123.0, 122.8, 121.3, 107.0, 73.0, 72.9, 27.7, 27.6, 26.9, 26.8, 26.2, 22.7, 22.4; (ESI⁺) m/z of $[\text{M}+\text{H}]^+$ detected: 742.2766, expected for $\text{C}_{39}\text{H}_{55}\text{ClNO}_2\text{PPd}$: 742.2779; ν_{max} (thin film)/ cm^{-1} 2924 (C-H, m), 1581 (m), 1456 (s), 1243 (s), 1112 (s), 1057 (s), 727 (s).

Crystallisation *via* vapour diffusion of pentane into a solution of the **title compound** in MeOH (10 mg/mL) yielded crystals suitable for X-ray diffraction study.

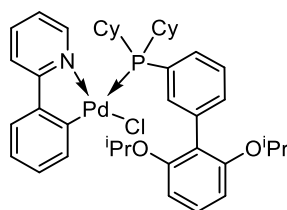
Pd(dmba)(Xantphos)Cl (70)



$[\text{Pd}(\text{dmba})(\mu\text{-Cl})_2]$ (28 mg, 50 μmol , 1.0 equiv.) and Xantphos (58 mg, 100 μmol , 2.0 equiv.) were combined in CH_2Cl_2 (2 mL). After 1 h, the mixture was concentrated *in vacuo*. MTBE (200 μL) and pentane (800 μL) were added, and the mixture was left to stand for 15 min. After which, the solvent was pipetted off, and the resulting solid was washed with pentane (2×1 mL) to yield the **title compound** (86 mg, >99 %) as a colourless solid: m.p. decomposes at 190 $^\circ\text{C}$; ^1H NMR (400 MHz, CDCl_3 , 323 K) δ 7.46 – 7.39 (m, 10H), 7.24 – 7.19 (m, 4H), 7.11 (m, 8H), 6.96 (t, $J = 7.7$ Hz, 1H), 6.90 – 6.85 (m, 2H), 6.80 (qd, $J = 4.5, 1.6$ Hz, 2H), 6.72 (ddd, $J = 7.3, 6.1, 2.3$ Hz, 1H), 6.30 – 6.23 (m, 2H), 3.84 (s, 2H), 2.64 (s, 6H), 1.51 – 1.46 (m, 6H); $^{13}\text{C}\{^1\text{H}\}$ NMR (101 MHz, CDCl_3) δ 152.9, 152.8, 151.1, 148.0, 137.1, 134.6, 134.5, 133.8, 130.4, 129.1, 128.0, 127.9, 124.5, 123.2, 123.1, 122.5, 72.5, 50.2, 34.4; $^{31}\text{P}\{^1\text{H}\}$ NMR (162 MHz, CDCl_3 , 323 K) δ 4.21; (ESI⁺) of $[\text{M}-\text{Cl}]^+$ detected: 814.1931, expected for $\text{C}_{48}\text{H}_{44}\text{NClOP}_2\text{Pd}$: 814.1949; ν_{max} (thin film)/ cm^{-1} 1434 (w), 1405 (s), 1239 (s), 739 (s), 695 (s).

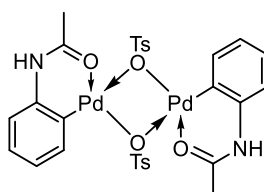
Crystallisation *via* liquid-liquid diffusion of hexane layered onto a solution of the **title compound** in CHCl_3 (10 mg/mL) yielded crystals suitable for X-ray diffraction study.

Pd(2-phenylpyridine)(RuPhos)Cl (77)



PdCl₂ (21 mg, 120 μmol, 1.0 equiv.) and 2-phenylpyridine (33 μL, 240 μmol, 2.0 equiv.) were combined in MeOH (1 mL) and stirred for 72 h. The solid formed was isolated *via* gravity filtration and washed with MeOH (5 mL), and CH₂Cl₂ (3 x 5mL). The solid (16 mg) was then combined with RuPhos (25 mg, 54 μmol, 2.0 equiv. to crude material) suspended in CH₂Cl₂ (5 mL) and heated to reflux for 2 h. After cooling, the solvent was removed *in vacuo* and MTBE (200 μL) and pentane (800 μL) were added. The suspension was placed into the freezer for 15 min, the supernatant pipetted off and the resulting solid washed with pentane (2 x 1 mL) to yield the **title compound** (39 mg, 43%) as a yellow solid: m.p. decomposes at 248 °C; ¹H NMR (400 MHz, CDCl₃) δ 9.75 – 9.68 (m, 1H), 7.97 – 7.86 (m, 1H), 7.77 (td, *J* = 7.7, 1.7 Hz, 1H), 7.72 – 7.66 (m, 1H), 7.44 (dd, *J* = 7.8, 1.5 Hz, 1H), 7.34 – 7.27 (m, 2H), 7.20 (t, *J* = 6.7 Hz, 1H), 7.05 – 6.96 (m, 2H), 6.90 (t, *J* = 7.4 Hz, 1H), 6.78 – 6.71 (m, 2H), 6.67 – 6.58 (m, 3H), 4.49 (s, 2H), 3.06 (s, 1H), 2.68 (s, 1H), 2.37 (s, 1H), 2.12 – 1.88 (m, 3H), 1.72 (d, *J* = 12.7 Hz, 2H), 1.55 (s, 17H), 1.29 – 1.07 (m, 15H); ³¹P{¹H} NMR (162 MHz, CDCl₃) δ 68.41; (ESI⁺) *m/z* of [M-Cl]⁺ detected: 722.2731, expected for C₄₁H₅₁NO₂PPd: 722.2708; *v*_{max} (thin film)/cm⁻¹ 2923 (C-H, w), 1578 (w), 1458 (m), 1243 (m), 1108 (s), 1058 (s), 759 (s), 743 (s), 731 (s).

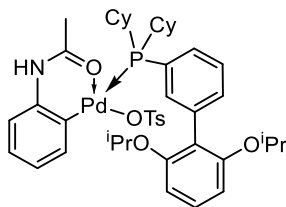
[Pd(acetanilide)(μ-OTs)]₂ (79)



Acetanilide (27 mg, 200 μmol, 1.0 equiv.), Pd(OAc)₂ (38 mg, 200 μmol, 1.0 equiv.) and *p*-toluenesulfonic acid hydrate (45 mg, 200 μmol, 1.0 equiv.) were combined in CH₂Cl₂ (2 mL) and heated for 1 min. The resulting yellow solid was isolated *via* gravity filtration, washed with CH₂Cl₂ (3 x 2 mL) to give the **title compound** (74 mg, 83%) as a yellow solid: ¹H NMR (400 MHz, Methanol-*d*₄) δ 11.49 (s, 1H), 7.71 (d, *J* = 8.2 Hz, 2H), 7.25 – 7.20 (m, 1H), 7.14 – 7.08 (m, 1H), 6.94 – 6.86 (m, 3H), 2.36 (s, 3H), 2.30 (s, 3H); ¹³C{¹H} NMR

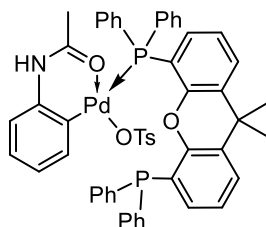
(101 MHz, MeOD) δ 168.1, 141.7, 133.1, 132.2, 129.8, 127.2, 127.0, 124.3, 117.4, 114.4, 21.3, 20.7. The spectral data are in agreement with reported literature values.¹⁸⁵

Pd(acetanilide)(RuPhos)OTs (80)



[Pd(acetanilide)(μ -OTs)]₂ (22 mg, 25 μ mol, 1.0 equiv.) and RuPhos (23 mg, 50 μ mol, 2.0 equiv.) were combined in CH₂Cl₂ (2 mL) and stirred for 1 h. The reaction mixture was filtered through a bed of Celite® and concentrated *in vacuo* to yield the **title compound** (43 mg, 96%) as a yellow solid: m.p. decomposes at 110 °C; ¹H NMR (400 MHz, CDCl₃) δ 12.05 (s, 1H), 7.88 (d, *J* = 8.0 Hz, 2H), 7.66 (t, *J* = 8.5 Hz, 1H), 7.58 (t, *J* = 7.5 Hz, 1H), 7.47 (tt, *J* = 7.5, 1.4 Hz, 1H), 7.13 (d, *J* = 7.9 Hz, 2H), 7.05 – 7.00 (m, 1H), 6.91 – 6.87 (m, 1H), 6.84 – 6.80 (m, 2H), 6.64 (d, *J* = 8.5 Hz, 2H), 4.59 (hept, *J* = 6.0 Hz, 2H), 2.43 (s, 3H), 2.32 (s, 3H), 2.25 (q, *J* = 11.5 Hz, 2H), 1.84 – 1.60 (m, 14H), 1.28 (d, *J* = 6.0 Hz, 6H), 1.03 (d, *J* = 6.0 Hz, 6H), 0.88 (t, *J* = 7.1 Hz, 6H); ³¹P{¹H} NMR (162 MHz, CDCl₃) δ 42.6; ¹³C{¹H} NMR (101 MHz, CDCl₃) δ 171.8, 171.7, 160.4, 143.9, 143.6, 143.5, 139.0, 136.7, 134.8, 132.8, 132.3, 128.6, 128.5, 126.9, 126.3, 126.2, 121.0, 109.4, 109.3, 106.7, 106.5, 106.3, 106.2, 71.9, 71.8, 33.1, 33.0, 32.8, 32.7, 29.0, 28.3, 26.9, 25.9, 25.8, 22.6, 22.3, 22.2, 22.1, 22.0, 21.8, 21.6, 21.5, 21.4, 21.3; (ESI⁺) *m/z* of [M-OTs]⁺ detected: 706.2664, expected for C₄₅H₅₈NO₆PPdS: 706.2641; ν_{max} (thin film)/cm⁻¹ 2974 (w), 2928 (m), 2857 (w), 1587 (m), 1454 (s), 1388 (m), 1256 (m), 1221 (m), 1175 (s), 1104 (s), 1028 (s), 1012 (s), 753 (m), 728 (s), 682 (s).

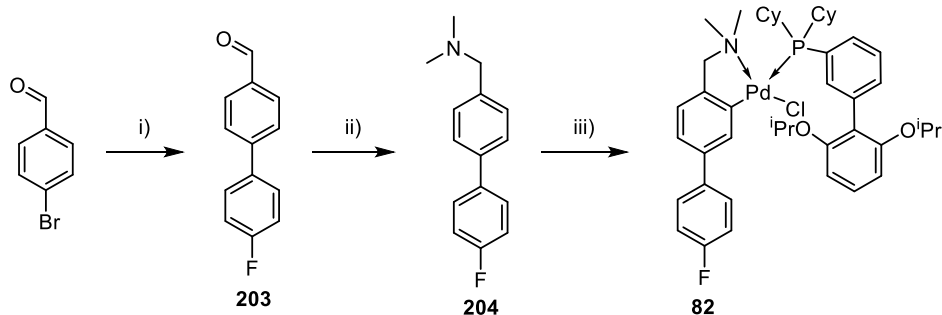
Pd(acetanilide)(Xantphos)OTs (81)



[Pd(acetanilide)(μ -OTs)]₂ (22 mg, 25 μ mol, 1.0 equiv.) and Xantphos (29 mg, 50 μ mol, 2.0 equiv.) were combined in CH₂Cl₂ (2 mL) and stirred for 1 h. The reaction mixture was filtered through a bed of Celite® and concentrated *in vacuo* to yield the **title compound**

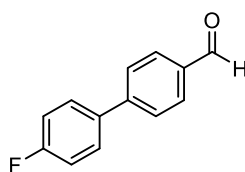
(43 mg, 96%) as a yellow solid: m.p. decomposes at 120 °C; ^1H NMR (400 MHz, CDCl_3) δ 7.57 (dd, $J = 7.8, 1.5$ Hz, 3H), 7.34 (d, $J = 7.8$ Hz, 2H), 7.18 – 7.07 (m, 14H), 7.03 (t, $J = 7.5$ Hz, 8H), 6.98 – 6.93 (m, 2H), 6.84 (d, $J = 7.9$ Hz, 2H), 6.74 – 6.69 (m, 1H), 6.57 – 6.52 (m, 1H), 6.26 (t, $J = 7.5$ Hz, 1H), 2.13 (s, 3H), 1.69 (s, 6H), 1.62 (s, 3H); $^{31}\text{P}\{^1\text{H}\}$ NMR (162 MHz, CDCl_3) δ 15.2 (broad); $^{13}\text{C}\{^1\text{H}\}$ NMR (101 MHz, CDCl_3) δ 170.0, 154.1, 154.1, 154.0, 144.2, 138.6, 133.6, 133.1, 130.6, 130.1, 128.6, 128.6, 128.3, 126.2, 125.5, 123.7, 119.8, 119.1, 35.6, 30.9, 22.8, 21.4; (ESI⁺) m/z of $[\text{M-OTs}]^+$ detected: 818.1590, expected for $\text{C}_{54}\text{H}_{47}\text{NO}_5\text{P}_2\text{PdS}$: 818.1569; ν_{max} (thin film)/ cm^{-1} 3371 (br, w), 2978 (m), 2876 (w), 1680 (w), 1410 (s), 1368 (m), 1291 (w), 1199 (m), 1153 (m), 1117 (m), 949 (s), 734 (m), 688 (s).

Synthesis of Pd(*N,N*-Dimethyl-4-(4-fluorophenyl)benzylamine)(RuPhos)Cl (**82**)



Scheme 67: Reagents and conditions: i) 4-Fluoroboronic acid (1.2 equiv.), $\text{Pd}(\text{PPh}_3)_4$ (4.0 mol%), aq. Na_2CO_3 (2.0 M), toluene/EtOH, Ar, reflux, 16 h, 77%; ii) $\text{NaBH}(\text{OAc})_3$ (1.5 equiv.), dimethylamine (2.0 M in THF, 1.5 equiv.), AcOH (cat.), DCE, rt, 2.5 h 95%; iii) PdCl_2 (1.0 equiv.), MeOH, rt, 1 h. then RuPhos (1.0 equiv.), CH_2Cl_2 , reflux, 3 h, 7%.

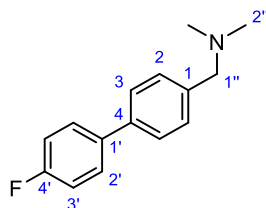
4-(4-Fluorophenyl)benzaldehyde (**203**)



To a solution of 4-bromobenzaldehyde (460 mg, 2.5 mmol, 1.0 equiv.) in toluene (17.5 mL) was added aq. Na_2CO_3 (2.0 M, 8.0 mL), and a solution of 4-fluorophenyl boronic acid (420 mg, 3.0 mmol, 1.2 equiv.) in EtOH (9.6 mL). The reaction mixture was purged with argon, and $\text{Pd}(\text{PPh}_3)_4$ (120mg, 0.10 mmol, 4.0 mol%) was added, and the reaction mixture was heated to reflux overnight. After allowing the mixture to cool, EtOAc (10 mL) and H_2O (10 mL) were added, and the organics were separated. The aqueous components were extracted with EtOAc (2×10 mL), and the combined organics were filtered through Celite® and concentrated *in vacuo*. The crude product was purified using flash column chromatography (neat CH_2Cl_2) to yield the **title compound** (384 mg, 77%) as a colourless

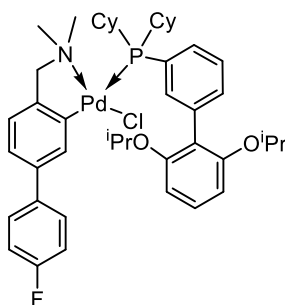
solid: R_f 0.55 (petroleum ether 40 – 60/ CH_2Cl_2 50:50); m.p. 78 – 79 °C from CH_2Cl_2 [lit.² 72 – 74 °C, lit.³ 79 – 79 °C]; ^1H NMR (400 MHz, CDCl_3) δ 10.06 (s, 1H), 7.95 (d, $J = 8.3$ Hz, 2H), 7.71 (d, $J = 8.3$ Hz, 2H), 7.67 – 7.55 (m, 2H), 7.23 – 7.06 (m, 2H); ^{19}F NMR (376 MHz, CDCl_3) δ -113.58. The spectral data are in agreement with reported literature values.¹⁸⁵

***N,N*-Dimethyl-4-(4-fluorophenyl)benzylamine (204)**



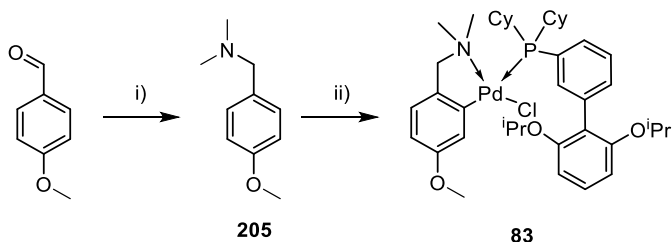
4-(4-Fluorophenyl)benzaldehyde (150 mg, 0.75 mmol, 1.0 equiv.), dimethylamine (2.0 M in THF, 0.58 mL, 1.16 mmol, 1.6 equiv.), $\text{NaBH}(\text{OAc})_3$ (240 mg, 1.1 mmol, 1.5 equiv.) and glacial acetic acid (2 drops) were combined in DCE (5 mL). The resulting mixture was stirred at rt for 2.5 hr, after which sat. aq. NaHCO_3 (20 mL) was added. The mixture was separated, and the aqueous components were extracted with CH_2Cl_2 (3×10 mL). The combined organics were washed with brine (20 mL), dried (Na_2SO_4) and concentrated *in vacuo*. The resulting crude oil was subjected to flash column chromatography (gradient up to 2% MeOH in CH_2Cl_2) to yield the **title compound** (162 mg, 95%) as a light brown oil: R_f 0.44 ($\text{CH}_2\text{Cl}_2/\text{MeOH}$ 98:2); ^1H NMR (400 MHz, Chloroform-*d*) δ 7.55 (dd, $J = 8.8, 5.3$ Hz, 2H, H-3'), 7.50 (d, $J = 8.3$ Hz, 2H, H-2), 7.37 (d, $J = 8.3$ Hz, 2H, H-3), 7.12 (t, $J = 8.8$ Hz, 2H, H-2'), 3.46 (s, 2H, H-1''), 2.27 (s, 6H, H-2''); ^{19}F NMR (376 MHz, CDCl_3) δ -116.00; $^{13}\text{C}\{^1\text{H}\}$ NMR (101 MHz, CDCl_3) δ 162.6 (d, $J = 246.2$ Hz, C-4'), 139.3, 137.7, 137.2 (d, $J = 3.3$ Hz, C-1'), 129.8, 128.7 (d, $J = 8.0$ Hz, C-2'), 127.0, 115.7 (d, $J = 21.4$ Hz, C-3'), 64.0; 45.4; (ESI⁺) m/z of $[\text{M}+\text{H}]^+$ detected: 230.1344, expected for $\text{C}_{15}\text{H}_{16}\text{FN}$: 230.1340; ν_{max} (thin film)/ cm^{-1} 2928 (C-H, w), 1498 (s), 1224 (s), 1021 (m), 839 (s), 802 (s).

Pd(*N,N*-Dimethyl-4-(4-fluorophenyl)benzylamine)(RuPhos)Cl (**82**)



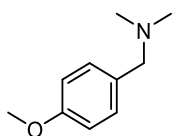
N,N-Dimethyl-4-(4-fluorophenyl)benzylamine (81 mg, 690 μmol , 1.0 equiv.) and PdCl_2 (159 mg, 690 μmol , 1.0 equiv.) were combined in MeOH and stirred for 16 h. The reaction mixture was concentrated and dissolved in CH_2Cl_2 , filtered through a column of silica, and concentrated *in vacuo*. The crude intermediate (43 mg) was then combined with RuPhos (59 mg, 120 μmol , 2.0 equiv. to intermediate) in CH_2Cl_2 (5 mL) and heated to reflux for 3 h. The solvent was removed *in vacuo*, MTBE (500 μL) and pentane (2 mL) were added, and the resulting suspension was placed in a $-20\text{ }^\circ\text{C}$ freezer for 15 min. After removal from the freezer, the supernatant was pipetted off, and the solid was washed with pentane ($2 \times 2\text{ mL}$) to give the **title compound** (43 mg, 7%); m.p. decomposes at $200\text{ }^\circ\text{C}$; ^1H NMR (500 MHz, CDCl_3 , 318 K) δ 7.81 (dd, $J = 13.6, 8.0\text{ Hz}$, 1H), 7.42 (t, $J = 7.6\text{ Hz}$, 1H), 7.33 – 7.22 (m, 1H), 7.17 (d, $J = 7.7\text{ Hz}$, 1H), 7.11 (t, $J = 7.7\text{ Hz}$, 1H), 6.95 (t, $J = 6.7\text{ Hz}$, 2H), 6.83 (t, $J = 8.5\text{ Hz}$, 2H), 6.76 (d, $J = 5.2\text{ Hz}$, 1H), 6.66 (t, $J = 6.8\text{ Hz}$, 2H), 6.56 (d, $J = 8.4\text{ Hz}$, 2H), 4.57 – 4.25 (m, 2H), 2.76 (s, 6H), 2.56 (s, 2H), 1.70 (s, 3H), 1.55 (s, 5H), 1.37 – 0.59 (m, 22H); $^{31}\text{P}\{^1\text{H}\}$ NMR (202 MHz, CDCl_3) δ 71.41; ^{19}F NMR (376 MHz, CDCl_3) δ -117.91; (ESI $^+$) m/z $[\text{M}-\text{Cl}]^+$ detected: 796.3248, expected for $\text{C}_{45}\text{H}_{58}\text{FCINO}_2\text{PPd}$: 796.3240; ν_{max} (thin film)/ cm^{-1} 2922 (C-H, m), 1509 (m), 1456 (s), 1244 (m), 1111 (s), 1056 (s), 807 (s), 744 (m).

Synthesis of Pd(*N,N*-dimethyl-4-methoxybenzylamine)(RuPhos)Cl (**83**)



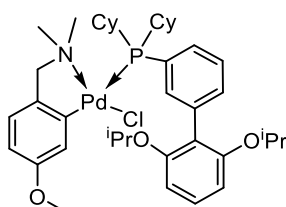
Scheme 68: **Reagents and conditions:** i) $\text{NaBH}(\text{OAc})_3$ (1.5 equiv.), dimethylamine (2.0 M in THF, 1.5 equiv.), CH_2Cl_2 , rt, 16 h, 71%; ii) PdCl_2 (1 equiv.), MeOH, rt, 24 h then RuPhos (2 equiv.), CH_2Cl_2 , 72 h, 12%.

N,N-Dimethyl-4-methoxybenzylamine (205)



4-Methoxybenzaldehyde (110 μ L, 1.0 mmol, 1.0 equiv.), dimethylamine (2.0 M in THF, 0.75 mL, 1.5 mmol, 1.5 equiv.), and $\text{NaBH}(\text{OAc})_3$ (320 mg, 1.5 mmol, 1.5 equiv.), combined in CH_2Cl_2 (20 mL) and stirred for 16 h. After which, sat. aq. NaHCO_3 (40 mL) was added, and the aqueous component was separated and extracted with CH_2Cl_2 (3×20 mL). The combined organics were then washed with brine (40 mL), dried (Na_2SO_4) and concentrated *in vacuo*. The crude residue was subjected to flash column chromatography (gradient up to 2:98 MeOH/ CH_2Cl_2 with 1% added NEt_3) to yield the title compound (118 mg, 71%) as a colourless liquid: R_f 0.21 (1:2:97 $\text{NEt}_3/\text{MeOH}/\text{CH}_2\text{Cl}_2$); ^1H NMR (400 MHz, CDCl_3) δ 7.21 (d, $J = 8.6$ Hz, 2H, H-3), 6.86 (d, $J = 8.6$ Hz, 2H, H-2), 3.80 (s, 3H, OCH_3), 3.36 (s, 2H, H-1'), 2.22 (s, 6H, H-2'); $^{13}\text{C}\{^1\text{H}\}$ NMR (101 MHz, CDCl_3) δ 158.8, 131.1, 130.4, 113.7, 63.8, 55.4, 45.3. The spectral data are in agreement with reported literature values.¹⁸⁶

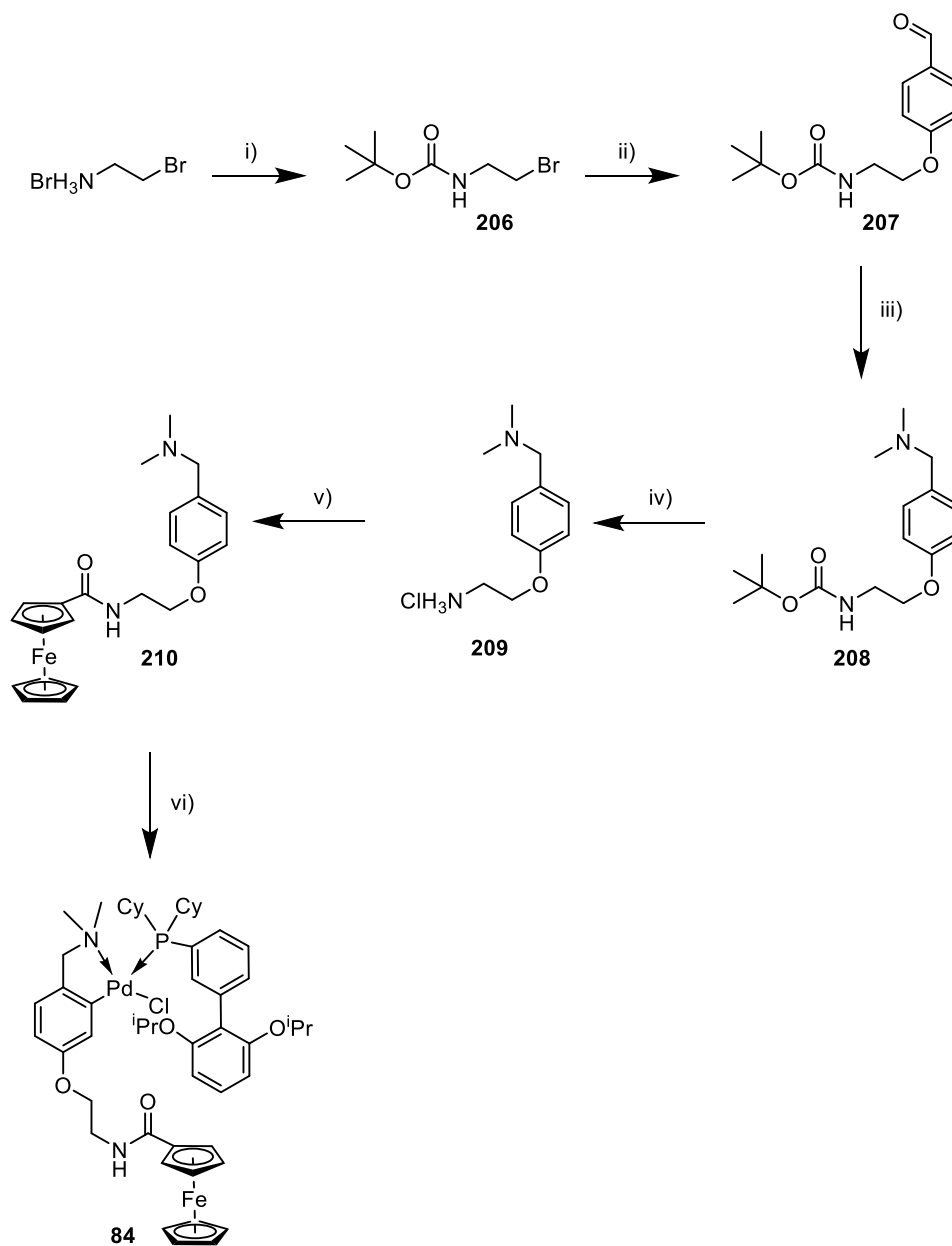
Pd(*N,N*-dimethyl-4-methoxybenzylamine)(*RuPhos*)Cl (83)



N,N-Dimethyl-4-methoxybenzylamine (20 mg, 120 μ mol, 1.0 equiv.) and PdCl_2 (21 mg, 120 μ mol, 1.0 equiv.) were combined in MeOH (500 μ L) and stirred for 24 h. After which, the solid formed was isolated *via* gravity filtration, washed with MeOH (5 mL) and H_2O (5 mL) and dried under high vacuum to yield a light green solid (13 mg).

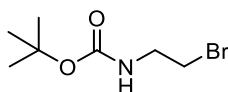
This intermediate (13 mg, 21 μ mol, 1.0 equiv.) was combined with *RuPhos* (20 mg, 42 μ mol, 2.0 equiv.) in CH_2Cl_2 (1 mL) and stirred for 72 h. After which, the reaction mixture was concentrated and washed with pentane (3×1 mL) to yield the **title compound** (11 mg, 12%) as a colourless solid: $^{31}\text{P}\{^1\text{H}\}$ NMR (162 MHz, CDCl_3 , 328 K) δ 66.87; (ESI⁺) m/z of $[\text{M}]^+$ detected: 767.2855, expected for $\text{C}_{40}\text{H}_{57}\text{ClINO}_3\text{PPd}$: 767.2815.

Synthesis of Pd(*N,N*-dimethyl-4-(*N'*-(ferrocene amide)-2-aminoethoxy)benzylamine) (RuPhos)Cl (84)



Scheme 69: Reagents and conditions: i) Boc_2O (1.1 equiv.), DIPEA (2.0 equiv.), THF, 0 °C – rt, 16 h, 82%; ii) 4-hydroxybenzaldehyde (1.0 equiv.), K_2CO_3 (2.0 equiv.), NaI (1.0 equiv.), DMF, Ar, 80 °C, 90 min, 63%; iii) $\text{NaBH}(\text{OAc})_3$ (1.5 equiv.), dimethylamine (2.0 M in THF, 1.5 equiv.), HOAc (cat.), CH_2Cl_2 , rt, 16 h, 58%; iv) 4 M HCl in dioxane, 0 °C – rt, N_2 , 30 min, 99%; v) EDC·HCl (1.1 equiv.), HOBt·H₂O (1.1 equiv.), ferrocene carboxylic acid (1.0 equiv.), NEt_3 (2.0 equiv.), CH_2Cl_2 , rt, 3 h, 65%; vi) PdCl_2 (1.0 equiv.), NaOAc (1.0 equiv.), NaCl (2.0 equiv.), MeOH, rt, 24 h, then RuPhos (1 equiv.), CH_2Cl_2 , rt, 1 h, 60%.

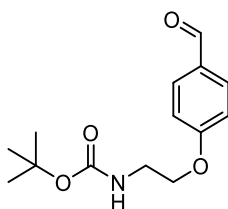
2-(Boc-amino)ethyl bromide (206)



2-(Boc-amino)ethyl bromide was prepared according to a literature procedure with minor modifications.⁶ 2-Bromoethylamine hydrobromide (1.02 g, 5.0 mmol, 1.0 equiv.) and

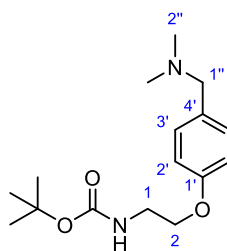
di-*tert*-butyl dicarbonate (1.20 g, 5.5 mmol, 1.1 equiv.) were combined in THF (15 mL) and cooled to 0 °C. *N,N*-Diisopropylethylamine (1.8 mL, 10 mmol, 2.0 equiv.) was added dropwise, the reaction mixture was warmed to rt, and stirred for 16 h. The reaction mixture was concentrated *in vacuo*. The residue was dissolved in EtOAc (20 mL), washed with K₂CO₃ (10%, aq., 20 mL) and brine (20 mL), and dried with Na₂SO₄ before being concentrated *in vacuo*. The crude product was subjected to flash column chromatography (gradient up to 10% Et₂O in petroleum ether) to yield the **title compound** (916 mg, 82%) as a colourless oil: R_f 0.16 (Et₂O/petroleum ether 5:95), ¹H NMR (400 MHz, CDCl₃) δ 4.94 (s, 1H), 3.59 – 3.50 (m, 2H), 3.45 (t, *J* = 5.8 Hz, 2H), 1.45 (s, 9H). The spectral data are in agreement with reported literature values.¹⁸⁷

***tert*-Butyl(2-(4-formylphenoxy)ethyl)carbamate (207)**



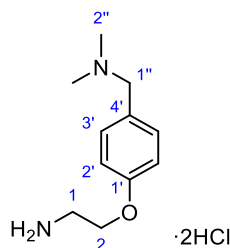
2-(Boc-amino)ethyl bromide (880 g, 3.9 mmol, 1.5 equiv.), 4-hydroxybenzaldehyde (320 mg, 2.6 mmol, 1.0 equiv.), NaI (390 mg, 2.6 mmol, 1.0 equiv.), and K₂CO₃ (730 mg, 5.2 mmol, 2.0 equiv.) were combined in DMF (10 mL) under argon and heated to 80 °C. After 90 min, 4-hydroxybenzaldehyde (80 mg, 0.65 mmol, 0.25 equiv.) and K₂CO₃ (180 mg, 1.3 mmol, 0.5 equiv.) were added, and the mixture stirred for another 2 h. The reaction mixture was cooled, diluted with H₂O (30 mL) and extracted with Et₂O (3 × 25 mL). The combined organics were washed with aq. LiCl (0.5 M, 2 × 25 mL), and brine (50 mL) before being dried with Na₂SO₄ and concentrated *in vacuo* to yield the **title compound** (542 mg, 63%) as an off-white solid: m.p. (62 – 64 °C); ¹H NMR (400 MHz, Chloroform-*d*) δ 9.89 (s, 1H), 7.84 (d, *J* = 8.8 Hz, 2H), 7.00 (d, *J* = 8.7 Hz, 2H), 4.97 (s, 1H), 4.11 (t, *J* = 5.1 Hz, 2H), 3.65 – 3.53 (m, 2H), 1.45 (s, 9H). The spectral data are in agreement with reported literature values.¹⁸⁸

***N,N*-Dimethyl-4-((*N'*-Boc)2-aminoethoxy)benzylamine (208)**



tert-Butyl(2-(4-formylphenoxy)ethyl)carbamate (620 mg, 2.3 mmol, 1.0 equiv.), dimethylamine (2.0 M in THF, 1.75 mL, 3.5 mmol, 1.5 equiv.), NaBH(OAc)₃ (740 mg, 3.5 mmol, 1.5 equiv.), and glacial acetic acid (5 drops) were combined in CH₂Cl₂ (20 mL) under an atmosphere of N₂. After 18 h, the reaction mixture was concentrated *in vacuo*, and sat. aq. NaHCO₃ (50 mL) was added. The aqueous suspension was extracted with CH₂Cl₂ (3 × 40 mL), and the combined organics were dried (Na₂SO₄), and concentrated *in vacuo*. The crude product was subjected to flash column chromatography (gradient up to 1:99 NEt₃/toluene) to yield the **title compound** (394 mg, 58%) as an off-white solid: m.p. (105 – 107 °C); ¹H NMR (500 MHz, CDCl₃) δ 7.21 (d, *J* = 8.6 Hz, 2H, H-2'), 6.84 (d, *J* = 8.6 Hz, 2H, H-3'), 4.99 (s, br, 1H, NH), 4.01 (t, *J* = 5.1 Hz, 2H, H-2), 3.55 – 3.50 (m, 2H, H-1), 3.35 (s, H, 2H, H-1'), 2.22 (s, 6H, H-2'), 1.45 (s, 9H, C(CH₃)₃); ¹³C{¹H} NMR (101 MHz, CDCl₃) δ 157.8 (C-1'), 156.0 (C=O), 131.5 (C-4'), 130.5 (C-3'), 114.3 (C-2'), 79.6 (C(CH₃)₃) 67.3 (C-1'), 63.8 (C-2), 45.4 (C-2'), 40.3 (C-1), 28.5 (C(CH₃)₃); (ESI⁺) *m/z* of [M+H]⁺ detected: 295.2021, expected for C₁₆H₂₆N₂O₃: 295.2016; *v*_{max} (thin film)/cm⁻¹ 3203 (N-H, s), 2945 (N-H, s), 2819 (C-H, s), 2775 (C-H, s), 1705 (C=O, s), 1613 (C-H bend, w), 1546 (m), 1514 (s), 1451 (m), 1368 (m), 1240 (s), 1173 (s), 1154 (s), 1110 (m).

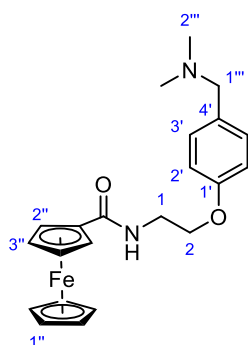
***N,N*-Dimethyl-4-(2-aminoethoxy)benzylamine dihydrochloride (209)**



N,N-Dimethyl-4-((*N'*-Boc)2-aminoethoxy)benzylamine (150 mg, 500 μmol, 1.0 equiv.) was added to 4 M HCl in dioxane (10 mL) that had been cooled to 0 °C under N₂. The reaction mixture was allowed to warm to rt and stirred for 30 min before being concentrated *in vacuo* to yield the **title compound** (130 mg, 99%) as an off-white solid; m.p. (decomposes at

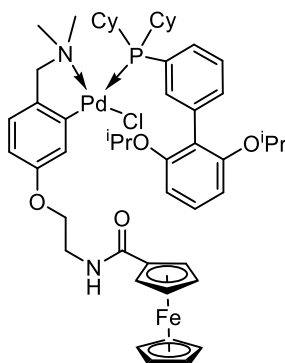
198 °C); R_f 0.32 (5:95:1 MeOH/CH₂Cl₂/NEt₃); ¹H NMR (400 MHz, Methanol-*d*₄) δ 7.50 (d, J = 8.7 Hz, 2H, H-2'), 7.13 (d, J = 8.7 Hz, 2H, H-3'), 4.33 – 4.23 (m, 4H, H-1'', H-1), 3.40 (t, J = 5.0 Hz, 2H, H-2), 2.83 (s, 6H, H-2''); ¹³C{¹H} NMR (101 MHz, MeOD) δ 160.8 (C-1'), 133.7 (C-3'), 124.0 (C-4'), 116.4 (C-2'), 65.5 (C-2), 61.6 (C-1''), 42.7 (C-1), 40.3 (C-2''); (ESI⁺) m/z of [M+H]⁺ detected: 195.1494, expected for C₁₁H₁₈N₂O: 195.1492; ν_{\max} (thin film)/cm⁻¹ 2953 (N-H, br, s), 2827 (C-H, s), 2771 (C-H, s), 1709 (s), 1613 (w), 1550 (w), 1514 (s), 1459 (w), 1368 (w), 1280 (m), 1237 (s), 1169 (m), 1150 (m).

***N,N*-Dimethyl-4-(*N'*-(ferrocene amide)-2-aminoethoxy)benzylamine (210)**



N,N-dimethyl-4-(2-aminoethoxy)benzylamine dihydrochloride (53 mg, 200 μmol, 1.0 equiv.) and NEt₃ (58 μL, 400 μmol, 2.0 equiv.) were combined in CH₂Cl₂ (5 mL). After stirring for 5 min, ferrocene carboxylic acid (46 mg, 200 μmol, 1.0 equiv.), HOBt·H₂O (34 mg, 220 μmol, 1.1 equiv.) and EDC·HCl (42 mg, 220 μmol, 1.1 equiv.) were added, and the resulting solution was stirred for 3 h. The reaction mixture was diluted with H₂O (30 mL) and extracted with CH₂Cl₂ (2 × 30 mL). The combined organics were washed with brine (50 mL), dried (Na₂SO₄) and concentrated *in vacuo*. The crude residue was subjected to flash column chromatography (1:99 NEt₃/CH₂Cl₂) to yield the **title compound** (53 mg, 65%) as an orange solid: m.p. (100 – 102 °C); ¹H NMR (400 MHz, CDCl₃) δ 7.15 (d, J = 8.6 Hz, 2H, H-3'), 6.83 (d, J = 8.6 Hz, 2H, H-2'), 6.08 (s, 1H, NH), 4.60 (t, J = 2.0 Hz, 2H, H-1), 4.27 (t, J = 2.0 Hz, 2H, H-2), 4.09 (s, 4H, H-1''), 4.06 (t, J = 5.0 Hz, 2H, H-3''), 3.75 – 3.68 (m, 2H, H-2''), 3.28 (s, 2H, NCH₂), 2.14 (s, 6H, NCH₃); ¹³C{¹H} NMR (101 MHz, CDCl₃) δ 170.7 (C=O), 157.8 (C-1'), 131.8 (C-4'), 130.6 (C-3'), 114.3 (C-2'), 76.0 (Cp-C), 70.6 (Cp-C), 69.9 (C-2), 68.3 (Cp-C), 67.1 (Cp-C), 63.8 (C-1'''), 45.4 (C-1), 39.3 (C-2'''); (ESI⁺) m/z of [M+H]⁺ detected: 405.1462, expected for C₂₂H₂₆FeN₂O₂: 405.1463; ν_{\max} (thin film)/cm⁻¹ 3290 (N-H, br, s), 2934 (C-H, br, m), 2815 (C-H, s), 2763 (C-H, s), 1625 (C=O, s), 1538 (s), 1506 (s), 1451 (m), 1296 (m), 1237 (s), 1177 (m), 1106 (m), 1023 (m), 809 (s).

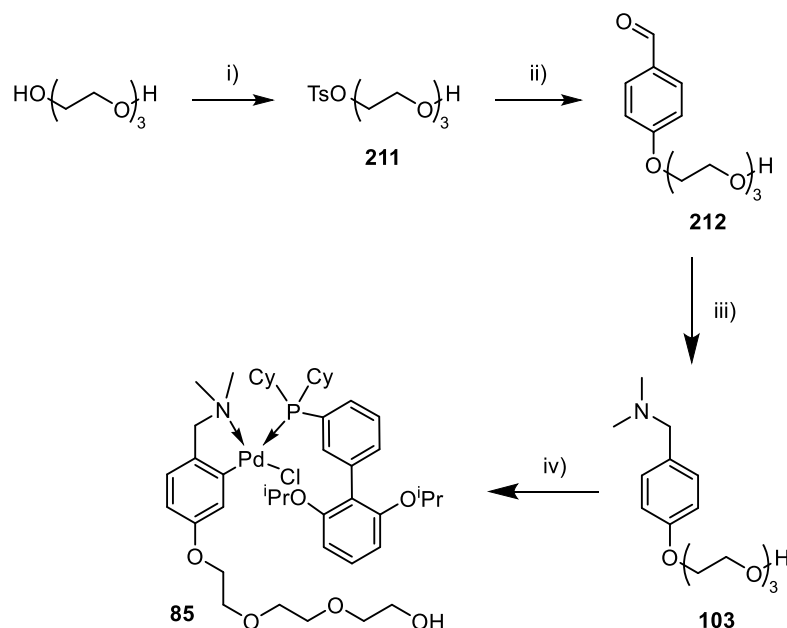
**Pd(*N,N*-dimethyl-4-(*N'*-(ferrocene amide)-2-aminoethoxy)benzylamine)(RuPhos)Cl
(84)**



N,N-Dimethyl-4-(*N'*-(ferrocene amide)-2-aminoethoxy)benzylamine (20 mg, 50 μ mol, 1.0 equiv.), PdCl₂ (9 mg, 50 μ mol, 1.0 equiv.), NaCl (6 mg, 100 μ mol, 2.0 equiv.), NaOAc (4 mg, 50 μ mol, 1.0 equiv.), and H₂O (3 μ L, 150 μ mol, 3.0 equiv.) were combined in MeOH (500 μ L) and stirred for 24 h. The resulting solid formed was isolated *via* gravity filtration, washed with H₂O (3 mL) and MeOH (2 \times 3 mL), and dried under high vacuum to an orange solid (16 mg).

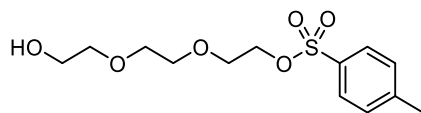
This intermediate (16 mg, 15 μ mol, 1.0 equiv.) was combined with RuPhos (14 mg, 30 μ mol, 2.0 equiv.) in CH₂Cl₂ (2 mL) and stirred for 1 h. After removal of the solvent, the resulting solid was dissolved in MTBE/Pentane (1:4, 2 mL) and placed in the freezer for 30 min. The supernatant was pipetted off and the solid was washed with pentane (2 \times 2 mL) to yield the **title compound** (23 mg, 60% yield over two steps) as an orange solid: ³¹P{¹H} NMR (162 MHz, CDCl₃) δ 66.87; (ESI⁺) *m/z* of [M-Cl]⁺ detected: 973.3322, expected for C₅₂H₆₈ClFeN₂O₄PPd: 973.3330.

Synthesis of Pd(*N,N*-dimethyl-4-(2-(2-(2-hydroxyethoxy)ethoxy)ethoxy)benzylamine) (RuPhos)Cl (85)



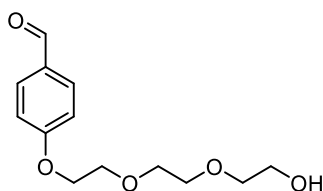
Scheme 70: **Reagents and conditions:** i) 4-Toluenesulfonyl chloride (0.25 equiv.), DMAP (0.5 mol%), NEt_3 (0.25 equiv.), CH_2Cl_2 , 0 °C – rt, 20 h, 56%; ii) 4-hydroxybenzaldehyde (1.3 equiv.), K_2CO_3 (2.0 equiv.), DMF, 100 °C, 2.5 h, 73%; iii) $\text{NaBH}(\text{OAc})_3$ (1.5 equiv.), dimethylamine (2.0 M in THF, 1.5 equiv.), CH_2Cl_2 , rt, 72 h; 85%; iv) Na_2PdCl_4 (1 equiv.), NEt_3 (1 equiv.), MeOH, rt, 1 h, then RuPhos (1 equiv.), CH_2Cl_2 , 72%.

2-(2-(2-Hydroxyethoxy)ethoxy)ethyl 4-methylbenzenesulfonate (211)



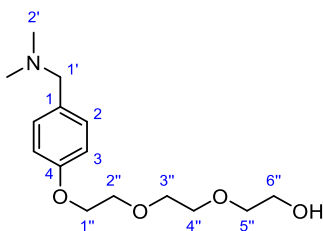
4-Toluenesulfonyl chloride (950 mg, 5.0 mmol, 1.0 equiv.) was added to a solution of triethylene glycol (2.8 mL, 21 mmol, 4.1 equiv.), 4-dimethylaminopyridine (12 mg, 0.10 mmol, 0.020 equiv.) and NEt_3 (0.80 mL, 5.5 mmol, 1.1 equiv.) in CH_2Cl_2 (25 mL) that had been cooled to 0 °C. After 20 h, the reaction mixture was diluted with CH_2Cl_2 (40 mL), washed with aq. HCl (1 M, 40 mL), H_2O (40 mL) and brine (40 mL). The organic component was dried (Na_2SO_4) and concentrated *in vacuo*. The crude residue was then subjected to flash column chromatography (4:1 EtOAc/Petrol ether 40 – 60) to yield the **title compound** (950 mg, 56%) as a clear oil: R_f 0.24 (4:1 EtOAc/Petrol ether 40 – 60); ^1H NMR (500 MHz, CDCl_3) δ 7.80 (d, $J = 8.3$ Hz, 2H), 7.35 – 7.33 (m, 2H), 4.17 (t, $J = 4.7$ Hz, 2H), 3.74 – 3.68 (m, 4H), 3.61 (s, 4H), 3.59 – 3.56 (m, 2H), 2.45 (s, 3H). The spectral data are in agreement with reported literature values.¹⁸⁹

4-(2-(2-(2-Hydroxyethoxy)ethoxy)ethoxy)benzaldehyde (212)



2-(2-(2-(2-Hydroxyethoxy)ethoxy)ethyl 4-methylbenzenesulfonate (940 mg, 3.1 mmol, 1.0 equiv.) was added to a solution of 4-hydroxybenzaldehyde (490 mg, 4.0 mmol, 1.3 equiv.) and K_2CO_3 (860 mg, 6.2 mmol, 2.0 equiv.) in anhydrous *N,N*-dimethylformamide (10 mL). The resulting solution was heated to 100 °C for 2.5 h before being diluted with aq. HCl (1 M, 50 mL), and extracted with CH_2Cl_2 (3 × 50 mL). The combined organics were washed with aq. LiCl (0.5 M, 3 × 50 mL), dried (Na_2SO_4) and concentrated *in vacuo*. The resulting crude residue was subjected to flash column chromatography (gradient from 4:1 EtOAc/Petrol ether 40 – 60 to 100% EtOAc) to yield the **title compound** (580 mg, 73%) as a colourless oil: 1H NMR (400 MHz, $CDCl_3$) δ 9.89 (s, 1H), 7.83 (d, $J = 8.7$ Hz, 2H), 7.03 (d, $J = 8.7$ Hz, 2H), 4.24 – 4.20 (m, 2H), 3.92 – 3.88 (m, 2H), 3.77 – 3.69 (m, 6H), 3.65 – 3.60 (m, 2H). The spectral data are in agreement with reported literature values.¹⁸⁹

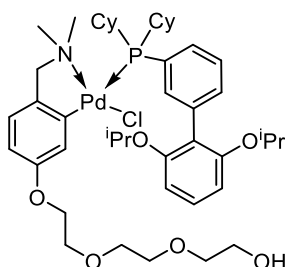
N,N-Dimethyl-4-(2-(2-(2-hydroxyethoxy)ethoxy)ethoxy)benzylamine (103)



4-(2-(2-(2-Hydroxyethoxy)ethoxy)ethoxy)benzaldehyde (510 mg, 2.0 mmol, 1.0 equiv.), dimethylamine (2.0 M in THF, 1.5 mL, 3.0 mmol, 1.5 equiv.) and $NaBH(OAc)_3$ (640 mg, 3.0 mmol, 1.5 equiv.) were combined in CH_2Cl_2 (20 mL) and stirred for 72 h at rt. After which, the reaction mixture was concentrated *in vacuo*, sat. aq. $NaHCO_3$ (60 mL) was added, and the aqueous mixture was extracted with $CH_2Cl_2/iPrOH$ (2:1, 60 mL). The organic component was washed with H_2O (60 mL), brine (60 mL), dried (Na_2SO_4), and concentrated *in vacuo*. The crude material was then purified *via* Strata® SCX (55 μm , 70 Å) 5g cartridge (eluted with $CH_2Cl_2/MeOH$ 90:10 then 2.0 M NH_3 in EtOH) to yield the **title compound** (461 mg, 85%) as a pale yellow oil: 1H NMR (400 MHz, $CDCl_3$) δ 7.21 (d, $J = 8.6$ Hz, 2H, H-3), 6.87 (d, $J = 8.6$ Hz, 1H, H-4), 4.15 – 4.11 (m, 2H, H-1''), 3.88 – 3.85 (m, 2H),

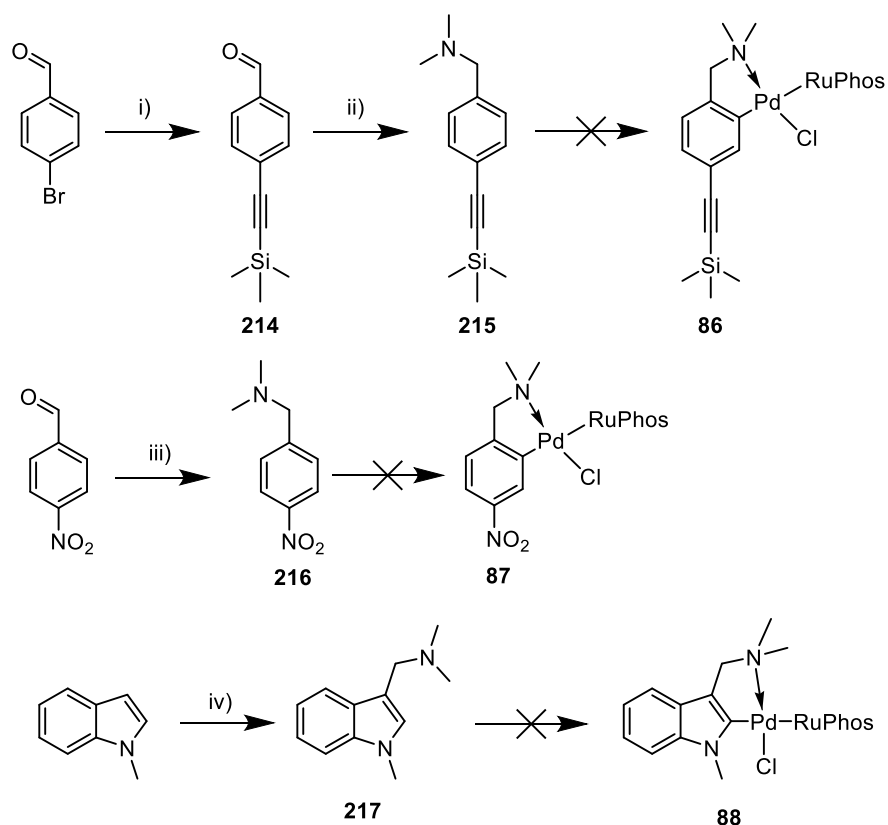
3.76 – 3.68 (m, 6H), 3.63 – 3.60 (m, 2H), 3.38 (s, 2H, H-1'), 2.23 (s, 6H, H-2'); $^{13}\text{C}\{^1\text{H}\}$ NMR (101 MHz, CDCl_3) δ 158.1 (C-4), 130.6 (C-1), 130.5 (C-2), 114.5 (C-3), 72.6, 70.9, 70.5, 69.9, 67.5, 63.6, 61.8, 45.1; (ESI⁺) m/z of $[\text{M}+\text{H}]^+$ detected: 284.1857, expected for $\text{C}_{15}\text{H}_{25}\text{NO}_4$: 284.1856; ν_{max} (thin film)/ cm^{-1} 3330 (O-H, br, w), 2930 (C-H, s), 2862 (C-H, s), 2819 (C-H, s), 2767 (C-H, s), 1613 (m), 1514 (s), 1451 (m), 1372 (w), 1237 (s), 1181 (w), 1122 (s), 1058 (C-O, s), 928 (w), 852 (m), 809 (m).

Pd(*N,N*-dimethyl-4-(2-(2-(2-hydroxyethoxy)ethoxy)ethoxy)benzylamine)(RuPhos)Cl (85)



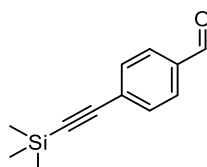
N,N-Dimethyl-4-(2-(2-(2-hydroxyethoxy)ethoxy)ethoxy)benzylamine (21 mg, 74 μmol , 1.0 equiv.), NEt_3 (11 μL , 74 μmol , 1.0 equiv.) and Na_2PdCl_4 (22 mg, 74 μmol , 1.0 equiv.) were combined in MeOH (500 μL) and stirred for 1 h before being concentrated. The residue was suspended in CH_2Cl_2 (1 mL) and filtered. RuPhos (35 mg, 74 μmol , 1.0 equiv.) was added to the filtrate and the mixture was stirred for 30 min before being concentrated. MTBE/pentane (1:4, 2 mL) was added to the residue, and the suspension was placed in the freezer for 2 h. The supernatant was pipetted off, the mixture suspended in Et_2O and filtered to remove any NEt_3HCl . The Et_2O was then removed *in vacuo* to yield the **title compound** (47 mg, 72%) as a crystalline solid: $^{31}\text{P}\{^1\text{H}\}$ NMR (162 MHz, CDCl_3) δ 34.01; (ESI⁺) m/z of $[\text{M}]^+$ detected: 850.3744, expected for $\text{C}_{45}\text{H}_{67}\text{NO}_6\text{PPd}$: 850.3756.

Failed Syntheses of 86 87 and 88



Scheme 71: **Reagents and conditions:** i) Trimethylsilylacetylene (1.5 equiv.), Pd(PPh₃)₄ (4 mol%), CuI (10 mol%), Et₃N (4.0 equiv.), THF, Ar, rt, 16 h, 96%; ii) dimethylamine (2.0 M in THF, 1.5 equiv.), NaBH(OAc)₃ (1.5 equiv.), AcOH (cat.), DCE, rt, 2.5 h, 95%; iii) dimethylamine (2.0 M in THF, 1.5 equiv.), NaBH(OAc)₃ (1.5 equiv.), AcOH (cat.), THF, rt, 1 h, 52%; iv) dimethylamine (40% in H₂O), AcOH, formaldehyde (37% in H₂O), 0 °C – rt, 1 h, 99%.

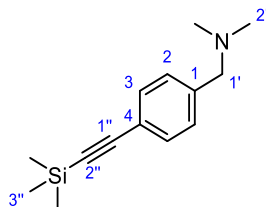
4-((Trimethylsilyl)ethynyl)benzaldehyde (214)



4-Bromobenzaldehyde (460 mg, 2.5 mmol, 1.0 equiv.), trimethylsilylacetylene (0.52 mL, 3.8 mmol, 1.5 equiv.), Pd(PPh₃)₄ (120 mg, 0.10 mmol, 4 mol%), CuI (48 mg, 0.25 mmol, 10 mol%), and Et₃N (1.4 mL, 10 mmol, 4.0 equiv.) were combined in dry THF in anhydrous conditions under an atmosphere of argon. The resulting mixture was stirred at rt overnight and concentrated *in vacuo*. The resulting crude mixture was treated with pentane (10 mL) and filtered through Celite® before being concentrated *in vacuo* and subjected to flash column chromatography (gradient up to 2% EtOAc in petroleum ether 40 – 60) to yield the **title compound** (484 mg, 96%) as a light brown solid: R_f 0.51 (petroleum ether 40 – 60/EtOAc 95:5); m.p. 63 – 65 °C (from petroleum ether 40 – 60) [lit.⁴ 66 – 67 °C];

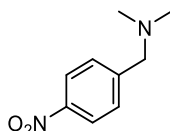
^1H NMR (400 MHz, CDCl_3) δ 10.00 (s, 1H), 7.82 (d, $J = 8.4$ Hz, 2H), 7.60 (d, $J = 8.4$ Hz, 2H), 0.27 (s, 9H). The data are in agreement with reported literature values.¹⁹⁰

N,N-Dimethyl-4-((trimethylsilyl)ethynyl)benzylamine (215)



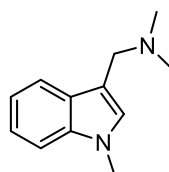
4-((Trimethylsilyl)ethynyl)benzaldehyde (480 mg, 2.25 mmol, 1.0 equiv.), dimethylamine (2.0 M in THF, 1.8 mL, 3.49 mmol, 1.6 equiv.), $\text{NaBH}(\text{OAc})_3$ (720 mg, 3.38 mmol, 1.5 equiv.) and glacial acetic acid (3 drops) were combined in DCE (10 mL). The resulting mixture was stirred at rt for 2.5 hr, after which sat. aq. NaHCO_3 (20 mL) was added. The mixture was separated, and the aqueous components were extracted with CH_2Cl_2 (3×10 mL). The combined organics were washed with brine (20 mL), dried (Na_2SO_4) and concentrated *in vacuo* to yield the **title compound** (494 mg, 95%) as a light brown oil: R_f 0.36 ($\text{CH}_2\text{Cl}_2/\text{MeOH}$ 95:5); ^1H NMR (500 MHz, CDCl_3) δ 7.42 (d, $J = 8.2$ Hz, 2H, H-2), 7.25 – 7.21 (m, 2H, H-3), 3.40 (s, 2H, H-1'), 2.21 (s, 6H, H-2'), 0.24 (s, 9H, H-3); $^{13}\text{C}\{^1\text{H}\}$ NMR (126 MHz, CDCl_3) δ 139.7 (C-1), 132.0 (C-2), 129.0 (C-3), 121.9 (C-4), 105.3 (C-1'), 94.0 (C-2'), 64.3 (C-1'), 45.5 (C-2'), 0.2 (C-3').

N,N-Dimethyl-4-nitrobenzylamine (216)



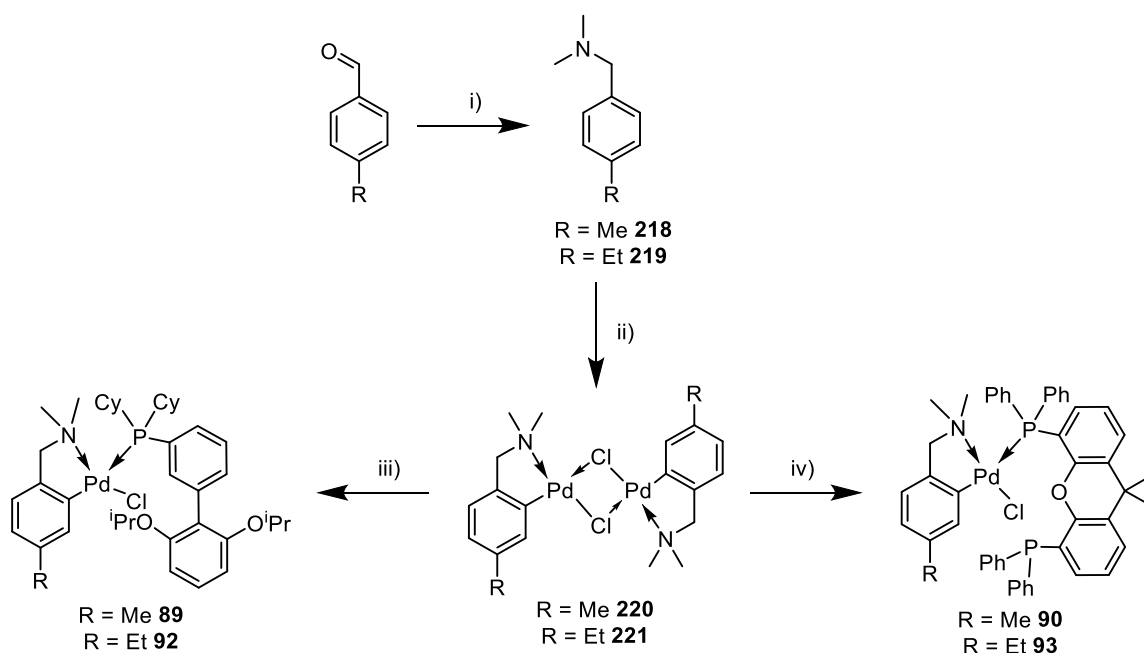
4-Nitrobenzaldehyde (300 mg, 2.0 mmol, 1.0 equiv.), dimethylamine (2.0 M in THF, 1.5 mL, 3.0 mmol, 1.5 equiv.), $\text{NaBH}(\text{OAc})_3$ (630 mg, 3.0 mmol, 1.5 equiv.), and glacial acetic acid (3 drops) were combined in THF (20 mL). After 1 h, the reaction mixture was concentrated *in vacuo*, and sat. aq. NaHCO_3 (25 mL) and CH_2Cl_2 (25 mL) were added. The organics were separated, and the aqueous component was further extracted with CH_2Cl_2 (2×25 mL). The combined organics were washed with brine (25 mL), dried (Na_2SO_4), and concentrated *in vacuo*. The crude residue was subjected to flash column chromatography (99:1 toluene/ NEt_3) to yield the **title compound** (186 mg, 52%) as a yellow oil; R_f 0.26 (99:1 toluene/ NEt_3); ^1H NMR (400 MHz, CDCl_3) δ 8.18 (d, $J = 8.7$ Hz, 2H), 7.50 (d, $J = 8.7$ Hz, 2H), 3.53 (s, 2H), 2.27 (s, 6H). The spectral data are in agreement with literature values.¹⁸⁶

3-(*N,N*-Dimethylaminomethyl)-1-methylindole (217)



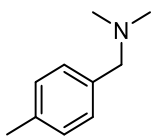
Dimethylamine (40% in H₂O, 290 μ L) and glacial acetic acid (440 μ L) were combined at 0 °C. Formaldehyde (37% in H₂O, 170 μ L) and 1-methylindole (250 μ L, 2.0 mmol) were added, and the resulting solution was allowed to warm to rt and stirred for 1 h. NaOH (10% in H₂O, 20 mL) was added, and the oil was extracted into Et₂O (3 \times 20 mL). The combined organics were dried (MgSO₄) and concentrated *in vacuo* to yield the **title compound** (370 mg, 99%) as a yellow oi. No further purification was necessary: *R_f* 0.35 (MeOH/CH₂Cl₂/NEt₃ 4:97:1); ¹H NMR (400 MHz, CDCl₃) δ 7.69 (d, *J* = 8.1 Hz, 1H), 7.30 (d, *J* = 8.1 Hz, 1H), 7.23 (ddd, *J* = 8.1, 7.0, 1.2 Hz, 1H), 7.12 (ddd, *J* = 8.1, 7.0, 1.2 Hz, 1H), 7.00 (s, 1H) 3.77 (s, 3H), 3.63 (s, 2H), 2.29 (s, 6H). The spectral data are in agreement with reported literature values.¹⁹¹

Syntheses of 89, 90, 92 and 93



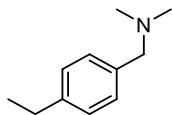
Scheme 72: Reagents and conditions: i) dimethylamine (2.0 M in THF, 1.5 equiv.), NaBH(OAc)₃ (1.5 equiv.), CH₂Cl₂, rt, 16 h, R = Me 58%, R = Et 31%; ii) PdCl₂ (1 equiv.), NaOAc (1 equiv.), MeOH, rt, 16 h, R = Me 68%, R = Et 41%; iii) RuPhos (1 equiv.), CH₂Cl₂, rt, 1 h, R = Me 75%, R = Et 89%; iv) Xantphos (1 equiv.), CH₂Cl₂, rt, 1 h, R = Me 70%, R = Et 93%.

N,N-Dimethyl-4-methylbenzylamine (218)



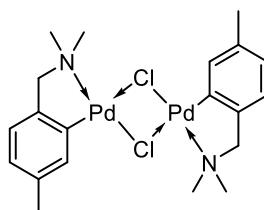
p-Tolualdehyde (120 mg, 1.0 mmol, 1.0 equiv.), dimethylamine (2.0 M in THF, 750 μ L, 1.5 mmol, 1.5 equiv.), and NaBH(OAc)₃ (320 mg, 1.5 mmol, 1.5 equiv.), were combined in CH₂Cl₂ (20 mL). After 1 h, the reaction mixture was concentrated *in vacuo*, and sat. aq. NaHCO₃ (25 mL) and CH₂Cl₂ (25 mL) were added. The organics were separated, and the aqueous component was further extracted with CH₂Cl₂ (2 \times 25 mL). The combined organics were washed with brine (25 mL), dried (Na₂SO₄), and concentrated *in vacuo*. The crude residue was subjected to flash column chromatography (gradient from 30:69:1 to 40:59:1 EtOAc/petroleum ether/NEt₃) to yield the **title compound** (87 mg, 58%) as a clear oil; ¹H NMR (400 MHz, CDCl₃) δ 7.19 (d, *J* = 8.1 Hz, 2H), 7.13 (d, *J* = 7.9 Hz, 2H), 3.39 (s, 2H), 2.34 (s, 3H), 2.23 (s, 6H); ¹³C{¹H} NMR (101 MHz, CDCl₃) δ 136.8, 135.8, 129.2, 129.0, 64.2, 45.4, 21.2. The spectral data are in agreement with reported literature values.¹⁹²

N,N-Dimethyl-4-ethylbenzylamine (219)



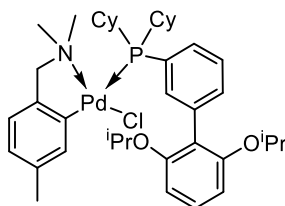
4-Ethylbenzaldehyde (127 μ L, 1.0 mmol, 1.0 equiv.), dimethylamine (2.0 M in THF, 750 μ L, 1.5 mmol, 1.5 equiv.), and NaBH(OAc)₃ (320 mg, 1.5 mmol, 1.5 equiv.), were combined in CH₂Cl₂ (20 mL). After 1 h, the reaction mixture was concentrated *in vacuo*, and sat. aq. NaHCO₃ (25 mL) and CH₂Cl₂ (25 mL) were added. The organics were separated, and the aqueous component was further extracted with CH₂Cl₂ (2 \times 25 mL). The combined organics were washed with brine (25 mL), dried (Na₂SO₄), and concentrated *in vacuo*. The crude residue was subjected to flash column chromatography (gradient from 20:79:1 to 30:69:1 Et₂O/toluene/NEt₃) to yield the **title compound** (51 mg, 31%) as a clear oil; ¹H NMR (400 MHz, CDCl₃) δ 7.22 (d, *J* = 8.1 Hz, 2H), 7.15 (d, *J* = 8.1 Hz, 2H), 3.39 (s, 2H), 2.64 (q, *J* = 7.6 Hz, 2H), 2.23 (s, 6H), 1.24 (t, *J* = 7.6 Hz, 3H); ¹³C{¹H} NMR (101 MHz, CDCl₃) δ 143.1, 136.2, 129.2, 127.8, 64.3, 45.5, 28.7, 15.7. The spectral data are in agreement with reported literature values.¹⁹³

[Pd(*N,N*-dimethyl-4-methylbenzylamine)(μ -Cl)]₂ (220**)**



4-Methyl-*N,N*-dimethylbenzylamine (72 mg, 440 μ mol, 1.0 equiv.), PdCl₂ (66 mg, 440 μ mol, 1.0 equiv.) and NaOAc (36 mg, 440 μ mol, 1.0 equiv.) were combined in MeOH (5 mL) and stirred at rt overnight. The reaction was filtered, and the isolated solid washed with MeOH (3 \times 2 mL). The solid was then suspended in CH₂Cl₂, filtered to remove Pd black that had formed during the reaction, and concentrated *in vacuo* to yield the **title compound** (87 mg, 68%) as a green solid: ¹H NMR (400 MHz, CDCl₃) δ 7.02 – 6.94 (m, 1H), 6.80 – 6.73 (m, 2H), 3.89 (s, 2H), 2.88 – 2.79 (m, 6H), 2.29 – 2.24 (m, 3H); ¹³C{¹H} NMR (101 MHz, CDCl₃) δ 144.0, 143.8, 143.0, 134.9, 134.8, 134.1, 133.5, 125.6, 121.3, 73.2, 73.1, 53.0, 52.6, 21.5; (ESI⁺) *m/z* [M-Cl]⁺ detected: 545.0016, expected for C₂₀H₂₈Cl₂N₂Pd₂: 545.0015; ν_{max} (thin film)/cm⁻¹ 2914 (w), 2170 (w), 2036 (w), 1585 (m), 1436 (m), 1399 (m), 1238 (w), 1200 (w), 1041 (w), 980 (w), 884 (w), 853 (s), 815 (m), 791 (w), 740 (w), 674 (w), 532 (m), 510 (m), 427 (m). (*N.B.* Observed complexity in ¹H and ¹³C spectra due to the presence of *cis*- and *trans*- isomers).

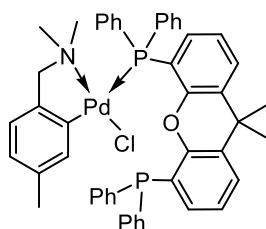
Pd(*N,N*-dimethyl-4-methylbenzylamine)(RuPhos)Cl (89**)**



[Pd(*N,N*-dimethyl-4-methylbenzylamine)(μ -Cl)]₂ (**220**) (29 mg, 50 μ mol, 1.0 equiv.) and RuPhos (47 mg, 100 μ mol, 2.0 equiv.) were combined in CH₂Cl₂ (2 mL). After 1 h, the mixture was concentrated *in vacuo*. MTBE (200 μ L) and pentane (800 μ L) were added, and the mixture was left to stand for 15 min. After which, the supernatant was pipetted off, and the resulting solid was washed with pentane (2 \times 1 mL) to yield the **title compound** (57 mg, 75%) as a colourless solid: m.p. decomposes at 190 $^{\circ}$ C; ¹H NMR (400 MHz, CDCl₃) δ 7.53 (dd, *J* = 14.2, 7.8 Hz, 1H), 7.31 – 7.21 (m, 2H), 6.98 – 6.89 (m, 2H), 6.74 (d, *J* = 7.4 Hz, 1H), 6.61 (d, *J* = 8.4 Hz, 2H), 6.58 – 6.52 (m, 1H), 6.06 (d, *J* = 5.4 Hz, 1H), 4.50 (s, 2H), 3.89 (s, 2H), 2.71 (s, 6H), 2.47 (s, 3H), 2.09 – 1.49 (m, 16H), 1.29 – 1.00 (m, 18H); ³¹P{¹H}

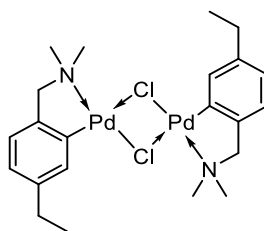
NMR (162 MHz, CDCl₃) δ 67.5; ¹³C{¹H} NMR (101 MHz, CDCl₃) δ 157.2, 151.8, 151.7, 144.5, 140.9, 140.7, 140.6, 139.9, 139.7, 133.7, 133.6, 133.5, 133.4, 128.8, 128.6, 128.6, 128.1, 127.8, 124.7, 124.6, 123.9, 122.6, 120.8, 106.3, 72.6, 70.8, 27.8, 27.7, 27.0, 26.9, 26.3, 22.4, 22.3, 21.9; (ESI⁺) *m/z* of [M–Cl]⁺ detected: 720.3171, expected for C₄₀H₅₇ClNO₂PPd: 720.3174; ν_{\max} (thin film)/cm⁻¹ 2989 (w), 2913 (m), 2847 (w), 1593 (w), 1447 (s), 1420 (m), 1249 (w), 1110 (s), 1057 (s), 996 (m), 847 (w), 798 (w), 760 (m), 728 (s), 568 (w), 538 (w), 476 (m), 453 (w), 428 (w).

Pd(*N,N*-dimethyl-4-methylbenzylamine)(Xantphos)Cl (90)



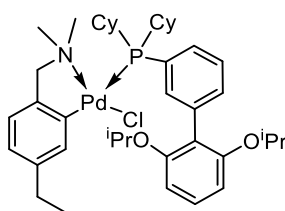
[Pd(*N,N*-dimethyl-4-methylbenzylamine)(μ -Cl)]₂ (**220**) (29 mg, 50 μ mol, 1.0 equiv.) and Xantphos (58 mg, 100 μ mol, 2.0 equiv.) were combined in CH₂Cl₂ (2 mL). After 1 h, the mixture was concentrated *in vacuo*. MTBE (200 μ L) and pentane (800 μ L) were added, and the mixture was left to stand for 15 min. After which, the solvent was pipetted off, and the resulting solid was washed with pentane (2 \times 1 mL) to yield the **title compound** (61 mg, 70%) as a yellow solid: ¹H NMR (400 MHz, CDCl₃) δ 7.60 – 7.07 (m, 22H), 6.98 (t, *J* = 7.7 Hz, 2H), 6.81 (s, 2H), 6.71 (d, *J* = 7.4 Hz, 1H), 6.53 – 6.43 (m, 1H), 5.98 (s, 1H), 3.78 (s, 2H), 2.60 (s, 6H), 1.84 – 1.51 (m, 8H); ¹³C{¹H} NMR (101 MHz, CDCl₃) δ 153.0, 151.7, 144.6, 137.6, 134.5, 134.0, 133.8, 130.6, 129.1, 128.0, 128.0, 128.0, 127.9, 123.6, 123.2, 122.1, 72.0, 49.9, 34.5, 21.4; (ESI⁺) *m/z* of [M–Cl]⁺ detected: 832.2103, expected for C₄₉H₄₆ClNOP₂Pd: 832.2101; ³¹P{¹H} NMR (162 MHz, CDCl₃) δ 3.4; m.p. decomposes at 201 °C; ν_{\max} (thin film)/cm⁻¹ 3064 (w), 3045 (w), 2978 (w), 1433 (m), 1402 (s), 1240 (s), 1093 (m), 853 (m), 741 (s), 694 (s), 515 (s), 462 (m), 439 (m).

[Pd(*N,N*-dimethyl-4-ethylbenzylamine)(μ -Cl)]₂ (221**)**



4-Ethyl-*N,N*-dimethylbenzylamine (51 mg, 310 μ mol, 1.0 equiv.), PdCl₂ (55 mg, 310 μ mol, 1.0 equiv.) and NaOAc (25 mg, 310 μ mol, 1.0 equiv.) were combined in MeOH (5 mL) and stirred at rt overnight. The reaction was filtered, and the isolated solid washed with MeOH (3 \times 2 mL). The solid was then suspended in CH₂Cl₂, filtered to remove Pd black that had formed during the reaction, and concentrated *in vacuo* to yield the **title compound** (39 mg, 41%) as a green solid: m.p. decomposes at 168 °C; ¹H NMR (400 MHz, CDCl₃) δ 7.05 – 6.96 (m, 1H), 6.83 – 6.75 (m, 2H), 3.90 (s, 2H), 2.90 – 2.77 (m, 6H), 2.64 – 2.50 (m, 2H), 1.24 – 1.15 (m, 3H); ¹³C{¹H} NMR (101 MHz, CDCl₃) δ 144.2, 144.1, 143.0, 141.4, 133.1, 132.5, 131.4, 124.3, 123.1, 121.4, 121.4, 73.3, 73.1, 53.0, 52.7, 29.0, 16.0; (ESI⁺) *m/z* [M-Cl]⁺ detected: 573.0330, expected for C₂₂H₃₂Cl₂N₂Pd₂: 573.0323; ν_{max} (thin film)/cm⁻¹ 3037 (m), 3002 (m), 2960 (s), 2911 (m), 2859 (w), 2833 (w), 2779 (w), 1586 (s), 1557 (m), 1451 (s), 1396 (s), 1197 (w), 1140 (w), 1037 (m), 1014 (m), 983 (s), 967 (s), 891 (m), 857 (s), 807 (s), 760 (m), 711 (m), 673 (w), 582 (m), 517 (m), 432 (m). (*N.B.* Observed complexity in ¹H and ¹³C spectra due to the presence of *cis*- and *trans*- isomers).

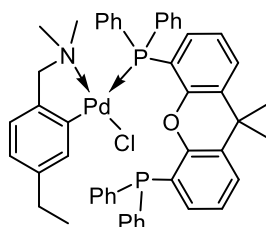
Pd(*N,N*-dimethyl-4-ethylbenzylamine)(RuPhos)Cl (92**)**



[Pd(*N,N*-dimethyl-4-ethylbenzylamine)(μ -Cl)]₂ (**221**) (15 mg, 25 μ mol, 1.0 equiv.) and RuPhos (23 mg, 50 μ mol, 2.0 equiv.) were combined in CH₂Cl₂ (2 mL). After 1 h, the mixture was concentrated *in vacuo*. MTBE (200 μ L) and pentane (800 μ L) were added, and the mixture was placed in a -20 °C freezer for 1 h. After which, the solvent was pipetted off, and the resulting solid was washed with pentane (3 \times 1 mL) to yield the **title compound** (34 mg, 89%) as a yellow solid: m.p. decomposes at 190 °C; ¹H NMR (400 MHz, CDCl₃) δ 7.66 – 7.55 (m, 1H), 7.31 – 7.22 (m, 2H), 7.02 – 6.92 (m, 2H), 6.80 (d, *J* = 7.5 Hz, 1H),

6.67 – 6.58 (m, 3H), 6.15 (d, $J = 5.2$ Hz, 1H), 4.53 – 4.43 (m, 2H), 3.90 (s, 2H), 2.71 (s, 6H), 2.51 (s, 2H), 2.13 – 1.48 (m, 16H), 1.20 – 1.02 (m, 18H), 0.88 (t, $J = 7.6$ Hz, 3H); $^{13}\text{C}\{^1\text{H}\}$ NMR (101 MHz, CDCl_3) δ 157.3, 151.6, 144.9, 140.9, 140.1, 139.5, 133.7, 133.7, 128.9, 128.8, 128.7, 124.9, 124.8, 122.8, 122.3, 121.1, 106.6, 72.7, 71.0, 28.9, 27.8, 27.7, 27.1, 26.3, 22.5, 21.9, 15.4; $^{31}\text{P}\{^1\text{H}\}$ NMR (162 MHz, CDCl_3) δ 67.1; (ESI⁺) m/z of $[\text{M}-\text{Cl}]^+$ detected: 734.3332, expected for $\text{C}_{41}\text{H}_{59}\text{ClINOPPd}$: 734.3328; ν_{max} (thin film)/ cm^{-1} 2915 (s), 2849 (s), 1590 (s), 1448 (s), 1381 (m), 1245 (s), 1110 (s), 1057 (s), 997 (m), 849 (m), 808 (m), 785 (m), 761 (m), 729 (m), 659 (w), 613 (w), 537 (m), 508 (w), 478 (m), 453 (m), 408 (w).

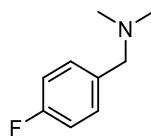
Pd(*N,N*-dimethyl-4-ethylbenzylamine)(Xantphos)Cl (93)



$[\text{Pd}(\text{N,N}\text{-dimethyl-4-ethylbenzylamine})(\mu\text{-Cl})_2$ (**221**) (15 mg, 25 μmol , 1.0 equiv.) and Xantphos (29 mg, 50 μmol , 2.0 equiv.) were combined in CH_2Cl_2 (2 mL). After 1 h, the mixture was concentrated *in vacuo*. MTBE (200 μL) and pentane (800 μL) were added, and the mixture was placed in a -20 $^\circ\text{C}$ freezer for 1 h. After which, the solvent was pipetted off, and the resulting solid was washed with pentane (3×1 mL) to yield the **title compound** (35 mg, 93%) as a yellow solid: m.p. decomposes at 205 $^\circ\text{C}$; ^1H NMR (400 MHz, CDCl_3) δ 7.51 – 7.02 (m, 22H), 6.96 (t, $J = 7.7$ Hz, 2H), 6.87 – 6.76 (m, 3H), 6.57 (dd, $J = 7.5$, 1.6 Hz, 1H), 6.17 (td, $J = 3.4$, 1.5 Hz, 1H), 3.82 (s, 2H), 2.62 (s, 6H), 1.91 (q, $J = 7.6$ Hz, 2H), 1.56 (br s, 6H), 0.66 (t, $J = 7.6$ Hz, 3H); $^{31}\text{P}\{^1\text{H}\}$ NMR (162 MHz, CDCl_3) δ 3.5; $^{13}\text{C}\{^1\text{H}\}$ NMR (101 MHz, CDCl_3) δ 152.9, 150.7, 145.3, 140.3, 137.1, 134.6, 134.6, 134.5, 133.8, 130.4, 129.0, 128.0, 128.0, 127.8, 123.1, 122.6, 122.2, 72.2, 50.2, 34.5, 28.6, 27.1, 15.2; (ESI⁺) m/z of $[\text{M}-\text{Cl}]^+$ detected: 846.2240, expected for $\text{C}_{50}\text{H}_{48}\text{ClINOP}_2\text{Pd}$: 846.2258; ν_{max} (thin film)/ cm^{-1} 2980 (w), 2927 (w), 1589 (w), 1434 (m), 1405 (s), 1246 (m), 1096 (w), 979 (m), 855 (s), 808 (w), 785 (w), 740 (s), 692 (s), 614 (w), 539 (w), 515 (s), 477 (w), 438 (m), 418 (m).

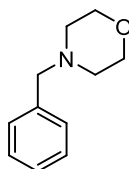
5.3.2. Synthesis of Compounds for *in situ* Arylation

N,N-Dimethyl-4-fluorobenzylamine (96)



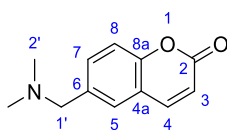
4-Fluorobenzaldehyde (210 μ L, 2.00 mmol, 1.0 equiv.), dimethylamine (2.0 M in THF, 1.5 mL, 3.0 mmol, 1.5 equiv.), and NaBH(OAc)₃ (640 mg, 3.00 mmol, 1.5 equiv.) were combined in CH₂Cl₂ (25 mL). The resulting mixture was stirred at rt for 3 hr, after which the mixture was concentrated *in vacuo*, and aq. NaOH (1 M, 40 mL) was added. The mixture was separated, and the aqueous components were extracted with Et₂O (3 \times 40 mL). The combined organics were dried (Na₂SO₄), concentrated *in vacuo*, and subjected to flash column chromatography (CH₂Cl₂/MeOH/Et₃N 98:1:1) to yield the **title compound** (256 mg, 84%) as a light brown oil: R_f 0.56 (CH₂Cl₂/MeOH/Et₃N 98:1:1); ¹H NMR (400 MHz, CDCl₃) δ 7.29 (dd, *J*_{H-H} = 8.6, *J*_{H-F} = 5.6 Hz, 2H), 7.01 (dd, *J*_{H-H} = 8.6 Hz, *J*_{H-F} = 8.7 Hz 2H), 3.44 (s, 2H), 2.26 (s, 6H); ¹⁹F NMR (376 MHz, CDCl₃) δ -115.47. The spectral data are in agreement with literature values.¹⁹⁴

N-Benzyl morpholine (98)



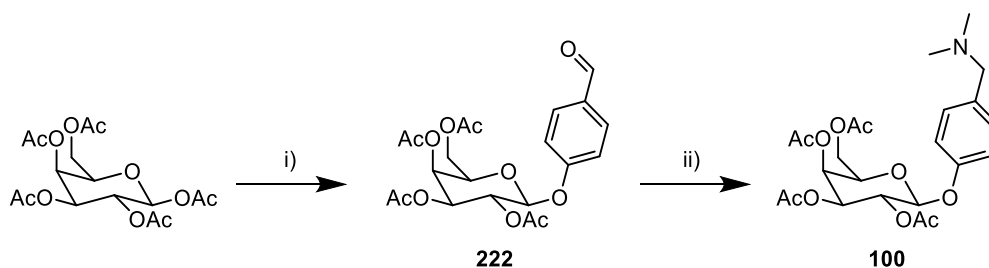
Benzyl bromide (400 μ L, 3.3 mmol, 1.1 equiv.) was added dropwise to a suspension of morpholine (260 μ L, 3.0 mmol, 1.0 equiv.) and K₂CO₃ (540 mg, 3.9 mmol, 1.3 equiv.) in MeCN (10 mL), and stirred for 16 h. After which, the resulting solids were filtered off, washed with EtOAc (3 \times 10 mL) and the combined organics were concentrated *in vacuo*. The crude material subjected to flash column chromatography (6:1 petroleum ether/EtOAc with 1% added NEt₃) to yield the **title compound** (530 mg, 99%) as a colourless liquid: ¹H NMR (400 MHz, CDCl₃) δ 7.34 – 7.23 (m, 5H), 3.75 – 3.66 (t, *J* = 4.7 Hz, 2H), 3.50 (s, 2H), 2.44 (t, *J* = 4.7 Hz, 2H); ¹³C{¹H} NMR (101 MHz, CDCl₃) δ 137.90, 129.33, 128.38, 127.27, 67.17, 63.61, 53.77. The spectral data are in agreement with reported literature values.¹⁹⁵

6-(*N,N*-Dimethylaminomethyl)coumarin (**99**)



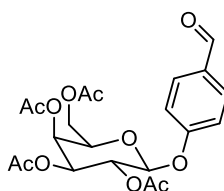
Coumarin-6-carboxaldehyde (210 mg, 1.0 mmol, 1.0 equiv.), dimethylamine (2.0 M in THF, 0.75 mL, 1.5 mmol, 1.5 equiv.), NaBH(OAc)₃ (210 mg, 1.0 mmol, 1.0 equiv.) and glacial acetic acid (3 drops) were combined in CH₂Cl₂ (25 mL) and stirred at rt. After which, sat. aq. NaHCO₃ (20 mL) was added, and the aqueous layer was extracted with CH₂Cl₂ (3 × 20 mL). The combined organic portions were dried (Na₂SO₄) and concentrated *in vacuo*. The crude material was subjected to flash column chromatography (gradient from 50:50 EtOAc/petroleum ether to 100% EtOAc with 1% NEt₃) to yield the **title compound** (156 mg, 77%) as a yellow oil; ¹H NMR (400 MHz, CDCl₃) δ 7.69 (d, *J* = 9.6 Hz, 1H, H-4), 7.51 – 7.42 (m, 2H, H-5, H-7), 7.29 (d, *J* = 8.4 Hz, 1H, H-8), 6.42 (d, *J* = 9.6 Hz, 1H, H-3), 3.46 (s, 2H, H-1'), 2.25 (s, 6H, H-2'); ¹³C{¹H} NMR (101 MHz, CDCl₃) δ 161.1 (C-2), 153.4 (C-8a), 143.6 (C-4), 135.7 (C-6), 132.7 (C-7), 128.0 (C-5), 118.8 (C-4a), 116.9 (C-8, C-3), 63.6 (C-1'), 45.5 (C-2'); (ESI⁺) *m/z* of [M+H]⁺ detected: 204.1021, expected for C₁₂H₁₃NO₂: 204.1019; ν_{max} (thin film)/cm⁻¹ 2921 (C-H, m), 2868 (C-H, m), 2827 (C-H, m), 2762 (C-H, m), 1723 (C=O, s), 1627 (m), 1572 (s), 1442 (s), 1385 (m), 1263 (m), 1169 (s), 1100 (s), 982 (m), 904 (m), 851 (m), 827 (s), 794 (s), 758 (m), 619 (m).

Synthesis of 4-(Per-(*O*)-acetyl-β-D-galactopyranosyl)oxy-*N,N*-dimethylbenzylamine (**100**)



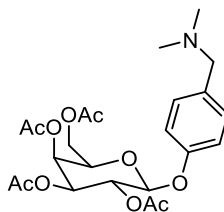
Scheme 73: Reagents and conditions: i) HBr (33 wt% in AcOH), AcOH, rt, 1 h, then 4-hydroxybenzaldehyde (2 equiv.), aq. NaOH (1 M), rt, 18 h, 44%; ii) dimethylamine (2.0 M in THF, 1.5 equiv.), NaBH(OAc)₃ (1.5 equiv.), CH₂Cl₂, rt, 16 h, 90%.

(Per-(*O*)-acetyl- β -D-galactopyranosyl)-4-oxybenzaldehyde (222)



β -D-Galactose pentaacetate (1.95 g, 5.0 mmol, 1.0 equiv.) was suspended in HBr (33 wt% in AcOH, 5 mL) and AcOH (2.5 mL) and stirred for 1 h, after which ice (20 g) was added. The aqueous phase was extracted with CH_2Cl_2 (3×40 mL). The combined organics were washed with sat. aq. NaHCO_3 (3×40 mL), dried (MgSO_4) and concentrated *in vacuo* to yield a colourless oil, which was taken forward without characterisation. The intermediate (1.99 g) in acetone (10 mL) was added dropwise to a solution of 4-hydroxybenzaldehyde (1.22 g, 10 mmol, 2.0 equiv.) in aq. NaOH (1 M, 10 mL) and the reaction mixture was stirred for 18 h. Aq. NaOH (50 mL) was added, and the reaction mixture was extracted with CH_2Cl_2 (3×50 mL), and the combined organics were washed with aq. NaOH (1 M, 2×50 mL), H_2O (50 mL), dried (MgSO_4) and concentrated *in vacuo* to give a pale yellow oil. The crude residue was subjected to flash column chromatography (gradient from 20:80 EtOAc/petroleum ether to 50:50 EtOAc/petroleum ether) to give a clear oil. Trituration with EtOH gave the **title compound** (1.0 g, 44% over two steps) as a colourless solid: ^1H NMR (400 MHz, CDCl_3) δ 9.93 (s, 1H), 7.85 (d, $J = 8.7$ Hz, 2H), 7.11 (d, $J = 8.7$ Hz, 2H), 5.52 (dd, $J = 10.4, 7.9$ Hz, 1H), 5.48 (d, $J = 3.3$ Hz, 1H), 5.17 (d, $J = 7.9$ Hz, 1H), 5.14 (dd, $J = 10.4, 3.3$ Hz, 1H), 4.27 – 4.09 (m, 3H), 2.19 (s, 3H), 2.07 (s, 6H), 2.02 (s, 3H). The spectral data are in agreement with reported literature values.¹⁹⁶

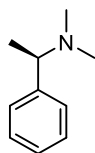
4-(Per-(*O*)-acetyl- β -D-galactopyranosyl)oxy-*N,N*-dimethylbenzylamine (100)



(Per-(*O*)-acetyl- β -D-galactopyranosyl)-4-oxybenzaldehyde (230 mg, 500 μmol , 1.0 equiv.) dimethylamine (2.0 M in THF, 0.38 mL, 750 μmol , 1.5 equiv.), and $\text{NaBH}(\text{OAc})_3$ (320 mg, 750 μmol , 1.5 equiv.) were combined in CH_2Cl_2 (20 mL) and stirred for 16 h. Sat. aq. NaHCO_3 (50 mL) was added, the aqueous component was extracted with CH_2Cl_2 (3×30 mL), and combined organics were concentrated *in vacuo*. The resulting residue was

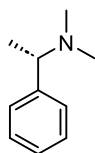
suspended in Et₂O, filtered, and concentrated *in vacuo* to yield the **title compound** (217 mg, 90%) as a colourless foam: R_f 0.49 (EtOAc/petroleum ether 50:50); m.p. 52 – 53 °C; ¹H NMR (400 MHz, CDCl₃) δ 7.22 (app d, *J* = 8.7 Hz, 2H), 6.95 (app d, *J* = 8.7 Hz, 2H), 5.51 – 5.44 (m, 2H), 5.10 (dd, *J* = 10.5, 3.4 Hz, 1H), 5.03 (d, *J* = 7.9 Hz, 1H), 4.26 – 4.13 (m, 2H), 4.07 – 4.03 (m, 1H), 3.37 (s, 2H), 2.22 (s, 6H), 2.18 (s, 3H), 2.06 (s, 3H), 2.06 (s, 3H), 2.01 (s, 3H); ¹³C{¹H} NMR (101 MHz, CDCl₃) δ 170.5, 170.4, 170.3, 169.5, 156.2, 134.0, 130.4, 116.9, 99.9, 71.2, 71.0, 68.8, 67.0, 63.7, 61.5, 45.4, 20.9, 20.8, 20.7; (ESI⁺) *m/z* of [M+H]⁺ detected: 482.2024, expected for C₂₃H₃₁NO₁₀: 482.2021; ν_{max} (thin film)/cm⁻¹ 2948 (w, C-H), 2861 (w, C-H), 2818 (w, C-H), 2775 (w, C-H), 1746 (s, C=O), 1502 (m), 1365 (m), 1208 (s), 1043 (s), 956 (w), 921 (w), 854 (w), 811 (w).

(R)-(+)-N,N-Dimethyl-1-phenylethylamine(101)



(R)-(+)-1-Phenylethylamine (0.64 mL, 5.0 mmol, 1.0 equiv.) was added dropwise to formic acid (0.95 mL, 25 mmol, 5.0 equiv.) that had been cooled to 0 °C. After which, formaldehyde (37% in H₂O, 1.23 mL, 3.0 equiv.) was added, and the resulting mixture was heated to 90 °C for 16 h. The mixture was allowed to cool, concentrated *in vacuo*, aq. NaOH (2.0 M, 25 mL) was added, and the aqueous component was extracted with CH₂Cl₂ (3 × 40 mL). The combined organics were dried with Na₂SO₄ and concentrated *in vacuo* to yield the **title compound** (520 mg, 70%) as a pale yellow oil: ¹H NMR (400 MHz, CDCl₃) δ 7.34 – 7.21 (m, 5H), 3.24 (q, *J* = 6.7 Hz, 1H), 2.20 (s, 6H), 1.37 (d, *J* = 6.7 Hz, 3H); [α]_D²³ +40 (*c* 1.0, CH₃OH). The spectral data are in agreement with reported literature values.¹⁹⁷

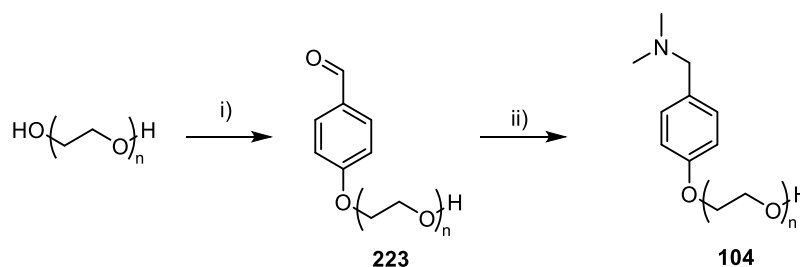
(S)-(-)-N,N-Dimethyl-1-phenylethylamine (102)



(S)-(-)-1-Phenylethylamine (0.64 mL, 5.0 mmol, 1.0 equiv.) was added dropwise to formic acid (0.95 mL, 25 mmol, 5.0 equiv.) that had been cooled to 0 °C. After which, formaldehyde (37% in H₂O, 1.23 mL, 3.0 equiv.) was added, and the resulting mixture was heated to 90 °C for 16 h. The mixture was allowed to cool, concentrated *in vacuo*, aq. NaOH (2.0 M, 25 mL) was added, and the aqueous component was extracted with CH₂Cl₂ (3 × 40 mL). The

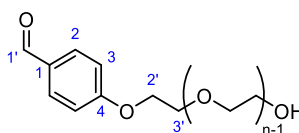
combined organics were dried with Na₂SO₄ and concentrated *in vacuo* to yield the **title compound** (520 mg, 70%) as a pale-yellow oil: ¹H NMR (400 MHz, CDCl₃) δ 7.35 – 7.21 (m, 5H), 3.24 (q, *J* = 6.7 Hz, 1H), 2.20 (s, 6H), 1.37 (d, *J* = 6.7 Hz, 3H); [α]_D²³ –44 (*c* = 1.0, CH₃OH). The spectral data are in agreement with reported literature values.¹⁹⁸

Synthesis of *N,N*-Dimethyl(4-(PEG-400))benzylamine (104)



Scheme 74: **Reagents and conditions:** i) 4-Toluenesulfonyl chloride (0.25 equiv.), DMAP (0.5 mol%), NEt₃ (0.25 equiv.), CH₂Cl₂, 0 °C – rt, 20 h, then 4-hydroxybenzaldehyde (1.3 equiv.), K₂CO₃ (2.0 equiv.), DMF, 100 °C, 2.5 h, 74%;
 iii) NaBH(OAc)₃ (1.5 equiv.), dimethylamine (2.0 M in THF, 1.5 equiv.), CH₂Cl₂, rt, 72 h; 63%.

4-(PEG-400)Benzaldehyde (223)



4-Toluenesulfonyl chloride (950 mg, 5.0 mmol, 1.0 equiv.) was added to a solution of PEG-400 (7.3 mL, 21 mmol, 4.1 equiv.), 4-dimethylaminopyridine (12 mg, 0.10 mmol, 0.020 equiv.) and NEt₃ (0.80 mL, 5.5 mmol, 1.1 equiv.) in CH₂Cl₂ (25 mL) that had been cooled to 0 °C. After 20 h, the reaction mixture was diluted with CH₂Cl₂ (40 mL), washed with aq. HCl (1 M, 40 mL), H₂O (40 mL) and brine (40 mL). The organic component was dried (Na₂SO₄) and concentrated *in vacuo* to yield PEG-400-OTs (2.46 g) as a colourless oil which was used without further purification.

4-Hydroxybenzaldehyde (600 mg, 4.9 mmol, 1.3 equiv.), PEG-400-OTs (2.1 g, 3.8 mmol, 1.0 equiv.) and K₂CO₃ (1.1 g, 7.6 mmol, 2.0 equiv.) were combined in DMF (20 mL) and heated to 100 °C for 90 min. After which, the reaction mixture was concentrated *in vacuo*, dissolved in IPA/CH₂Cl₂ (1:2, 60 mL), the organics washed with HCl (1 M, aq., 60 mL), NaOH (1 M, aq., 60 mL), LiCl (0.5 M, aq., 5 × 60 mL) to yield the **title compound** (1.86 g, 74% over 2 steps) as a colourless oil: ¹H NMR (400 MHz, CDCl₃) δ 9.88 (s, 1H, H-1'), 7.82 (d, *J* = 8.7 Hz, 2H, H-2), 7.02 (d, *J* = 8.7 Hz, 2H, H-3), 4.23 – 4.19 (t, *J* = 4.9 Hz, 2H, H-2'), 3.90 – 3.87 (t, *J* = 4.9 Hz, 2H, H-3'), 3.75 – 3.59 (m, 30H, -OCH₂), 2.50 (s, 1H, -OH); ¹³C{¹H} NMR (101 MHz, CDCl₃) δ 190.9 (C-1'), 164.0 (C-4), 132.1 (C-2), 130.2 (C-1), 115.0 (C-3), 72.7, 71.1, 70.8, 70.8, 70.7, 70.7, 70.5, 69.6, 67.9, 61.9; (ESI⁺) *m/z* of [M+H]⁺

detected: 475.2505, expected for $C_{23}H_{38}O_{10}$ ($n = 7$): 475.2538 (Figure 21); ν_{\max} (thin film)/ cm^{-1} 3485 (O-H, br, w), 2866 (C-H, br, s), 1689 (C=O, s), 1605 (s), 1574 (m), 1518 (w), 1455 (w), 1359 (w), 1300 (w), 1253 (s), 1094 (C-O, br, s).

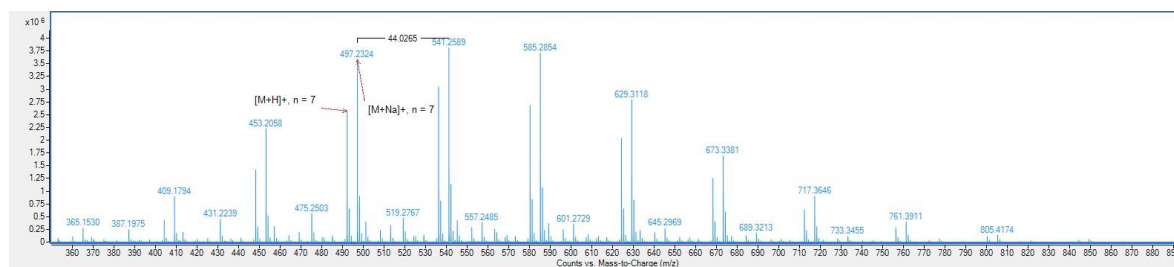
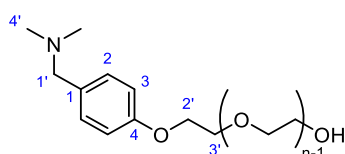


Figure 21: Mass spectrum of 223 showing distribution of peaks.

N,N-Dimethyl(4-(PEG-400))benzylamine (104)



4-(PEG-400)Benzaldehyde (1.1 g mg, 2.2 mmol, 1.0 equiv.), dimethylamine (2.0 M in THF, 1.7 mL, 3.3 mmol, 1.5 equiv.) and $NaBH(OAc)_3$ (700 mg, 3.3 mmol, 1.5 equiv.) were combined in CH_2Cl_2 (20 mL) and stirred for 72 h at rt. After which, the reaction mixture was diluted with sat. aq. $NaHCO_3$ (60 mL), and the aqueous mixture was extracted with $CH_2Cl_2/iPrOH$ (2:1, 60 mL). The organic component was washed with H_2O (60 mL), brine (60 mL), dried (Na_2SO_4), and concentrated *in vacuo*. The crude material was then purified *via* Strata® SCX (55 μm , 70 Å) 5g cartridge (eluted with $CH_2Cl_2/MeOH$ 90:10 then 2.0 M NH_3 in MeOH) to yield the **title compound** (750 mg, 63%) as a pale yellow oil: 1H NMR (400 MHz, $CDCl_3$) δ 7.19 (d, $J = 8.5$ Hz, 2H), 6.86 (d, $J = 8.6$ Hz, 2H), 4.14 – 4.09 (m, 2H), 3.86 – 3.83 (m, 2H), 3.74 – 3.58 (m, 30H), 3.36 (s, 2H), 2.22 (s, 6H); $^{13}C\{^1H\}$ NMR (101 MHz, $CDCl_3$) δ 158.1 (C-4), 130.7 (C-1), 130.4 (C-2), 114.4 (C-3), 72.7, 70.9, 70.7, 70.6, 70.4, 69.8, 67.5, 63.6, 61.7, 45.1 (C-4'); (ESI⁺) m/z of $[M+H]^+$ detected: 504.3166, expected for $C_{25}H_{45}NO_9$ ($n = 7$): 504.3167 (Figure 22); ν_{\max} (thin film)/ cm^{-1} 3461 (O-H, br, w), 2866 (C-H, br, s), 2815 (C-H, w), 2775 (C-H, w), 1609 (w), 1506 (m), 1455 (w), 1352 (w), 1300 (w), 1241 (s), 1094 (C-O, br, s), 951 (br, w).

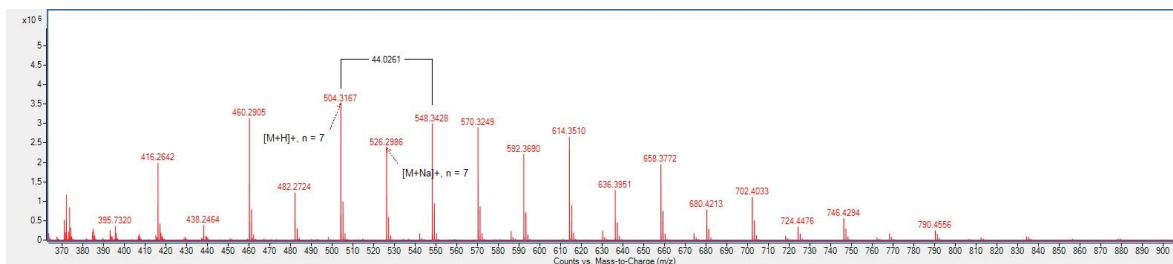
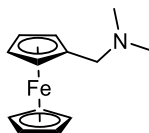


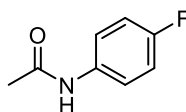
Figure 22: Mass spectrum of **104** showing distribution of peaks.

(Dimethylaminomethyl)ferrocene (**105**)



Ferrocene carboxaldehyde (210 mg, 1.0 mmol, 1.0 equiv.), dimethylamine (2.0 M in THF, 0.75 mL, 1.5 mmol, 1.5 equiv.), $\text{NaBH}(\text{OAc})_3$ (210 mg, 1.0 mmol, 1.0 equiv.) and glacial acetic acid (3 drops) were combined in DCE (10 mL) and stirred at rt. After 2 h, $\text{NaBH}(\text{OAc})_3$ (110 mg, 0.50 mmol, 0.50 equiv.) was added, and the reaction was stirred for a further 1 h at rt. After which, sat. aq. NaHCO_3 (20 mL) was added, and the aqueous layer was extracted with CH_2Cl_2 (3×20 mL). The combined organic portions were washed with brine (30 mL), dried (Na_2SO_4) and concentrated *in vacuo*. The crude residue was subjected to flash column chromatography (gradient from 0:100 to 100:0 EtOAc/Petroleum ether with 1% NEt_3 additive) to yield the **title compound** (212 mg, 84%) as a brown liquid: R_f 0.27 (99:1 EtOAc/ NEt_3); $^1\text{H NMR}$ (400 MHz, CDCl_3) δ 4.17 (t, $J = 1.8$ Hz, 2H), 4.11 (m, 7H), 3.30 (s, 3H), 2.18 (s, 6H). The spectral data are in agreement with reported literature values.¹⁹⁴

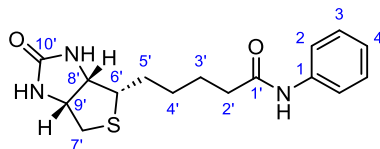
4-Fluoroacetanilide (**106**)



Acetyl chloride (160 μL , 2.2 mmol, 1.1 equiv.) was added dropwise to a solution of 4-fluoroaniline (190 μL , 2.0 mmol, 1.0 equiv.) and NEt_3 (560 μL , 4.0 mmol, 2.0 equiv.) in CH_2Cl_2 at 0 $^\circ\text{C}$. Following complete addition, the solution was allowed to warm to rt, and stirred for 90 min. The reaction mixture was washed with sat. aq. NH_4Cl (30 mL) and sat. aq. NaHCO_3 (30 mL), dried (Na_2SO_4) and concentrated *in vacuo* to give the **title compound** (305 mg, >99%) as an off-white solid: $^1\text{H NMR}$ (400 MHz, Chloroform-*d*) δ 7.48 – 7.42 (m,

2H), 7.15 (s, 1H), 7.01 (t, $J = 8.5$ Hz, 2H), 2.17 (s, 3H, CH₃); ¹⁹F NMR (376 MHz, CDCl₃) δ -118.01. The spectral data are in agreement with reported literature values.¹⁹⁹

Biotin-*N*-phenyl amide (108)



Biotin (122 mg, 500 μ mol, 1.0 equiv.), EDC·HCl (115 mg, 600 μ mol, 1.2 equiv.), HOBT·H₂O (81 mg, 600 μ mol, 1.2 equiv.) and NEt₃ (70 μ L, 500 μ mol, 1.0 equiv.) were combined in anhydrous DMF (3 mL) and stirred for 15 min. After which, aniline (46 μ L, 500 μ mol, 1.0 equiv.) was added, the mixture was heated to 40 °C and stirred for 3 h before being concentrated *in vacuo*. The residue was suspended in CH₂Cl₂ (10 mL) and filtered. The collected solid was further washed with CH₂Cl₂ (2 \times 5 mL) to yield the **title compound** (117 mg, 73 %) as a colourless solid: m.p. decomposes at 150 °C; ¹H NMR (400 MHz, Methanol-*d*₄) δ 7.61 – 7.52 (m, 2H, H-2), 7.34 – 7.29 (m, 2H, H-3), 7.14 – 7.06 (m, 1H, H-4), 4.51 (ddd, $J = 7.9, 5.0, 1.0$ Hz, 1H, H-9'), 4.33 (dd, $J = 7.9, 4.5$ Hz, 1H, H-8'), 3.28 – 3.22 (m, 1H, H-6'), 2.95 (dd, $J = 12.8, 5.0$ Hz, 1H, H-7), 2.72 (d, $J = 12.7$ Hz, 1H, H-7), 2.42 (t, $J = 7.3$ Hz, 2H, H-2'), 1.81 – 1.49 (m, 6H, H-3', H-4', H-5'); ¹³C{¹H} NMR (101 MHz, MeOD) δ 174.5 (C-1'), 166.1 (C-10'), 139.9 (C-1), 129.8 (C-3), 125.1 (C-2), 121.3 (C-4), 63.4 (C-9'), 61.6 (C-8'), 57.0 (C-6'), 41.0 (C-7'), 37.7 (C-2'), 29.8 (C-4'), 29.5 (C-3'), 26.8 (C-5'); ν_{\max} (thin film)/cm⁻¹ 3293 (br, C-H), 2936 (w, C-H), 2861 (w, C-H), 1695 (s, C=O), 1659 (m), 1600 (m), 1530 (m), 1432 (m), 1310 (w), 1266 (w), 1078 (w), 878 (w), 756 (m), 689 (s).

5.3.3. Bioconjugation Reactions

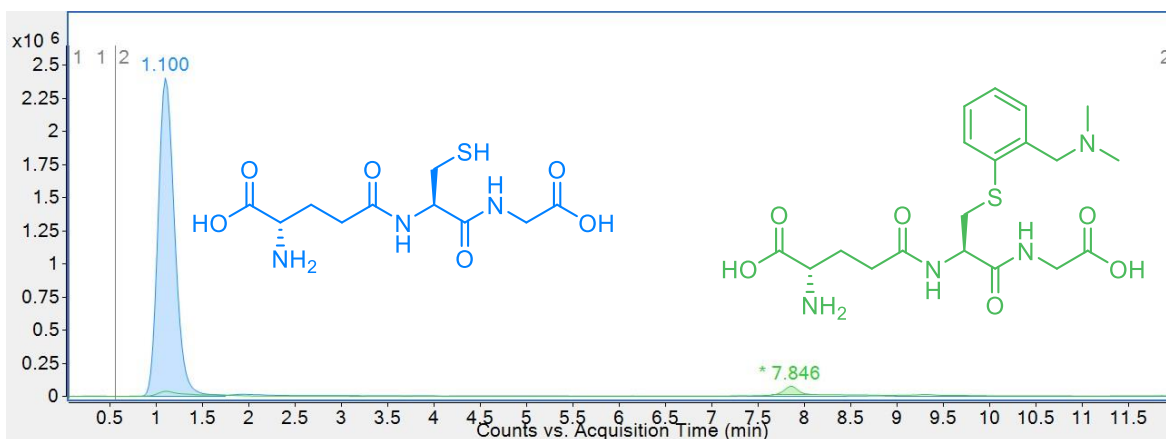
General procedure for glutathione arylation was adapted from the work of Buchwald and Pentelute.⁷⁴ Glutathione (4 μ L, 150 μ M in H₂O), H₂O (47 μ L), organic solvent (2 μ L), and phosphate buffer (6 μ L, 100 mM, pH 7.5) were combined in a 1.5 mL plastic Eppendorf tube and the resulting solution was mixed by vortexing for 5 s. A stock solution of the palladium complex (1 μ L, 1.2 mM in organic solvent) as added, the Eppendorf was vortexed for 5 s and left at rt for 5 min. The reaction was quenched by the addition of 3-mercaptopropionic acid (6.3 μ L, 0.5 μ L/mL solution in water, 3 equiv. to the palladium complex), H₂O (1000 μ L) was added to the Eppendorf and the reaction mixture was analysed by LC-MS. Final concentrations of the reaction before quenching: peptide – 10 μ M, Pd(II) complex – 20 μ M, phosphate buffer – 10 mM; organic solvent: H₂O = 5:95.

5.3.3.1. Initial Ligand Screen

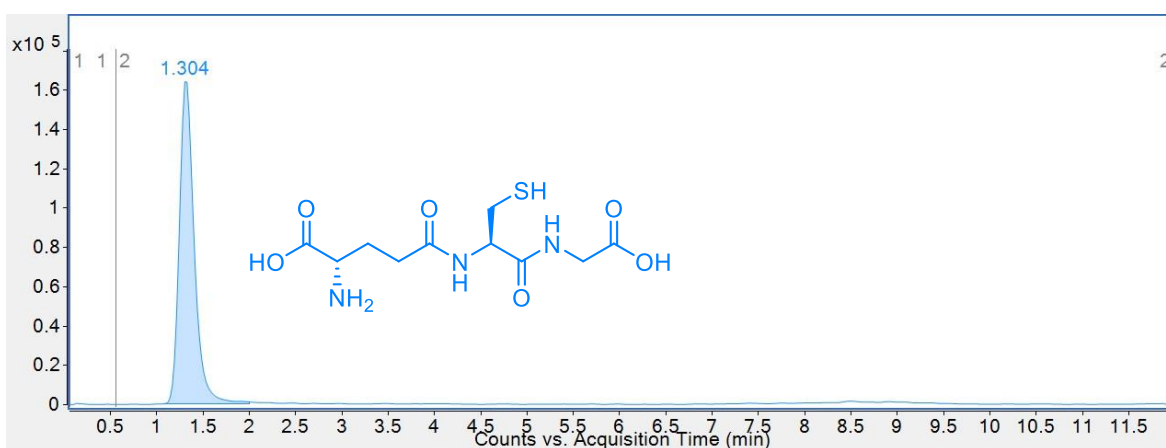
Reactions were run according to **general procedure for glutathione arylation** with compounds **65**, **66**, **67**, **68**, **69** and **70** and MeCN as the organic solvent but were not diluted. Samples were analysed using the **peptide LC-MS** method.

Entry	Pd(II) Complex	GSH EIC Peak Area	72 EIC Peak Area	LC-MS Yield ^[a]
1 (EIC 2)	65	29,964,849	671,613	2%
2 (EIC 3)	66	1,850,112	0	0%
3 (EIC 4)	67	113,003,095	56,877,386	33%
4 (EIC 5)	68	465,836	6,810,977	93%
5 (EIC 6)	69	202,906	11,164,671	98%
6 (EIC 7)	70	37,593,264	490,385,612	93%

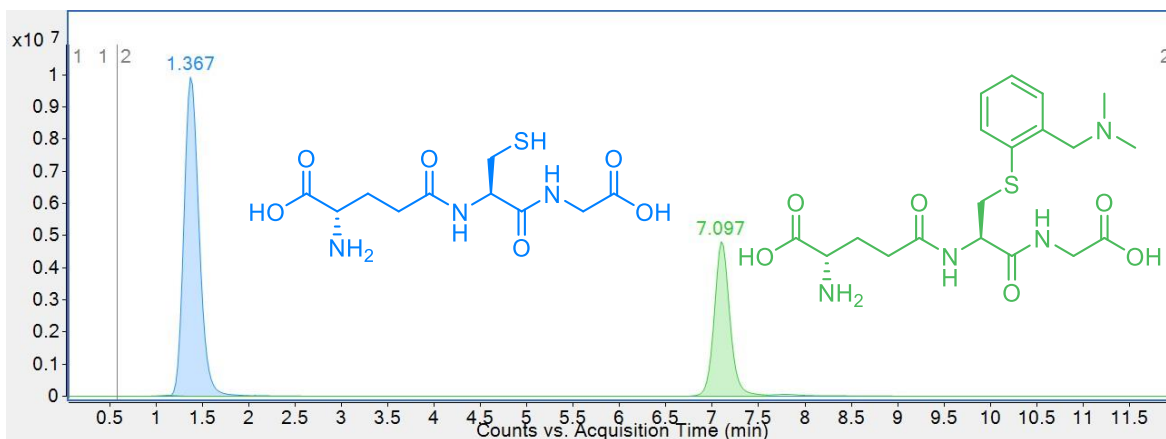
Table 19: Arylation of glutathione with Pd(II)(*dmba*) complexes. ^[a] Obtained by dividing the EIC peak area of 72 by the sum of the EIC peak area for glutathione (**48**) and 72.



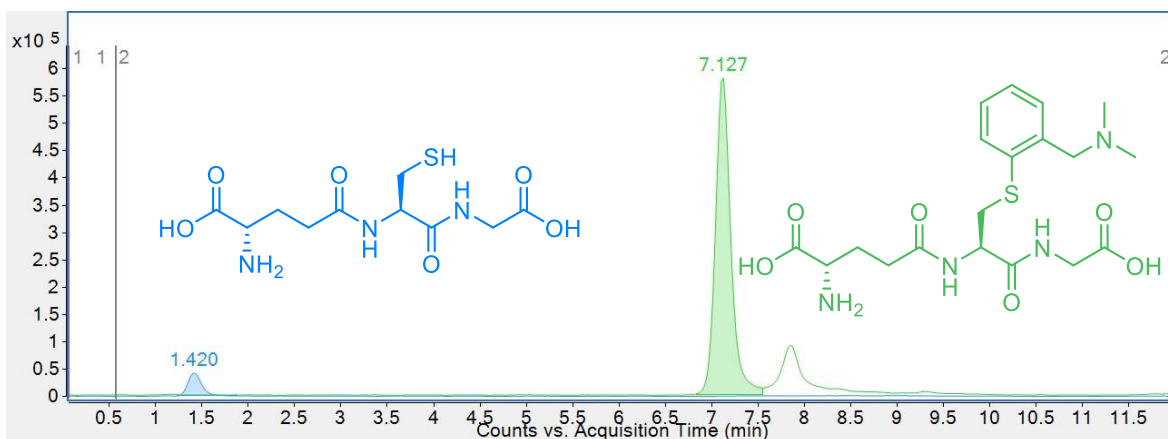
EIC 2: Reaction of glutathione with 65. GSH (ESI^+) m/z of $[M+H]^+$ detected: 308.0914, expected for $C_{10}H_{17}N_3O_6S$: 308.0911. GSH peak area: 29,964,849 (rt = 1.10 min). Arylated GSH (ESI^+) m/z of $[M+H]^+$ detected: 441.1800, expected for $C_{19}H_{28}N_4O_6S$: 441.1802. Arylated GSH peak area: 671,613 (rt = 7.85 min).



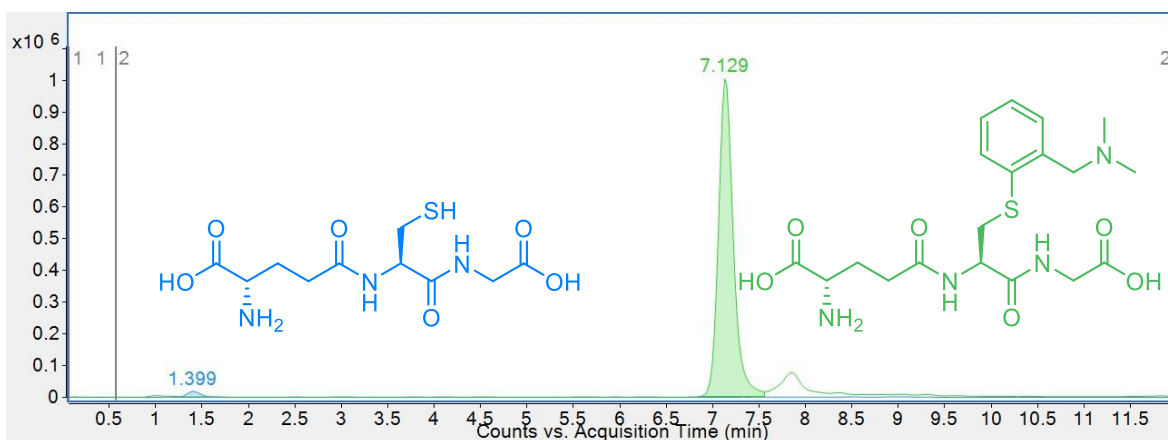
EIC 3: Reaction of glutathione with 66. GSH (48) (ESI^+) m/z of $[M+H]^+$ detected: 308.0908, expected for $C_{10}H_{17}N_3O_6S$: 308.0911. GSH peak area: 1,850,112 (rt = 1.3min). Arylated GSH (ESI^+) m/z of $[M+H]^+$ not detected.



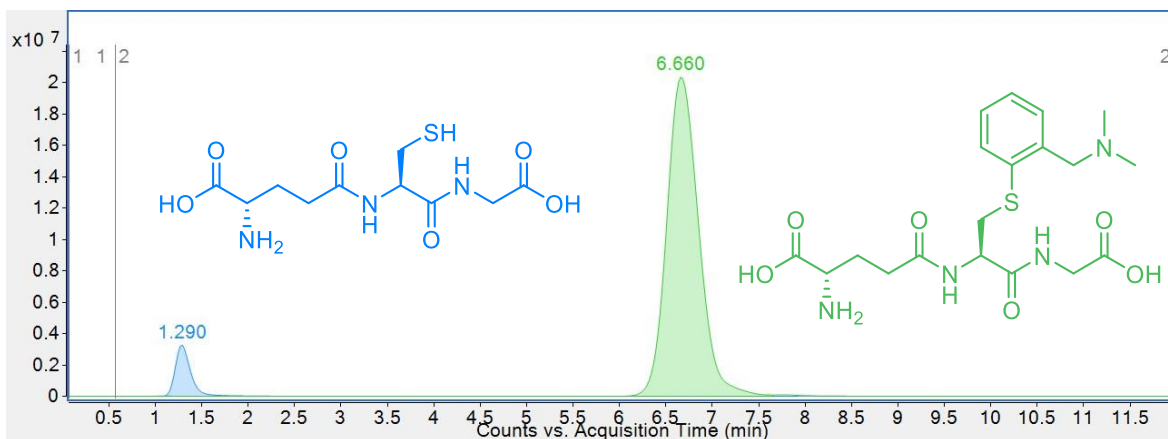
EIC 4: Reaction of glutathione with 67. GSH (ESI^+) m/z of $[M+H]^+$ detected: 308.0914, expected for $C_{10}H_{17}N_3O_6S$: 308.0911. GSH peak area: 113,003,095 (rt = 1.37 min). Arylated GSH (ESI^+) m/z of $[M+H]^+$ detected: 441.1800, expected for $C_{19}H_{28}N_4O_6S$: 441.1805. Arylated GSH peak area: 56,877,386 (rt = 7.10 min).



EIC 5: Reaction of glutathione with 68. GSH (ESI^+) m/z of $[M+H]^+$ detected: 308.0914, expected for $C_{10}H_{17}N_3O_6S$: 308.0909. GSH peak area: 465,836 ($rt = 1.42$ min). Arylated GSH (ESI^+) m/z of $[M+H]^+$ detected: 441.1799, expected for $C_{19}H_{28}N_4O_6S$: 441.1805. Arylated GSH peak area: 6,810,977 ($rt = 7.13$ min).



EIC 6: Reaction of glutathione with 69. GSH (ESI^+) m/z of $[M+H]^+$ detected: 308.0910, expected for $C_{10}H_{17}N_3O_6S$: 308.0909. GSH peak area: 202,906 ($rt = 1.40$ min). Arylated GSH (ESI^+) m/z of $[M+H]^+$ detected: 441.1800, expected for $C_{19}H_{28}N_4O_6S$: 441.1805. Arylated GSH peak area: 11,164,671 ($rt = 7.13$ min).



EIC 7: Reaction of glutathione with 70. GSH (ESI^+) m/z of $[M+H]^+$ detected: 308.0914, expected for $C_{10}H_{17}N_3O_6S$: 308.0911. GSH peak area: 37,593,264 ($rt = 1.29$ min). Arylated GSH (ESI^+) m/z of $[M+H]^+$ detected: 441.1800, expected for $C_{19}H_{28}N_4O_6S$: 441.1805. Arylated GSH peak area: 490,385,612 ($rt = 6.66$ min).

5.3.3.2. Residue Selectivity of Pd(dmba)(Xantphos)Cl (**70**)

Reactions were run according to **general procedure for glutathione arylation** using compound **70** with MeCN as the organic solvent but were not diluted and were analysed using the **peptide LC-MS** method and **peptide MS/MS** method.

5.3.3.3. Glutathione Calibration Curve

H₂O (47 μ L), CH₃CN (2 μ L), a solution (RuPhos)Pd(II)(dmba)Cl (**69**) (1 μ L, 1.2 mM in CH₃CN), phosphate buffer (6 μ L, 100 mM, pH 7.5) and 3-MPA (6.3 μ L, 0.5 μ L/mL in H₂O) were combined in a 1.5 mL plastic Eppendorf tube and the resulting solution was mixed by vortexing for 5 s. After 5 min, glutathione (4 μ L, varying concentrations) was added, H₂O (1000 μ L) was added to the Eppendorf and the reaction mixture was analysed by **peptide LC-MS**.

Entry	Glutathione Reaction Concentration / μ M	Glutathione EIC Peak Area
1	12.5	15,473,411
2	10.0	11,805,745
3	6.25	7,467,338
4	3.13	3,532,585
5	1.56	1,807,997
6	0.781	1,066,961
7	0.500	443,673
8	0.250	130,441
9	0.125	62,833

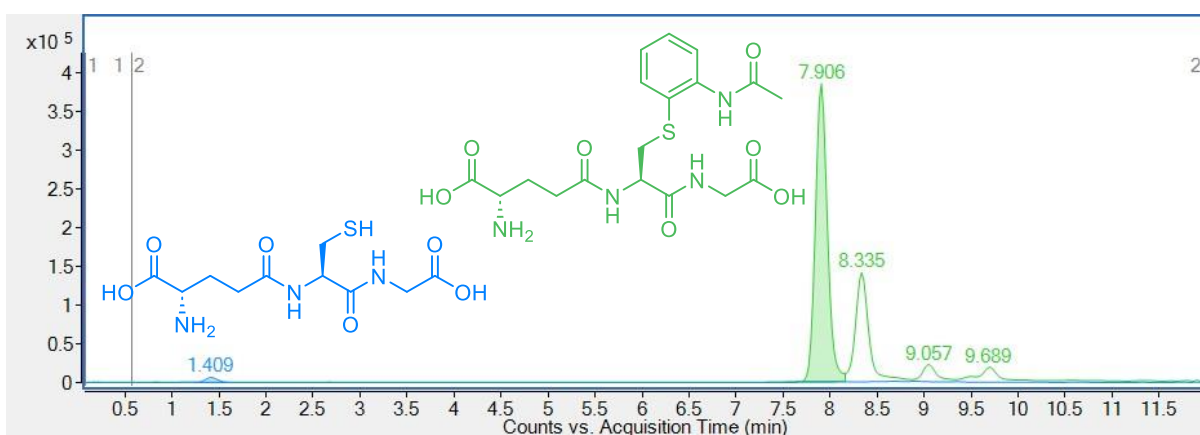
Table 20: Glutathione EIC peak area after reaction of **69** with 3-MPA was spiked with varying concentrations of glutathione. Graph plotted in section 2.2.3.

5.3.3.4. Acetanilide and 2-Phenylpyridine Pd(II) Complexes

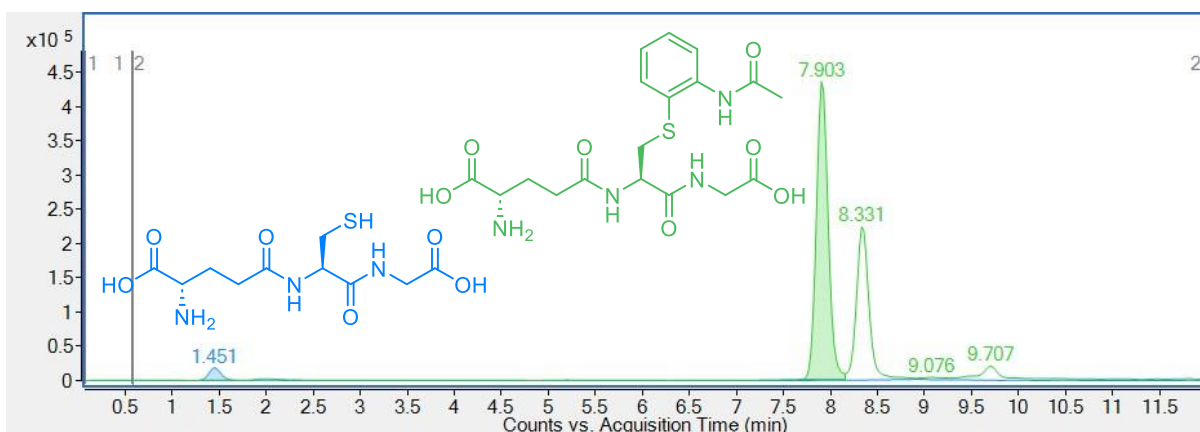
Reactions were run according to **general procedure for glutathione arylation** with compounds **77**, **80** and **81**. Samples were analysed using the **peptide LC-MS** method.

Entry	Pd(II) Complex	Co-solvent	Glutathione EIC Peak Area	Glutathione Conversion ^[a]
1 (EIC 8)	80	DMF	66,539	98%
2 (EIC 9)	81	DMF	170,837	97%
3	77	THF	N/A	N/A

Table 21: Conversions to arylated glutathione using Pd(II) complexes synthesised from acetanilide and 2-phenylpyridine.
^[a] Conversions calculated using glutathione calibration curve.



EIC 8: Reaction of glutathione with **80**. GSH (ESI⁺) m/z of [M+H]⁺ detected: 308.0916, expected for C₁₀H₁₇N₃O₆S: 308.0911. GSH peak area: 66,539 (rt = 1.41 min). Arylated GSH (ESI⁺) m/z of [M+H]⁺ detected: 441.1447, expected for C₁₈H₂₄N₄O₇S: 441.1438. Arylated GSH peak area: 3,414,065 (rt = 7.91 min).



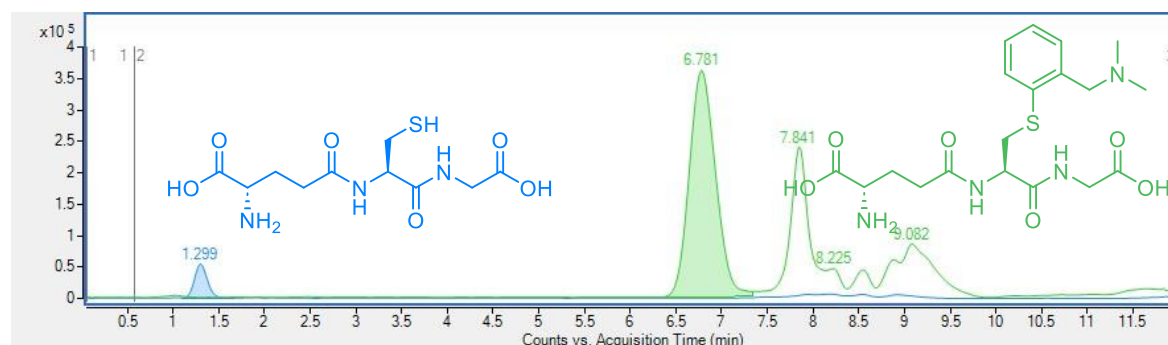
EIC 9: Reaction of glutathione with **81**. GSH (ESI⁺) m/z of [M+H]⁺ detected: 308.0916, expected for C₁₀H₁₇N₃O₆S: 308.0911. GSH peak area: 170,837 (rt = 1.45 min). Arylated GSH (ESI⁺) m/z of [M+H]⁺ detected: 441.1448, expected for C₁₈H₂₄N₄O₇S: 441.1438. Arylated GSH peak area: 3,814,698 (rt = 7.90 min).

5.3.3.5. Pd(II)-dmdba Substrate Scope

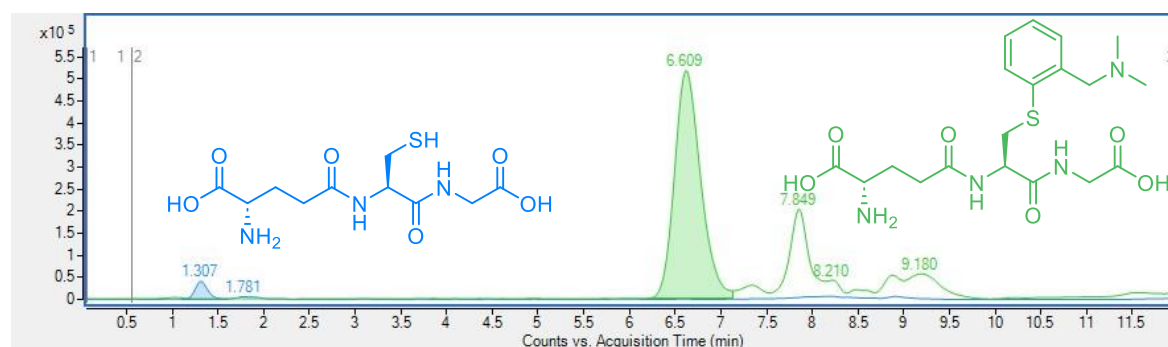
Reactions were run according to **general procedure for glutathione arylation** with compounds **69**, **70**, **82**, **83**, **84** and **85**, and MeCN as the organic co-solvent. Samples were analysed using the **peptide LC-MS** method.

Entry	Pd(II) Complex	Glutathione EIC Peak Area (corrected for dilution)	Glutathione Conversion ^[a]
1 (EIC 10)	69	540,454	94%
2 (EIC 11)	70	396,801	95%
3 (EIC 12)	82	2,064,537	82%
4 (EIC 13)	83	700,161	93%
5 (EIC 14)	84	1,033,322	90%
6 (EIC 15)	85	3,887,346	67%

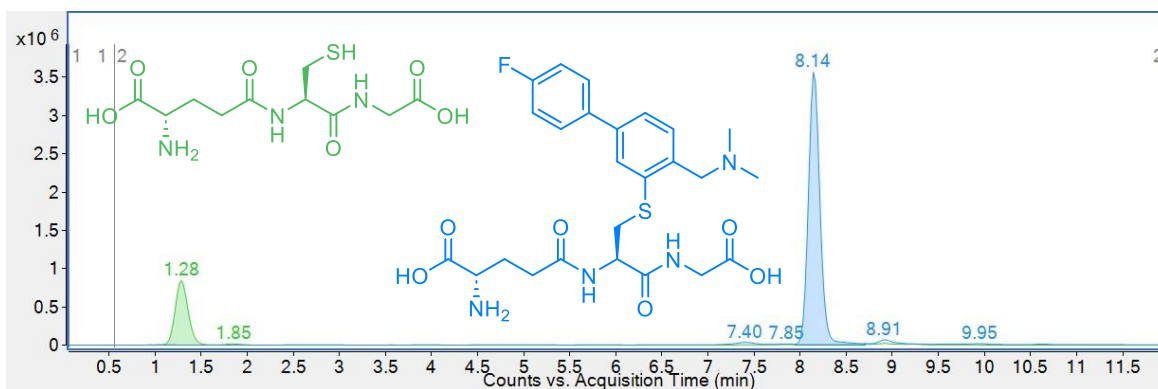
Table 22: Conversions to arylated glutathione using Pd(II) complexes synthesised from dmdba derivatives. ^[a] Conversions calculated using glutathione calibration curve.



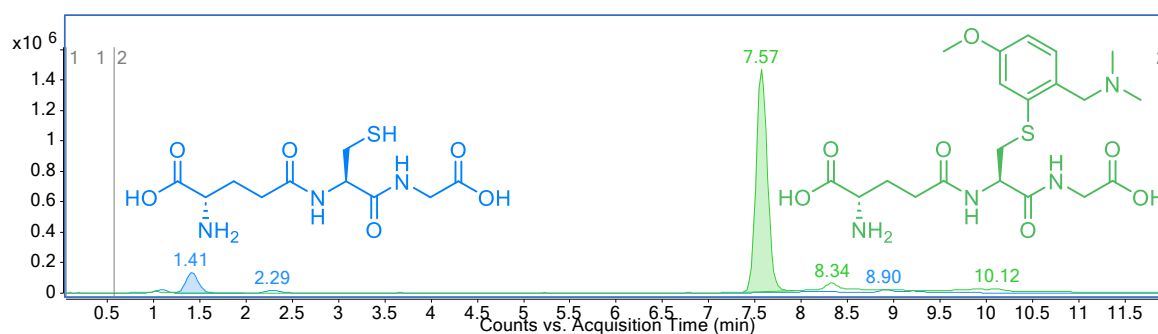
EIC 10: Reaction of glutathione with **69**. GSH (ESI⁺) m/z of [M+H]⁺ detected: 308.0910, expected for C₁₀H₁₇N₃O₆S: 308.0911. GSH peak area: 540454 (rt = 1.30 min). Arylated GSH (ESI⁺) m/z of [M+H]⁺ detected: 441.1800, expected for C₁₉H₂₈N₄O₆S: 441.1802. Arylated GSH peak area: 7223664 (rt = 6.78 min).



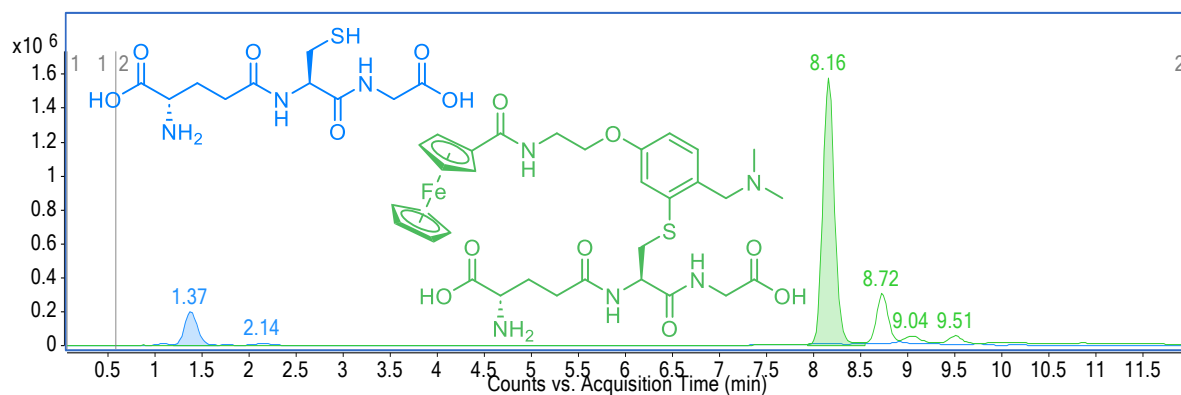
EIC 11: Reaction of glutathione with **70**. GSH (ESI⁺) m/z of [M+H]⁺ detected: 308.0910, expected for C₁₀H₁₇N₃O₆S: 308.0911. GSH peak area: 396801 (rt = 1.31 min). Arylated GSH (ESI⁺) m/z of [M+H]⁺ detected: 441.1800, expected for C₁₉H₂₈N₄O₆S: 441.1802. Arylated GSH peak area: 10289154 (rt = 6.61 min).



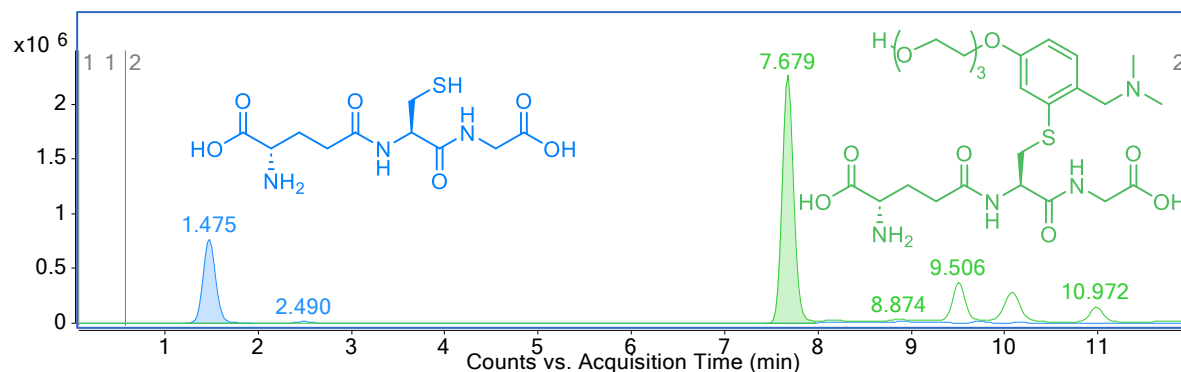
EIC 12: Reaction of glutathione with 82. GSH (ESI^+) m/z of $[M+H]^+$ detected: 308.0909, expected for $C_{10}H_{17}N_3O_6S$: 308.0911. GSH peak area: 8266674 (rt = 1.28 min). Arylated GSH (ESI^+) m/z of $[M+H]^+$ detected: 535.2012, expected for $C_{25}H_{31}FN_4O_6S$: 535.2021. Arylated GSH peak area: 31245140 (rt = 8.14 min).



EIC 13: Reaction of glutathione with 83. GSH (ESI^+) m/z of $[M+H]^+$ detected: 308.0910, expected for $C_{10}H_{17}N_3O_6S$: 308.0911. GSH peak area: 1311860 (rt = 1.41 min). Arylated GSH (ESI^+) m/z of $[M+H]^+$ detected: 471.1886, expected for $C_{20}H_{30}N_4O_7S$: 471.1908. Arylated GSH peak area: 12487789 (rt = 7.57 min).



EIC 14: Reaction of glutathione with 84. GSH (ESI^+) m/z of $[M+H]^+$ detected: 308.0911, expected for $C_{10}H_{17}N_3O_6S$: 308.0911. GSH peak area: 1909012 (rt = 1.37 min). Arylated GSH (ESI^+) m/z of $[M]^+$ detected: 710.2131 expected for $C_{32}H_{41}FeN_5O_8S$: 710.2145. Arylated GSH peak area: 13869245 (rt = 8.16 min).



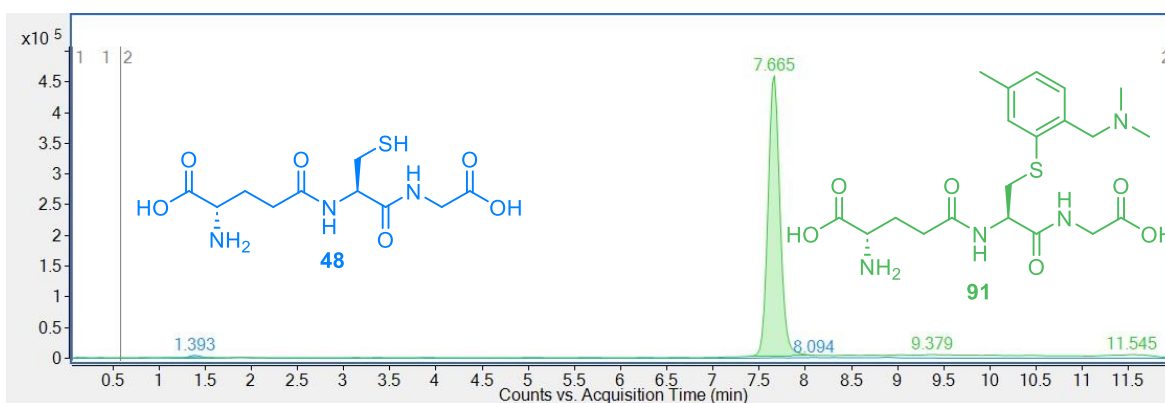
EIC 15: Reaction of glutathione with **85**. GSH (ESI^+) m/z of $[M+H]^+$ detected: 308.0912, expected for $C_{10}H_{17}N_3O_6S$: 308.0911. GSH peak area: 19675679 (rt = 1.48 min). Arylated GSH (ESI^+) m/z of $[M+H]^+$ detected: 589.2534, expected for $C_{23}H_{40}N_4O_{10}S$: 589.2538. Arylated GSH peak area: 26995863 (rt = 7.68 min).

5.3.3.6. Competition Experiments

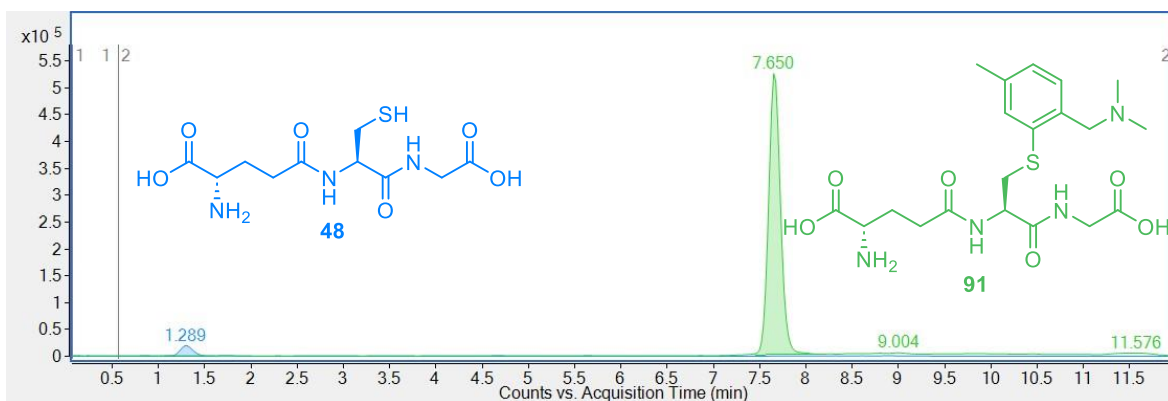
Glutathione arylation with synthesised complexes: Reactions were run according to **general procedure for glutathione arylation** with compounds **89**, **90**, **92** and **93** and DMF as the organic co-solvent. Samples were analysed using the **peptide LC-MS** method.

Entry	Palladium Complex	Glutathione EIC Peak Area	Glutathione Conversion ^[a]
1 (EIC 16)	89	49,680	98%
2 (EIC 17)	90	202,589	97%
3 (EIC 18)	92	not found	>99%
4 (EIC 19)	93	337,230	96%

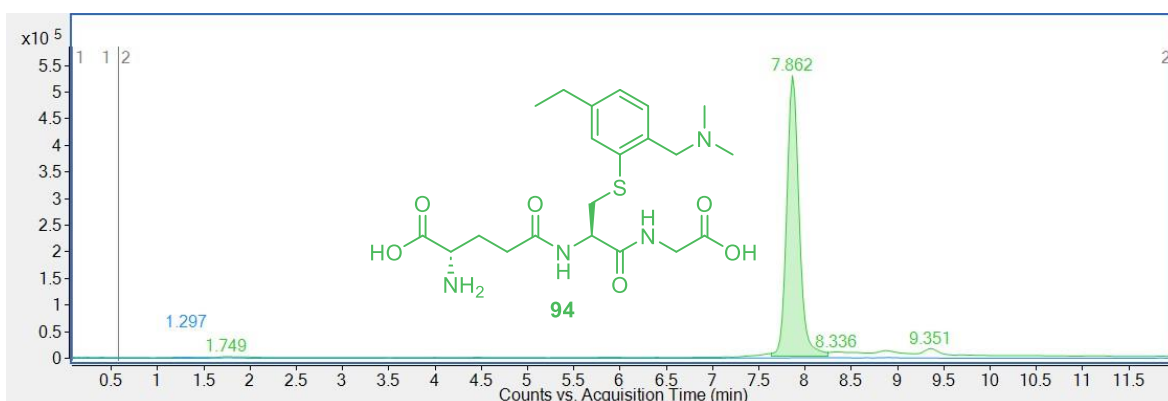
Table 23: Glutathione arylation with **89**, **90**, **92**, and **93**. ^[a] Conversions calculated using glutathione calibration curve.



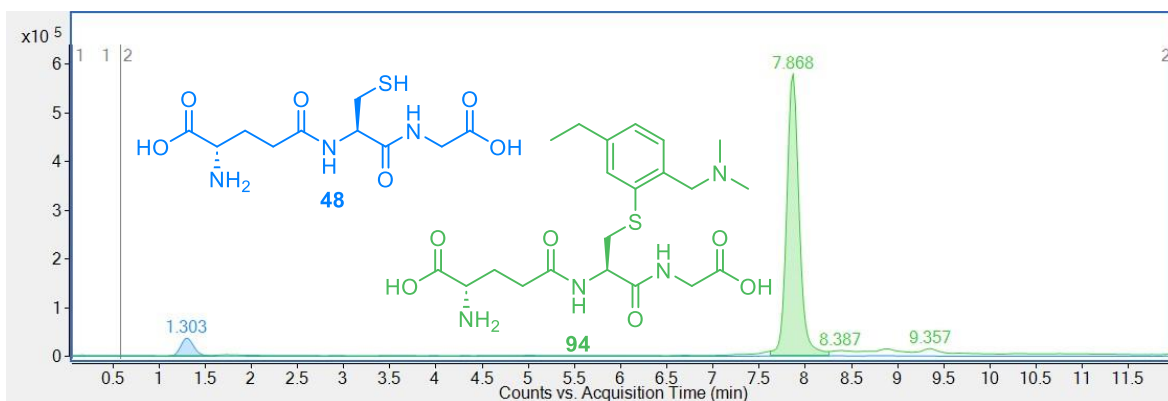
EIC 16: Reaction of glutathione with **89**. GSH (ESI^+) m/z of $[M+H]^+$ detected: 308.0906, expected for $C_{10}H_{17}N_3O_6S$: 308.0911. GSH peak area: 49,680 (rt = 1.39 min). **91** (ESI^+) m/z of $[M+H]^+$ detected: 455.1950, expected for $C_{20}H_{30}N_4O_6S$: 455.1959. **91** peak area: 4,111,961 (rt = 7.67 min).



EIC 17: Reaction of glutathione with **90**. GSH (ESI^+) m/z of $[M+H]^+$ detected: 308.0908, expected for $C_{10}H_{17}N_3O_6S$: 308.0911. GSH peak area: 202,589 ($rt = 1.29$ min). **91** (ESI^+) m/z of $[M+H]^+$ detected: 455.1949, expected for $C_{20}H_{30}N_4O_6S$: 455.1959. **91** peak area: 4,684,932 ($rt = 7.65$ min).



EIC 18: Reaction of glutathione with **92**. GSH (ESI^+) m/z of $[M+H]^+$ not found, expected for $C_{10}H_{17}N_3O_6S$: 308.0911. **94** (ESI^+) m/z of $[M+H]^+$ detected: 469.2109, expected for $C_{21}H_{32}N_4O_6S$: 469.2115. **94** peak area: 4,929,165 ($rt = 7.86$ min).



EIC 19: Reaction of glutathione with **93**. GSH (ESI^+) m/z of $[M+H]^+$ detected: 308.0909, expected for $C_{10}H_{17}N_3O_6S$: 308.0911. GSH counts: 337,230 ($rt = 1.30$ min). **94** (ESI^+) m/z of $[M+H]^+$ detected: 469.2111, expected for $C_{21}H_{32}N_4O_6S$: 469.2115. **94** peak area: 5,541,152 ($rt = 7.86$ min).

General competition experiment procedure: H_2O (47 μL), DMF (1 μL), and phosphate buffer (6 μL , 100 mM, pH 7.5), palladium complex A (1 μL , 1.2 mM in DMF), and palladium complex B (1 μL , 1.2 mM in DMF) were combined in a 1.5 mL plastic Eppendorf tube and the resulting solution was mixed by vortexing for 5 s. Glutathione (4 μL , 150 μM) as added, the Eppendorf was vortexed for 5 s and left at rt for 5 min. The reaction was quenched by the addition of 3-mercaptopropionic acid (6.3 μL , 1 $\mu L/mL$ solution in water, 3 equiv. to the

palladium complexes), H₂O (1000 μ L) was added to the Eppendorf and the reaction mixture was analysed by LC-MS. Final concentrations of the reaction before quenching: peptide – 10 μ M, Pd(II) complex A – 20 μ M, Pd(II) complex B – 20 μ M, phosphate buffer – 10 mM; organic solvent: H₂O = 5:95.

Compounds **69**, **70**, **89**, and **90** were used in the **general competition experiment procedure** and analysed by the **peptide LC-MS** method.

Entry	Palladium Complex A	Palladium Complex B	Glutathione Conversion ^[a]	72 EIC Peak Area	91 EIC Peak Area	72:91
1	69	90	97%	410,993	4,645,602	8:92
2	70	89	97%	2,920,276	1,690,215	63:37
3	70	90	98%	2,704,104	2,608,085	51:49
4	69	89	98%	869,653	3,358,638	21:79

Table 24: Competition experiment between RuPhos- and Xantphos-ligated Pd(II)-dmba complexes **69**, **70**, **89**, and **90**.
^[a] Conversions calculated using glutathione calibration curve.

Compounds **89**, **90**, **92**, and **93** were used in the **general competition experiment procedure** and analysed by the **peptide LC-MS** method.

Entry	Palladium Complex A	Palladium Complex B	Glutathione Conversion ^[a]	91 EIC Peak Area	94 EIC Peak Area	91:94
1	89	93	97%	1,805,988	3,375,124	35:65
2	90	92	97%	3,252,816	2,026,730	62:38
3	90	93	98%	2,989,668	2,763,355	52:48
4	90	93	98%	2,401,995	2,763,061	47:53

Table 25: Competition experiment between RuPhos- and Xantphos-ligated Pd(II)-dmba complexes **89**, **90**, **92**, and **93**.
^[a] Conversions calculated using glutathione calibration curve.

5.3.3.7. *In situ* Protocols

***In situ* conditions A:** Ar (15 μ L, 80 mM solution in MeOH, 2.0 equiv.) and Na₂PdCl₄ (15 μ L, 40 mM solution in MeOH, 1.0 equiv.) and MeOH (20 μ L) were combined and stirred for 1 h at rt. After which, RuPhos (30 μ L, 20 mM in MeCN, 1.0 equiv.) was added, the reaction mixture was diluted with MeCN (420 μ L) and stirred for another 1 h at rt, resulting in a stock solution of Pd(II) complex (500 μ L, 1.2 mM). This stock solution was then used in the **general procedure for glutathione arylation**.

***In situ* conditions B:** Ar (15 μ L, 80 mM solution in MeOH, 2.0 equiv.) and Na₂PdCl₄ (15 μ L, 40 mM solution in MeOH, 1.0 equiv.) and MeOH (20 μ L) were combined and stirred for 1 h at rt. After which, Xantphos (30 μ L, 20 mM in DMF, 1.0 equiv.) was added, the reaction mixture was diluted with DMF (420 μ L) and stirred for another 1 h at rt, resulting in a stock solution of Pd(II) complex (500 μ L, 1.2 mM). This stock solution was then used in the **general procedure for glutathione arylation**.

***In situ* conditions C:** Ar (15 μ L, 40 mM solution in MeOH, 1.0 equiv.), Na₂PdCl₄ (15 μ L, 40 mM solution in MeOH, 1.0 equiv.), NaOAc (15 μ L, 40 mM solution in MeOH, 1.0 equiv.), and MeOH (20 μ L) were combined and stirred for 1 h at rt. After which, RuPhos (30 μ L, 20 mM in MeCN, 1.0 equiv.) was added, the reaction mixture was diluted with MeCN (420 μ L) and stirred for another 1 h at rt, resulting in a stock solution of Pd(II) complex (500 μ L, 1.2 mM). This stock solution was then used in the **general procedure for glutathione arylation**.

***In situ* conditions D:** Ar (15 μ L, 40 mM solution in MeOH, 1.0 equiv.), Na₂PdCl₄ (15 μ L, 40 mM solution in MeOH, 1.0 equiv.), NaOAc (15 μ L, 40 mM solution in MeOH, 1.0 equiv.), and MeOH (20 μ L) were combined and stirred for 1 h at rt. After which, Xantphos (30 μ L, 20 mM in DMF, 1.0 equiv.) was added, the reaction mixture was diluted with DMF (420 μ L) and stirred for another 1 h at rt, resulting in a stock solution of Pd(II) complex (500 μ L, 1.2 mM). This stock solution was then used in the **general procedure for glutathione arylation**.

***In situ* conditions E:** Ar (15 μ L, 80 mM solution in MeOH, 2.0 equiv.), Na₂PdCl₄ (15 μ L, 40 mM solution in MeOH, 1.0 equiv.), NaOAc (15 μ L, 80 mM solution in MeOH, 2.0 equiv.), and MeOH (20 μ L) were combined and stirred for 1 h at rt. After which, RuPhos (30 μ L, 20 mM in MeCN, 1.0 equiv.) was added, the reaction mixture was diluted with MeCN (420 μ L) and stirred for another 1 h at rt, resulting in a stock solution of Pd(II) complex (500 μ L, 1.2 mM). This stock solution was then used in the **general procedure for glutathione arylation**.

***In situ* conditions F:** Ar (15 μ L, 80 mM solution in MeOH, 2.0 equiv.), Na₂PdCl₄ (15 μ L, 40 mM solution in MeOH, 1.0 equiv.), NaOAc (15 μ L, 80 mM solution in MeOH, 2.0 equiv.), and MeOH (20 μ L) were combined and stirred for 1 h at rt. After which, Xantphos (30 μ L, 20 mM in DMF, 1.0 equiv.) was added, the reaction mixture was diluted with DMF (420 μ L) and stirred for another 1 h at rt, resulting in a stock solution of Pd(II) complex (500 μ L,

1.2 mM). This stock solution was then used in the **general procedure for glutathione arylation**.

In situ conditions G: Ar (15 μ L, 80 mM solution in dioxane, 2.0 equiv.), Pd(OAc)₂ (15 μ L, 40 mM solution in dioxane, 1.0 equiv.), *p*TSA (15 μ L, 40 mM solution in dioxane) and dioxane (5 μ L) were combined and stirred for 1 h at rt. After which, RuPhos (30 μ L, 20 mM in MeCN, 1.0 equiv.) was added, the reaction mixture was diluted with MeCN (420 μ L) and stirred for another 1 h at rt, resulting in a stock solution of Pd(II) complex (500 μ L, 1.2 mM). This stock solution was then used in the **general procedure for glutathione arylation**.

In situ conditions H: Ar (15 μ L, 80 mM solution in dioxane, 2.0 equiv.), Pd(OAc)₂ (15 μ L, 40 mM solution in dioxane, 1.0 equiv.), *p*TSA (15 μ L, 40 mM solution in dioxane) and dioxane (5 μ L) were combined and stirred for 1 h at rt. After which, RuPhos (30 μ L, 20 mM in MeCN, 1.0 equiv.) was added, the reaction mixture was diluted with MeCN (420 μ L) and stirred for another 1 h at rt, resulting in a stock solution of Pd(II) complex (500 μ L, 1.2 mM). This stock solution was then used in the **general procedure for glutathione arylation**.

5.3.3.8. Optimisation of *In Situ* Pd(II)-dmba Generation

N,N-Dimethylbenzylamine (**57**) was used in *in situ* conditions **A, B, C, D, E, and F**.

Entry	<i>In Situ</i> Conditions	Glutathione EIC Peak Area	Glutathione Conversion ^[a]
1	A	2,596,898	78%
2	B	2,252,129	80%
3	C	666,901	93%
4	D	60,647	98%
5	E	1,134,861	89%
6	F	1,326,943	88%

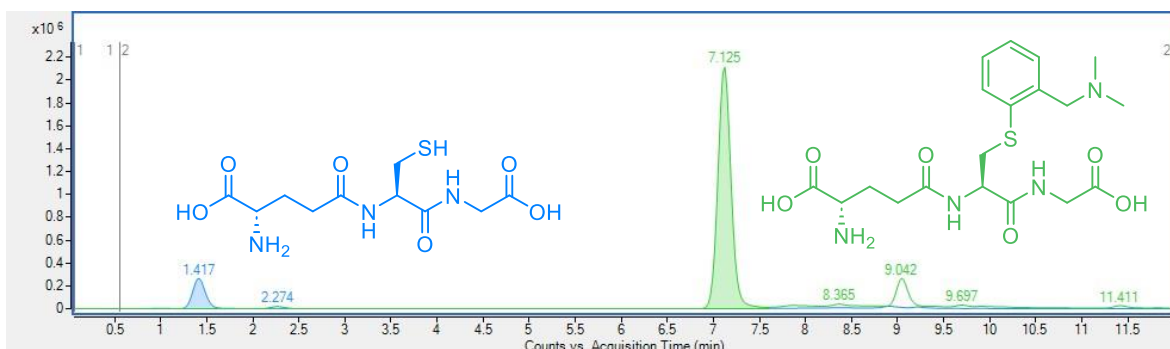
Table 26: Optimisation of *in situ* conditions for glutathione arylation with dmba. ^[a] Conversions calculated using glutathione calibration curve.

5.3.3.9. *In situ* Generated Pd(II)-dmba Substrate Scope

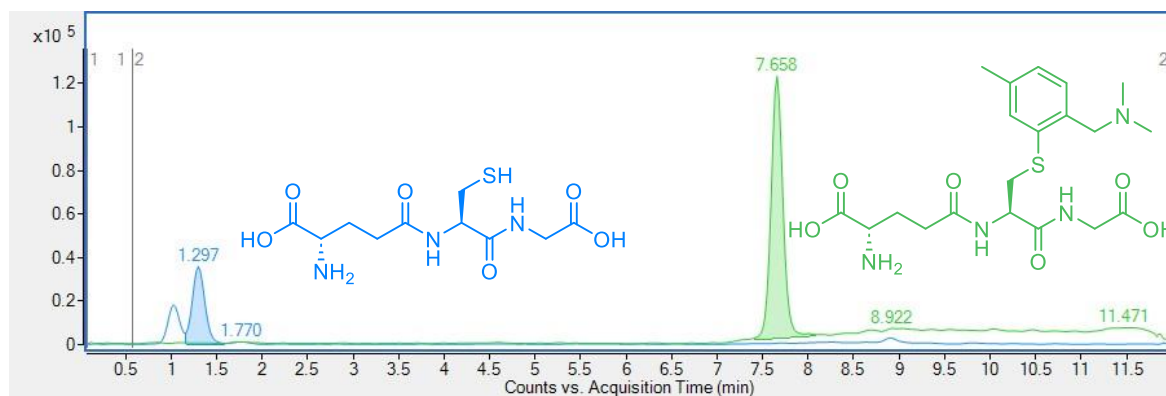
Various dmba derivatives (**57, 95 – 105**) were used in *in situ* conditions **A, B, C, and D**. One EIC per substrate included for the purpose of characterisation of the bioconjugate.

Entry	Ar =	Glutathione EIC Peak Area (and Conversion) for <i>in situ</i> Conditions ^[a]			
		A	B	C	D
1 (EIC 20)	57	2,596,898 (78%)	2,252,129 (80%)	666,901 (93%)	60,647 (98%)
2 (EIC 21)	95			348,721 (96%)	306,639 (96%)
3 (EIC 22)	96	5,891,705 (51%)	9,554,814 (21%)	1,404,054 (87%)	3,464,725 (71%)
4 (EIC 23)	97	4,508,158 (62%)	3,011,416 (74%)	170,258 (97%)	1,201,472 (89%)
5 (EIC 24)	98	3,262,707 (72%)	3,992,355 (66%)		
6 (EIC 25)	99	3,049,893 (74%)	6,650,626 (45%)	3,382,310 (71%)	3,886,774 (67%)
7 (EIC 26)	100			1,781,986 (84%)	761,146 (93%)
8 (EIC 27)	101	3,273,043 (72%)	4,402,912 (63%)	6,345,336 (47%)	4,677,660 (61%)
9 (EIC 28)	102	5,504,666 (54%)	2,450,568 (79%)	5,000,751 (58%)	5,218,068 (56%)
10 (EIC 29)	103	2,019,699 (82%)	533,460 (94%)		
11 (EIC 30)	104	1,494,721 (87%)	2,410,473 (79%)		
12 (EIC 31)	105	9,511,125 (22%)	8,569,304 (29%)	3,988,540 (66%)	2,709,453 (77%)

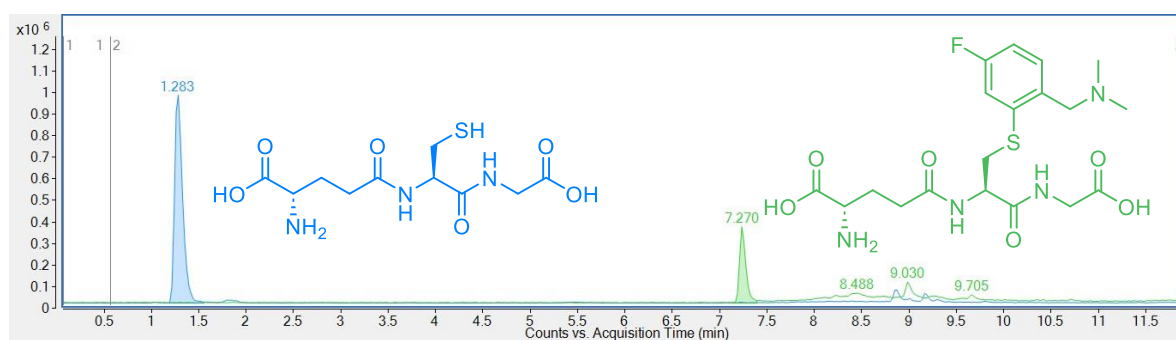
Table 27: Results for *in situ* generated Pd(II)-*dmba* substrate scope. ^[a] Conversions calculated using glutathione calibration curve. Entries 10 and 11 required 18 h reaction time for cyclopalladation step of *in situ* methods.



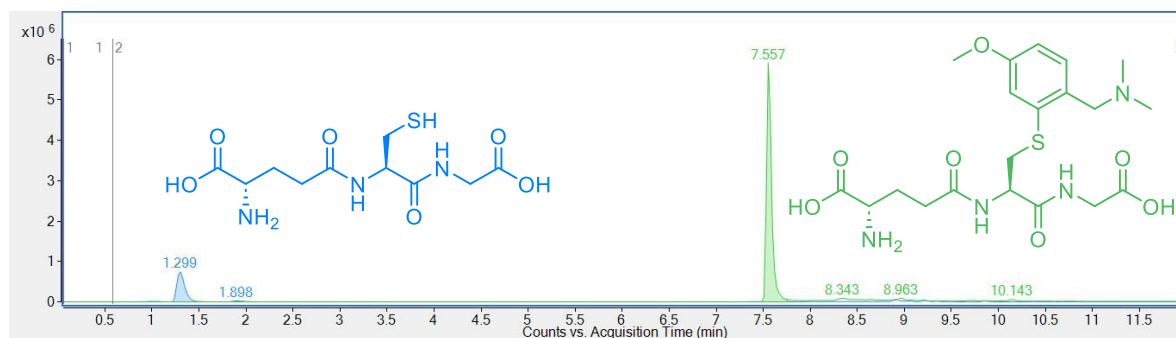
EIC 20: *In situ* arylation of glutathione with **57**. GSH (ESI⁺) *m/z* of [M+H]⁺ detected: 308.0912, expected for C₁₀H₁₇N₃O₆S: 308.0911. GSH peak area: 2,596,898 (rt = 1.42 min). Arylated GSH (ESI⁺) *m/z* of [M+H]⁺ detected: 441.1803, expected for C₁₉H₂₈N₄O₆S: 441.1802. Arylated GSH peak area: 21,083,331 (rt = 7.13 min). **In situ conditions A** were used.



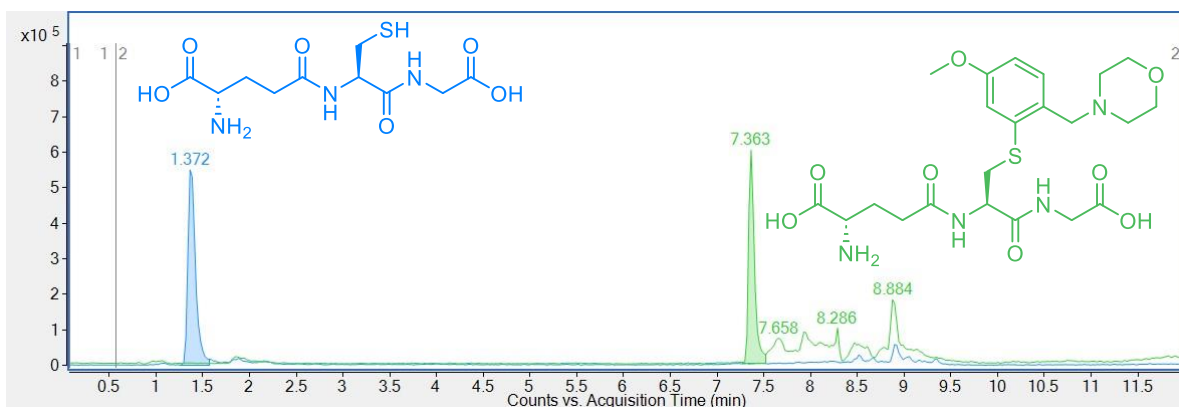
EIC 21: In situ arylation of glutathione with 95. GSH (ESI⁺) m/z of [M+H]⁺ detected: 308.0906, expected for C₁₀H₁₇N₃O₆S: 308.0911. GSH peak area: 348,721 (rt = 1.30 min). Arylated GSH (ESI⁺) m/z of [M+H]⁺ detected: 455.1948, expected for C₂₀H₃₀N₄O₆S: 455.1959. Arylated GSH peak area: 1,105,920 (rt = 7.66 min). **In situ conditions C** were used.



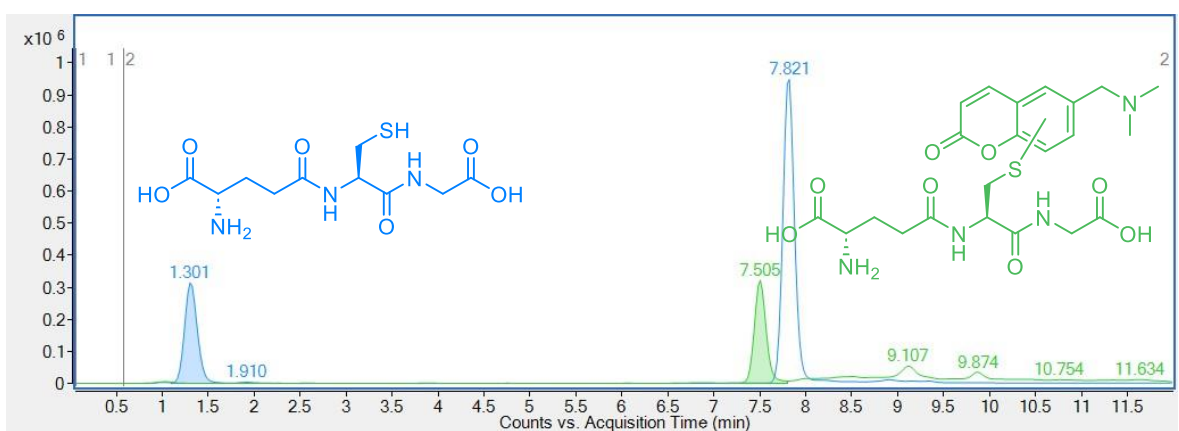
EIC 22: In situ arylation of glutathione with 96. GSH (ESI⁺) m/z of [M+H]⁺ detected: 308.0913, expected for C₁₀H₁₇N₃O₆S: 308.0911. GSH peak area: 5,891,705 (rt = 1.28 min). Arylated GSH (ESI⁺) m/z of [M+H]⁺ detected: 459.1706, expected for C₁₉H₂₇FN₄O₆S: 459.1708. Arylated GSH peak area: 1,743,145 (rt = 7.27 min). **In situ conditions A** were used.



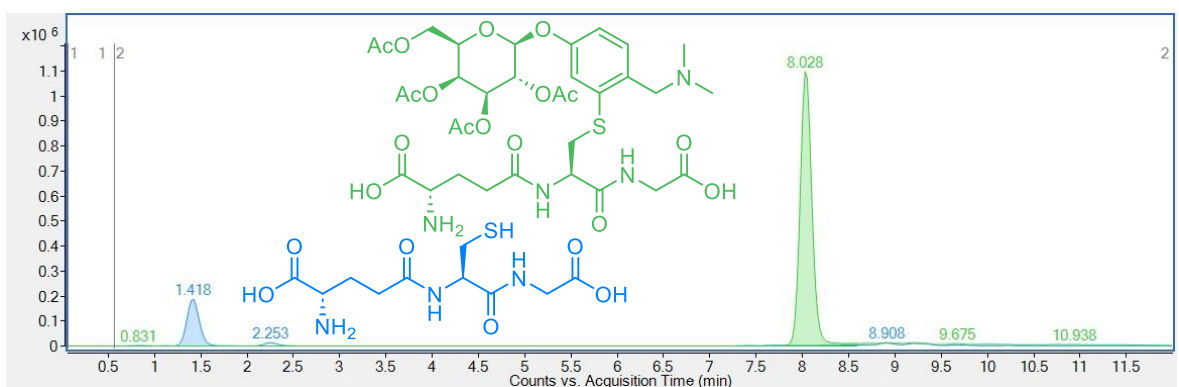
EIC 23: In situ arylation of glutathione with 97. GSH (ESI⁺) m/z of [M+H]⁺ detected: 308.0913, expected for C₁₀H₁₇N₃O₆S: 308.0911. GSH peak area: 4,508,158 (rt = 1.30 min). Arylated GSH (ESI⁺) m/z of [M+H]⁺ detected: 471.1906, expected for C₂₀H₃₀N₄O₇S: 471.1908. Arylated GSH peak area: 22,898,497 (rt = 7.56 min). **In situ conditions A** were used.



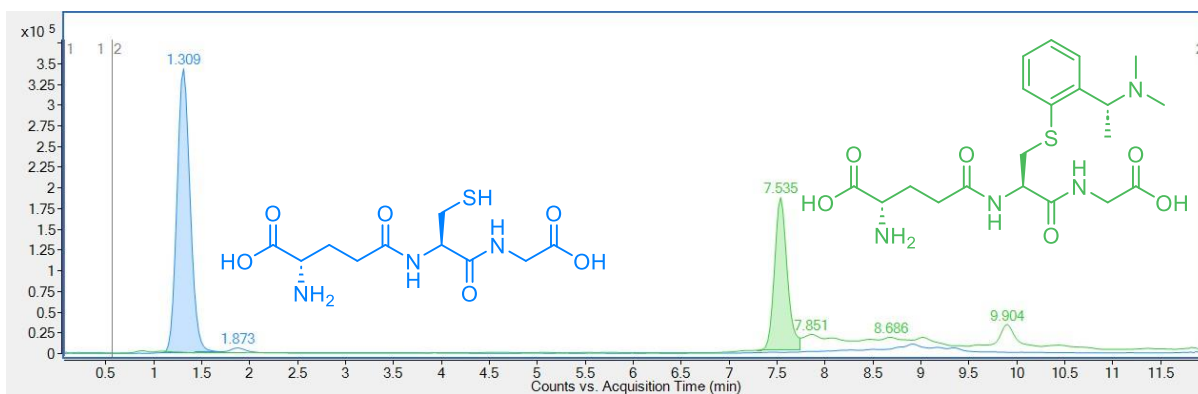
EIC 24: In situ arylation of glutathione with **98**. GSH (ESI^+) m/z of $[M+H]^+$ detected: 308.0909, expected for $C_{10}H_{17}N_3O_6S$: 308.0911. GSH peak area: 3,262,707 ($rt = 1.37$ min). Arylated GSH (ESI^+) m/z of $[M+H]^+$ detected: 483.1901, expected for $C_{21}H_{30}N_4O_7S$: 483.1908. Arylated GSH peak area: 2,746,639 ($rt = 7.37$ min). **In situ conditions A** were used.



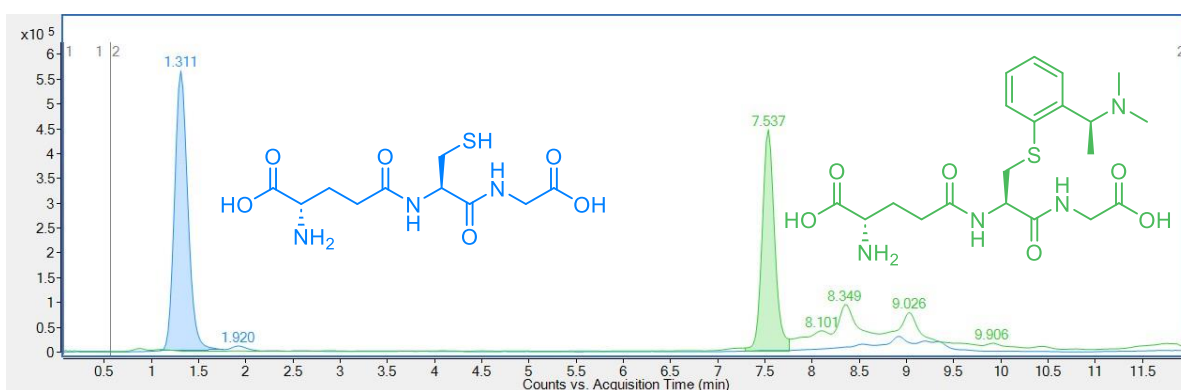
EIC 25: In situ arylation of glutathione with **99**. GSH (ESI^+) m/z of $[M+H]^+$ detected: 308.0910, expected for $C_{10}H_{17}N_3O_6S$: 308.0911. GSH peak area: 3,049,893 ($rt = 1.30$ min). Arylated GSH (ESI^+) m/z of $[M+H]^+$ detected: 501.1695, expected for $C_{22}H_{28}N_4O_8S$: 501.1701. Arylated GSH peak area: 2,889,766 ($rt = 7.51$ min). Note: GSH peak at 7.82 min likely due to degradation of conjugate. **In situ conditions A** were used.



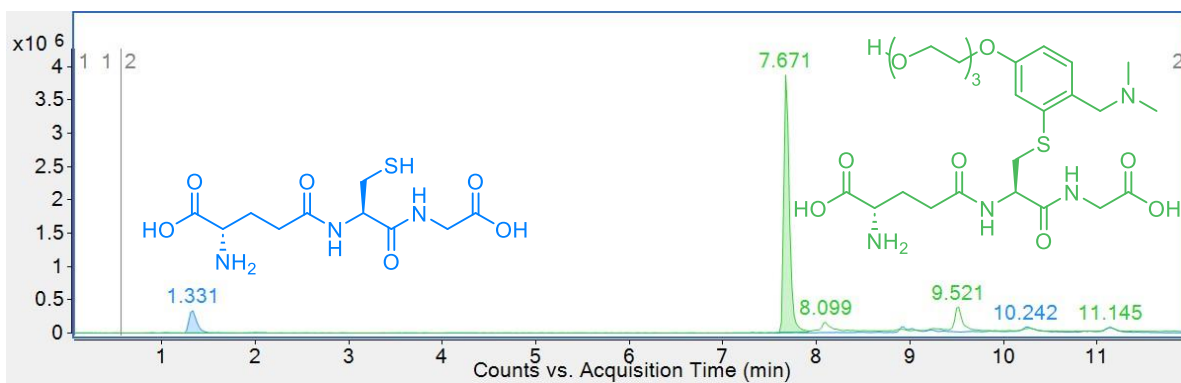
EIC 26: In situ arylation of glutathione with **100**. GSH (ESI^+) m/z of $[M+H]^+$ detected: 308.0907, expected for $C_{10}H_{17}N_3O_6S$: 308.0911. GSH peak area: 1,781,986 ($rt = 1.42$ min). Arylated GSH (ESI^+) m/z of $[M+H]^+$ detected: 787.2692, expected for $C_{33}H_{46}N_4O_{16}S$: 787.2702. Arylated GSH peak area: 9,841,686 ($rt = 8.03$ min). **In situ conditions D** were used.



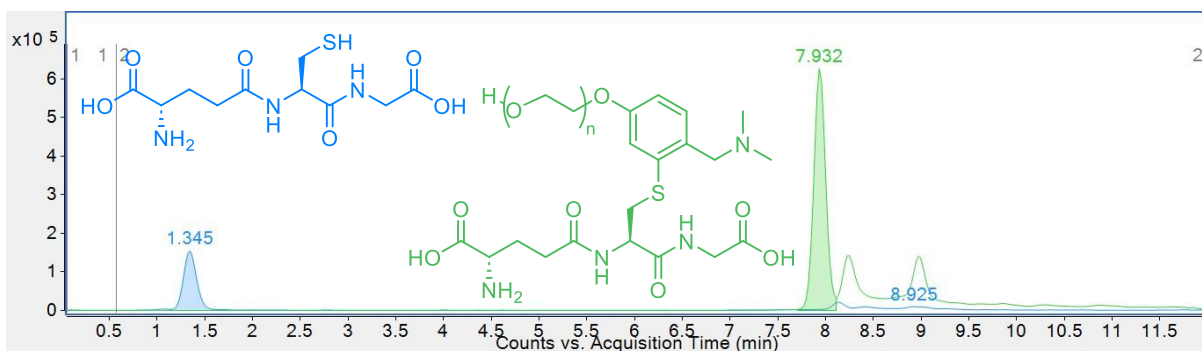
EIC 27: In situ arylation of glutathione with **101**. GSH (ESI^+) m/z of $[M+H]^+$ detected: 308.0910, expected for $C_{10}H_{17}N_3O_6S$: 308.0911. GSH peak area: 3,273,043 ($rt = 1.31$ min). Arylated GSH (ESI^+) m/z of $[M+H]^+$ detected: 455.1955, expected for $C_{20}H_{30}N_4O_6S$: 455.1959. Arylated GSH peak area: 1,697,237 ($rt = 7.54$ min). **In situ conditions** **A** were used.



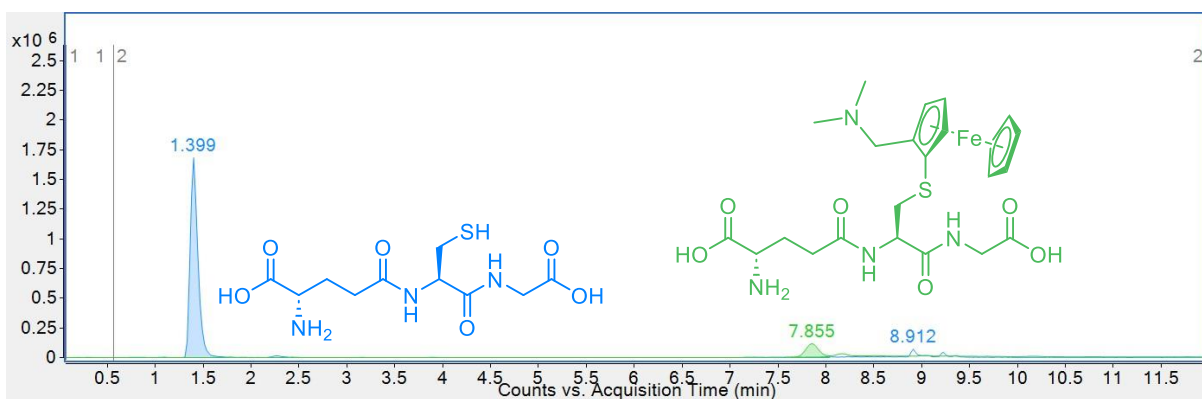
EIC 28: In situ arylation of glutathione with **102**. GSH (ESI^+) m/z of $[M+H]^+$ detected: 308.0909, expected for $C_{10}H_{17}N_3O_6S$: 308.0911. GSH peak area: 5,504,666 ($rt = 1.31$ min). Arylated GSH (ESI^+) m/z of $[M+H]^+$ detected: 455.1952, expected for $C_{20}H_{30}N_4O_6S$: 455.1959. Arylated GSH peak area: 4,127,423 ($rt = 7.54$ min). **In situ conditions** **A** were used.



EIC 29: In situ arylation of glutathione with **103**. GSH (ESI^+) m/z of $[M+H]^+$ detected: 308.0912, expected for $C_{10}H_{17}N_3O_6S$: 308.0911. GSH peak area: 2,019,699 ($rt = 1.33$ min). Arylated GSH (ESI^+) m/z of $[M+H]^+$ detected: 589.2532, expected for $C_{25}H_{40}N_4O_{10}S$: 589.2538. Arylated GSH peak area: 16,095,002 ($rt = 7.67$ min). **In situ conditions** **A** were used.



EIC 30: In situ arylation of glutathione with **104**. GSH (ESI^+) m/z of $[M+H]^+$ detected: 308.0911, expected for $C_{10}H_{17}N_3O_6S$: 308.0911. GSH peak area: 1,494,721 ($rt = 1.35$ min). Arylated GSH (ESI^+) m/z of $[M+Na]^+$ detected: 831.3653, expected for $C_{35}H_{60}N_4O_{16}S$ ($n = 8$): 831.3668 ($rt = 7.93$ min). Note: $n = 8$ chosen as representative arylation product, other lengths of polymer chain also detected. **In situ conditions A** were used.



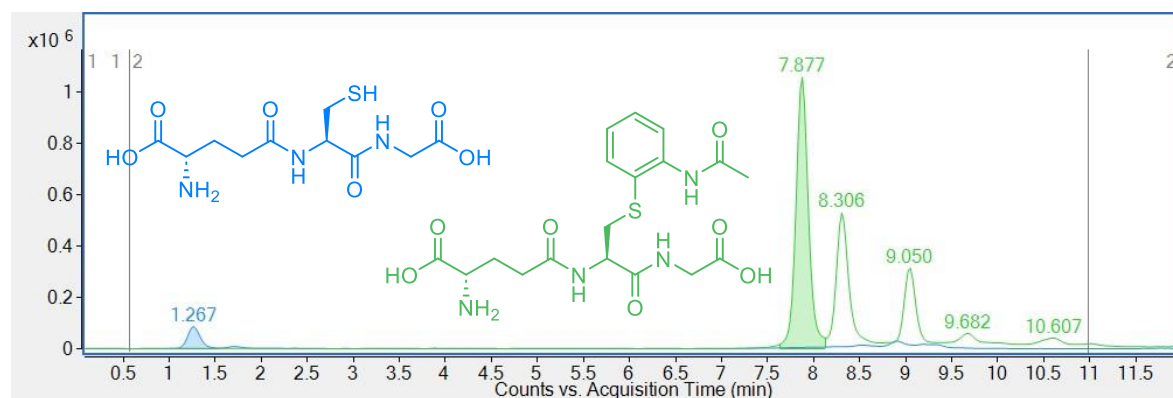
EIC 31: In situ arylation of glutathione with **105**. GSH (ESI^+) m/z of $[M+H]^+$ detected: 308.0913, expected for $C_{10}H_{17}N_3O_6S$: 308.0911. GSH peak area: 9,511,125 ($rt = 1.40$ min). Arylated GSH (ESI^+) m/z of $[M+H]^+$ detected: 549.1459, expected for $C_{23}H_{32}FeN_4O_6S$: 549.1465. Arylated GSH peak area: 117,128 ($rt = 7.86$ min). **In situ conditions A** were used.

5.3.3.10. *In situ* Generated Pd(II)-acetanilide Substrate Scope

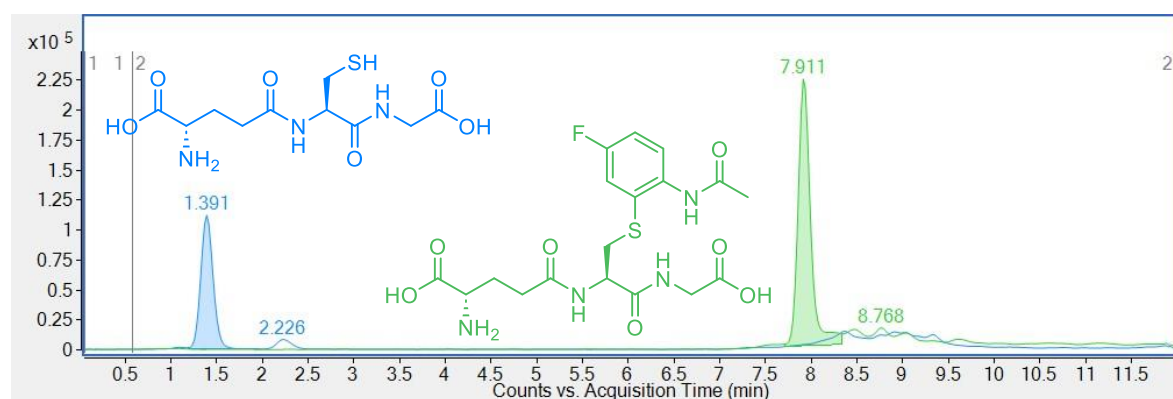
Various acetanilide derivatives (**78**, **106** and **107**) were used in *in situ* conditions **G** and **H**. One EIC per substrate included for the purpose of characterisation of the bioconjugate.

Entry	Ar =	Glutathione EIC Peak Area (and Conversion) for <i>in situ</i> Conditions ^[a]	
		G	H
1 (EIC 32)	78	1,459,491 (87%)	840,635 (92%)
2 (EIC 33)	106	1,036,095 (90%)	2,561,539 (78%)
3 (EIC 34)	107	288,511 (96%)	1,911,222 (83%)

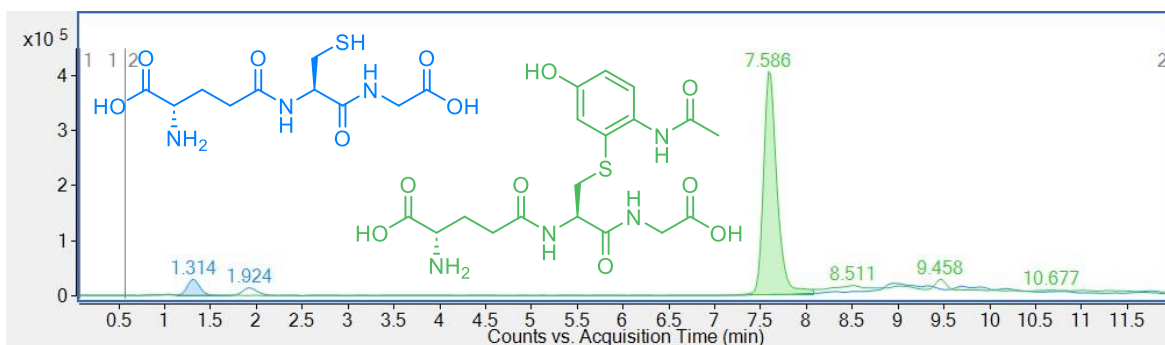
Table 28: Results for *in situ* generated Pd(II)-acetanilide substrate scope. ^[a] Conversions calculated using glutathione calibration curve.



EIC 32: *In situ* arylation of glutathione with **78**. GSH (ESI⁺) *m/z* of [M+H]⁺ detected: 308.0907, expected for C₁₀H₁₇N₃O₆S: 308.0911. GSH peak area: 1,459,491 (rt = 1.27 min). Arylated GSH (ESI⁺) *m/z* of [M+H]⁺ detected: 441.1438, expected for C₁₈H₂₄N₄O₇S: 441.1438. Arylated GSH peak area: 10,040,154 (rt = 7.88 min). *In situ* conditions **G** were used.



EIC 33: *In situ* arylation of glutathione with **106**. GSH (ESI⁺) *m/z* of [M+H]⁺ detected: 308.0904, expected for C₁₀H₁₇N₃O₆S: 308.0911. GSH peak area: 1,036,095 (rt = 1.39 min). Arylated GSH (ESI⁺) *m/z* of [M+H]⁺ detected: 459.1339, expected for C₁₈H₂₃FN₄O₇S: 459.1344. Arylated GSH peak area: 2,165,093 (rt = 7.91 min). *In situ* conditions **G** were used.



EIC 34: In situ arylation of glutathione with 107. GSH (ESI⁺) m/z of [M+H]⁺ detected: 308.0904, expected for C₁₀H₁₇N₃O₆S: 308.0911. GSH peak area: 288,511 (rt = 1.31 min). Arylated GSH (ESI⁺) m/z of [M+H]⁺ detected: 457.1383, expected for C₁₈H₂₄N₄O₈S: 457.1388. Arylated GSH peak area: 4,228,258 (rt = 7.59 min). In situ conditions G were used.

5.3.3.9. Intact Protein Bioconjugation With Complex 85

Using isolated Pd(II) complex: 85 (10 μ L, 10 mM in MeCN) was added to a mixture of BSA (10 μ L, 1 mM in H₂O) and PBS (80 μ L, Dulbecco A) in a 1.5 mL Eppendorf tube. After vortexing, the reaction mixture was held at 37 °C for 1 h before being diluted with H₂O (400 μ L). An aliquot (100 μ L) was then analysed by **intact protein LC-MS**. A control reaction containing no complex **85** (PEG) was also conducted.

5.3.3.10. Intact Protein Bioconjugation with *In Situ* Generated Complexes

Using *in situ* generated complexes: 100 or 103 (50 μ L, 80 mM in MeOH) and Na₂PdCl₄ (50 μ L, 40 mM in MeOH) were combined in a 1.5 mL Eppendorf tube and vortexed. After 16 h, phosphine ligand (100 μ L, 20 mM in MeCN or DMF) was added, the reaction was vortexed, and left to stand for 1 h to form a stock solution (10 mM) of Pd(II) complex.

Pd(II) stock solution (10 μ L, 10 mM in MeOH/MeCN or DMF 50:50, 10 equiv.) was added to a mixture of BSA (10 μ L, 1 mM in H₂O, 1 equiv.) and PBS (80 μ L, Dulbecco A) in a 1.5 mL Eppendorf tube. After vortexing, the reaction mixture was held at 37 °C for 1 h before being diluted with H₂O (400 μ L). An aliquot (100 μ L) was then analysed by **intact protein LC-MS**.

Using *in situ* generated complexes followed by trypsin digest: 100 or 103 (25 μ L, 80 mM in MeOH), NaOAc (25 μ L, 80 mM in MeOH) and Na₂PdCl₄ (50 μ L, 40 mM in MeOH) were combined in a 1.5 mL Eppendorf tube and vortexed. After 1 h, phosphine ligand (100 μ L, 20 mM in MeCN or DMF) was added, the reaction was vortexed, and left to stand for 1 h to form a stock solution of Pd(II) complex (10 mM).

Pd(II) stock solution (10 μ L, 10 mM in MeOH/MeCN or DMF 50:50, 10 equiv.) was added to a mixture of BSA (10 μ L, 1 mM in H₂O, 1 equiv.) and PBS (80 μ L, Dulbecco A) in a

1.5 mL Eppendorf tube. After vortexing, the reaction mixture was held at 37 °C for 1 h. An aliquot (15 µL) was taken and combined with trypsin (50:1 protein/trypsin) in NH₄HCO₃ (85 µL, 50 mM). After vortexing, the reaction mixture was held at 37 °C for 20 h, and then analysed by **peptide MS/MS**.

Estimation of conversions: Since only arylated Cys-34 (confirmed by MS/MS) was detected, conversions to arylated BSA are estimated by examining the EIC peak area of the modified and unmodified Cys-34 containing peptide (H-GLVLIAFSQYLQQCPFDEHVK-OH) following trypsin digest. Conversions are estimated as follows:

$$\frac{\text{Peak area(modified)}}{\text{Peak area(total)}} \times 100.$$

Entry	Ar =	Ligand/Solvent	Unmodified peptide EIC Peak Area	Modified peptide EIC Peak Area	Estimated Conversion
1	103	RuPhos/MeCN	980,095	43,031,491	98%
2	103	Xantphos/DMF	73,763	11,164,356	99%
3	100	RuPhos/MeCN	1,426,750	18,339,359	93%
4	100	Xantphos/DMF	1,341,270	13,691,649	91%

Table 29: Estimation of conversion to arylated BSA at Cys-34.

MS/MS Data:

Data for Table 29 entry 1:

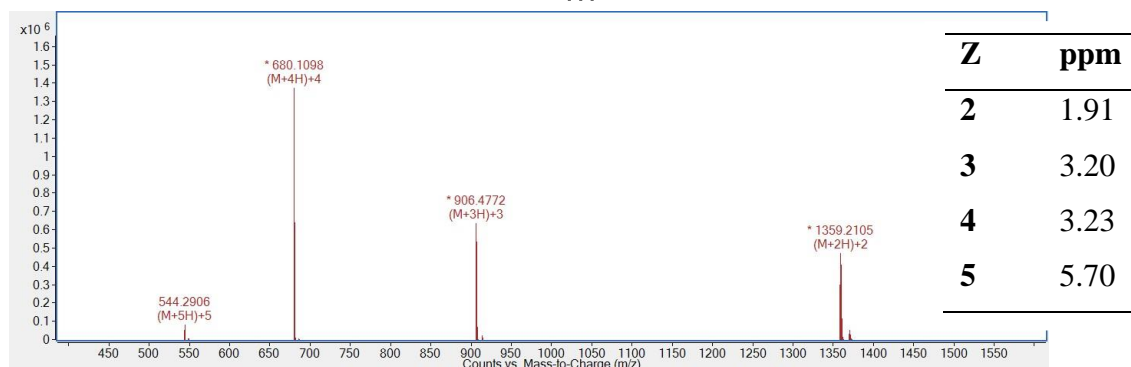
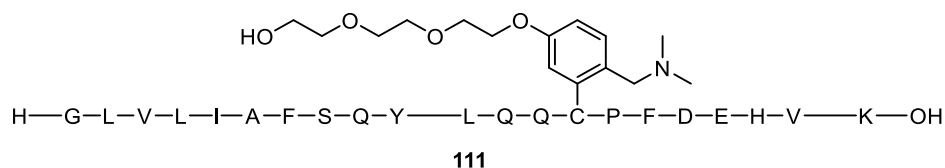


Figure 23: MS spectrum of arylated GLVLIAFSQYLQQCPFDEHVK with ppm errors for parent ions.

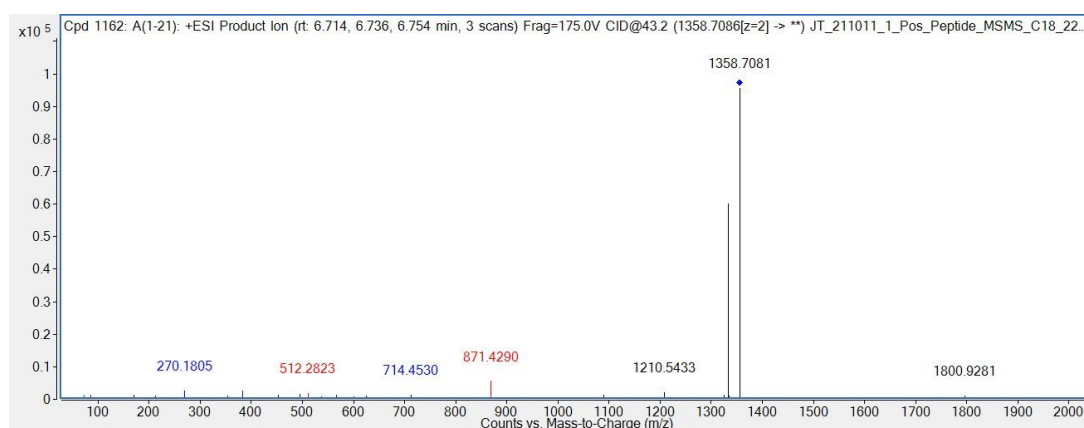


Figure 24: MS/MS spectrum from (Z = 2) parent ion.

Sequence	m/z	m/z (predicted)	Diff (ppm)	Z (prod.)	Ion
GL	171.1128	171.1123	-2.8	1	b2
GLV	270.1812	270.1805	-2.7	1	b3
GLVL	383.2653	383.2641	-3.1	1	b4
GLVLI	496.3493	496.3481	-2.6	1	b5
GLVLIA	567.3865	567.387	1	1	b6
GLVLIAF	714.4549	714.453	-2.7	1	b7
GLVLIAFSQY	1092.6088	1092.6083	-0.5	1	b10
HVK	383.2401	383.2392	-2.4	1	y3
EHVK	512.2827	512.2823	-0.9	1	y4
PFDEHVK	871.4308	871.429	-2.1	1	y7
L	86.0964	86.0959	-6.1	1	L
V	72.0808	72.0805	-4	1	V
I	86.0964	86.0959	-6.1	1	I

Table 30: Confirmation of b and y ions from Z = 2 parent ion.

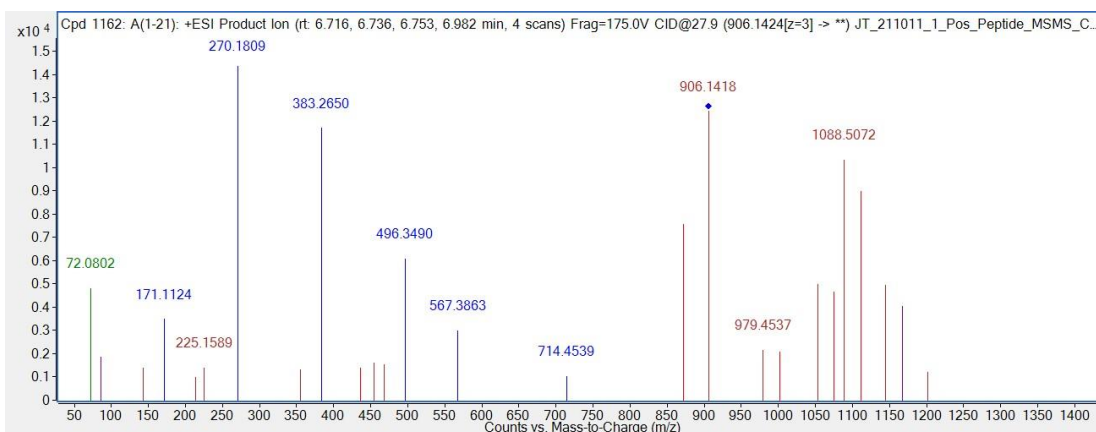


Figure 25: MS/MS spectrum from (Z = 3) parent ion.

Sequence	m/z	m/z (predicted)	Diff (ppm)	Z (prod.)	Ion
GL	171.1128	171.1124	-2.1	1	b2
GLV	270.1812	270.1809	-1.3	1	b3
GLVL	383.2653	383.265	-0.6	1	b4
GLVLI	496.3493	496.349	-0.7	1	b5
GLVLIA	567.3865	567.3863	-0.2	1	b6
GLVLIAF	714.4549	714.4539	-1.4	1	b7
GLVLIAFSQYLQQCPFDE	1167.59	1167.5773	-10.8	2	b18
PFDEHVK	871.4308	871.4302	-0.7	1	y7
PFDEHVK	436.2191	436.2186	-1	2	y7
SQYLQQCPFDEHVK	1001.9826	1001.9827	0.1	2	y14
FSQYLQQCPFDEHVK	1075.5168	1075.518	1.1	2	y15
AFSQYLQQCPFDEHVK	1111.0354	1111.0366	1.1	2	y16
IAFSQYLQQCPFDEHVK	1167.5774	1167.5773	0	2	y17
L	86.0964	86.0959	-6.6	1	L
V	72.0808	72.0802	-7.5	1	V

Table 31 Confirmation of b and y ions from Z = 3 parent ion.

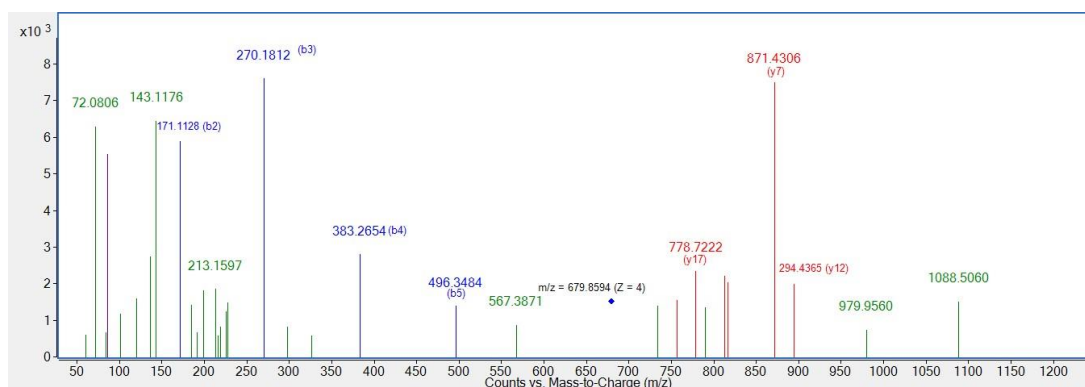


Figure 26: MS/MS spectrum from (Z = 4) parent ion.

Sequence	m/z	m/z (predicted)	Diff (ppm)	Z (prod.)	Ion
V	72.0806	72.0808	-2.7	1	V
L	86.0963	86.0964	-1.4	1	L
I	86.0963	86.0964	-1.4	1	I
Q	101.0703	101.0709	-5.9	1	Q
Y	136.0752	136.0757	-3.4	1	Y
GL	171.1128	171.1128	-0.1	1	b2
GLV	270.1812	270.1812	-0.2	1	b3
GLVL	383.2654	383.2653	0.4	1	b4
GLVLI	496.3484	496.3493	-2	1	b5
QQCPFDEHVK	756.3652	756.3636	2.2	2	y10
IAFSQYLQQCPFDEHVK	778.7222	778.7207	2	3	y17
LQQCPFDEHVK	812.9065	812.9056	1.1	2	y11
LIAFSQYLQQCPFDEHVK	816.4168	816.4154	1.7	3	y18
PFDEHVK	871.4306	871.4308	-0.2	1	y7
YLQQCPFDEHVK	894.4365	894.4373	-0.8	2	y12

Table 32: Confirmation of b and y ions from Z = 4 parent ion.

Data for Table 29 entry 2:

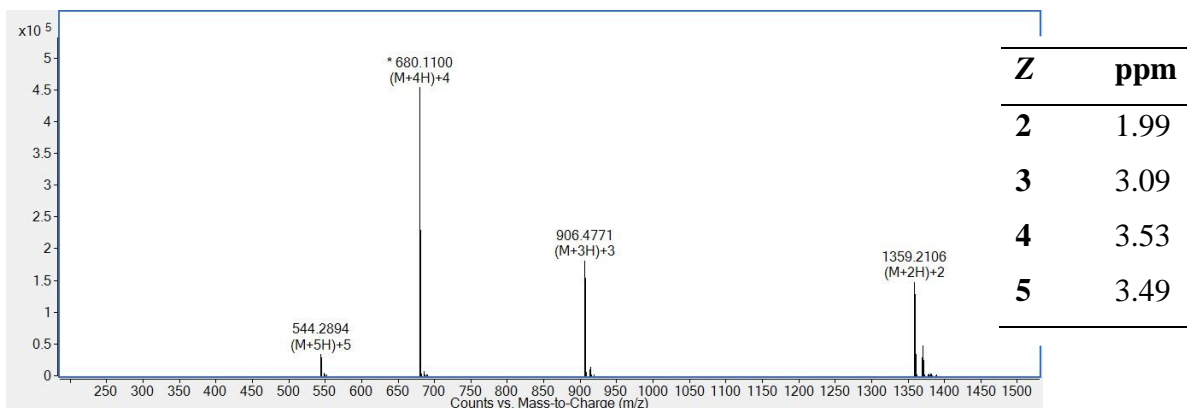
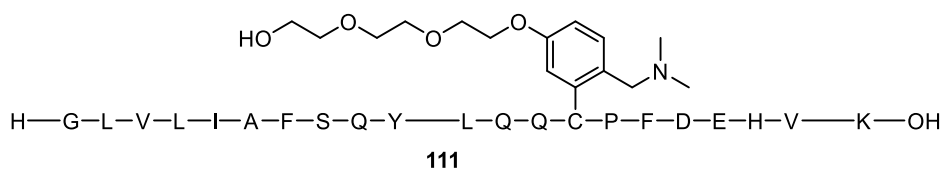


Figure 27: MS spectrum of arylated GLVLIAFSQYLQQC PFDEHVK with ppm errors for parent ions.

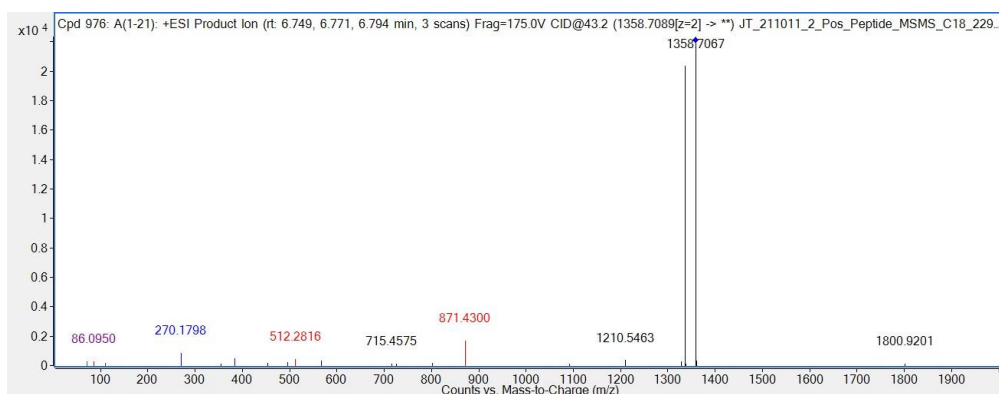


Figure 28: MS/MS spectrum from (Z = 2) parent ion.

Sequence	m/z	m/z (predicted)	Diff (ppm)	Z (prod.)	Ion
GLV	270.1812	270.1798	-5.2	1	b3
GLVL	383.2653	383.2632	-5.4	1	b4
GLVLI	496.3493	496.3497	0.8	1	b5
GLVLIA	567.3865	567.3843	-3.8	1	b6
GLVLIAFS	801.4869	801.4811	-7.2	1	b8
GLVLIAFSQY	1092.6088	1092.6072	-1.5	1	b10
EHVK	512.2827	512.2816	-2.2	1	y4
PFDEHVK	871.4308	871.43	-0.9	1	y7
L	86.0964	86.095	-16.7	1	L
V	72.0808	72.0805	-4.5	1	V
I	86.0964	86.095	-16.7	1	I
H	110.0713	110.0708	-4	1	H

Table 33: Confirmation of b and y ions from Z = 2 parent ion.

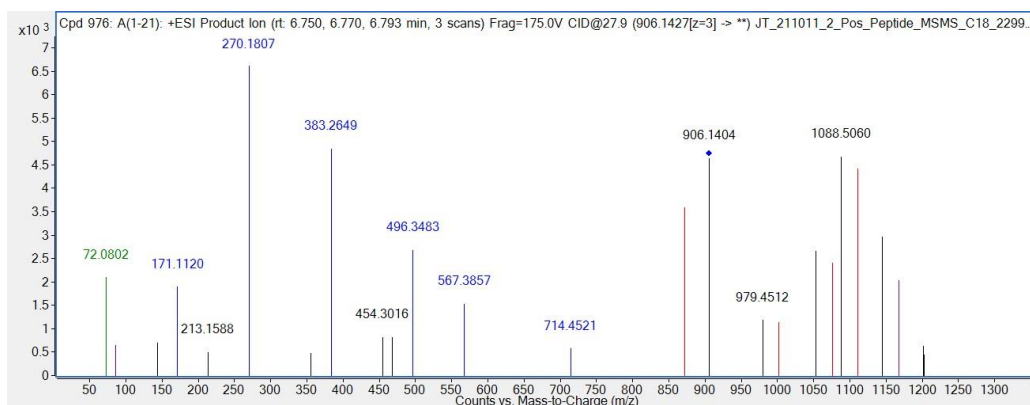


Figure 29: MS/MS spectrum from (Z = 3) parent ion.

Sequence	m/z	m/z (predicted)	Diff (ppm)	Z (prod.)	Ion
GL	171.1128	171.112	-4.5	1	b2
GLV	270.1812	270.1807	-1.8	1	b3
GLVL	383.2653	383.2649	-1.1	1	b4
GLVLI	496.3493	496.3483	-2.1	1	b5
GLVLIA	567.3865	567.3857	-1.4	1	b6
GLVLIAF	714.4549	714.4521	-3.8	1	b7
GLVLIAFSQYLQQCPFDE	1167.59	1167.5774	-10.8	2	b18
PFDEHVK	871.4308	871.4306	-0.3	1	y7
SQYLQQCPFDEHVK	1001.9826	1001.9833	0.7	2	y14
FSQYLQQCPFDEHVK	1075.5168	1075.5174	0.6	2	y15
AFSQYLQQCPFDEHVK	1111.0354	1111.0339	-1.3	2	y16
IAFSQYLQQCPFDEHVK	1167.5774	1167.5774	0	2	y17
L	86.0964	86.0953	-12.6	1	L
V	72.0808	72.0802	-8.2	1	V
I	86.0964	86.0953	-12.6	1	I

Table 34: Confirmation of b and y ions from Z = 3 parent ion.

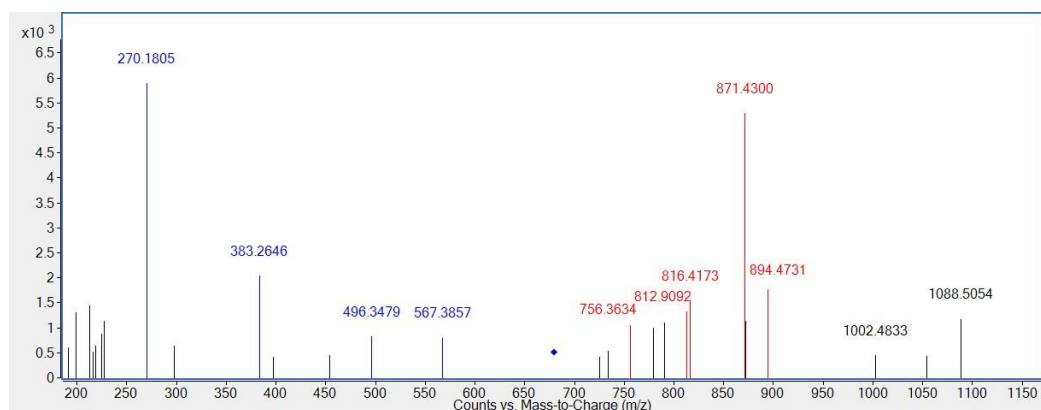


Figure 30: MS/MS spectrum from (Z = 4) parent ion.

Sequence	m/z	m/z (predicted)	Diff (ppm)	Z (prod.)	Ion
V	72.0803	72.0808	-5.9	1	V
L	86.0962	86.0964	-2.1	1	L
I	86.0962	86.0964	-2.1	1	I
Q	101.0704	101.0709	-5.1	1	Q
Y	136.0752	136.0757	-3.6	1	Y
GL	171.1126	171.1128	-1.4	1	b2
GLV	270.1805	270.1812	-2.5	1	b3
GLVL	383.2646	383.2653	-1.8	1	b4
GLVLI	496.3479	496.3493	-2.9	1	b5
GLVLIA	567.3857	567.3865	-1.3	1	b6
QQCPFDEHVK	756.3634	756.3636	-0.2	2	y10
LQQCPFDEHVK	812.9092	812.9056	4.5	2	y11
LIAFSQYLQQCPFDEHVK	816.4173	816.4154	2.4	3	y18
PFDEHVK	871.43	871.4308	-0.9	1	y7
YLQQCPFDEHVK	894.4371	894.4373	-0.2	2	y12

Table 35: Confirmation of b and y ions from Z = 4 parent ion.

Data for Table 29 entry 3:

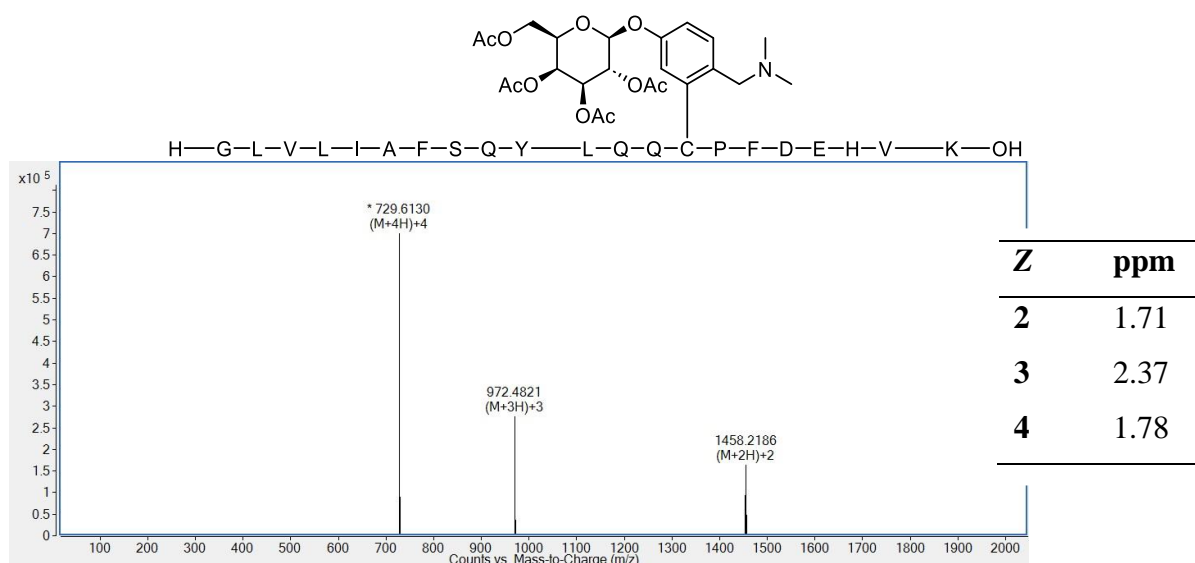


Figure 31: MS spectrum of arylated GLVLI-AF-S-Q-Y-L-Q-Q-C-P-F-D-E-H-V-K-OH with ppm errors for parent ions.

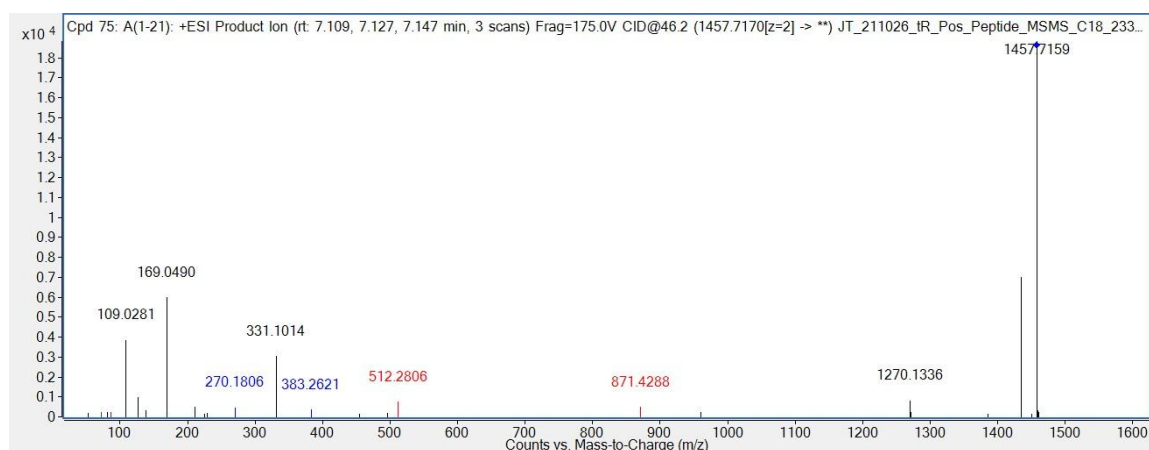


Figure 32: MS/MS spectrum from (Z = 2) parent ion.

Sequence	m/z	m/z (predicted)	Diff (ppm)	Z (prod.)	Ion
GLV	270.1812	270.1806	-2.4	1	b3
GLVL	383.2653	383.2621	-8.3	1	b4
HVK	383.2401	383.2389	-3.3	1	y3
EHVK	512.2827	512.2806	-4.1	1	y4
PFDEHVK	871.4308	871.4288	-2.4	1	y7
L	86.0964	86.0949	-18.2	1	L
V	72.0808	72.0801	-10	1	V
I	86.0964	86.0949	-18.2	1	I

Table 36: Confirmation of b and y ions from Z = 2 parent ion.

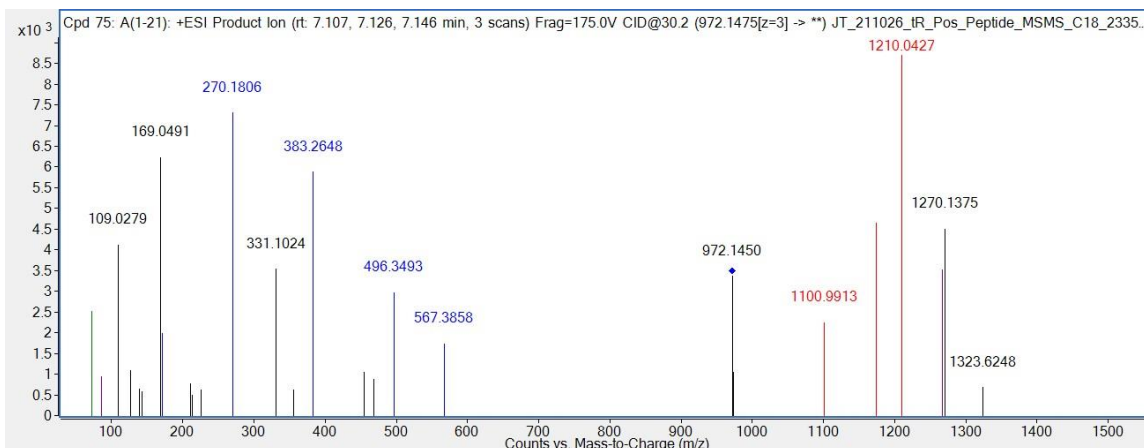


Figure 33: MS/MS spectrum from (Z = 3) parent ion.

Sequence	m/z	m/z (predicted)	Diff (ppm)	Z (prod.)	Ion
GL	171.1128	171.112	-4.8	1	b2
GLV	270.1812	270.1806	-2.2	1	b3
GLVL	383.2653	383.2648	-1.2	1	b4
GLVLI	496.3493	496.3493	-0.1	1	b5
GLVLIA	567.3865	567.3858	-1.1	1	b6
GLVLIAFSQYLQCCPFDE	1266.5982	1266.5832	-11.8	2	b18
SQYLQCCPFDEHVK	1100.9908	1100.9913	0.5	2	y14
FSQYLQCCPFDEHVK	1174.525	1174.5244	-0.5	2	y15
AFSQYLQCCPFDEHVK	1210.0436	1210.0427	-0.8	2	y16
IAFSQYLQCCPFDEHVK	1266.5856	1266.5832	-1.9	2	y17
L	86.0964	86.0965	1.2	1	L
V	72.0808	72.0806	-2.3	1	V
I	86.0964	86.0965	1.2	1	I

Table 37: Confirmation of b and y ions from Z = 3 parent ion.

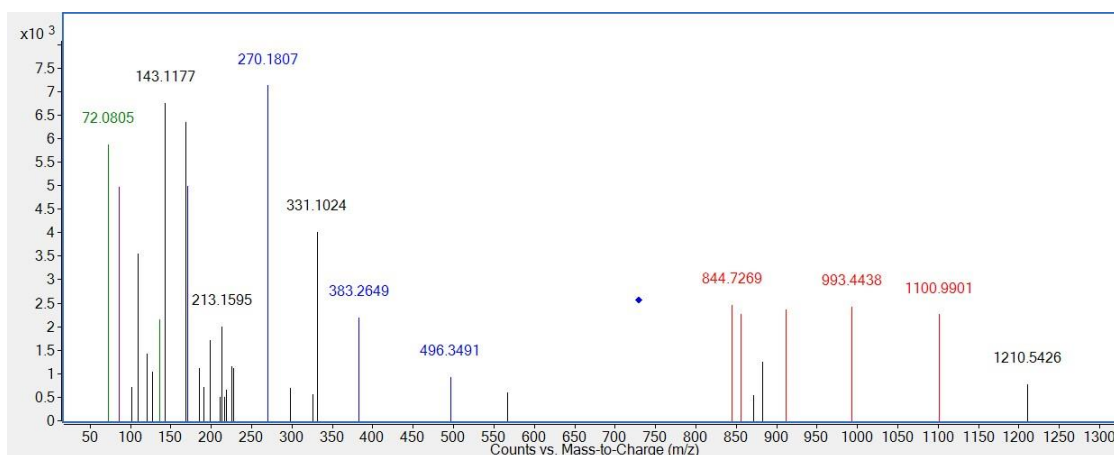


Figure 34: MS/MS spectrum from (Z = 4) parent ion.

Sequence	m/z	m/z (predicted)	Diff (ppm)	Z (prod.)	Ion
V	72.0805	72.0808	-3.3	1	V
L	86.0963	86.0964	-1.6	1	L
I	86.0963	86.0964	-1.6	1	I
Y	136.0754	136.0757	-1.8	1	Y
GL	171.1124	171.1128	-2.6	1	b2
GLV	270.1807	270.1812	-2	1	b3
GLVL	383.2649	383.2653	-0.9	1	b4
GLVLI	496.3491	496.3493	-0.6	1	b5
IAFSQYLQPCPFDEHVK	844.7269	844.7262	0.9	3	y17
QQCPFDEHVK	855.3713	855.3718	-0.6	2	y10
LQQCPFDEHVK	911.9146	911.9138	0.9	2	y11
YLQQCPFDEHVK	993.4438	993.4455	-1.7	2	y12
SQYLQPCPFDEHVK	1100.9901	1100.9908	-0.6	2	y14

Table 38: Confirmation of b and y ions from Z = 4 parent ion.

Data for Table 29 entry 4:

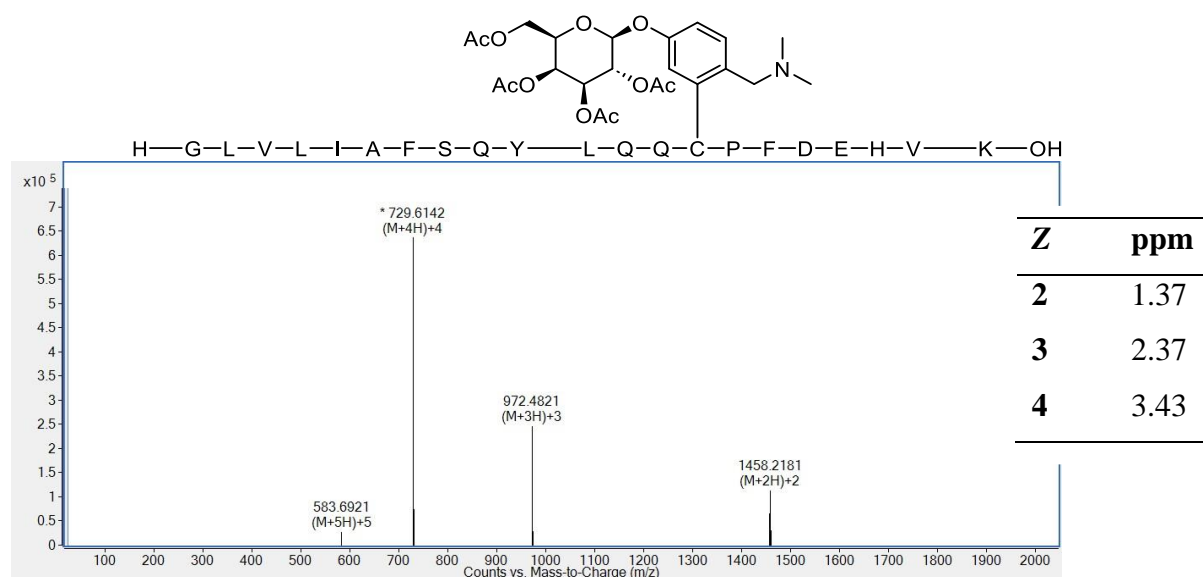


Figure 35: MS spectrum of arylated GLVLI AFSQYLQQC PFDEHVK with ppm errors for parent ions.

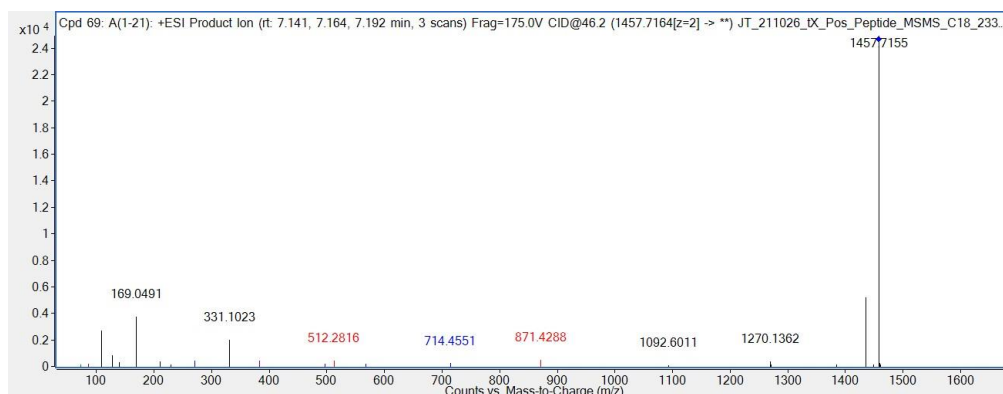


Figure 36: MS/MS spectrum from (Z = 2) parent ion.

Sequence	m/z	m/z (predicted)	Diff (ppm)	Z (prod.)	Ion
V	72.0805	72.0808	-3.3	1	V
L	86.0963	86.0964	-1.6	1	L
I	86.0963	86.0964	-1.6	1	I
Y	136.0754	136.0757	-1.8	1	Y
GL	171.1124	171.1128	-2.6	1	b2
GLV	270.1807	270.1812	-2	1	b3
GLVL	383.2649	383.2653	-0.9	1	b4
GLVLI	496.3491	496.3493	-0.6	1	b5
IAFSQYLQQC PFDEHVK	844.7269	844.7262	0.9	3	y17
QQC PFDEHVK	855.3713	855.3718	-0.6	2	y10
LQC PFDEHVK	911.9146	911.9138	0.9	2	y11
YLQC PFDEHVK	993.4438	993.4455	-1.7	2	y12
SQYLQC PFDEHVK	1100.9901	1100.9908	-0.6	2	y14

Table 39: Confirmation of b and y ions for Z = 2.

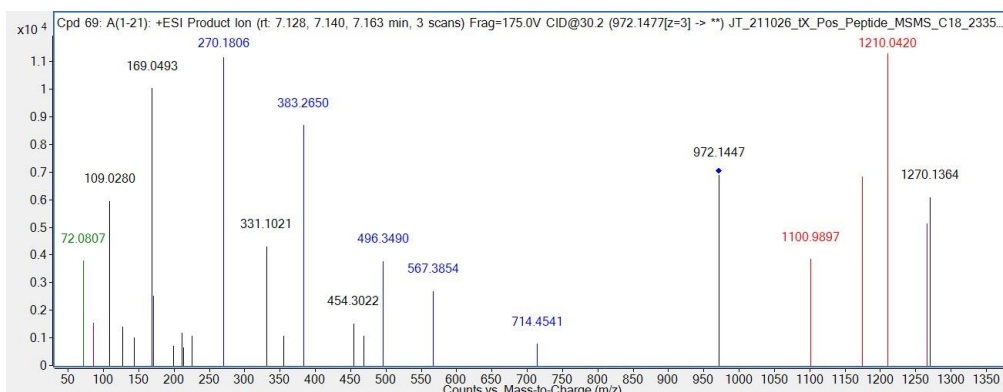


Figure 37: MS/MS spectrum from ($Z = 3$) parent ion.

Sequence	m/z	m/z (predicted)	Diff (ppm)	Z (prod.)	Ion
GL	171.1128	171.1119	-5.5	1	b2
GLV	270.1812	270.1806	-2.1	1	b3
GLVL	383.2653	383.265	-0.7	1	b4
GLVLI	496.3493	496.349	-0.7	1	b5
GLVLIA	567.3865	567.3854	-1.9	1	b6
GLVLIAF	714.4549	714.4541	-1.1	1	b7
GLVLIAFSQYLQCCPFDE	1266.5982	1266.5843	-10.9	2	b18
SQYLQCCPFDEHVK	1100.9908	1100.9897	-1	2	y14
FSQYLQCCPFDEHVK	1174.525	1174.5242	-0.7	2	y15
AFSQYLQCCPFDEHVK	1210.0436	1210.042	-1.3	2	y16
IAFSQYLQCCPFDEHVK	1266.5856	1266.5843	-1	2	y17
L	86.0964	86.0961	-4	1	L
V	72.0808	72.0807	-1.6	1	V
I	86.0964	86.0961	-4	1	I

Table 40: Confirmation of b and y ions for $Z = 3$.

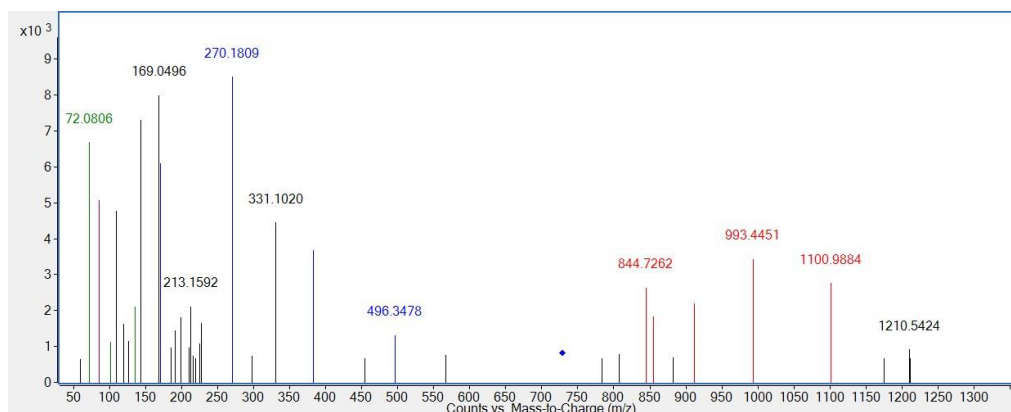


Figure 38: MS/MS spectrum from ($Z = 4$) parent ion.

Sequence	m/z	m/z (predicted)	Diff (ppm)	Z (prod.)	Ion
V	72.0806	72.0808	-2.6	1	V
L	86.0964	86.0964	-0.5	1	L
I	86.0964	86.0964	-0.5	1	I
Q	101.0709	101.0709	-0.8	1	Q
Y	136.0757	136.0757	0.3	1	Y
GL	171.1122	171.1128	-3.7	1	b2
GLV	270.1809	270.1812	-1.3	1	b3
GLVL	383.2647	383.2653	-1.4	1	b4
GLVLI	496.3478	496.3493	-3.1	1	b5
IAFSQYLQPCPFDEHVK	844.7262	844.7262	0.1	3	y17
QQCPFDEHVK	855.3708	855.3718	-1.2	2	y10
LQQCPFDEHVK	911.9118	911.9138	-2.2	2	y11
YLQQCPFDEHVK	993.4451	993.4455	-0.4	2	y12
SQYLQPCPFDEHVK	1100.9884	1100.9908	-2.2	2	y14

Table 41: Confirmation of b and y ions for Z = 4.

5.3.4. Crystallographic Data

Pd(dmba)(RuPhos)Cl (69)

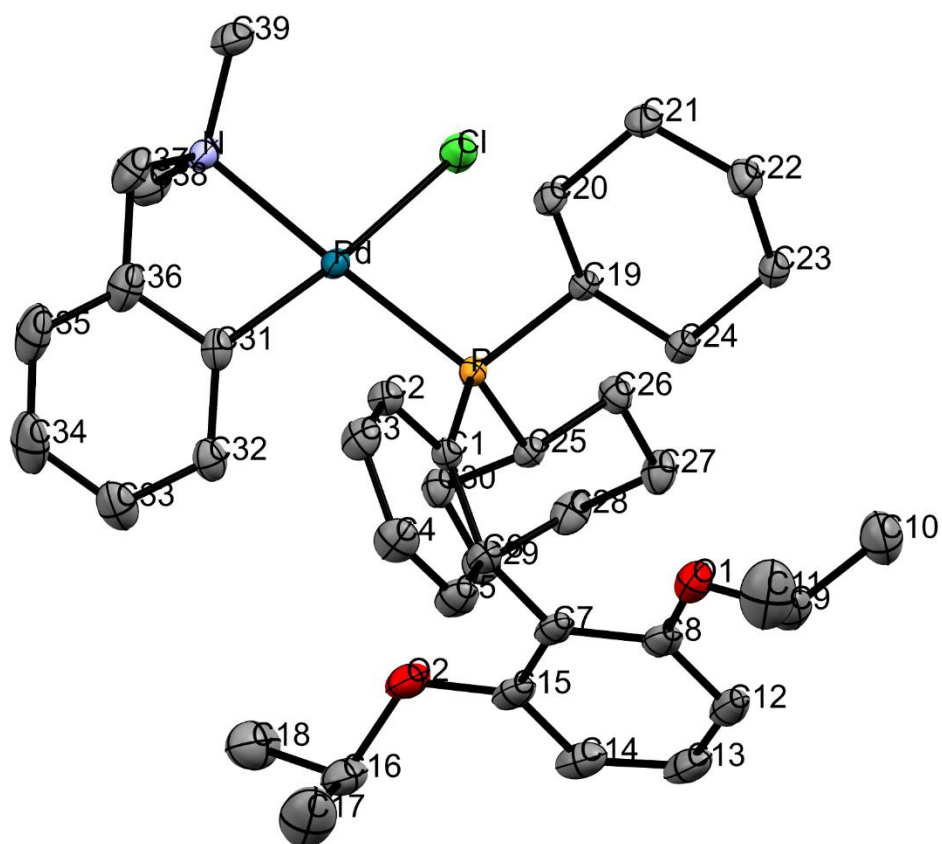


Figure 39: X-ray crystal structure of Pd(dmba)(RuPhos)Cl (69). Hydrogen atoms and one molecule of MeOH omitted for clarity. Thermal ellipsoids drawn at 50% probability.

Empirical formula	C ₄₀ H ₅₉ ClNO ₃ PPd	
Formula weight	774.7	
Temperature	150.01(10) K	
Wavelength	1.54184 Å	
Crystal system	Monoclinic	
Space group	P2 ₁ /c	
Unit cell dimensions	a = 15.21639(15) Å	a = 90°
	b = 22.61775(15) Å	b = 113.9415(11)°
	c = 12.35903(11) Å	g = 90°
Volume	3887.52(7) Å ³	
Z	4	
Density (calculated)	1.324 Mg/m ³	
Absorption coefficient	5.149 mm ⁻¹	
F(000)	1632	
Crystal size	0.110 × 0.070 × 0.020 mm ³	
Theta range for data collection	3.178 to 73.062°	
Index ranges	-16 ≤ h ≤ 18, -27 ≤ k ≤ 27, -15 ≤ l ≤ 15	
Reflections collected	34752	
Independent reflections	7724 [R(int) = 0.0318]	
Completeness to theta = 67.684°	100.00%	
Absorption correction	Semi-empirical from equivalents	
Max. and min. transmission	1.00000 and 0.69031	
Refinement method	Full-matrix least-squares on F ²	
Data / restraints / parameters	7724 / 1 / 435	
Goodness-of-fit on F²	1.016	
Final R indices [I > 2σ(I)]	R1 = 0.0246, wR2 = 0.0621	
R indices (all data)	R1 = 0.0269, wR2 = 0.0635	
Extinction coefficient	n/a	
Largest diff. peak and hole	0.533 and -0.618 e.Å ⁻³	

Table 42: Crystal data and structure refinement for Pd(dmba)(RuPhos)Cl (**69**).

Pd(dmba)(Xantphos)Cl (70)

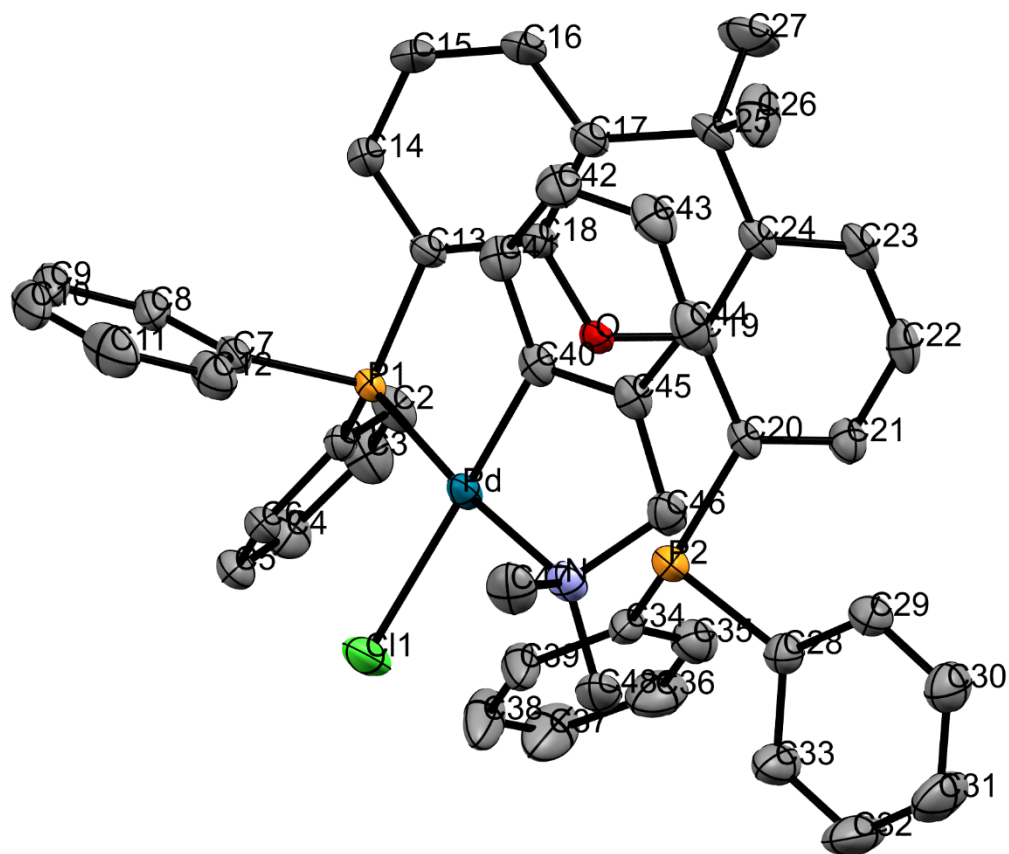


Figure 40: X-ray crystal structure of Pd(dmba)(Xantphos)Cl (70). Hydrogen atoms and one molecule of CHCl₃ omitted for clarity. Thermal ellipsoids drawn at 50% probability.

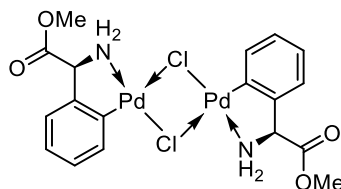
Empirical formula	C ₄₉ H ₄₅ Cl ₄ NOP ₂ Pd	
Formula weight	974	
Temperature	150.0(3) K	
Wavelength	0.71073 Å	
Crystal system	Monoclinic	
Space group	P2 ₁ /n	
Unit cell dimensions	a = 11.7378(3) Å	α = 90°.
	b = 23.3003(5) Å	β = 98.135(2)°.
	c = 16.2116(3) Å	γ = 90°.
Volume	4389.16(17) Å ³	
Z	4	
Density (calculated)	1.474 Mg/m ³	
Absorption coefficient	0.778 mm ⁻¹	
F(000)	1992	
Crystal size	0.468 × 0.425 × 0.082 mm ³	
Theta range for data collection	3.004 to 27.482°	
Index ranges	-15 ≤ h ≤ 15, -30 ≤ k ≤ 30, -21 ≤ l ≤ 21	
Reflections collected	40882	
Independent reflections	10037 [R(int) = 0.0345]	
Completeness to theta = 67.684°	99.80%	
Absorption correction	Semi-empirical from equivalents	
Max. and min. transmission	1.00000 and 0.91801	
Refinement method	Full-matrix least-squares on F ²	
Data / restraints / parameters	10037 / 0 / 527	
Goodness-of-fit on F²	1.107	
Final R indices [I > 2σ(I)]	R1 = 0.0473, wR2 = 0.1042	
R indices (all data)	R1 = 0.0581, wR2 = 0.1095	
Extinction coefficient	n/a	
Largest diff. peak and hole	1.401 and -1.011 e.Å ⁻³	

Table 43: Crystal data and structure refinement for Pd(dmba)(Xantphos)Cl (70).

5.4. Pd(II)-Mediated Amino Acid Side Chain-Side Chain Bioconjugation

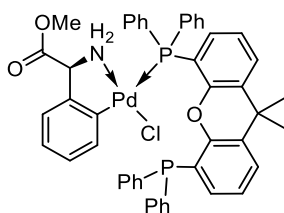
5.4.1. Synthesis of Pd(II)-Amino Acid Complexes

(*S,S*)-[Pd(μ -Cl)(C₆H₄CHCO₂MeNH₂)]₂ (**121**)



(*S*)-(-)-2-Phenylglycine methyl ester hydrochloride (100 mg, 500 μ mol, 1.0 equiv.) and Pd(OAc)₂ (110 mg, 500 μ mol, 1.0 equiv.) were combined in acetone and heated to reflux under an atmosphere of N₂ for 48 h. The reaction mixture was allowed to cool and diluted with hexane. The resulting precipitate was isolated *via* filtration and subjected to flash column chromatography (EtOAc/petroleum ether gradient from 40:60 to 100:0) to yield the **title compound** (126 mg, 82%) as a yellow solid: m.p. decomposed at 181 °C; $[\alpha]_D^{25}$ -205 (*c* 0.20, CHCl₃); ¹H NMR (400 MHz, DMSO-*d*₆) δ 7.67 (d, *J* = 7.7 Hz, 1H), 7.11 (d, *J* = 7.2 Hz, 1H), 7.02 (app t, *J* = 6.9 Hz, 1H), 6.97 (t, *J* = 7.4 Hz, 1H), 6.25 (dd, *J* = 10.1, 5.8 Hz, 1H), 4.94 (d, *J* = 10.1 Hz, 1H), 4.79 – 4.76 (m, 1H), 3.71 (s, 3H); ¹³C{¹H} NMR (101 MHz, DMSO-*d*₆) δ 170.9, 150.7, 149.2, 132.9, 125.9, 125.0, 122.9, 65.2, 52.6; ν_{\max} (thin film)/cm⁻¹ 3283 (s), 3213 (s), 3046 (w), 2951 (w), 1720 (s), 1560 (s), 1433 (s), 1352 (m), 1233 (s), 1139 (m), 1026 (s), 967 (w), 739 (s), 696 (m), 532 (w), 474 (w), 425 (w).

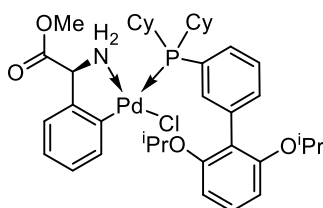
(*S*)-Pd(Cl)(C₆H₄CHCO₂MeNH₂)(Xantphos) (**122**)



(*S,S*)-[Pd(μ -Cl)(C₆H₄CHCO₂MeNH₂)]₂ (31 mg, 50 μ mol, 1.0 equiv.) and Xantphos (58 mg, 100 μ mol, 2.0 equiv.) were combined in CH₂Cl₂ (2 mL) and stirred for 1 h. The reaction mixture was concentrated *in vacuo* and subjected to flash column chromatography (CH₂Cl₂/MeOH gradient from 100:0 to 90:10) to yield the **title compound** (43 mg, 48%) as an orange solid: m.p. decomposes at 192 °C; $[\alpha]_D^{25}$ +30 (*c* 0.20, CHCl₃); ¹H NMR (400 MHz, CDCl₃) δ 7.54 – 7.46 (m, 5H), 7.41 (t, *J* = 8.6 Hz, 4H), 7.33 – 7.23 (m, 8H), 7.20 (td, *J* = 7.5,

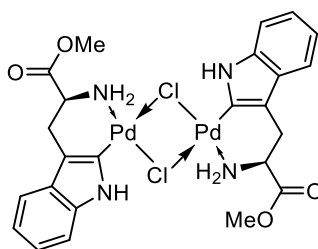
1.4 Hz, 2H), 7.12 – 7.05 (m, 5H), 6.98 (d, $J = 7.7$ Hz, 1H), 6.89 – 6.78 (m, 3H), 6.51 – 6.39 (m, 2H), 4.86 (s, 1H), 4.22 (s, 2H), 3.76 (s, 3H), 1.57 (s, 6H); $^{31}\text{P}\{^1\text{H}\}$ NMR (162 MHz, CDCl_3) δ 22.1; $^{13}\text{C}\{^1\text{H}\}$ NMR (101 MHz, CDCl_3) δ 171.9, 153.9, 153.8, 149.3, 137.8, 137.8, 137.7, 134.9, 134.2, 134.0, 132.9, 131.9, 131.8, 130.3, 129.6, 129.4, 128.7, 128.6, 128.3, 128.2, 127.7, 126.1, 126.1, 126.0, 124.3, 123.9, 123.8, 122.8, 121.3, 121.0, 65.0, 52.6, 35.2, 31.7; (ESI⁺) m/z of $[\text{M}-\text{Cl}]^+$ detected: 848.1690, expected for $\text{C}_{48}\text{H}_{42}\text{ClNO}_3\text{P}_2\text{Pd}$: 848.1686; ν_{max} (thin film)/ cm^{-1} 3049 (w), 2954 (w), 1737 (s), 1574 (m), 1433 (s), 1402 (s), 1226 (s), 1094 (m), 788 (w), 741 (s), 694 (s), 535 (w), 513 (s), 469 (w).

(S,S)-Pd(Cl)(C₆H₄CHCO₂MeNH₂)(RuPhos) (123)



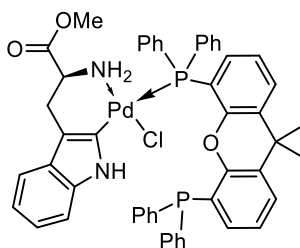
(*S,S*)-[$\{\text{Pd}(\mu\text{-Cl})(\text{C}_6\text{H}_4\text{CHCO}_2\text{MeNH}_2)\}_2$] (31 mg, 50 μmol , 1.0 equiv.) and RuPhos (58 mg, 100 μmol , 2.0 equiv.) were combined in CH_2Cl_2 (2 mL) and stirred for 1 h. The reaction mixture was concentrated *in vacuo* and subjected to flash column chromatography ($\text{CH}_2\text{Cl}_2/\text{MeOH}$ gradient from 100:0 to 90:10) to yield the **title compound** (56 mg, 72%) as an off-white solid: m.p. decomposes at 147 °C; $[\alpha]_{\text{D}}^{25}$ -40 (c 0.20, CHCl_3); ^1H NMR (400 MHz, CDCl_3) δ 7.68 (dd, $J = 14.6, 7.9$ Hz, 1H), 7.30 – 7.23 (m, 2H), 6.98 – 6.91 (m, 3H), 6.80 (td, $J = 7.3, 1.4$ Hz, 1H), 6.65 – 6.51 (m, 4H), 5.04 (s, 1H), 4.51 – 4.41 (m, 2H), 4.30 (s, 1H), 3.88 (s, 4H), 1.73 (s, 3H), 1.55 (s, 4H), 1.31 – 1.20 (m, 8H), 1.10 (t, $J = 6.0$ Hz, 6H); $^{31}\text{P}\{^1\text{H}\}$ NMR (162 MHz, CDCl_3) δ 66.7; $^{13}\text{C}\{^1\text{H}\}$ NMR (101 MHz, CDCl_3) δ 171.6, 157.5, 151.4, 149.4, 140.8, 140.3, 139.8, 139.6, 133.2, 129.1, 126.2, 124.8, 124.7, 123.5, 122.7, 106.9, 106.8, 71.8, 64.0, 53.0, 31.7, 27.5, 27.3, 26.9, 26.7, 26.2, 22.8, 22.6, 22.3; (ESI⁺) m/z of $[\text{M}-\text{Cl}]^+$ detected: 736.2764, expected for $\text{C}_{39}\text{H}_{53}\text{NO}_4\text{PPd}$: 736.2756; ν_{max} (thin film)/ cm^{-1} 3049 (w), 2954 (w), 1737 (s), 1574 (m), 1433 (s), 1402 (s), 1226 (s), 1094 (m), 788 (w), 741 (s), 694 (s), 535 (w), 513 (s), 469 (w).

(*S,S*)-[Pd₂{κ²-*C,N*-C₈H₅NCH₂CH(CO₂Me)NH₂-2}₂(μ-Cl)₂] (115)



L-Tryptophan methyl ester hydrochloride (127 mg, 500 μmol, 1.0 equiv.) and Pd(OAc)₂ (112 mg, 500 μmol, 1.0 equiv.) were combined in MeCN (9 mL) and heated to 30 °C for 48 h. The precipitate formed was isolated *via* filtration and washed with MeCN (3 × 3 mL) and Et₂O (3 × 3 mL) to yield a tan solid. This crude solid was suspended in acetone (50 mL), filtered through a pad of Mg(SO)₄ and concentrated to approximately 3 mL. The yellow precipitate formed was isolated *via* filtration, and washed with acetone (2 × 2 mL) and Et₂O (3 × 3 mL) to yield the **title compound** (89 mg, 49%) as a yellow solid: ¹H NMR (400 MHz, DMSO-*d*₆) δ 10.48 (s, 1H), 7.34 – 7.28 (m, 1H), 7.25 – 7.21 (m, 1H), 6.92 – 6.84 (m, 2H), 5.24 – 5.13 (m, 2H), 3.64 (s, 4H), 3.17 (dd, *J* = 15.5, 3.8 Hz, 1H), 3.04 (dd, *J* = 15.5, 9.0 Hz, 1H); ¹³C{¹H} NMR (101 MHz, DMSO-*d*₆) δ 172.0, 135.4, 130.0, 127.9, 119.2, 117.7, 116.1, 109.9, 106.4, 52.8, 52.1, 27.2. . The spectral data are in agreement with reported literature values.²⁰⁰

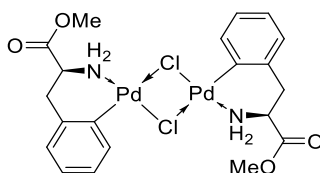
(*S*)-[Pd₂{κ²-*C,N*-C₈H₅NCH₂CH(CO₂Me)NH₂-2}Cl(Xantphos)] (125)



(*S,S*)-[Pd₂{κ²-*C,N*-C₈H₅NCH₂CH(CO₂Me)NH₂-2}₂(μ-Cl)₂] (27 mg, 75 μmol, 1.0 equiv.) and Xantphos (43 mg, 75 μmol, 1.0 equiv.) were combined in CH₂Cl₂ (2 mL) and stirred for 1 h. The reaction mixture was concentrated and treated with MTBE/pentane (50:50, 1000 μL), the supernatant was pipetted off and the resulting solid was washed with pentane (3 × 2 mL) to yield the **title compound** (70 mg, 99%) as an orange solid; m.p. decomposes at 143 °C; [α]_D²⁵ +40 (*c* 0.20, CHCl₃); ¹H NMR (400 MHz, CDCl₃) δ 7.64 – 6.92 (m, 25H), 6.89 (ddd, *J* = 7.9, 7.0, 1.0 Hz, 1H), 6.79 – 6.71 (m, 3H), 6.59 – 6.52 (m, 1H), 3.68 (s, 1H), 3.46 (s, 3H), 3.31 (dd, *J* = 14.6, 4.1 Hz, 1H), 3.14 (dd, *J* = 14.6, 6.0 Hz, 1H), 3.07 – 3.03 (m, 1H), 1.57 (s, 6H), 1.20 (s, 2H); ³¹P{¹H} NMR (162 MHz, CDCl₃) δ 22.1, 15.7 (br), -9.7 (br);

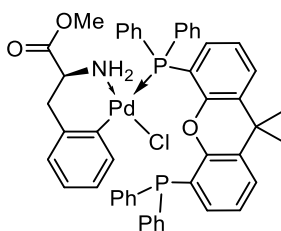
$^{13}\text{C}\{^1\text{H}\}$ NMR (101 MHz, CDCl_3) δ 172.7, 153.7, 138.2, 137.2, 134.5, 134.3, 134.0, 133.8, 131.0, 131.0, 128.7, 128.5, 128.4, 127.9, 127.7, 123.5, 123.5, 118.3, 118.0, 115.7, 109.5, 107.9, 52.5, 50.8, 49.6, 34.8, 30.7, 27.1; (ESI $^+$) m/z of $[\text{M}-\text{Cl}]^+$ detected: 901.1934, expected for $\text{C}_{51}\text{H}_{45}\text{ClN}_2\text{O}_3\text{P}_2\text{Pd}$: 901.1953; ν_{max} (thin film)/ cm^{-1} 3447 (w), 2933 (w), 1734 (m), 1435 (m), 1408 (m), 1332 (w), 1247 (s), 1226 (m), 1057 (s), 997 (m), 907 (w), 811 (w), 784 (w), 731 (s), 691 (s), 579 (w), 537 (m), 510 (s), 472 (s), 427 (w), 418 (w).

(*S,S*)-[Pd $_2\{\kappa^2(\text{C},\text{N})\text{-C}_6\text{H}_4\text{CH}_2\text{CH}(\text{CO}_2\text{Me})\text{NH}_2\text{-2}\}_2(\mu\text{-Cl})_2]$ (126)



Phenylalanine methyl ester hydrochloride (108 mg, 500 μmol , 1.0 equiv.) and $\text{Pd}(\text{OAc})_2$ (112 mg, 500 μmol , 1.0 equiv.) were combined in MeCN (7 mL) at 40 $^\circ\text{C}$ for 24 h. The reaction mixture was filtered through a plug of MgSO_4 and concentrated *in vacuo*. The crude oil was taken up in CH_2Cl_2 (1 mL) and Et_2O was added until a precipitate formed, which was isolated *via* gravity filtration, washed with Et_2O , and dried to give the cyclopalladated intermediate (72 mg) as a red solid which could not be purified and was not characterised.¹⁴³

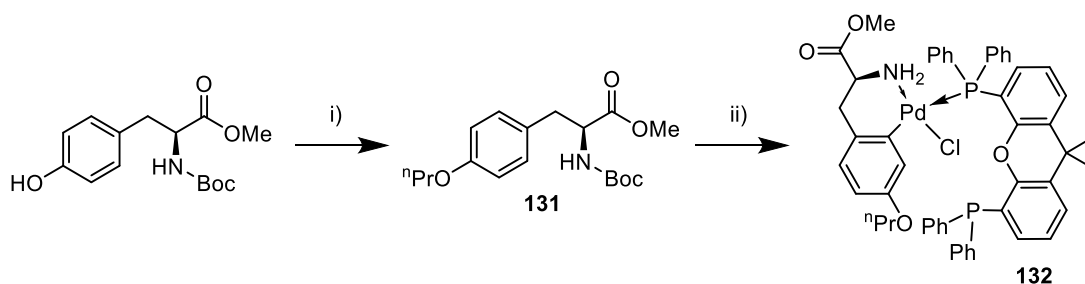
(*S*)-[Pd $\{\kappa^2(\text{C},\text{N})\text{-C}_6\text{H}_4\text{CH}_2\text{CH}(\text{CO}_2\text{Me})\text{NH}_2\text{-2}\}\text{Cl}(\text{Xantphos})]$ (127)



(S,S) -[Pd $_2\{\kappa^2(\text{C},\text{N})\text{-C}_6\text{H}_4\text{CH}_2\text{CH}(\text{CO}_2\text{Me})\text{NH}_2\text{-2}\}_2(\mu\text{-Cl})_2]$ (16 mg, 50 μmol , 1.0 equiv.) and Xantphos (29 mg, 50 μmol , 1.0 equiv.) were combined in CH_2Cl_2 (2 mL) and stirred for 1 h at rt. The solvent was removed, and the crude residue was subjected to flash column chromatography (gradient 3:97 to 5:95 $\text{MeOH}/\text{CH}_2\text{Cl}_2$). The product obtained was crystallised by adding MTBE (500 μL) followed by pentane (500 μL), and then washed with pentane (3×2 mL) to give the **title compound** (19 mg, 42%) as a yellow solid: m.p. decomposes at 159 $^\circ\text{C}$; $[\alpha]_{\text{D}}^{25} +20$ (c 0.20, CHCl_3); ^1H NMR (400 MHz, CDCl_3) δ 7.58 (s, 5H), 7.39 (d, $J = 7.7$ Hz, 2H), 7.35 – 7.02 (br m, 15H), 6.97 (t, $J = 7.6$ Hz, 2H), 6.76 (t, $J = 7.5$ Hz, 2H), 6.63 – 6.58 (m, 1H), 6.53 (t, $J = 7.2$ Hz, 1H), 6.41 (d, $J = 7.1$ Hz, 1H), 6.20 (t,

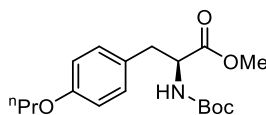
$J = 7.7$ Hz, 1H), 3.52 (s, 2H), 3.47 (s, 3H), 3.34 – 3.23 (br m, 1H), 3.06 (br s, 1H), 2.64 (br s, 1H), 1.45 (s, 6H); $^{31}\text{P}\{^1\text{H}\}$ NMR (162 MHz, CDCl_3) δ 22.1; $^{13}\text{C}\{^1\text{H}\}$ NMR (101 MHz, CDCl_3) δ 172.9, 137.2, 134.6, 134.4, 133.5, 132.2, 130.8, 130.3, 129.4, 128.3, 128.3, 128.2, 127.7, 126.6, 124.7, 123.5, 123.3, 52.6, 50.1, 46.2, 34.6, 27.1; (ESI⁺) m/z of $[\text{M}-\text{Cl}]^+$ detected: 862.1833, expected for $\text{C}_{49}\text{H}_{44}\text{ClNO}_3\text{P}_2\text{Pd}$: 862.1843; ν_{max} (thin film)/ cm^{-1} 3052 (w), 2954 (m), 2920 (m), 2851 (w), 1737 (s), 1573 (w), 1434 (s), 1401 (s), 1229 (s), 1197 (m), 1095 (m), 876 (w), 789 (w), 742 (s), 691 (s), 536 (s), 510 (s).

Synthesis of 132



Scheme 75: **Reagents and conditions:** i) 1-Bromopropane (4 equiv.), K_2CO_3 (2 equiv.), DMF, 70 °C, 21 h, 53%; ii) 4 M HCl in dioxane (15 equiv.), rt, 15 min, then $\text{Pd}(\text{OAc})_2$ (1 equiv.), 40 °C, 24 h, then Xantphos (1 equiv.), CH_2Cl_2 , rt, 1h, 14% over three steps.

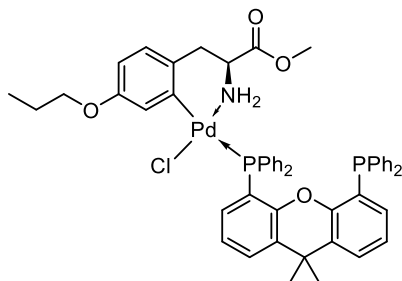
Boc-Tyr(*O-nPr*)-OMe (131)



Boc-Tyr-OMe (150 mg, 0.50 mmol, 1.0 equiv.), bromopropane (92 μL , 1.0 mmol, 2.0 equiv.), and K_2CO_3 (140 mg, 1.0 mmol, 2.0 equiv.) were combined in DMF (5 mL) and heated to 70 °C. After 5 h, bromopropane (92 μL , 1.0 mmol, 2.0 equiv.) was added, and the reaction was stirred for a further 16 h at 70 °C. The reaction mixture was allowed to cool, concentrated *in vacuo*, diluted with aq. HCl (1 M, 50 mL), and extracted with CH_2Cl_2 (3 \times 30 mL). The combined organics were dried (Na_2SO_4) and concentrated *in vacuo*. The crude residue was subjected to flash column chromatography (EtOAc/Petroleum ether gradient from 0:100 to 10:90) to yield the **title compound** (89 mg, 53%) as a colourless oil which crystallised on standing: m.p. 53 – 55 °C (from CH_2Cl_2 /hexane); $[\alpha]_{\text{D}}^{25} +45$ (c 0.40, CHCl_3); ^1H NMR (400 MHz, CDCl_3) δ 6.95 (d, $J = 8.5$ Hz, 2H), 6.75 (d, $J = 8.6$ Hz, 2H), 4.88 (d, $J = 8.3$ Hz, 1H), 4.47 (q, $J = 6.6$ Hz, 1H), 3.82 (t, $J = 6.6$ Hz, 2H), 3.64 (s, 3H), 3.00 – 2.88 (m, 2H), 1.72 (h, $J = 7.1$ Hz, 2H), 1.35 (s, 9H), 0.96 (t, $J = 7.4$ Hz, 3H); $^{13}\text{C}\{^1\text{H}\}$ NMR (101 MHz, CDCl_3) δ 172.6, 158.4, 130.4, 127.8, 114.7, 80.0, 69.6, 54.7, 52.3, 37.6, 28.5, 22.7, 10.7; (ESI⁺) m/z of $[\text{M}+\text{Na}]^+$ detected: 360.1785, expected for $\text{C}_{18}\text{H}_{27}\text{NO}_5$:

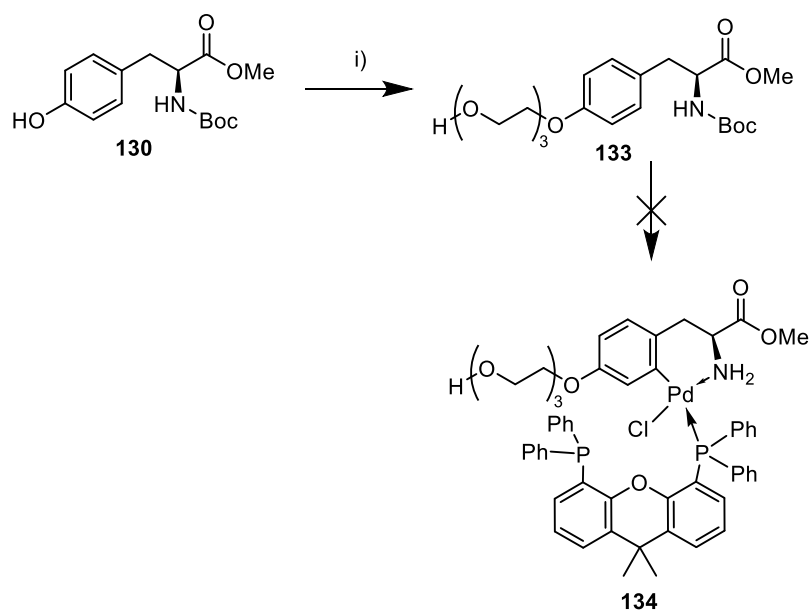
360.1781; ν_{\max} (thin film)/ cm^{-1} 3350 (s), 2959 (s), 2934 (w), 2874 (m), 1736 (s), 1689 (s), 1616 (w), 1512 (s), 1439 (m), 1366 (m), 1288 (s), 1247 (s), 1218 (s), 1162 (s), 1110 (m), 1060 (s), 1023 (m), 992 (s), 887 (w), 822 (s), 801 (m), 759 (w), 658 (s), 551 (s), 508 (w).

Pd(Boc-Tyr(*O*-*n*Pr)-OMe)(Xantphos)Cl (132)



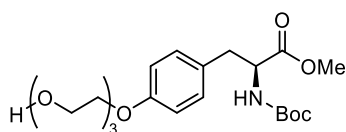
Boc-Tyr(*O*-*n*Pr)-OMe (67 mg, 200 μmol , 1.0 equiv.) was dissolved in 4 M HCl in dioxane (750 μL , 3.0 mmol, 15 equiv.) and stirred at rt for 15 min before being concentrated *in vacuo* to yield a colourless solid that was not isolated. Pd(OAc)₂ (45 mg, 200 μmol , 1.0 equiv.) and MeCN (4 mL) were added, and the resulting mixture was heated to 40 °C for 24 h before being concentrated *in vacuo*. The resulting solid was suspended in Et₂O (5 mL), filtered, and hexane (10 mL) was added to precipitate an orange solid (28 mg) which was not isolated. The crude solid (20 mg) was combined with Xantphos (27 mg, 47 μmol , 1.0 equiv. intermediate) in CH₂Cl₂ (2 mL) for 1 h, before being concentrated *in vacuo*. The crude residue was subjected to flash column chromatography (gradient from 99:1 to 90:10 CH₂Cl₂/MeOH) to yield the **title compound** (18 mg, 14% over 3 steps) as a yellow solid: m.p. decomposes at 150 °C; $[\alpha]_{\text{D}}^{25}$ +130 (*c* 0.20, CHCl₃); ¹H NMR (400 MHz, Chloroform-*d*) δ 7.59 – 7.13 (m, 24H), 6.99 (t, *J* = 7.7 Hz, 2H), 6.75 (t, *J* = 7.3 Hz, 2H), 6.42 (d, *J* = 8.0 Hz, 1H), 6.23 – 6.19 (m, 1H), 6.16 (d, *J* = 8.2 Hz, 1H), 3.54 (s, 3H), 3.43 (s, 1H), 3.23 – 3.04 (m, 3H), 2.74 (s, 1H), 1.62 – 1.41 (m, 8H), 0.81 (t, *J* = 7.4 Hz, 3H); ³¹P{¹H} NMR (162 MHz, CDCl₃) δ 22.1; ¹³C{¹H} NMR (101 MHz, CDCl₃) δ 173.1, 155.3, 155.3, 155.3, 134.4, 134.3, 133.2, 131.2, 131.1, 129.4, 128.3, 128.3, 127.7, 126.9, 123.6, 123.5, 121.9, 110.8, 68.6, 52.6, 50.5, 45.4, 34.8, 22.6, 10.6; (ESI⁺) *m/z* of [M-Cl]⁺ detected: 920.2234, expected for C₅₂H₅₀ClNO₄P₂Pd: 920.2263; ν_{\max} (thin film)/ cm^{-1} 3085 (w), 3051 (w), 2958 (w), 1737 (s), 1580 (s), 1434 (s), 1402 (s), 1230 (s), 1095 (w), 1048 (w), 877 (w), 788 (w), 742 (s), 693 (s), 512 (s), 466 (w).

Failed Synthesis of 134:



Scheme 76: **Reagents and conditions:** i) 2-(2-(2-Hydroxyethoxy)ethoxy)ethyl 4-methylbenzenesulfonate (1 equiv.), K_2CO_3 (1 equiv.), DMF, 80 °C, 18 h, 27%.

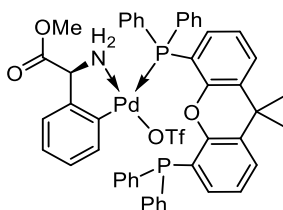
Boc-Tyr(O-PEG₃)-OMe



Boc-Tyr-OMe (220 mg, 0.75 mmol, 1.4 equiv.), 2-(2-(2-Hydroxyethoxy)ethoxy)ethyl 4-methylbenzenesulfonate (160 mg, 0.54 mmol, 1.0 equiv.) and K_2CO_3 (150 mg, 1.1 mmol, 1.0 equiv.) were combined in DMF (10 mL) and heated to 80 °C for 18 h. The reaction was allowed to cool, diluted with HCl (1 M, 40 mL), and extracted with CH_2Cl_2 (3 × 30 mL). The combined organics were washed with aq. NaOH (1 M, 40 mL), aq. LiCl (0.5 M, 3 × 30 mL) and brine (50 mL) before being dried (Na_2SO_4) and concentrated *in vacuo*. The crude residue was subjected to automated flash column chromatography (gradient from 0:100 acetone/petroleum ether to 100:0) to yield the **title compound** (116 mg, 27%) as a colourless oil: $[\alpha]_D^{25} +25$ (*c* 0.40, $CHCl_3$); 1H NMR (400 MHz, $CDCl_3$) δ 7.02 (d, *J* = 8.5 Hz, 2H), 6.84 (d, *J* = 8.6 Hz, 2H), 4.97 (d, *J* = 8.4 Hz, 1H), 4.59 – 4.48 (m, 1H), 4.19 – 4.07 (m, 2H), 3.92 – 3.81 (m, 2H), 3.75 – 3.68 (m, 9H), 3.64 – 3.60 (m, 2H), 3.02 (q, *J* = 7.5, 7.0 Hz, 2H), 1.42 (s, 9H); $^{13}C\{^1H\}$ NMR (101 MHz, $CDCl_3$) δ 172.4, 157.8, 155.1, 130.3, 128.3, 114.7, 79.9, 72.5, 70.8, 70.4, 69.8, 67.4, 61.8, 54.5, 52.2, 37.5, 28.3; (ESI⁺) *m/z* of $[M+H]^+$ detected: 428.2285, expected for $C_{21}H_{33}NO_8$: 428.2279; ν_{max} (thin film)/ cm^{-1} 3371 (br, s), 2974 (s),

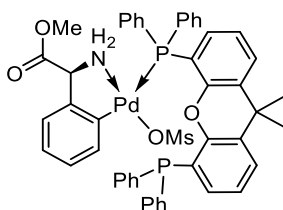
2929 (w), 2873 (s), 1742 (m), 1708 (s), 1612 (w), 1510 (s), 1454 (m), 1365 (s), 1245 (s), 1162 (s), 1057 (s), 940 (w), 825 (m), 531 (w).

(S,S)-Pd(OTf)(C₆H₄CHCO₂MeNH₂)(Xantphos) (135)



(*S,S*)-[$\{\text{Pd}(\mu\text{-Cl})(\text{C}_6\text{H}_4\text{CHCO}_2\text{MeNH}_2)\}_2$] (15 mg, 25 μmol , 1.0 equiv.) and AgOTf (13 mg, 50 μmol , 2.0 equiv.) were combined in CH₂Cl₂ (2 mL) and stirred for 1 h. The reaction mixture was filtered through Celite® into a flask containing Xantphos (29 mg, 50 μmol , 1.0 equiv.). The resulting solution was stirred for 1 h, concentrated *in vacuo* and subjected to flash column chromatography (CH₂Cl₂/MeOH gradient from 99:1 to 90:10) to yield the **title compound** (26 mg, 52%) as a yellow solid: m.p. decomposed at 161 °C (from CH₂Cl₂/MeOH); $[\alpha]_D^{25} +300$ (*c* 0.20, CHCl₃); ¹H NMR (500 MHz, CDCl₃) δ 7.76 – 7.70 (m, 2H), 7.37 – 6.99 (m, 25H), 6.92 – 6.86 (m, 1H), 6.59 – 6.50 (m, 2H), 5.27 (s, 1H), 3.90 (s, 3H), 1.80 (s, 6H), 1.67 (s, 2H); ¹⁹F NMR (470 MHz, CDCl₃) δ -78.2; ³¹P{¹H} NMR (202 MHz, CDCl₃) δ 33.4, 20.0, 1.5; ¹³C{¹H} NMR (126 MHz, CDCl₃) δ 172.8, 154.3, 149.5, 135.9, 135.8, 135.7, 133.9, 133.6, 132.7, 130.4, 128.9, 128.6, 126.8, 126.7, 125.8, 125.2, 125.2, 124.7, 122.1, 67.8, 53.1, 36.3, 29.8; (ESI⁺) *m/z* of [M-OTf]⁺ detected: 848.1699, expected for C₄₉H₄₂NO₆P₂PdSF₃: 848.1686; ν_{max} (thin film)/cm⁻¹ 3343 (w), 3226 (w), 3055 (m), 2957 (m), 2922 (m), 2858 (w), 1732 (s), 1574 (m), 1481 (w), 1435 (s), 1409 (s), 1224 (s), 1151 (s), 1094 (m), 1029 (s), 911 (w), 779 (w), 739 (s), 692 (s), 635 (s), 511 (s), 415 (w).

(S,S)-Pd(OMs)(C₆H₄CHCO₂MeNH₂)(Xantphos) (136)

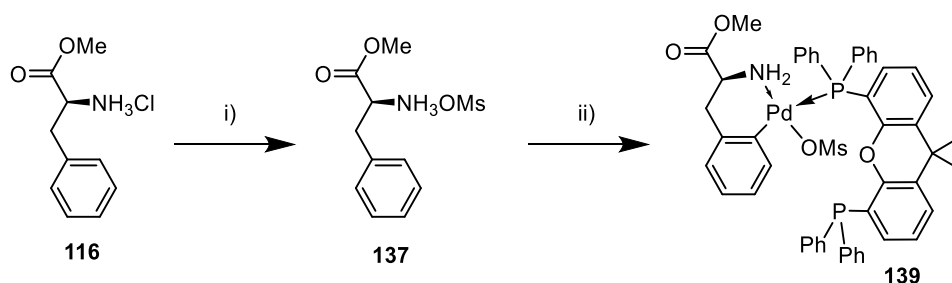


(*S,S*)-[$\{\text{Pd}(\mu\text{-Cl})(\text{C}_6\text{H}_4\text{CHCO}_2\text{MeNH}_2)\}_2$] (15 mg, 25 μmol , 1.0 equiv.) and AgOMs (10 mg, 50 μmol , 2.0 equiv.) were combined in CH₂Cl₂ (2 mL) and stirred for 1 h. The reaction mixture was filtered through celite, and *n*-Hexane (5 mL) was added to produce a light yellow precipitate. The supernatant was pipetted off, and the solid was further washed with

hexane (3 × 1 mL) to yield (*S,S*)-[Pd(μ -OTf)(C₆H₄CHCO₂MeNH₂)]₂ (15 mg) which was used without further purification.

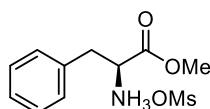
(*S,S*)-[Pd(μ -OMs)(C₆H₄CHCO₂MeNH₂)]₂ (15 mg, 21 μ mol, 1.0 equiv.) and Xantphos (24 mg, 42 μ mol, 2.0 equiv.) were combined in CH₂Cl₂ (2 mL) and stirred for 1 h. The solvent was removed *in vacuo* and the crude residue was subjected to flash column chromatography (CH₂Cl₂/MeOH gradient from 99:1 to 90:10) to yield the **title compound** (23 mg, 49% over two steps) as a yellow solid: m.p. decomposes at 173 °C; [α]_D²⁵ +50 (*c* 0.20, CHCl₃); ¹H NMR (500 MHz, CDCl₃) δ 7.68 (d, *J* = 7.6 Hz, 2H), 7.38 – 6.92 (m, 25H), 6.91 – 6.84 (m, 1H), 6.59 – 6.48 (m, 2H), 5.32 (s, 1H), 3.87 (s, 3H), 2.31 (s, 3H), 1.92 – 1.71 (m, 8H); ³¹P{¹H} NMR (202 MHz, CDCl₃) δ 33.3, 22.1, 11.4 (broad); ¹³C{¹H} NMR (126 MHz, CDCl₃) δ 173.1, 154.3, 154.2, 150.0, 136.3, 136.2, 136.1, 134.0, 133.4, 133.3, 132.8, 132.4, 130.1, 129.0, 128.9, 128.6, 128.5, 128.4, 126.5, 126.5, 126.4, 125.4, 125.0, 124.9, 124.5, 67.9, 52.9, 39.1, 36.1, 31.7; (ESI⁺) *m/z* of [M-OMs]⁺ detected: 848.1695, expected for C₄₉H₄₅NO₆P₂PdS: 848.1686; ν_{\max} (thin film)/cm⁻¹ 3053 (m), 2956 (m), 2928 (w), 1731 (s), 1574 (s), 1435 (s), 1407 (s), 1175 (s), 1038 (s), 740 (s), 692 (s), 551 (m), 511 (s), 415 (w).

Synthesis of 139:



Scheme 77: **Reagents and conditions:** Na₂CO₃ (1.2 equiv.), H₂O, then MeSO₃H (1.0 equiv.), Et₂O, 70%; ii) Pd(OAc)₂ (1 equiv.), MeCN, 60 °C – 78 °C, 4 h, then Xantphos (2 equiv.), CH₂Cl₂, rt, 1 h.

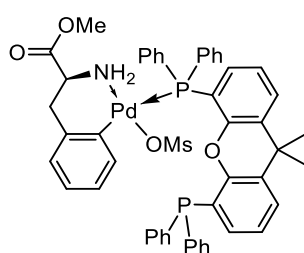
Phenylglycine methyl ester mesylate (137)



L-Phenylalanine methyl ester hydrochloride (430 mg, 2.0 mmol, 1.0 equiv.) added to a solution of Na₂CO₃ (250 mg, 2.4 mmol, 1.2 equiv.) in H₂O (10 mL) and stirred for 10 min. The reaction mixture was extracted with CH₂Cl₂ (3 × 10 mL), the combined organics were dried and concentrated *in vacuo*. Et₂O (5 mL) was added, and a solution of methanesulfonic acid (130 μ L, 2.0 mmol, 1.0 equiv.) in Et₂O (10 mL) was added dropwise with stirring. The

solid formed was isolated *via* gravity filtration, washed with Et₂O (3 × 10 mL) and dried under vacuum to yield the **title compound** (386 mg, 70%) as a colourless crystalline solid: m.p. decomposes at 200 °C; [α]_D²⁵ +18 (*c* 0.40, MeOH); ¹H NMR (400 MHz, Methanol-*d*₄) δ 7.40 – 7.25 (m, 5H), 4.33 (app t, *J* = 6.8 Hz, 1H), 3.26 (dd, *J* = 14.3, 6.8 Hz, 1H), 3.18 (dd, *J* = 14.3, 6.8 Hz, 1H), 2.70 (s, 3H); ¹³C{¹H} NMR (101 MHz, MeOD) δ 170.5, 135.3, 130.4, 130.2, 128.9, 55.2, 53.6, 39.5, 37.4; ν_{max} (thin film)/cm⁻¹ 3088 (w, C-H), 3003 (w, C-H), 2906 (s, br, N-H), 1751 (s, C=O), 1608 (w), 1526 (m), 1440 (w), 1145 (s), 1766 (w), 1034 (s), 947 (w), 846 (m), 775 (m), 733 (m), 694 (w), 545 (s), 523 (s), 454 (w).

(S)-[Pd{ κ^2 (C,N)-C₆H₄CH₂CH(CO₂Me)NH₂-2}OMs(Xantphos)] (139)

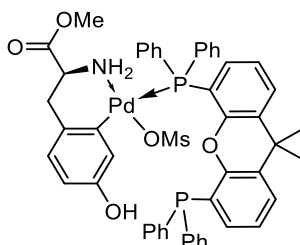


L-Phenylglycine methyl ester mesylate (55 mg, 200 μ mol, 1.0 equiv.) was combined with Pd(OAc)₂ (55 mg, 220 μ mol, 1.1 equiv.) in MeCN (10 mL) and heated to 60 °C for 1 h, then 78 °C for 3 h. The reaction mixture was allowed to cool, filtered through a pad of Celite® and NaCO₃, and concentrated *in vacuo*. The crude residue was dissolved in a minimum amount of CH₂Cl₂ and Et₂O was added until new precipitate stopped forming. The resulting precipitate was isolated *via* gravity filtration and washed with Et₂O (3 × 3 mL) to yield the dimeric cyclopalladated intermediate (71 mg) as a light green solid which was not characterised.

The intermediate (71 mg) and Xantphos (113 mg, 190 μ mol, 0.95 equiv.) were combined in CH₂Cl₂ (2 mL) and stirred at rt for 1 h. The solvent was removed, and the residue was subjected to flash column chromatography (gradient from 0:100 MeOH/CH₂Cl₂ to 3.5:96.5, then eluted with 10:90). The resulting solid was crystallised from CH₂Cl₂/hexane and washed with copious pentane to yield the **title compound** (109 mg, 58%) as a light-green solid: m.p. decomposes at 175 °C; [α]_D²⁵ +15 (*c* 0.20, CHCl₃); ¹H NMR (400 MHz, CD₃CN) δ 7.81 (d, *J* = 7.7 Hz, 2H), 7.34 – 7.11 (m, 22H), 6.94 – 6.80 (m, 4H), 6.64 – 6.57 (m, 1H), 6.48 (t, *J* = 7.5 Hz, 1H), 3.62 (s, 7H), 3.22 (d, *J* = 12.7 Hz, 1H), 2.37 (s, 3H), 1.73 (s, 6H); ³¹P{¹H} NMR (162 MHz, CD₃CN) δ 7.1; ¹³C{¹H} NMR (101 MHz, CD₃CN) δ 173.4, 155.3, 155.3, 135.1, 135.0, 134.1, 133.3, 131.7, 131.3, 130.8, 129.8, 129.7, 129.6, 128.9, 126.7,

126.4, 126.0, 126.0, 53.5, 51.6, 45.9, 39.8, 37.0; (ESI⁺) *m/z* of [M–OMs]⁺ detected: 862.1849, expected for C₅₀H₄₇NO₆P₂PdS: 862.1843; ν_{\max} (thin film)/cm⁻¹ 3285 (br, m), 2991 (w), 2949 (w), 1732 (s), 1637 (m), 1573 (m), 1412 (s), 1252 (m), 1172 (s), 1038 (s), 822 (w), 757 (m), 726 (m), 691 (m), 651 (w), 553 (m), 522 (s), 510 (s), 471 (m), 452 (m), 413 (w).

(S)-[Pd{ κ^2 (C,N)-4-(OH)C₆H₃CH₂CH(CO₂Me)NH₂-2}OMs(Xantphos)] (140)



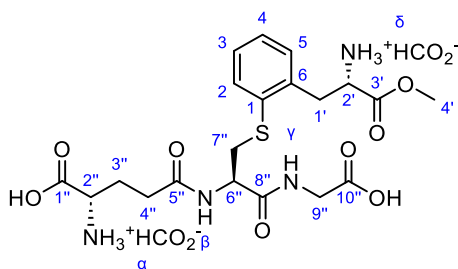
L-Tyrosine methyl ester mesylate (58 mg, 200 μ mol, 1.0 equiv.) and Pd(OAc)₂ (45 mg, 200 μ mol, 1.0 equiv.) were combined in MeCN (7 mL) and heated to 60 °C for 1 h, then 78 °C for 3 h. The reaction mixture was allowed to cool, filtered through a pad of Celite® and NaCO₃, and concentrated *in vacuo*. Et₂O (10 mL) was added, and the resulting precipitate was isolated *via* gravity filtration, and washed with Et₂O (3 \times 2 mL) to give the crude intermediate (92 mg) as a solid which was not isolated. Xantphos (116 mg, 200 μ mol, 1.0 equiv.) and CH₂Cl₂ (5 mL) were added, and the resulting mixture was stirred for 1 h before being concentrated *in vacuo* and subjected to automated flash column chromatography (gradient from 0:100 to 10:90 MeOH/CH₂Cl₂, 10 CV then 10:90 MeOH/CH₂Cl₂ 30 CV) to yield the **title compound** (74 mg, 38% over two steps) as a yellow solid: m.p. decomposes at 190 °C (from MeOH/pentane); $[\alpha]_{\text{D}}^{25}$ –120 (*c* 0.20, CHCl₃); ¹H NMR (500 MHz, CD₃CN) δ 7.81 (d, *J* = 7.8 Hz, 2H), 7.24 (m, 23H), 6.84 (s, 1H), 6.68 (s, 1H), 6.33 (d, *J* = 7.9 Hz, 1H), 6.10 (td, *J* = 7.0, 2.3 Hz, 1H), 3.62 (s, 3H), 3.56 – 3.32 (m, 5H), 3.12 (s, 1H), 2.40 (s, 3H), 1.72 (s, 6H); ¹³C{¹H} NMR (126 MHz, CD₃CN) δ 173.5, 155.3, 134.2, 133.3, 131.4, 131.3, 129.8, 129.7, 129.6, 129.5, 128.8, 126.0, 125.9, 122.3, 113.1, 53.4, 52.2, 45.1, 39.8, 36.9, 28.3; ³¹P{¹H} NMR (202 MHz, CD₃CN) δ 6.3 (broad); (ESI⁺) *m/z* of [M–OMs]⁺ detected: 878.1788, expected for C₅₀H₄₇NO₆P₂PdS: 878.1792; ν_{\max} (thin film)/cm⁻¹ 3210 (br, s), 2956 (s), 1732 (s), 1572 (s), 1434 (s), 1408 (s), 1155 (s), 1038 (s), 876 (m), 742 (s), 692 (s), 551 (w), 512 (s), 465 (w).

5.4.2. Isolation of Glutathione Bioconjugate

Reverse phase automated flash column chromatography was performed on a Teledyne ISCO CombiFlash® NextGen 300+ with a UV/Vis detector using RediSep® Gold C18 reversed phase columns.

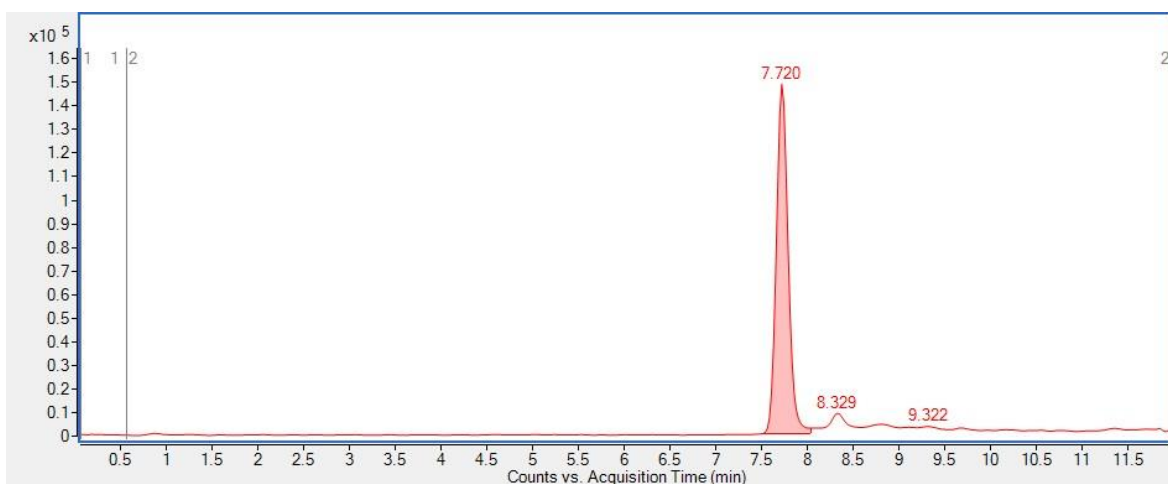
Method for purification of 141: Column: C18 12-16g, flow rate: 13 ml/min, equilibration volume: 6.0 CV, initial waste: 0.0 CV, air purge: 0.0 min, solvent A: water +0.1% FA, solvent B: methanol +0.1% FA. The column was operated starting with 1 % mobile phase B for 5 min, thereafter the gradient was initiated and ran for 10 min to 20% B, then for 10 min to 100% B, held at 100% B for 5 min, and reduced to 80% B for 5 min for a total of 40 min run time.

(141)



(*S,S*)-[Pd{κ²(*C,N*)-C₆H₄CH₂CH(CO₂Me)NH₂-2}OMs(Xantphos)] (**139**) (94 mg, 100 μmol, 1.0 equiv.) in MeCN (5 mL) was added to a solution of glutathione (31 mg, 100 μmol, 1.0 equiv.) in aq. tris buffer (5 mL, 0.1 M, pH 8.0) in a polypropylene 50 mL centrifuge tube. The resulting mixture was vortexed for 5 s then left to stand for 30 min at rt. 3-MPA (32 μL in 2 mL H₂O) was added, the mixture was vortexed and then filtered through a cotton wool plug, which was washed with 0.1% formic acid in H₂O (5 mL). The filtrate was concentrated *in vacuo* to remove any organic solvent, and then subjected to reverse phase automated flash column chromatography. The product-containing fractions were combined and lyophilized to yield the **title compound** (18 mg, 31%) as a colourless solid: m.p. 158 – 160 °C (from H₂O); ¹H NMR (500 MHz, D₂O) δ 7.64 (dd, *J* = 7.7, 1.3 Hz, 1H, H-2), 7.43 (app td, *J* = 7.7, 1.7 Hz, 1H, H-3), 7.37 (td, *J* = 7.7, 1.3 Hz, 1H, H-4), 7.33 (dd, *J* = 7.7, 1.7 Hz, 1H, H-5), 4.57 (dd, *J* = 8.0, 5.0 Hz, 1H, H-6''), 4.42 (t, *J* = 7.5 Hz, 1H, H-2'), 3.81 (s, 3H, H-4'), 3.73 (t, *J* = 6.5 Hz, 1H, H-2''), 3.69 (d, *J* = 17.4 Hz, 1H, H-9''), 3.64 (d, *J* = 17.4 Hz, 1H, H-9''), 3.57 (dd, *J* = 14.3, 7.5 Hz, 1H, H-1'), 3.51 (dd, *J* = 14.5, 5.0 Hz, 1H, H-7''), 3.39 (dd, *J* = 14.6, 8.0 Hz, 1H, H-7''), 3.36 (dd, *J* = 14.3, 7.5 Hz, 1H, H-1'), 2.49 – 2.34 (m, 2H, H-4''), 2.15 – 2.01 (m, 2H, H-3''); ¹³C{¹H} NMR (126 MHz, D₂O) δ 175.4 (C-10''), 174.6

(C-5''), 173.8 (C-1''), 171.3 (C-8''), 169.9 (C-3'), 135.1 (C-3), 133.7 (C-4), 132.1 (C-5), 131.1 (C-2), 129.1 (C-6), 128.2 (C-1), 54.0 (C-2''), 53.6 (C-9''), 53.3 (C-6'), 53.3 (C-2'), 42.9 (C-4'), 35.3 (C-7''), 34.5 (C-1'), 31.3 (C-4''), 26.0 (C-3''); (ESI⁺) *m/z* of [M+H]⁺ detected: 485.1700, expected for C₂₀H₂₈N₄O₈S: 485.1701 (EIC 35); ν_{\max} (thin film)/cm⁻¹ 3267 (w), 3053 (w), 2929 (br, s), 1745 (m), 1633 (s), 1530 (br, s), 1441 (w), 1392 (s), 1236 (s), 1067 (w), 757 (s), 537 (m).



EIC 35: LC-MS of purified **141** using *peptide LC-MS* method.

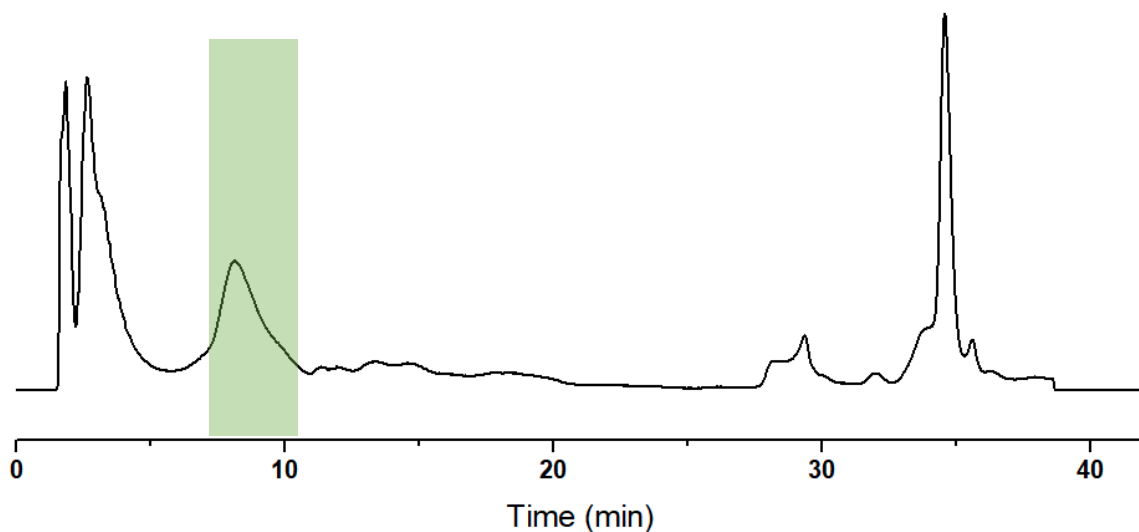


Figure 41: UV trace of automated flash column chromatography with corresponding to **141** highlighted in green.

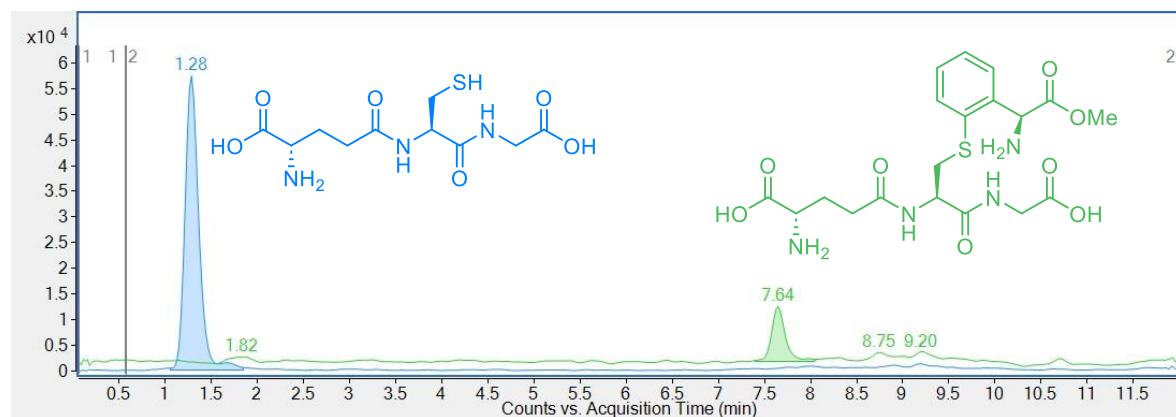
5.4.3. Bioconjugation Reactions

5.4.3.1. Glutathione Arylation

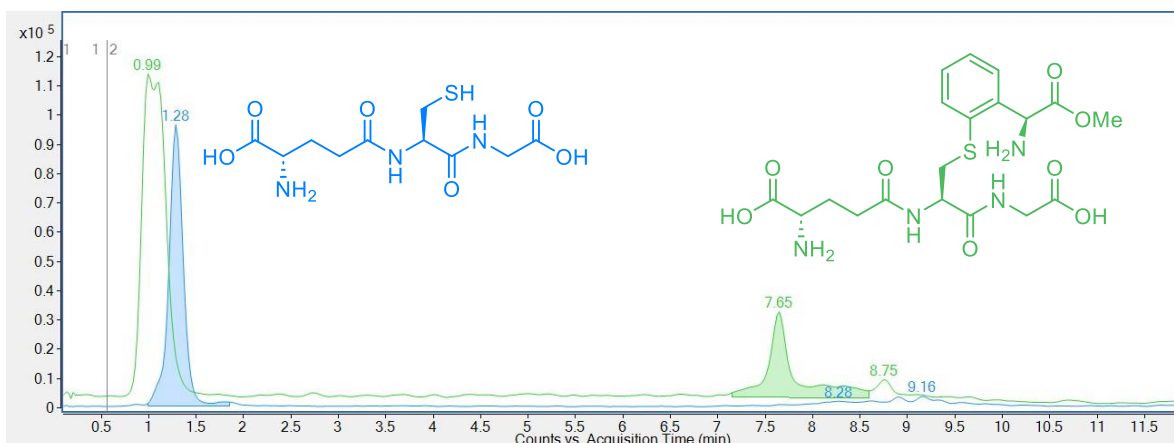
Reactions were run according to **general procedure for glutathione arylation** with compounds **122**, **135**, **136**, **125**, **127**, **139**, **132** and **140** and DMF as the organic co-solvent. Samples were analysed using the **peptide LC-MS** method.

Entry	Compound	Glutathione EIC Peak Area	Glutathione Conversion ^[a]
1 (EIC 36)	122	604,030	94%
2 (EIC 37)	135	1,038,148	90%
3 (EIC 38)	136	629,985	94%
4 (EIC 39)	125	273,229	96%
5 (EIC 40)	127	319,561	96%
6 (EIC 41)	139	80,227	98%
7 (EIC 42)	132	911,493	91%
8 (EIC 43)	140	180,268	97%

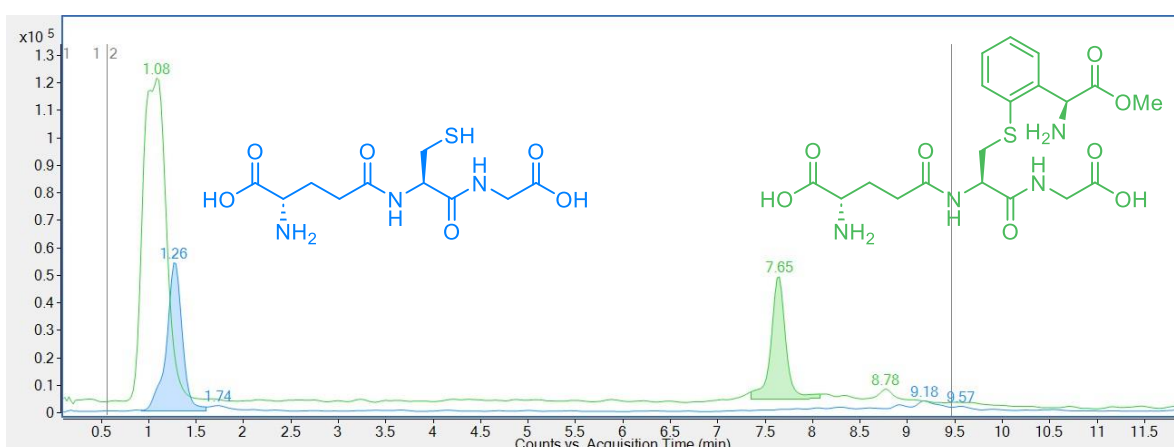
Table 44: Results for glutathione arylation using Pd(II)-amino acid complexes. ^[a] Conversions calculated using glutathione calibration curve.



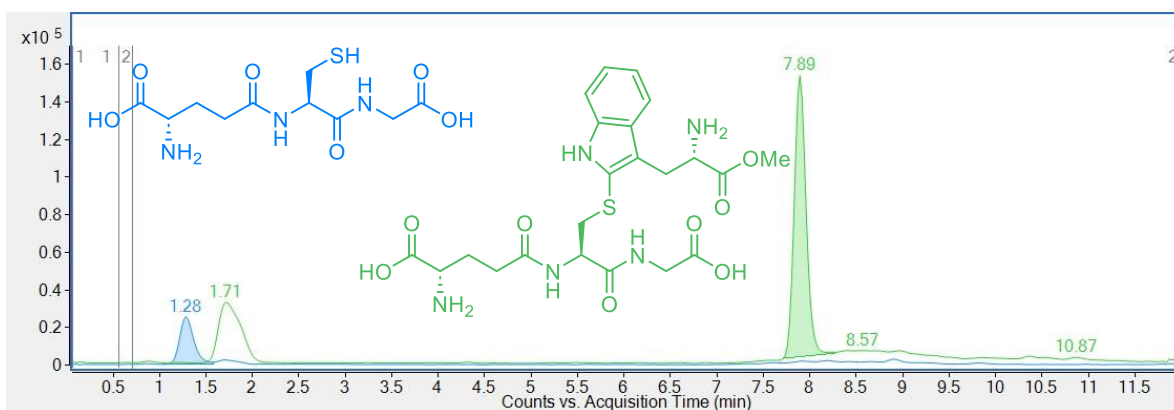
EIC 36: Reaction of glutathione with **122**. GSH (ESI⁺) *m/z* of [M+H]⁺ detected: 308.0908, expected for C₁₀H₁₇N₃O₆S: 308.0911. GSH peak area: 604,030 (rt = 1.28 min). Arylated GSH (ESI⁺) *m/z* of [M+H]⁺ detected: 471.1537, expected for C₁₉H₂₆N₄O₈S: 471.1544. Arylated GSH peak area: 110,267 (rt = 7.64 min).



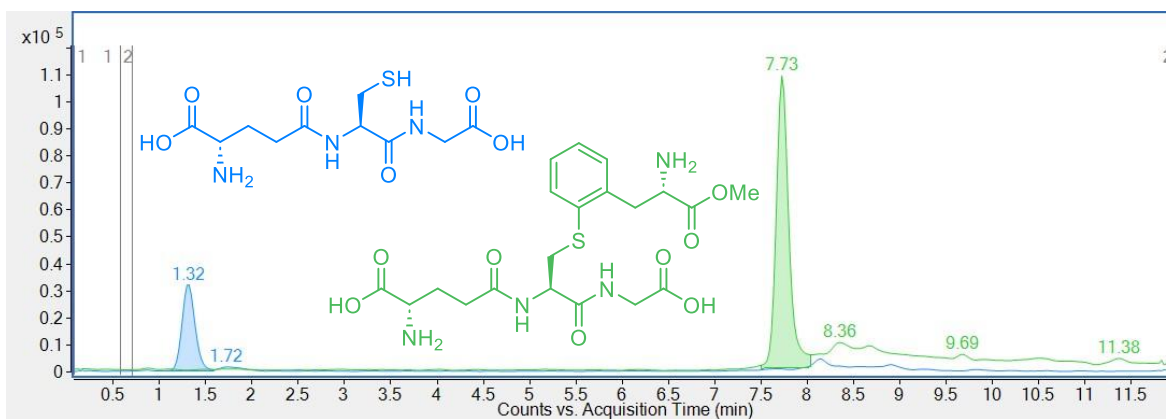
EIC 37: Reaction of glutathione with 135. GSH (ESI⁺) m/z of [M+H]⁺ detected: 308.0908, expected for C₁₀H₁₇N₃O₆S: 308.0911. GSH peak area: 1,038,148 (rt = 1.28 min). Arylated GSH (ESI⁺) m/z of [M+H]⁺ detected: 471.1541, expected for C₁₉H₂₆N₄O₈S: 471.1544. Arylated GSH peak area: 566,004 (rt = 7.65 min).



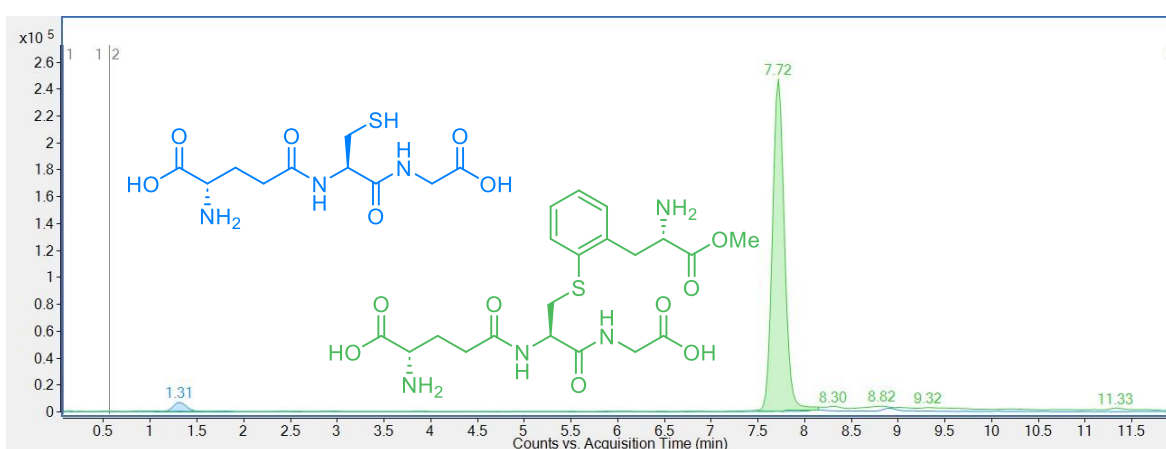
EIC 38: Reaction of glutathione with 136. GSH (ESI⁺) m/z of [M+H]⁺ detected: 308.0907, expected for C₁₀H₁₇N₃O₆S: 308.0911. GSH peak area: 629,985 (rt = 1.26 min). Arylated GSH (ESI⁺) m/z of [M+H]⁺ detected: 471.1539, expected for C₁₉H₂₆N₄O₈S: 471.1544. Arylated GSH peak area: 491,353 (rt = 7.65 min).



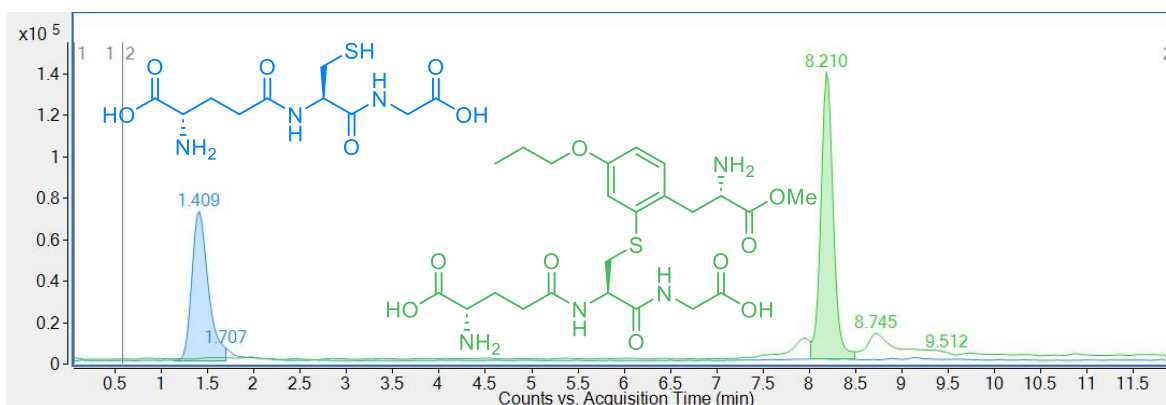
EIC 39: Reaction of glutathione with 125. GSH (ESI⁺) m/z of [M+H]⁺ detected: 308.0907, expected for C₁₀H₁₇N₃O₆S: 308.0911. GSH peak area: 273,229 (rt = 1.28 min). Arylated GSH (ESI⁺) m/z of [M+H]⁺ detected: 524.1799, expected for C₂₂H₂₉N₅O₈S: 524.1810. Arylated GSH peak area: 1,327,648 (rt = 7.89 min).



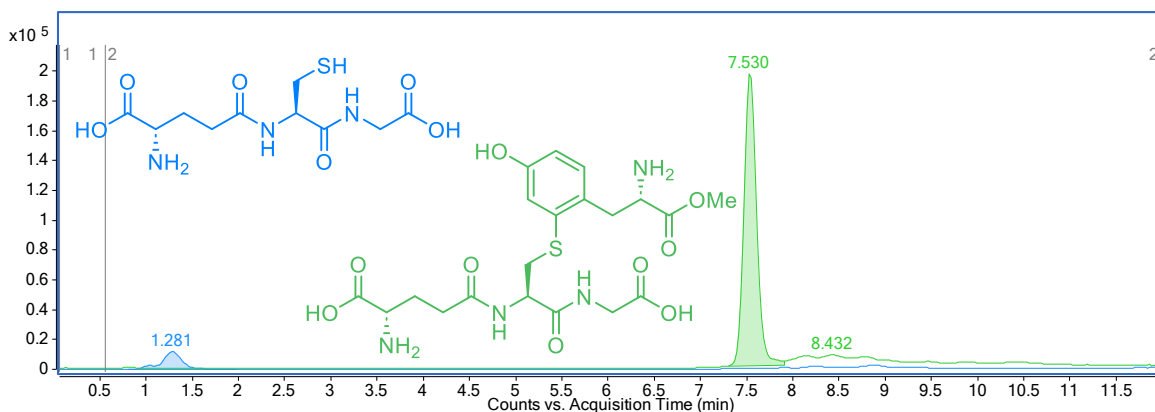
EIC 40: Reaction of glutathione with 127. GSH (ESI⁺) m/z of [M+H]⁺ detected: 308.0908, expected for C₁₀H₁₇N₃O₆S: 308.0911. GSH peak area: 319,561 (rt = 1.32 min). Arylated GSH (ESI⁺) m/z of [M+H]⁺ detected: 485.1690, expected for C₂₀H₂₈N₄O₈S: 485.1701. Arylated GSH peak area: 1,033,969 (rt = 7.73 min).



EIC 41: Reaction of glutathione with 139. GSH (ESI⁺) m/z of [M+H]⁺ detected: 308.0908, expected for C₁₀H₁₇N₃O₆S: 308.0911. GSH peak area: 80,227 (rt = 1.31 min). Arylated GSH (ESI⁺) m/z of [M+H]⁺ detected: 485.1696, expected for C₂₀H₂₈N₄O₈S: 485.1701. Arylated GSH peak area: 2,205,442 (rt = 7.73 min).



EIC 42: Reaction of glutathione with 132. GSH (ESI⁺) m/z of [M+H]⁺ detected: 308.0908, expected for C₁₀H₁₇N₃O₆S: 308.0911. GSH peak area: 911,493 (rt = 1.41 min). Arylated GSH (ESI⁺) m/z of [M+H]⁺ detected: 543.2113, expected for C₂₃H₃₄N₄O₉S: 543.2119. Arylated GSH peak area: 1,305,925 (rt = 8.21 min).



EIC 43: Reaction of glutathione with 140. GSH (ESI⁺) m/z of $[M+H]^+$ detected: 308.0907, expected for $C_{10}H_{17}N_3O_6S$: 308.0911. GSH peak area: 180,268 (rt = 1.28 min). Arylated GSH (ESI⁺) m/z of $[M+H]^+$ detected: 501.1646, expected for $C_{20}H_{28}N_4O_9S$: 501.1650. Arylated GSH peak area: 1,874,448 (rt = 7.53 min).

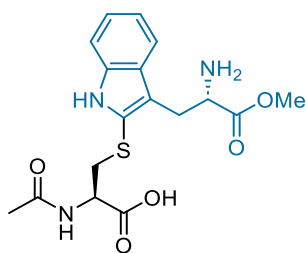
5.4.3.2. BSA Arylation

Complex **127** (10 μ L, 1 mM in DMF, 10 equiv.) was added to a mixture of BSA (10 μ L, 100 μ M in H₂O, 1 equiv.), PBS (80 μ L, Dulbecco A), H₂O (815 μ L), and DMF (90 μ L) in a 1.5 mL Eppendorf tube. After vortexing, the reaction mixture was held at 37 °C for 1 h before being analysed by **intact protein LC-MS**. Final reaction conditions: BSA – 1 μ M, **127** – 10 μ M, H₂O/DMF (90:10). A control reaction containing no complex **127** was also conducted.

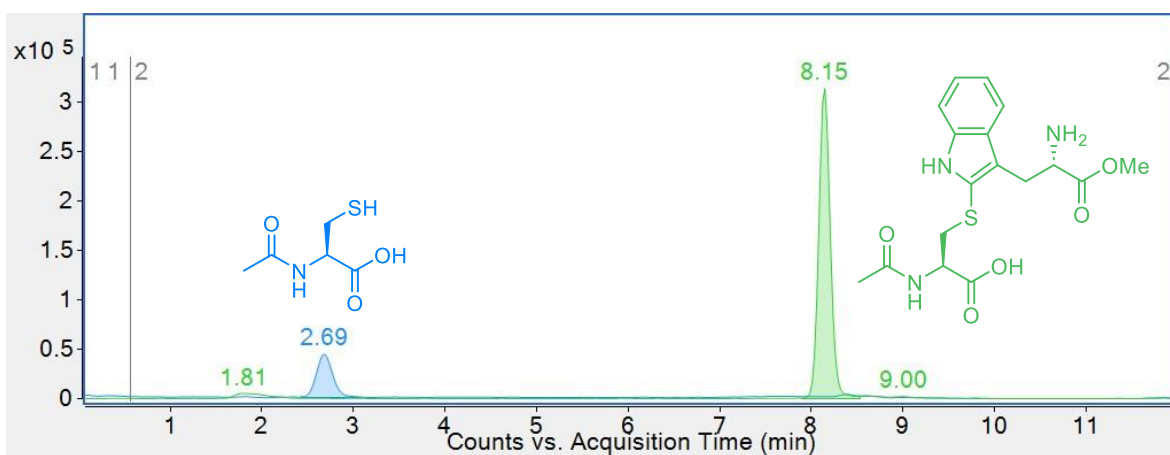
5.4.3.3. Macrocycle formation

Procedure for *N*-acetylcysteine arylation: Pd(II) complex (4 μ L, 1 mM in DMF, 1 equiv.), *N*-acetylcysteine (4 μ L, 1 mM in DMF 1 equiv.), and DIPEA (4 μ L, 1 mM in DMF 1 equiv.) were combined in a 1.5 mL Eppendorf tube. After vortexing, the reactions were left to stand for 5 min, before 3-MPA (4 μ L, 3 mM in DMF) was added. The reactions were then diluted with H₂O (1000 μ L) and analysed by **peptide LC-MS**.

145



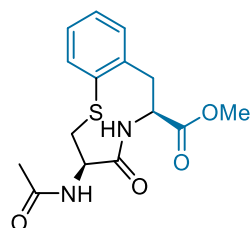
125 was used in procedure for *N*-acetylcysteine arylation.



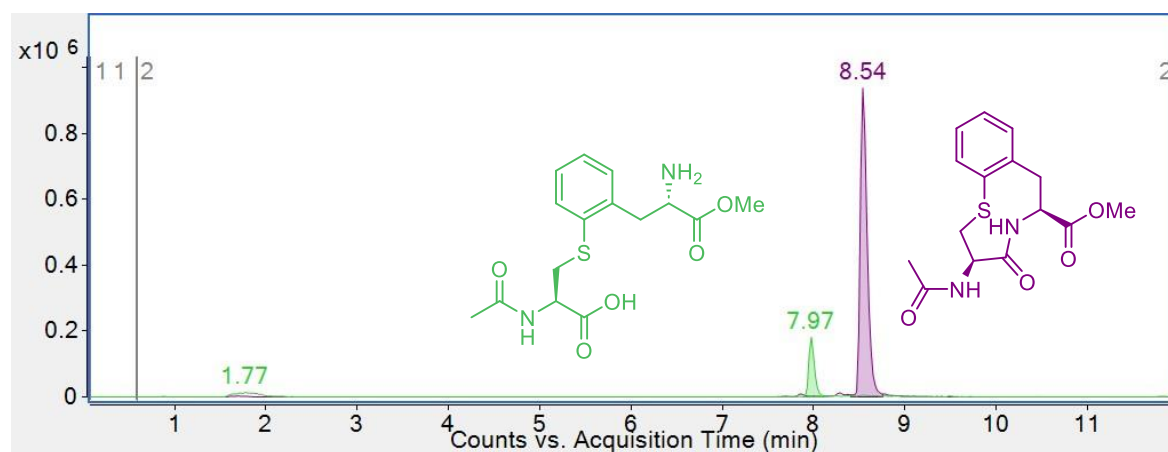
EIC 45: Reaction of *N*-acetylcysteine with **125**. NAC. (ESI⁺) *m/z* of [M+H]⁺ detected: 164.0374, expected for C₅H₉NO₃S: 164.0376. NAC peak area: 530,025 (rt = 2.69 min). **145** (ESI⁺) *m/z* of [M+H]⁺ detected: 380.1270, expected for C₁₇H₂₁N₃O₅S: 380.1275. **145** peak area: 2,752,430 (rt = 8.15 min).

Procedure for macrocycle formation: Pd(II) complex (4 μL , 1.0 mM in DMF, 1.0 equiv.), *N*-acetylcysteine (4 μL , 1.0 mM in DMF, 1.0 equiv.), and DIPEA (4 μL , 1.0 mM in DMF, 1.0 equiv.) were combined in a 1.5 mL Eppendorf tube. After vortexing, the reactions were left to stand for 5 min. DIPEA (4 μL , 1.0 mM in DMF, 1.0 equiv.), EDC·HCl (2 μL , 6.0 mM in DMF, 3.0 equiv.), and HOBt·H₂O (2 μL , 12 mM in DMF, 6.0 equiv.) were then added, and the resulting mixture was vortexed and left to stand for 4 h. The reactions were then diluted with H₂O (1000 μL) and analysed by **peptide LC-MS**.

144

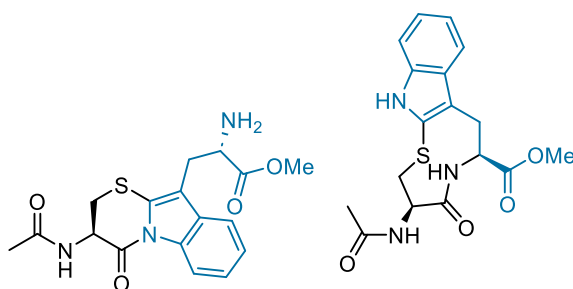


127 was used in **procedure for macrocycle formation**.

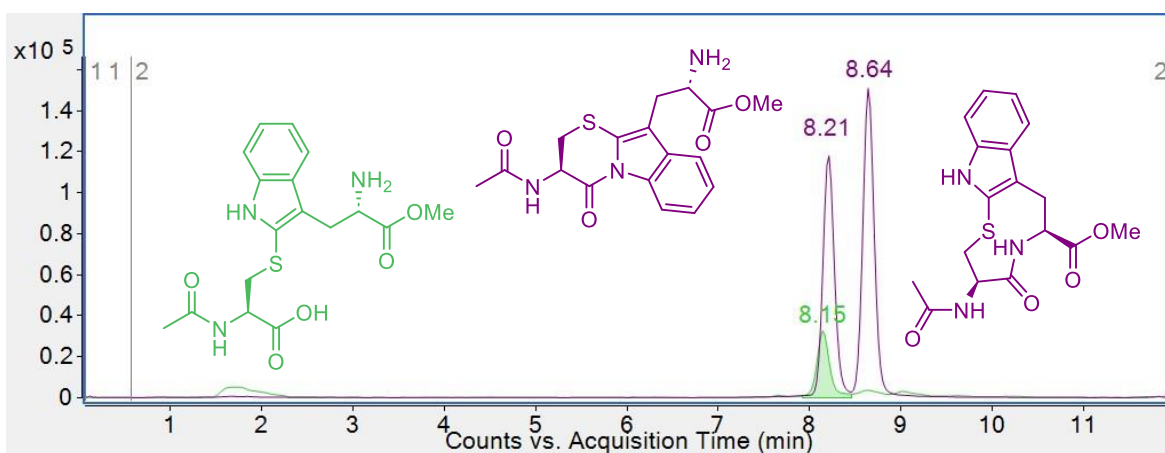


EIC 46: Cyclisation of **143**. **143** (ESI⁺) *m/z* of [M+H]⁺ detected: 341.1162, expected for C₁₅H₂₀N₂O₅S: 341.1166. **143** peak area: 835,142 (rt = 7.96 min). **144** (ESI⁺) *m/z* of [M+H]⁺ detected: 341.1166, expected for C₁₅H₁₈N₂O₄S: 341.1166. **144** peak area: 5,147,819 (rt = 8.54 min).

146 and 147



125 was used in procedure for macrocycle formation.



EIC 47: Cyclisation of **145**. **145** (ESI⁺) *m/z* of [M+H]⁺ detected: 380.1270, expected for C₁₇H₂₁N₃O₅S: 380.1275. **145** peak area: 323,333 (rt = 8.14 min). **146/147** (ESI⁺) *m/z* of [M+H]⁺ detected: 363.1199, expected for C₁₇H₁₉N₃O₄S: 363.1199. **146/147** peak area: 1,051,984 (rt = 8.21 min), 1,353,131 (rt = 8.64 min).

5.5. General Synthetic Experimental for Chapter 4

Reagents were purchased from Sigma Aldrich, Strem Chemicals, ChemImpex, Oakwood Chemicals, TCI, Fisher Scientific, Combi-Blocks, Alfa Aesar, Biomatik, or Integrated DNA Technologies (IDT) and used as received unless otherwise noted. Dichloromethane, acetone, acetonitrile (MeCN), hexanes, diethyl ether (Et₂O), *N,N*-dimethylformamide (DMF), ethyl acetate, and tetrahydrofuran (THF) were used as received without further purification unless otherwise specified. Toluene and cyclohexane were dried over activated 3 Å molecular sieves prior to distillation under a N₂ atmosphere followed by degassing via three freeze-pump-thaw cycles and stored under an atmosphere of purified N₂ in a Vacuum Atmospheres NexGen glovebox prior to use. 2-(di(*tert*-butyl)phosphino)-*N,N*-dimethylbenzenamine (**173**) and RuPhos (**63**) were purchased from Strem Chemicals and Oakwood Chemicals respectively and stored under an atmosphere of purified N₂ in a Vacuum Atmospheres NexGen glovebox prior to use. Glutathione (**48**) was purchased from Sigma Aldrich and stored at -20 °C prior to use. AgSbF₆ was purchased from Fisher Scientific and stored under an atmosphere of purified N₂ in a Vacuum Atmospheres NexGen glovebox prior to use. 1-Hydroxy-7-azabenzotriazole solution (HOAt, 0.6 M in DMF), hexafluorophosphate azabenzotriazole tetramethyl uronium (HATU), hexafluorophosphate benzotriazole tetramethyl uronium (HBTU), Fmoc-rink amide resin (0.7 – 0.9 mmol/g, 70-90 mesh), Fmoc-L-Ala-OH, Fmoc-L-Asp(*Ot*Bu)-OH, Fmoc-L-Arg(PbF)OH, Fmoc-L-Cys(Trt)-OH, Fmoc-L-Lys(Boc)-OH, and Fmoc-Thr(But)-OH were purchased from ChemImpex International and stored at 4 °C prior to use. Deuterated solvents (CD₂Cl₂, DMSO-*d*₆, CD₃CN, CD₃OD, and CDCl₃) were obtained from Cambridge Isotope Laboratories and used as received. Aqueous solutions of tris (tris(hydroxymethyl)aminomethane) buffer were prepared by dissolution of tris base (Sigma Aldrich) in Milli-Q water and adjusted to the appropriate pH with concentrated HCl. Me-DalPhos (**172**),²⁰¹ 2-(dicyclohexylphosphino)-*N,N*-dimethylbenzenamine (**174**),²⁰² AuCl(Me-DalPhos),²⁰³ **42**,²⁰⁴ **184**,²⁰⁴ **162**,⁹⁶ **183**,²⁰⁴ Au(2-(di(*tert*-butyl)phosphino)-*N,N*-dimethylbenzenamine)Cl,⁹⁸ **181**,⁹⁸ [(1,5-COD)PdCl₂],²⁰⁵ [(1,5-COD)Pd(CH₂TMS)₂] (**56**),⁷⁴ and **157**,⁷⁴ were previously prepared in the Spokoyny group according to reported literature procedures.

NMR spectra were recorded on a Bruker AV 300 spectrometer (¹H NMR at 300 MHz and ¹³C{¹H} NMR at 75.5 MHz) or a Bruker AV 400 spectrometer (¹H NMR at 400 MHz and ¹³C{¹H} NMR at 101 MHz). Proton chemical shifts are reported in parts per million

downfield from tetramethylsilane and are referenced to residual protium in the solvent. Carbon chemical shifts are reported in parts per million downfield from tetramethylsilane and are referenced to the carbon resonances of the solvent peak. Fluorine chemical shifts are reported in parts per million downfield from trichlorofluoromethane. NMR data are represented as follows: chemical shift, integration, multiplicity (s = singlet, d = doublet, dd = doublet of doublets, ddd = doublet of doublet of doublets, t = triplet, q = quartet, m = multiplet), coupling constants (Hz). All spectra were recorded at 298 K, unless otherwise stated.

High-resolution mass spectrometry data were collected using either an Agilent 1260 Infinity 6530 Q-TOF ESI instrument or a Thermo Exactive Plus Orbitrap instrument with IonSense ID-CUBE DART source.

5.6. HPLC and LC-MS Experimental for Chapter 4

HPLC purification was performed on an Agilent Technologies 1260 Infinity II HPLC instrument equipped with a Variable Wavelength Detector (VWD, 254, 214 nm) and using an Agilent ZORBAX SB-C18 (9.4 × 250 mm, 5 μm) reversed-phase column. All methods utilized a gradient elution of 0.1% TFA in water (solvent A) and 0.1% TFA in acetonitrile (solvent B) as the mobile phase with a column temperature of 23 °C and a flow rate of 3 mL/min. The fractions containing the desired products were combined and the solvent was lyophilized to afford the purified product.

Method A: Gradient: 0–5 min, 99% A : 1% B, 5 – 45 min, 99–60% A: 1 – 40% B, 45 – 55 min, 60 – 1% A: 40 – 99% B, 55 – 65 min, 1% A: 99% B.

Method B: Gradient: 0 – 10 min, 99% A : 1% B, 10 – 50 min, 99 – 1% A: 1 – 99% B, 50 – 60 min, 1% A: 99% B.

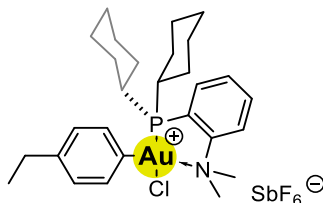
LC-MS data were collected on an Agilent 1260 Infinity 6530 Q-TOF ESI instrument operating in positive or negative mode using an Agilent ZORBAX 300SB-C18 column (2.1 × 150 mm, 5 μm) reversed-phase column. All methods utilized a gradient elution of 0.1% FA in water (solvent A) and 0.1% FA in acetonitrile (solvent B) as the mobile phase with a column temperature of 40 °C and a flow rate of 0.6 mL/min.

Method A: Operating in positive mode. Gradient: 0 – 1 min, 99% A : 1% B, 1 – 12 min, 99 – 1% A: 1 – 99% B, 12 – 15 min, 1% A: 99% B. LC stream switched from waste to MS at 30 sec and from MS to waste at 12 min.

5.7. Applications of Organometallic Au(III) Complexes for Bioconjugation

5.7.1. Preparation of Novel Organometallic Compounds[‡]

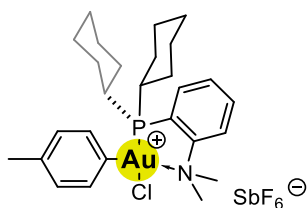
Au(2-(dicyclohexylphosphino)-*N,N*-dimethylbenzenamine)(4-EtPh)ClSbF₆ (**179**)



To a solution of AgSbF₆ (12 mg, 36 μmol, 1.0 equiv.) in CH₂Cl₂ (1 mL) was added a cooled solution of 4-iodoethylbenzene (26 mg, 110 μmol, 3.0 equiv.) and Au(2-(dicyclohexylphosphino)-*N,N*-dimethylbenzenamine)Cl (20 mg, 36 μmol, 1.0 equiv.) in CH₂Cl₂ (1 mL) at -20 °C, under protection from light. The resulting mixture was stirred overnight at rt, before being filtered through a pad of Celite® and concentrated *in vacuo*. Et₂O (10 mL) was added to the resulting oil, causing precipitation of a solid which was washed with, hexanes (10 mL), and then Et₂O (10 mL). The remaining solid residue was then dissolved in MeCN (5 mL), filtered through a fine frit and concentrated *in vacuo* to yield the **title compound** (21 mg, 66%) as a colourless powder: ¹H NMR (400 MHz, CD₂Cl₂) δ 8.02 – 7.95 (m, 1H), 7.91 (dd, *J* = 8.0, 4.3 Hz, 1H), 7.82 – 7.72 (m, 2H), 7.24 (d, *J* = 8.1 Hz, 2H), 7.16 (d, *J* = 7.8 Hz, 2H), 3.44 (s, 6H), 2.74 – 2.62 (m, 4H), 1.92 – 1.68 (m, 10H), 1.64 – 1.54 (m, 2H), 1.44 – 1.30 (m, 4H), 1.26 (t, *J* = 7.6 Hz, 3H), 1.17 – 1.04 (m, 2H), 0.75 – 0.62 (m, 2H). ³¹P{¹H} NMR (162 MHz, CD₂Cl₂) δ 58.91.

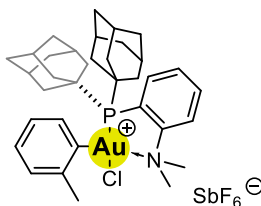
[‡] **179**, **180**, **187**, **188** and **200** Synthesised by Dr Evan Doud (UCLA). **224**, **198** and **199** Synthesised by Billy Treacy (UCLA).

Au(2-(dicyclohexylphosphino)-*N,N*-dimethylbenzenamine)(4-MePh)ClSbF₆ (180)



To a solution of AgSbF₆ (12 mg, 0.036 mmol, 1.0 equiv.) in CH₂Cl₂ (1 mL) was added a cooled solution of 4-iodotoluene (23 mg, 0.11 mmol, 3.0 equiv.) and Au(2-(dicyclohexylphosphino)-*N,N*-dimethylbenzenamine)Cl (20 mg, 0.036 mmol, 1.0 equiv.) in CH₂Cl₂ (1 mL) at -20 °C, under protection from light. The resulting mixture was stirred overnight at rt, before being filtered through a pad of Celite® and concentrated *in vacuo*. Et₂O (10 mL) was added to the resulting oil, causing precipitation of a solid which was washed with, hexanes (10 mL), and then Et₂O (10 mL). The remaining solid residue was then dissolved in MeCN (5 mL), filtered through a fine frit and concentrated *in vacuo* to yield the **title compound** (19 mg, 59%) as a colourless powder: ¹H NMR (400 MHz, CD₂Cl₂) δ 8.01 – 7.95 (m, 1H), 7.90 (dd, *J* = 8.0, 4.3 Hz, 1H), 7.82 – 7.73 (m, 2H), 7.22 (d, *J* = 8.7 Hz, 2H), 7.13 (d, *J* = 7.5 Hz, 2H), 3.43 (s, 6H), 2.73 – 2.62 (m, 2H), 2.39 (s, 3H), 1.92 – 1.70 (m, 10H), 1.66 – 1.56 (m, 2H), 1.43 – 1.28 (m, 4H), 1.18 – 1.05 (m, 2H), 0.80 – 0.68 (m, 2H). ³¹P{¹H} NMR (162 MHz, CD₂Cl₂) δ 58.62.

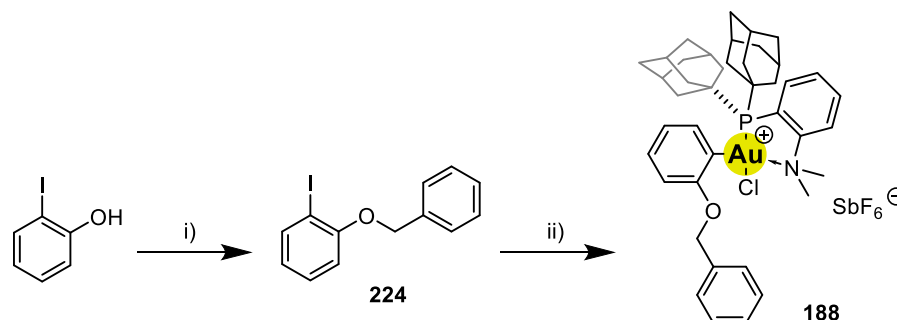
Au(Me-DalPhos)(2-MePh)ClSbF₆ (187)



To a solution of AgSbF₆ (10 mg, 30 μmol, 1.0 equiv.) in CH₂Cl₂ (1 mL) was added a cooled solution of 2-iodotoluene (20 mg, 90 μmol, 3.0 equiv.) and AuCl(Me-DalPhos) (20 mg, 30 μmol, 1.0 equiv.) in CH₂Cl₂ (1 mL) at -20 °C, under protection from light. The resulting mixture was stirred overnight at rt, before being filtered through a pad of Celite® and concentrated *in vacuo*. Et₂O (10 mL) was added to the resulting oil, causing precipitation of a solid which was washed with, hexanes (10 mL), and then Et₂O (10 mL). The remaining solid residue was then dissolved in MeCN (5 mL), filtered through a fine frit and concentrated *in vacuo* to yield the **title compound** (21.8 mg, 73%) as a pale-orange powder. ¹H NMR (400 MHz, CD₂Cl₂) δ 8.01 – 7.90 (m, 3H), 7.78 – 7.71 (m, 1H), 7.52 (d, *J* = 7.6 Hz,

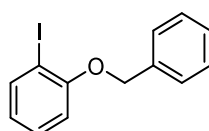
1H), 7.21 – 7.12 (m, 3H), 3.51 (s, 3H), 3.45 (s, 3H), 2.64 (s, 3H), 2.38 – 2.33 (m, 2H), 2.25 – 2.14 (m, 7H), 2.13 – 2.06 (m, 3H), 2.00 (s, 3H), 1.97 – 1.89 (m, 2H), 1.82 (d, $J = 2.9$ Hz, 5H), 1.76 – 1.66 (m, 8H). $^{31}\text{P}\{^1\text{H}\}$ NMR (162 MHz, CD_2Cl_2) δ 75.33.

Synthesis of 188



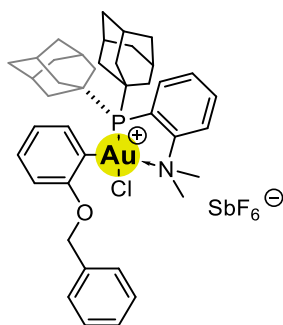
Scheme 78: **Reagents and conditions:** i) K_2CO_3 (1.6 equiv.), BnBr (1.5 equiv.), acetone, rt, 19 h, 94%; ii) $\text{AuCl}(\text{Me-DalPhos})$ (0.3 equiv.), AgSbF_6 (0.3 equiv.), -20 °C to rt, 16 h, protection from light, 65%.

1-Iodo-2-(phenylmethoxy)benzene (224)



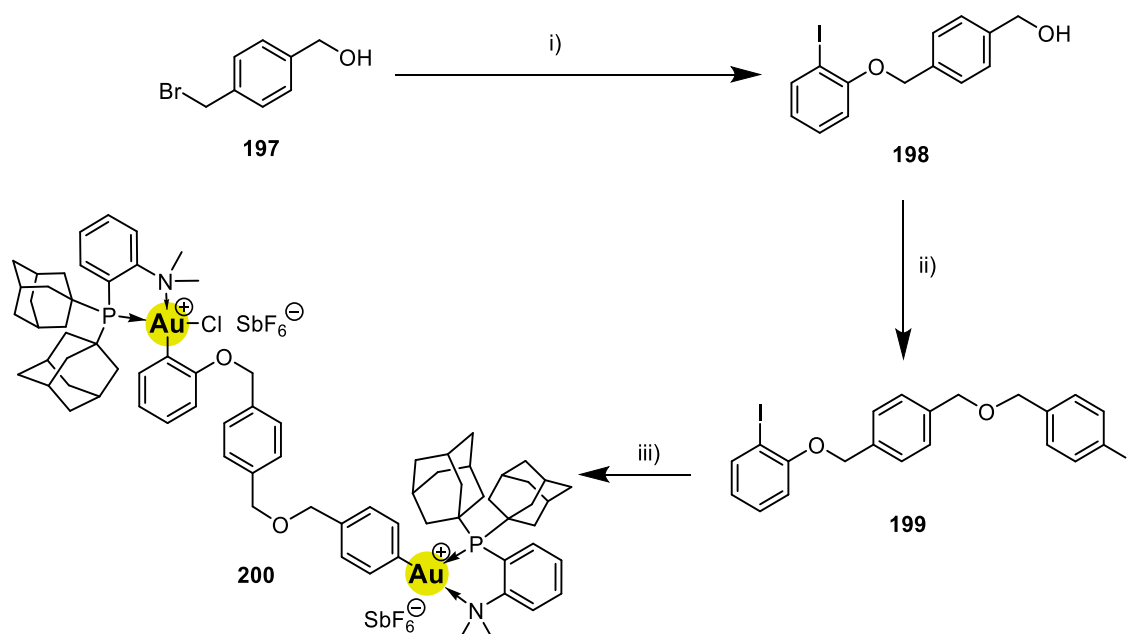
2-Iodophenol (500 mg, 2.3 mmol, 1.0 equiv.), K_2CO_3 , (500 mg, 3.6 mmol, 1.6 equiv.), and benzyl bromide (405 μL , 3.4 mmol, 1.5 equiv.) were combined in acetone (20 mL) and stirred at rt for 19 h before being concentrated *in vacuo*. The residue was dissolved in CH_2Cl_2 (150 mL), washed with brine (50 mL), dried (MgSO_4) and concentrated *in vacuo*. The residue was subjected to flash column chromatography (gradient from 0:100 to 40:60 EtOAc/hexanes) to yield the **title compound** (660 mg, 94%) as a yellow oil: ^1H NMR (300 MHz, CD_3CN) δ 7.81 (dd, $J = 7.7, 1.6$ Hz, 1H), 7.54 – 7.48 (m, 2H), 7.45 – 7.30 (m, 4H), 7.01 (dd, $J = 8.3, 1.4$ Hz, 1H), 6.76 (td, $J = 7.7, 1.4$ Hz, 1H), 5.16 (s, 2H); $^{13}\text{C}\{^1\text{H}\}$ NMR (75 MHz, CD_3CN) δ 158.2, 140.4, 137.8, 130.7, 129.5, 128.9, 128.5, 123.8, 114.0, 86.9, 71.6. The spectral data are in agreement with reported literature values.²⁰⁶

Au(Me-DalPhos)(2-(OBn)Ph)ClSbF₆ (188)



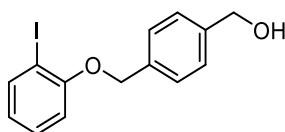
To a solution of AgSbF₆ (20 mg, 60 μ mol, 1.0 equiv.) in CH₂Cl₂ (2 mL) was added a cooled solution of 1-iodo-2-(phenylmethoxy)benzene (57 mg, 180 μ mol, 3.0 equiv.) and AuCl(Me-DalPhos) (40 mg, 60 μ mol, 1.0 equiv.) in CH₂Cl₂ (1 mL) at -20 °C, under protection from light. The resulting mixture was stirred overnight at rt, before being filtered through a pad of Celite® and concentrated *in vacuo*. Et₂O (10 mL) was added to the resulting oil, causing precipitation of a solid which was washed with, hexanes (10 mL), and then Et₂O (10 mL). The remaining solid residue was then dissolved in MeCN (5 mL), filtered through a fine frit and concentrated *in vacuo* to yield the **title compound** (43 mg, 65%) as a yellow crystalline powder: ¹H NMR (400 MHz, CD₂Cl₂) δ 7.95 – 7.90 (m, 1H), 7.88 – 7.83 (m, 2H), 7.71 – 7.65 (m, 1H), 7.54 (dd, *J* = 7.6, 1.9 Hz, 2H), 7.44 (dd, *J* = 7.9, 1.4 Hz, 1H), 7.37 – 7.28 (m, 4H), 7.04 (td, *J* = 7.6, 1.4 Hz, 1H), 6.97 (dd, *J* = 8.0, 1.4 Hz, 1H), 5.18 (d, *J* = 9.9 Hz, 1H), 5.06 (d, *J* = 9.9 Hz, 1H), 3.50 (s, 3H), 3.21 (s, 3H), 2.37 – 2.28 (m, 2H), 2.20 – 2.08 (m, 8H), 1.83 – 1.70 (m, 11H), 1.66 – 1.53 (m, 9H). ³¹P{¹H} NMR (162 MHz, CD₂Cl₂) δ 78.17.

Preparation of 200



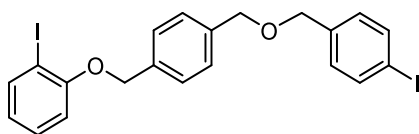
Scheme 79: **Reagents and conditions:** i) 2-Iodophenol (1.1 equiv.), K_2CO_3 (1.2 equiv.), acetone, reflux, 20 h, 88%;
ii) TBAB (0.3 equiv.), KOH (3 equiv.), 4-iodobenzyl bromide (2 equiv.), CH_2Cl_2/H_2O (3:1), 0 °C – rt, 20 h, 66%;
iii) $AgSbF_6$ (2.2 equiv.), (Me-DalPhos)AuCl (2.2 equiv.), CH_2Cl_2 , -20 °C – rt, protection from light, 16 h, 79%.

(4-((2-Iodophenoxy)methyl)phenyl)methanol (198)



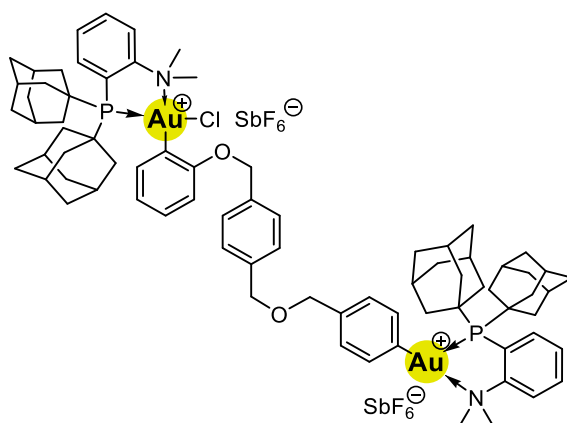
4-(Bromomethyl)benzyl alcohol (920 mg, 4.6 mmol, 1.0 equiv.), 2-iodophenol (1.1 g, 5.0 mmol, 1.1 equiv.), and K_2CO_3 (760 mg, 5.5 mmol, 1.2 equiv.) were combined in acetone (45 mL) and stirred at 75 °C for 20 h before being concentrated *in vacuo*. EtOAc (150 mL) was added, and the resulting solution was washed with brine (50 mL), dried ($MgSO_4$) and concentrated *in vacuo*. The resulting residue was subjected to flash column chromatography (gradient from 0:100 to 80:20 EtOAc/hexanes) to yield the **title compound** (1.4 g, 88%) as a colourless solid: 1H NMR (400 MHz, $DMSO-d_6$) δ 7.79 (dd, $J = 7.8, 1.6$ Hz, 1H), 7.49 – 7.43 (m, 2H), 7.39 – 7.31 (m, 3H), 7.08 (dd, $J = 8.3, 1.3$ Hz, 1H), 6.76 (td, $J = 7.5, 1.3$ Hz, 1H), 5.22 (t, $J = 5.7$ Hz, 1H), 5.16 (s, 2H), 4.53 (d, $J = 5.7$ Hz, 2H); $^{13}C\{^1H\}$ NMR (101 MHz, $DMSO-d_6$) δ 156.7, 142.2, 139.0, 135.0, 129.7, 127.2, 126.5, 122.8, 113.2, 86.9, 70.0, 62.7; (ESI⁻) m/z of $[M-H]^-$ detected: 338.9881, expected for $C_{14}H_{13}IO_2$: 338.9888.

1-Iodo-2-((4-(((4-iodobenzyl)oxy)methyl)benzyl)oxy)benzene (199)



KOH (490 mg, 8.8 mmol, 3.0 equiv.) was added to a solution of 4-((2-Iodophenoxy)methyl)phenyl)methanol (1.0 g, 2.9 mmol, 1.0 equiv.) and TBAB (280 mg, 0.88 mmol, 0.30 equiv.) in $\text{CH}_2\text{Cl}_2/\text{H}_2\text{O}$ (3:1, 20 mL) at 0 °C and stirred for 15 min. 4-Iodobenzyl bromide (1.7 g, 5.9 mmol, 2.0 equiv.) was added, the solution was allowed to warm to rt and stirred for 20 h. The reaction was diluted with CH_2Cl_2 (200 mL), washed with brine (50 mL), dried (MgSO_4), and concentrated *in vacuo*. The crude residue was subjected to flash column chromatography (gradient from 0:100 to 100:0 Et_2O /hexanes) to yield the **title compound** (1.1 g, 66%) as a colourless oil which crystallised after being placed in a -20 °C freezer: ^1H NMR (400 MHz, $\text{DMSO}-d_6$) δ 7.78 (dd, $J = 7.8, 1.6$ Hz, 1H), 7.74 – 7.68 (m, 2H), 7.52 – 7.45 (m, 2H), 7.41 – 7.31 (m, 3H), 7.21 – 7.13 (m, 2H), 7.08 (dd, $J = 8.3, 1.3$ Hz, 1H), 6.76 (td, $J = 7.5, 1.3$ Hz, 1H), 5.18 (s, 2H), 4.53 (s, 2H), 4.49 (s, 2H); $^{13}\text{C}\{^1\text{H}\}$ NMR (101 MHz, $\text{DMSO}-d_6$): δ 157.2, 139.5, 138.7, 138.3, 137.5, 136.4, 130.2, 130.2, 128.1, 127.7, 123.4, 113.6, 93.8, 87.3, 71.7, 71.2, 70.3; (ESI⁺) m/z of $[\text{M}]^+$ detected: 555.9359, expected for $\text{C}_{31}\text{H}_{18}\text{I}_2\text{O}_2$: 555.9396.

200



To a solution of AgSbF_6 (25 mg, 73 μmol , 2.2 equiv.) in CH_2Cl_2 (5 mL) was added a cooled solution of 1-Iodo-2-((4-(((4-iodobenzyl)oxy)methyl)benzyl)oxy)benzene (19 mg, 33 μmol , 1.0 equiv.) and $\text{AuCl}(\text{Me-DalPhos})$ (50 mg, 73 μmol , 3.0 equiv.) in CH_2Cl_2 (5 mL) at -20 °C, under protection from light. The resulting mixture was stirred overnight at rt, before being filtered through a pad of Celite® and concentrated *in vacuo*. EtOAc (10 mL) was added to

the resulting oil, causing precipitation of a solid which was washed with, hexanes (10 mL), and then Et₂O (10 mL). The remaining solid residue was then dissolved in MeCN (5 mL), filtered through a fine frit and concentrated *in vacuo* to yield the **title compound** (57 mg, 79%) as a yellow crystalline solid: ¹H NMR (400 MHz, CD₂Cl₂) δ 8.01 – 7.89 (m, 4H), 7.88 – 7.82 (m, 2H), 7.74 (tt, *J* = 8.3, 6.4 Hz, 1H), 7.70 – 7.65 (m, 1H), 7.54 (d, *J* = 8.1 Hz, 2H), 7.49 – 7.42 (m, 3H), 7.37 – 7.30 (m, 4H), 7.27 (m, 1H), 7.07 – 7.01 (m, 1H), 6.97 (dd, *J* = 8.1, 1.4 Hz, 1H), 5.20 (d, *J* = 10.1 Hz, 1H), 5.07 (d, *J* = 10.0 Hz, 1H), 4.56 (d, *J* = 1.9 Hz, 2H), 4.53 (s, 2H), 3.50 (s, 6H), 3.49 (s, 3H), 3.18 (s, 3H), 2.37 – 2.24 (m, 10H), 2.19 – 2.05 (d, 20H), 1.84–1.71 (m, 22H), 1.66 – 1.55 (m, 8H); ³¹P{¹H} NMR (162 MHz, CD₂Cl₂) δ 78.32, 74.90.

5.7.2. Preparation of H-DRKCAT-NH₂ (175)[‡]

The following general protocol was followed for the solid-phase peptide synthesis of H-DRKCAT-NH₂ (175).

Preparation of Resin: Rink amide resin (0.5 g, 0.84 mmol/g) was added to a 12.5 mL peptide synthesis vessel fitted with a coarse-porosity fritted glass resin support. DMF (2.5 mL) and CH₂Cl₂ (2.5 mL) were added to the vessel, and the mixture was shaken for a minimum of 1 h to allow the resin to swell. The resin was subsequently washed with DMF (3 × 10 mL).

First Deprotection: A 20% solution of 4-methylpiperidine in DMF (10 – 15 mL/g of resin) was added to the vessel, and the mixture was shaken for 20 min. After shaking, the 4-methylpiperidine solution was removed and the resin was washed with DMF (1 x 5 mL). A new solution of 4-methylpiperidine in DMF (10 – 15 mL/g of resin) was added to the vessel, and the vessel was shaken for an additional 5 min. The resin was then washed with DMF (3 × 5 mL, 1 min of shaking each wash) to ensure complete removal of 4-methylpiperidine.

Amino Acid Coupling Conditions: Amino acid (5.00 equiv. to resin) and HBTU (4.75 equiv. to resin) were dissolved in DMF (5 mL). DIPEA (6 equiv. to resin) was then added to the mixture, and the solution was stirred for 1 min. This mixture was then added to the peptide synthesis vessel containing the resin, and the vessel was shaken for 45 min. After

[‡] H-DRKCAT-NH₂ synthesis performed by Dr Evan Doud (UCLA).

shaking, the solution was removed, and the resin was washed with DMF (5×10 mL) to ensure complete removal of excess amino acid, HBTU, and DIPEA.

Cysteine Coupling Conditions: Cysteine coupling was performed following a procedure previously reported.²⁰⁷

Fmoc-Cys(Trt)-OH (5.00 equiv. to resin), HATU (6.66 equiv. to resin), and HOAt (0.6 M in DMF, 6.66 equiv. to resin) were combined in DMF (2.5 mL) and CH_2Cl_2 (2.5 mL). Once dissolved, 2,4,6-trimethylpyridine (6.66 equiv. to resin) was added and the mixture stirred quickly (1 – 2 sec) and added to the resin. The mixture was shaken for 1 h. After shaking, the resin was washed with DMF (5×10 mL) to ensure the removal of excess Fmoc-Cys(Trt)-OH, HATU, and HOAt. After cysteine coupling, the normal protocol was followed.

Amino Acid Deprotection Conditions: A 20% solution of 4-methylpiperidine in DMF (10 – 15 mL/g of resin) was added to the vessel and the mixture was shaken for 10 min. After shaking, the 4-methylpiperidine solution was removed and the resin was washed once with DMF (5 mL). A fresh solution of 4-methylpiperidine in DMF (10 – 15 mL/g of resin) was added to the vessel, and the mixture was shaken for an additional 5 min. The solution was removed, and the resin was washed with DMF (3×10 mL, 1 min of shaking each wash) to ensure the complete removal of 4-methylpiperidine.

Cleavage from Resin: After deprotection of the final amino acid residue, the resin was washed with CH_2Cl_2 (3×5 mL), and then transferred to a 50 mL round bottom flask. A light stream of N_2 was flowed over the resin for 5 min to evaporate residual CH_2Cl_2 . To the dry resin was added freshly prepared cleavage cocktail consisting of a 95:2.5:2.5 (v/v/v) mixture of TFA:H₂O:TIPS (10 ml of cocktail/gram of resin). The slurry was stirred under an atmosphere of N_2 for 3 – 4 h. The suspension was then transferred back to the peptide vessel, and the solution was filtered away from the resin. The resulting filtrate was transferred to a 50 mL conical tube and concentrated under a stream of N_2 to a final volume of 1/2 the original cocktail volume. To this solution was added cold (-20 °C) Et_2O ($4 \times$ original cocktail volume), resulting in the precipitation of the crude peptide. The suspension was centrifuged ($2,500 \times g$, 5 min), and the supernatant was removed and discarded. To the tube containing the solids was added Et_2O ($4 \times$ original cocktail volume), and the tube was sonicated (5 min) to suspend the crude peptide. The suspension was centrifuged ($2,500 \times g$, 5 min), the supernatant was decanted, and the crude peptide was dried under reduced pressure and stored at -20 °C prior to purification.

The crude **175** was purified by reversed-phase HPLC using **Method A**. HPLC fractions were analysed by LC-MS using **method A** and the pure HPLC fractions were combined and lyophilized. Both crude and purified **175** were stored in sealed containers under a N₂ atmosphere at -20 °C.

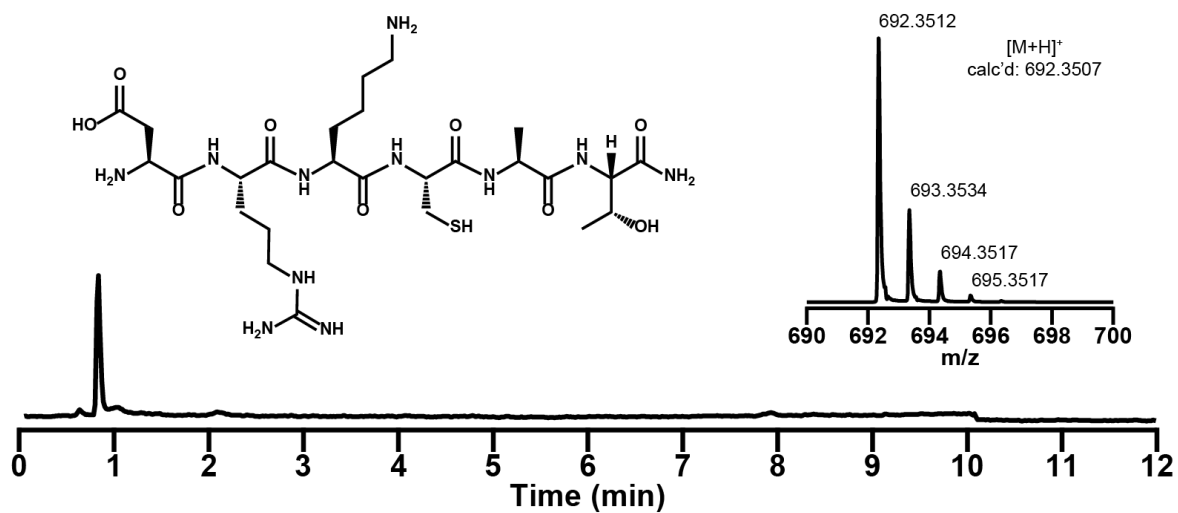


Figure 42: LC-MS Data of purified H-DRKCAT-NH₂ (**175**).

5.7.3. Competition Experiments[‡]

General procedure for competition experiments: Bioconjugation reagent A (100 μ L, 0.30 μ M in MeCN) and bioconjugation reagent B (100 μ L, 0.30 μ M in MeCN) were combined in a 1.5 mL Eppendorf tube and vortexed for 15 s resulting in a solution of bioconjugation reagents A and B (1.5 mM in MeCN). Solution of bioconjugation reagents A and B (50 μ L, 1.5 mM in MeCN, both reagents 3.0 equiv.) was combined with H-DRKCAT-NH₂ (**175**) (50 μ L, 500 μ M in 200 mM tris at pH 8.0, 1.0 equiv.) in a separate 1.5 mL Eppendorf tube, which was vortexed for 15 s and allowed to stand at rt for 15 min. An aliquot (10 μ L) of the reaction mixture was added to 0.1% TFA in H₂O/MeCN (50:50, 90 μ L). For experiments using Pd complex **191**, 3-MPA (10 μ L, 0.3 M in H₂O) was also added. The resulting solution was analysed by LC-MS using **method A**. Percentage conversions were determined by integrating the TIC for each product according to $\%(\text{Product A}) = \frac{\text{Counts}(\text{Product A})}{\text{Counts}(\text{Product A}) + \text{Counts}(\text{Product B})}$. Each reaction was repeated in triplicate and the percentage conversions are the mean of the three conversions, with errors reported as standard error of the mean.

[‡] Experiments performed by Dr Evan Doud (UCLA).

***N*-Ethylmaleimide (158) versus 162:** *N*-Ethylmaleimide (158) and 162 were used as bioconjugation reagent A and B, respectively, in the **general procedure for competition experiments**. Percentages of product A : product B $10.3 \pm 1.6\%$: $89.7 \pm 1.6\%$.

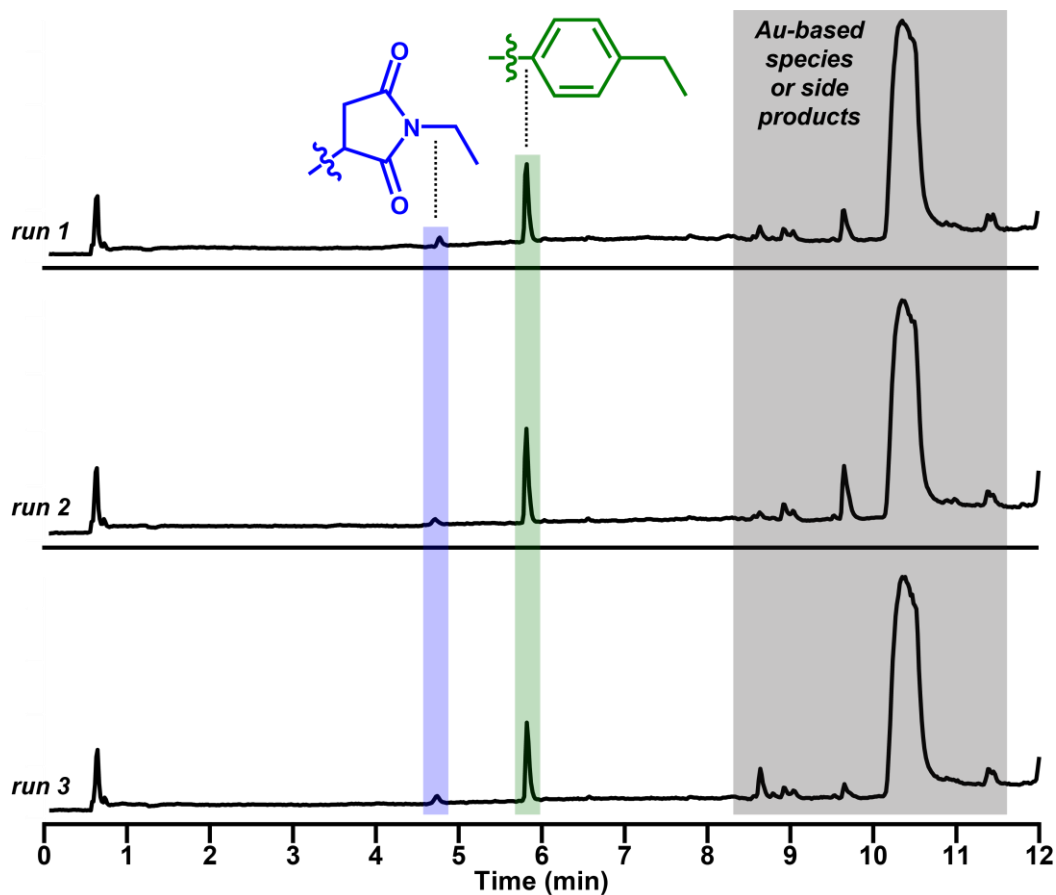


Figure 43: LC-MS TICs for the competition experiments between *N*-ethylmaleimide and 162 in the arylation of *H*-DRKCAT-NH₂ (175). Full structure of products A (blue) and B (green) not shown.

180 versus 162: **180** and **162** were used as bioconjugation reagent A and B, respectively, in the **general procedure for competition experiments**. Percentages of product A : product B $87.4 \pm 3.0\%$: $12.6 \pm 3.0\%$.

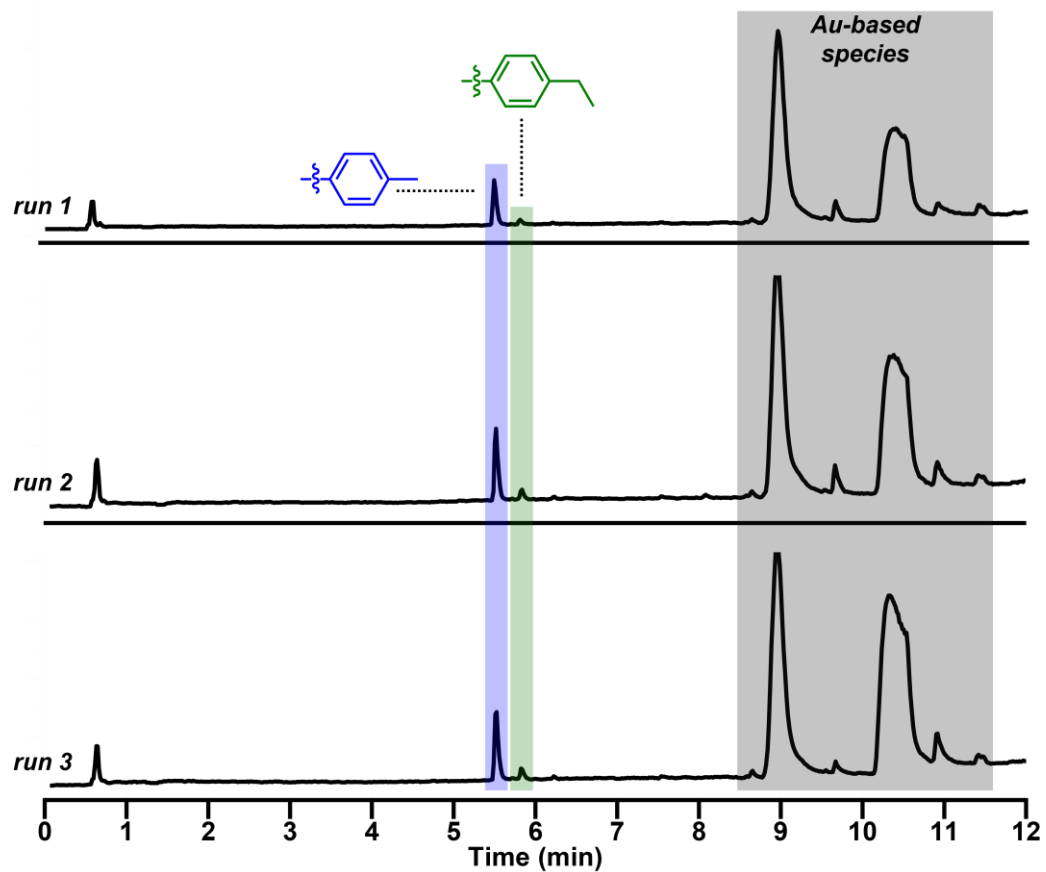


Figure 44: LC-MS TICs for the competition experiments between **180** and **162** in the arylation of H-DRKCAT-NH₂ (**175**). Full structure of products A (blue) and B (green) not shown.

180 versus 178: 180 and 178 were used as bioconjugation reagent A and B, respectively, in the **general procedure for competition experiments**. Percentages of product A : product B $57.0 \pm 0.6\%$: $42.9 \pm 0.6\%$.

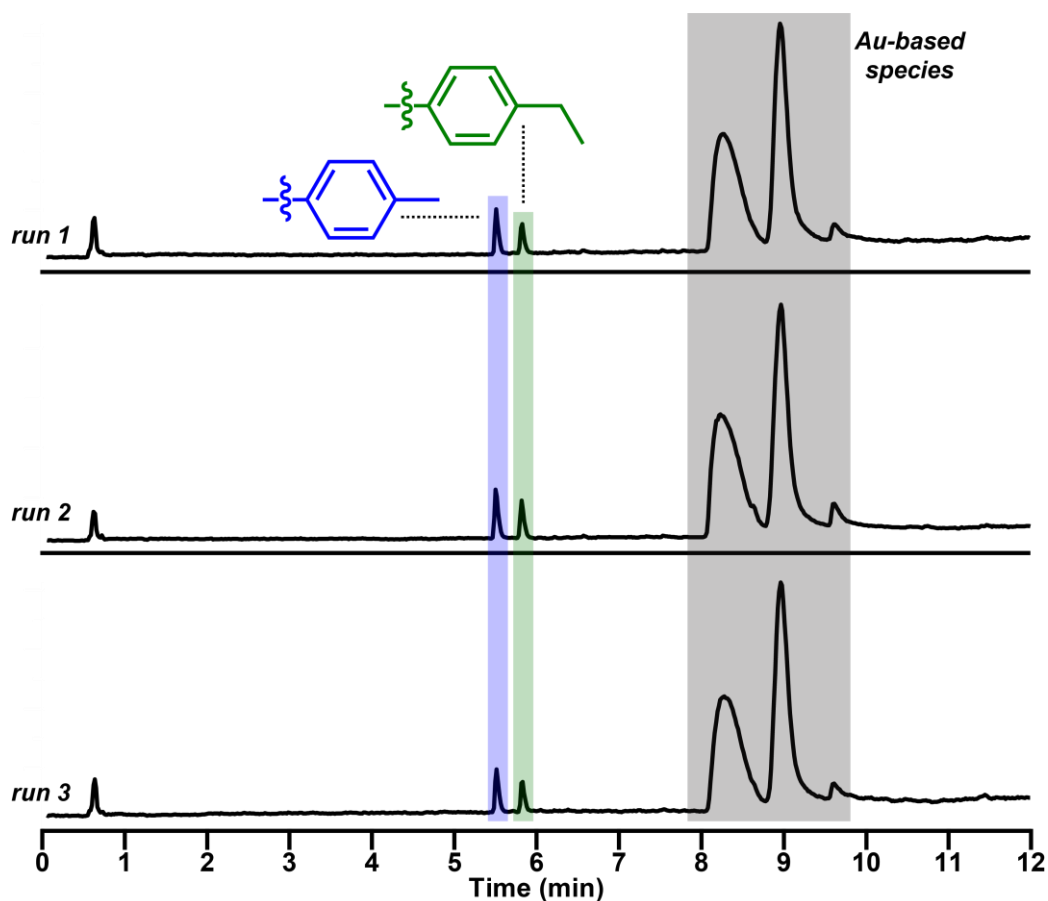


Figure 45: LC-MS TICs for the competition experiments between 180 and 178 in the arylation of H-DRKCAT-NH₂ (175). Full structure of products A (blue) and B (green) not shown.

181 versus 179: **181** and **179** were used as bioconjugation reagent A and B, respectively, in the **general procedure for competition experiments**. Percentages of product A : product B $34.1 \pm 1.0\%$: $65.9 \pm 1.0\%$.

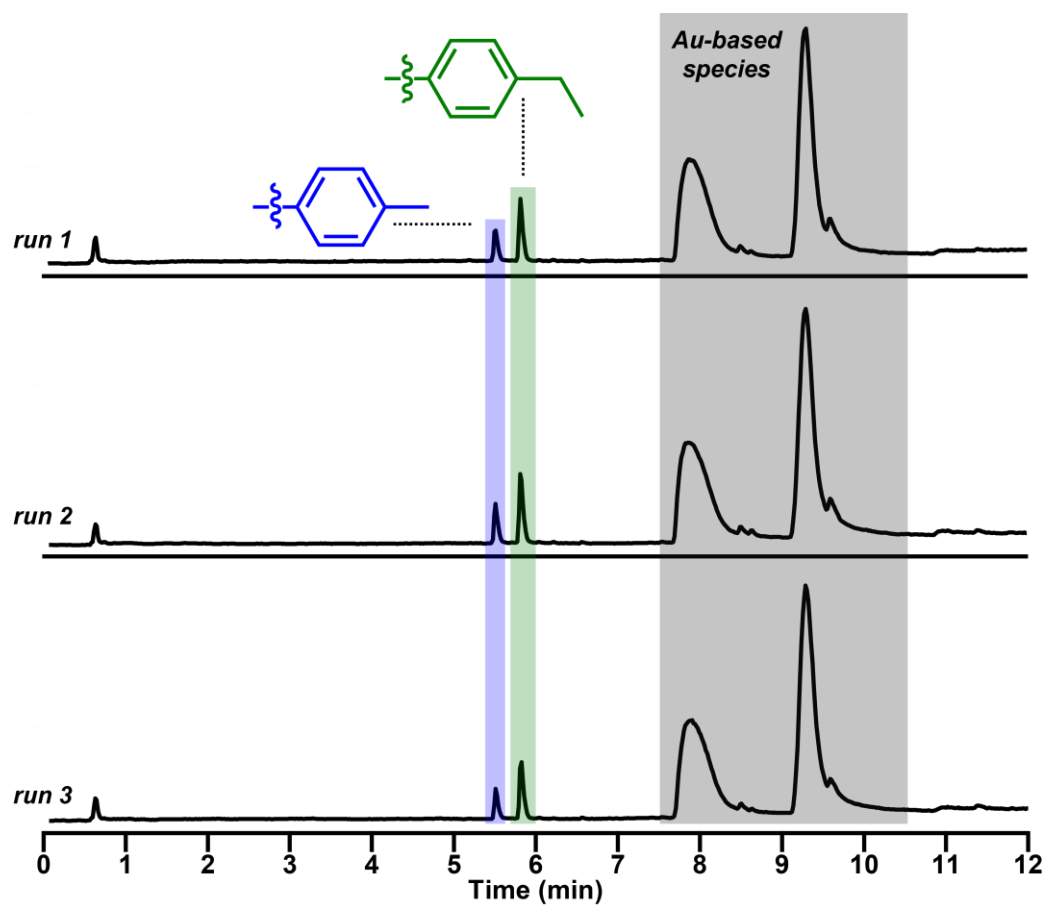


Figure 46: LC-MS TICs for the competition experiments between **181** and **179** in the arylation of *H*-DRKCAT-NH₂ (**175**). Full structure of products A (blue) and B (green) not shown.

184 versus 183: **184** and **183** were used as bioconjugation reagent A and B, respectively, in **general procedure for competition experiments**. Percentages of product A : product B $99.5 \pm 0.1\% : 0.5 \pm 0.1\%$.

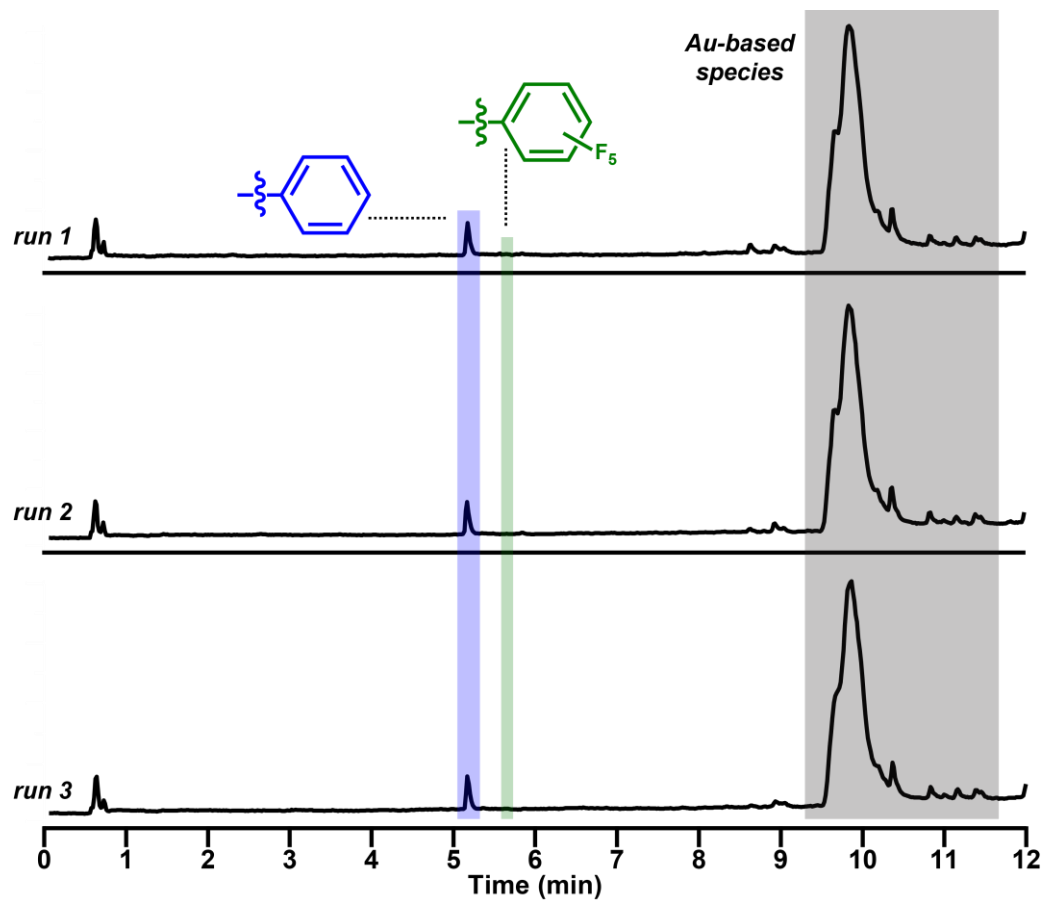


Figure 47: LC-MS TICs for the competition experiments between **184** and **183** in the arylation of *H*-DRKCAT-NH₂ (**175**). Full structure of products A (blue) and B (green) not shown.

184 versus 187: **184** and **187** were used as bioconjugation reagent A and B, respectively, in **general procedure for competition experiments**. Percentages of product A : product B $95.2 \pm 1.1\% : 4.8 \pm 1.1\%$.

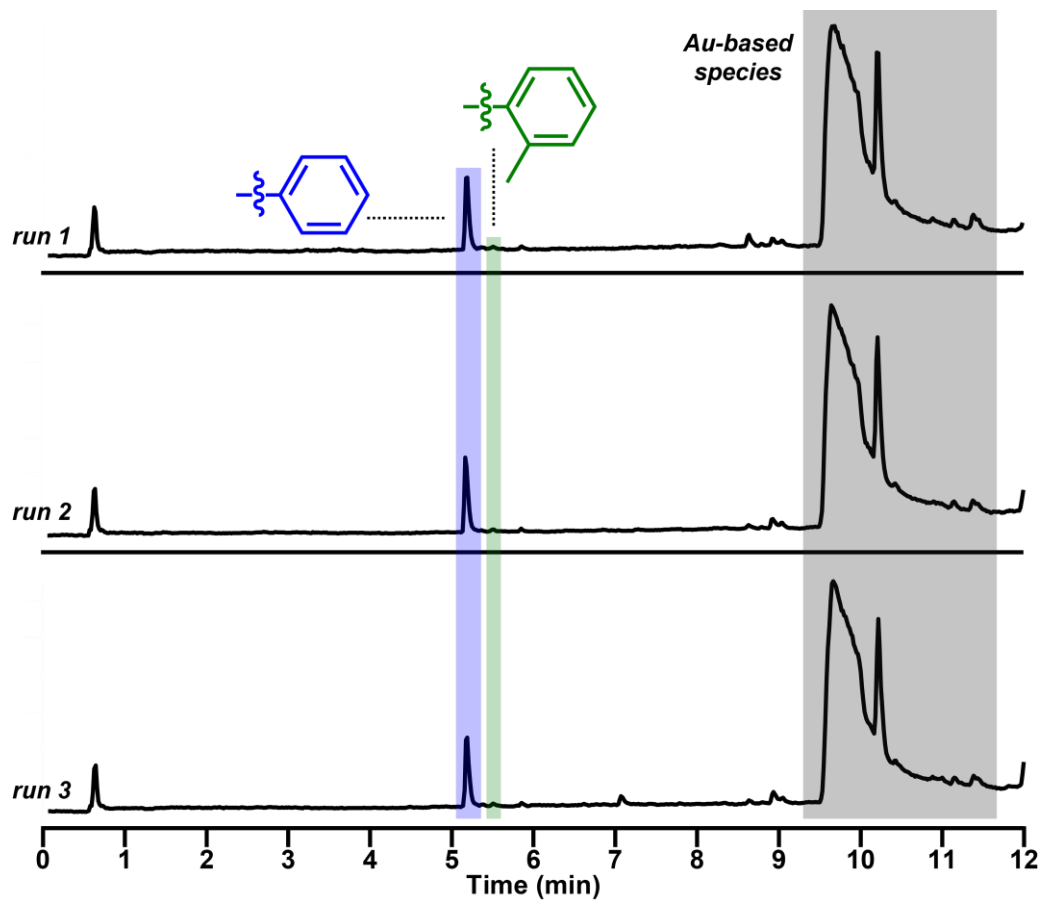


Figure 48: LC-MS TICs for the competition experiments between **184** and **187** in the arylation of H-DRKCAT-NH₂ (**175**). Full structure of products A (blue) and B (green) not shown.

184 versus 188: **184** and **188** were used as bioconjugation reagent A and B, respectively, in **general procedure for competition experiments**. Percentages of product A : product B $99.9 \pm 0.002\% : 0.1 \pm 0.002\%$.

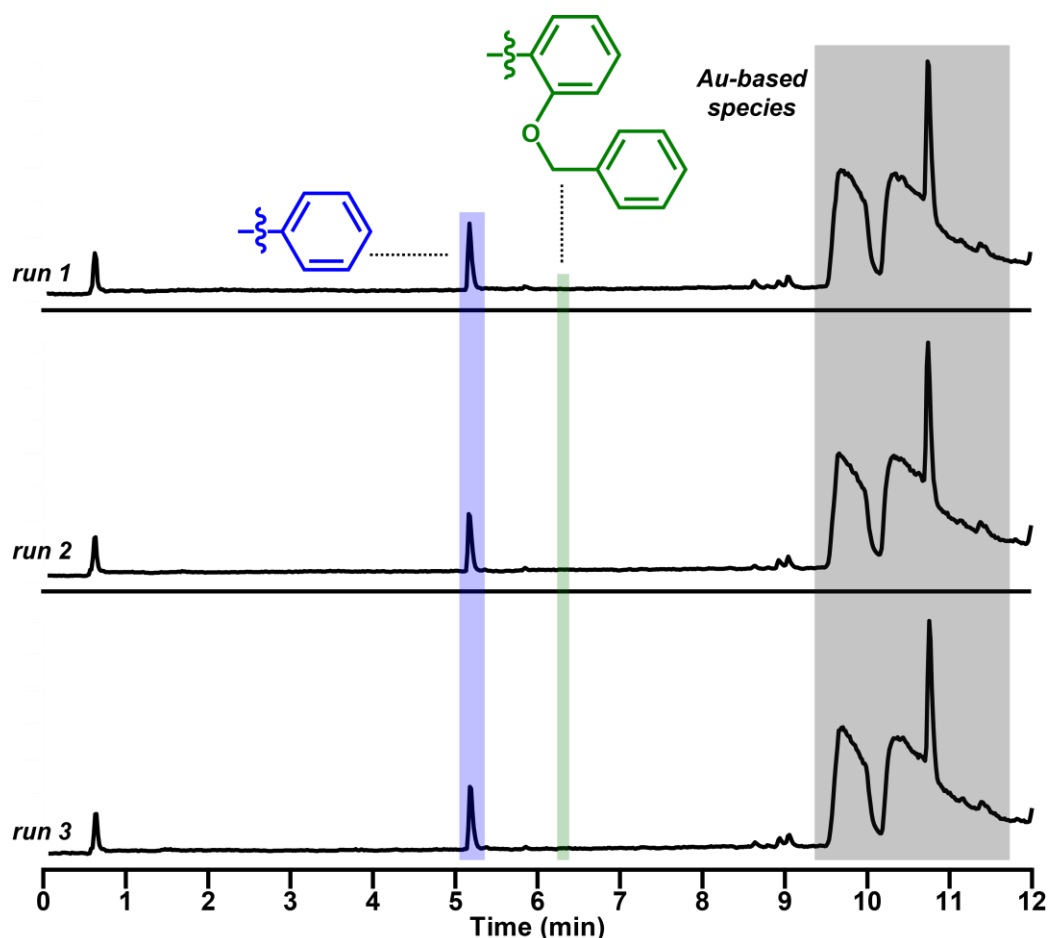


Figure 49: LC-MS TICs for the competition experiments between **184** and **187** in the arylation of *H*-DRKCAT-NH₂ (**175**). Full structure of products A (blue) and B (green) not shown.

5.7.4. Stopped-Flow Kinetic Analysis

Stopped-Flow Kinetics experiments were carried out using an Applied Photophysics SX20, using the Absorbance Photomultiplier or Photodiode Array detectors for single-wavelength and multi-wavelength data collection, respectively. For single-wavelength data collection, the monochromator was set to a pre-defined wavelength, and the slit width to 1.0 mm. The instrument was configured setting the cell path-length to 10 mm. When collecting full spectra with the Photodiode Array, buffered reaction solvent was used as the reference sample. Reaction volumes were set to 90 μ L of solution A, and 90 μ L of solution B for a total of 180 μ L. The apparatus was kept at 20.0 $^{\circ}$ C using a water recirculation bath. For single wavelength measurements, a minimum of 1000 data points were collected for durations ranging from 0.1 s to 300 s. For full spectra, a minimum of 10 spectra were taken,

which themselves were the average of a minimum of 100 spectra at a frequency of 1000 s^{-1} to minimise noise. Trigger mode was set to external, and a pressure hold was used for reactions below 5 s to remove artifacts observed due to cavitation. Instrument syringes and lines were rinsed firstly with Milli-Q® water, and then reaction buffer system prior to use. For any given bioconjugation reaction, the concentration of glutathione was at least 100 times larger than the concentration of bioconjugation reagent to ensure pseudo first-order conditions. Raw data was exported as ProData CSV files and processed in OriginPro 9.1.

5.7.4.1. Collection of Full UV/vis Spectra

Procedure for collection of full UV/vis spectra: Using the SX-20 fitted with the Photodiode Array, UV/vis spectra of all bioconjugation reagents (Solution A: $10\text{ }\mu\text{M}$ bioconjugation reagent, $\text{H}_2\text{O}/\text{MeCN}$ 50:50, $100\text{ }\mu\text{M}$ tris, pH 7.5) were collected. Pseudo first order reactions were then run using a 100-fold excess of glutathione (Solution B: 1 mM glutathione, $\text{H}_2\text{O}/\text{MeCN}$ 50:50, $100\text{ }\mu\text{M}$ tris, pH 7.5) and at least 10 UV/vis spectra were collected over the course of the reaction (variable times). Full spectra of bioconjugation reagents were referenced to the reaction solvent ($\text{H}_2\text{O}/\text{MeCN}$ 50:50, $100\text{ }\mu\text{M}$ Tris, pH 7.5). Bioconjugation reaction spectra were referenced to Solution B.

N-Ethylmaleimide (**158**) was used in solution A in **procedure for collection of full UV/vis spectra**. The reaction with glutathione was monitored over 90 seconds.

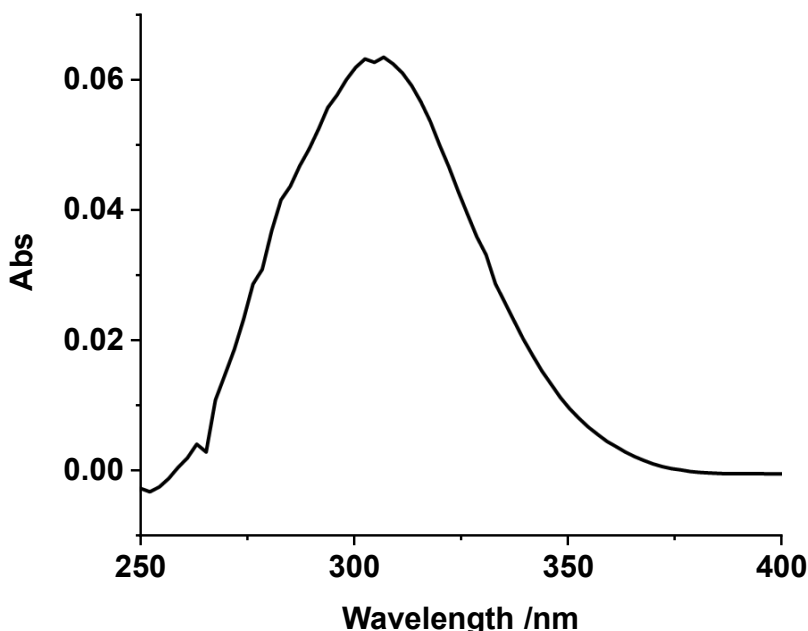


Figure 50: UV/vis spectrum of $10\text{ }\mu\text{M}$ *N*-ethylmaleimide (**158**) in $\text{H}_2\text{O}/\text{MeCN}$ (50:50) buffered to pH 7.5 with 100 mM tris. Spectra: 1. Sample period: 1 ms. Samples per spectrum: 1000.

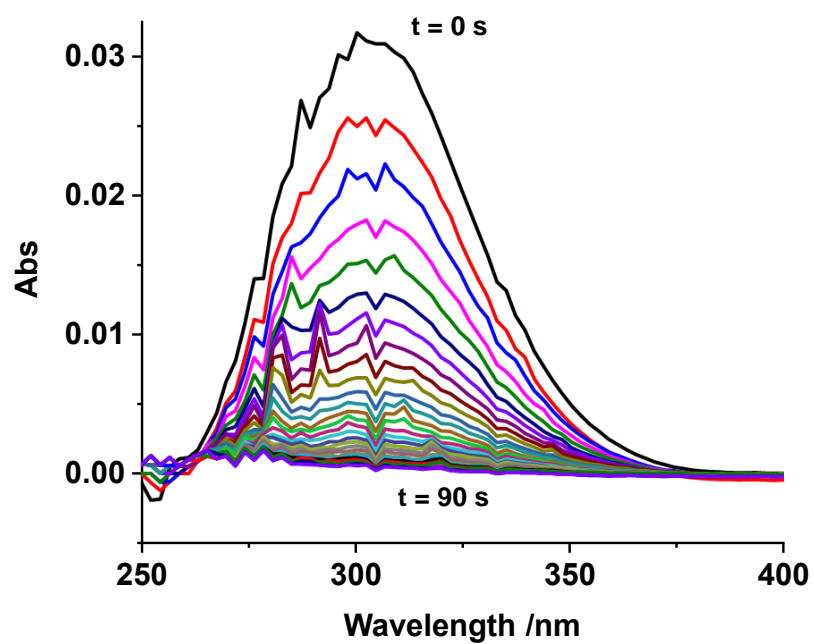


Figure 51: 10 μM N-ethylmaleimide (158) plus 1 mM GSH in $\text{H}_2\text{O}/\text{MeCN}$ (50:50) buffered to pH 7.4 with 100 mM tris. Reaction time: 90 s. Spectra: 30. Sample period: 1 ms. Samples per spectrum: 3000.

157 was used in solution A in **procedure for collection of full UV/vis spectra**. The reaction with glutathione was monitored over 120 seconds.

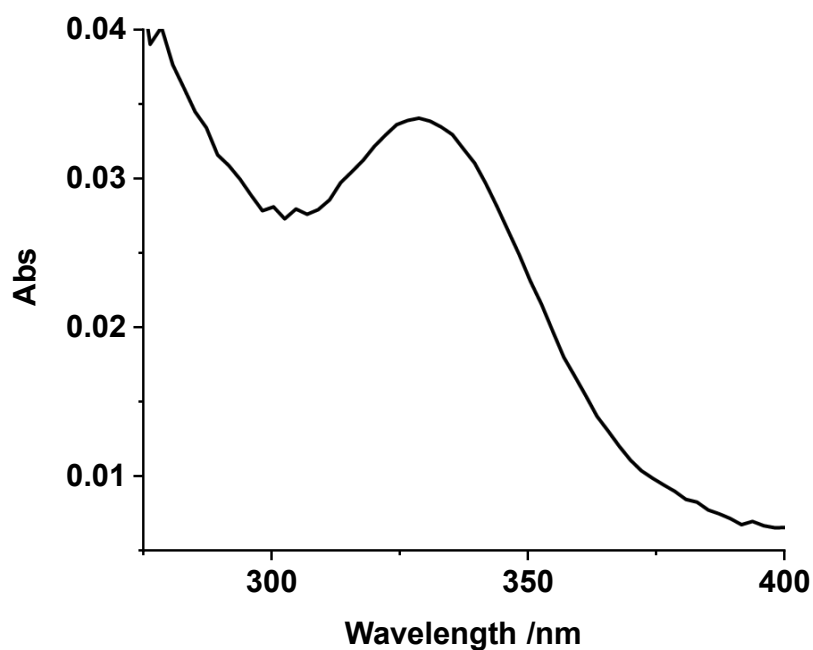


Figure 52: 10 μM 157 in $\text{H}_2\text{O}/\text{MeCN}$ (50:50) buffered to pH 7.5 with 100 mM tris. Spectra: 1. Sample period: 1 ms. Samples per spectrum: 1000.

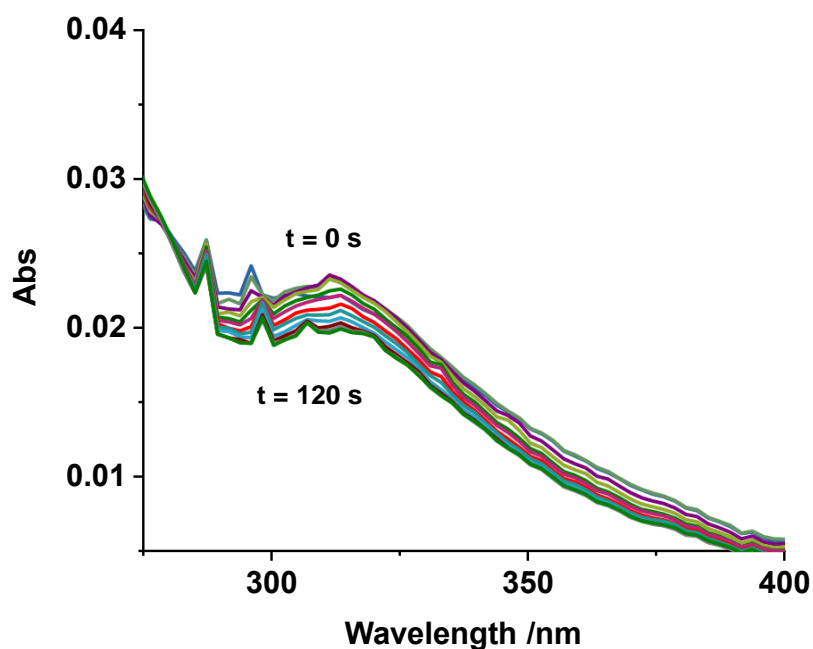


Figure 53: 10 μM 157 plus 1 mM GSH in $\text{H}_2\text{O}/\text{MeCN}$ (50:50) buffered to pH 7.5 with 100 mM tris. Reaction time: 120 s. Spectra: 10. Sample period: 1 ms. Samples per spectrum: 1000.

42 was used in solution A in **procedure for collection of full UV/vis spectra**. The reaction with glutathione was monitored over 10 seconds.

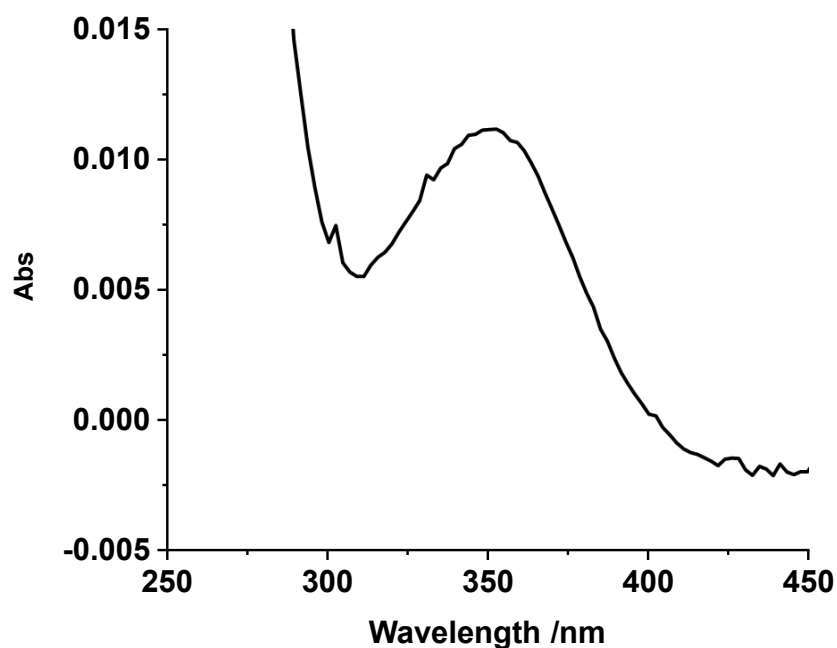


Figure 54: $10\ \mu\text{M}$ **42** in $\text{H}_2\text{O}/\text{MeCN}$ (50:50) buffered to pH 7.5 with 100 mM tris. Spectra: 1. Sample period: 1 ms. Samples per spectrum: 1000.

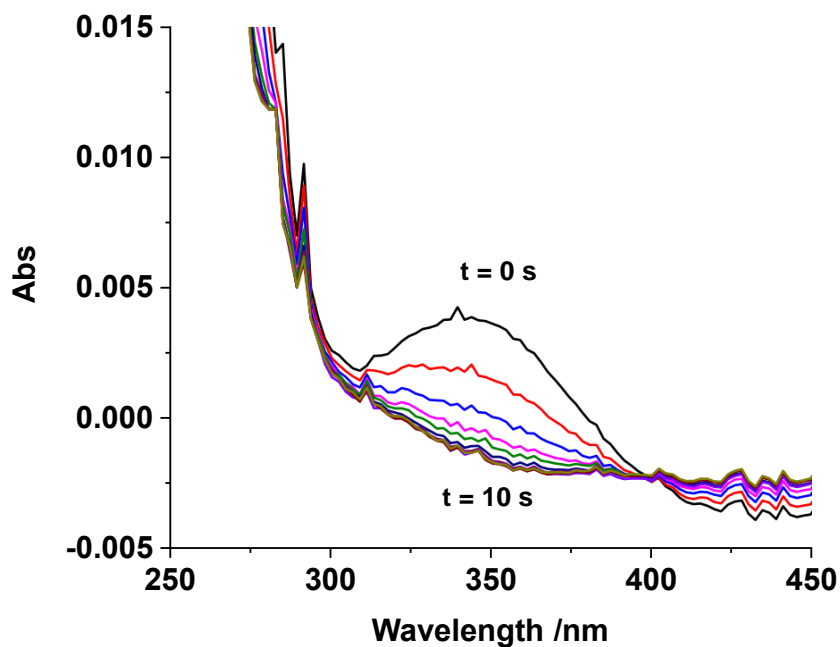


Figure 55: $10\ \mu\text{M}$ **42** plus 1 mM GSH in $\text{H}_2\text{O}/\text{MeCN}$ (50:50) buffered to pH 7.5 with 100 mM tris. Reaction time: 10 s. Spectra: 10. Sample period: 1 ms. Samples per spectrum: 1000.

181 was used in solution A in **procedure for collection of full UV/vis spectra**. The reaction with glutathione was monitored over 1 second.

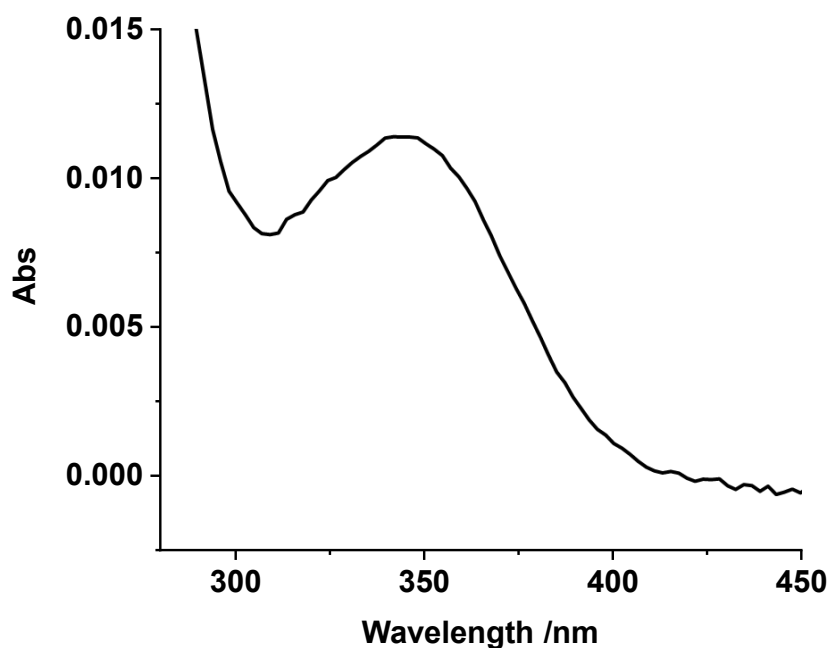


Figure 56: $10\ \mu\text{M}$ **181** in $\text{H}_2\text{O}/\text{MeCN}$ (50:50) buffered to pH 7.5 with 100 mM tris. Spectra: 1. Sample period: 1 ms. Samples per spectrum: 1000.

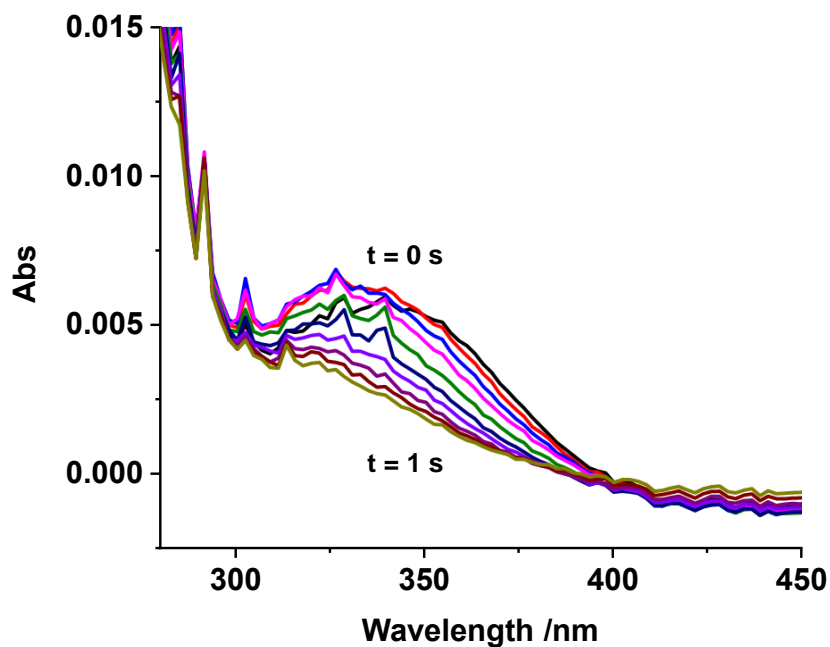


Figure 57: $10\ \mu\text{M}$ **181** plus 1 mM GSH in $\text{H}_2\text{O}/\text{MeCN}$ (50:50) buffered to pH 7.5 with 100 mM tris. Reaction time: 1 s. Spectra: 10. Sample period: 1 ms. Samples per spectrum: 100.

180 was used in solution A in **procedure for collection of full UV/vis spectra**. The reaction with glutathione was monitored over 1 second.

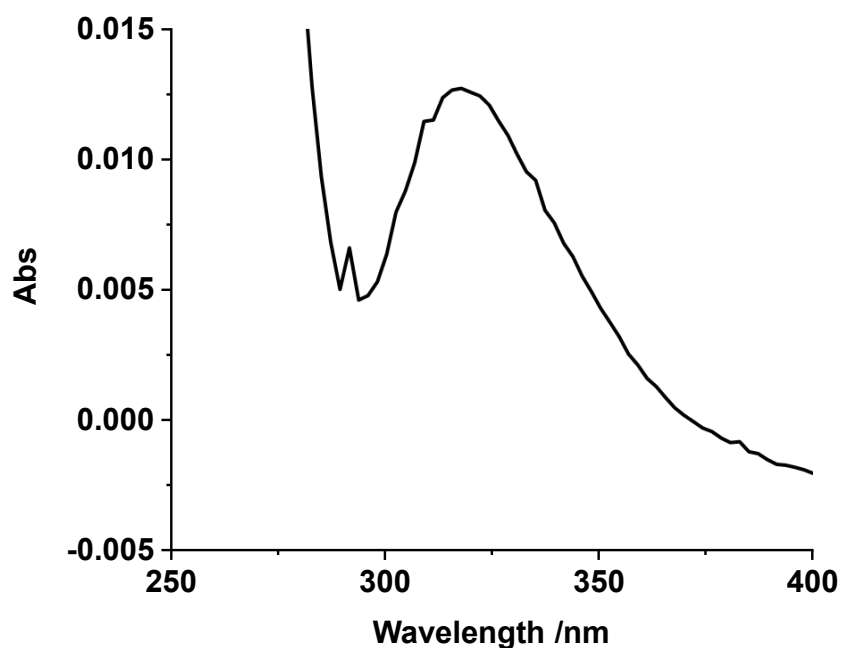


Figure 58: $10\ \mu\text{M}$ **180** in $\text{H}_2\text{O}/\text{MeCN}$ (50:50) buffered to pH 7.5 with 100 mM tris. Spectra: 1. Sample period: 1 ms. Samples per spectrum: 1000.

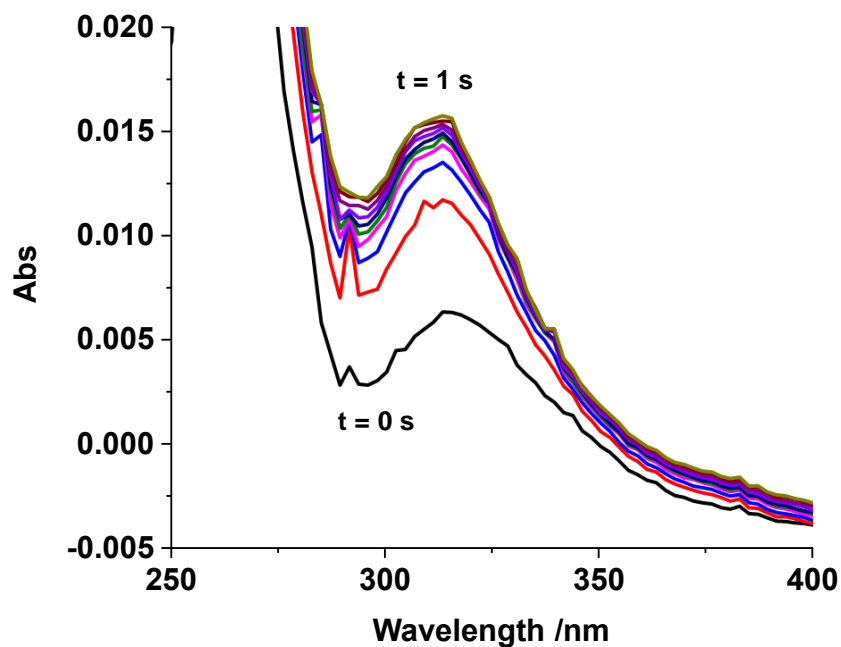


Figure 59: $10\ \mu\text{M}$ **180** plus 1 mM GSH in $\text{H}_2\text{O}/\text{MeCN}$ (50:50) buffered to pH 7.5 with 100 mM tris. Reaction time: 1 s. Spectra: 10. Sample period: 1 ms. Samples per spectrum: 100.

183 was used in solution A in **procedure for collection of full UV/vis spectra**. The reaction with glutathione was monitored over 300 seconds.

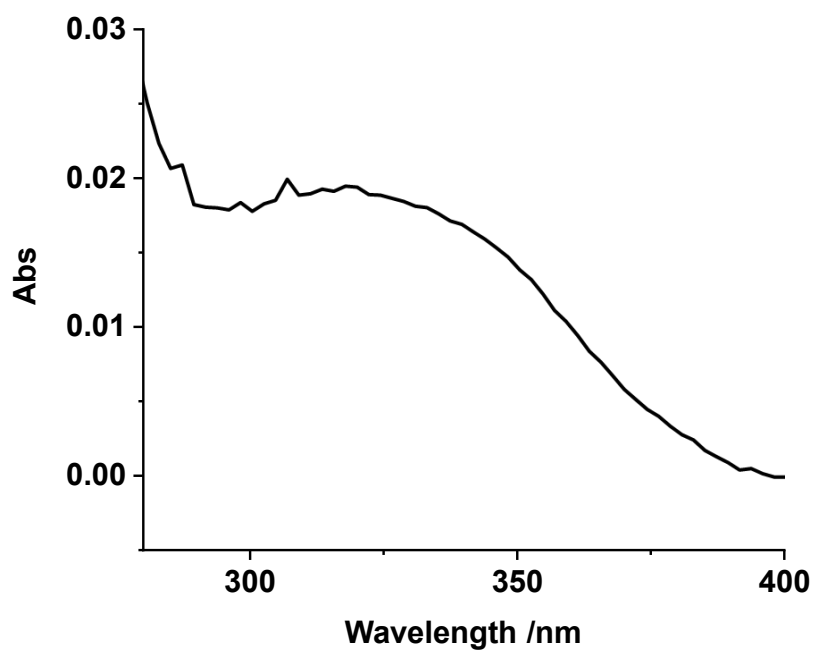


Figure 60: 10 μM 183 in $\text{H}_2\text{O}/\text{MeCN}$ (50:50) buffered to pH 7.5 with 100 mM tris. Spectra: 1. Sample period: 1 ms. Samples per spectrum: 1000.

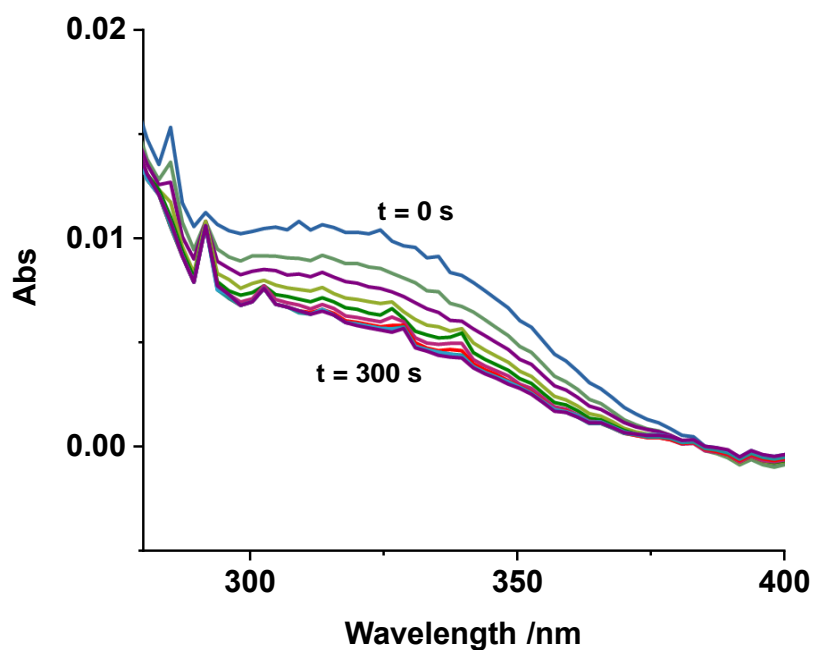


Figure 61: 10 μM 183 plus 1 mM GSH in $\text{H}_2\text{O}/\text{MeCN}$ (50:50) buffered to pH 7.5 with 100 mM tris. Reaction time: 300 s. Spectra: 10. Sample period: 1 ms. Samples per spectrum: 3000.

187 was used in solution A in **procedure for collection of full UV/vis spectra**. The reaction with glutathione was monitored over 300 seconds.

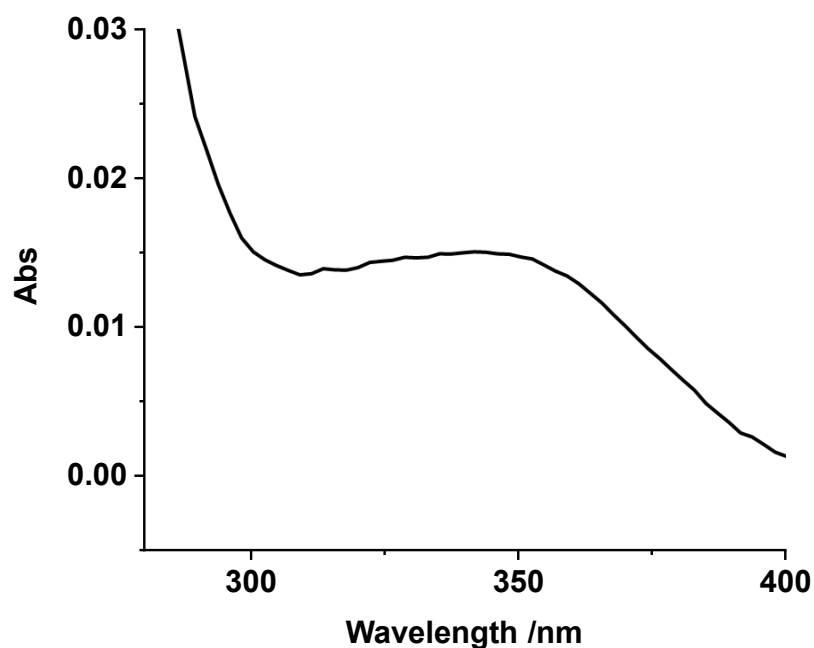


Figure 62: $10\ \mu\text{M}$ **187** in $\text{H}_2\text{O}/\text{MeCN}$ (50:50) buffered to pH 7.5 with 100 mM tris. Spectra: 1. Sample period: 1 ms. Samples per spectrum: 1000.

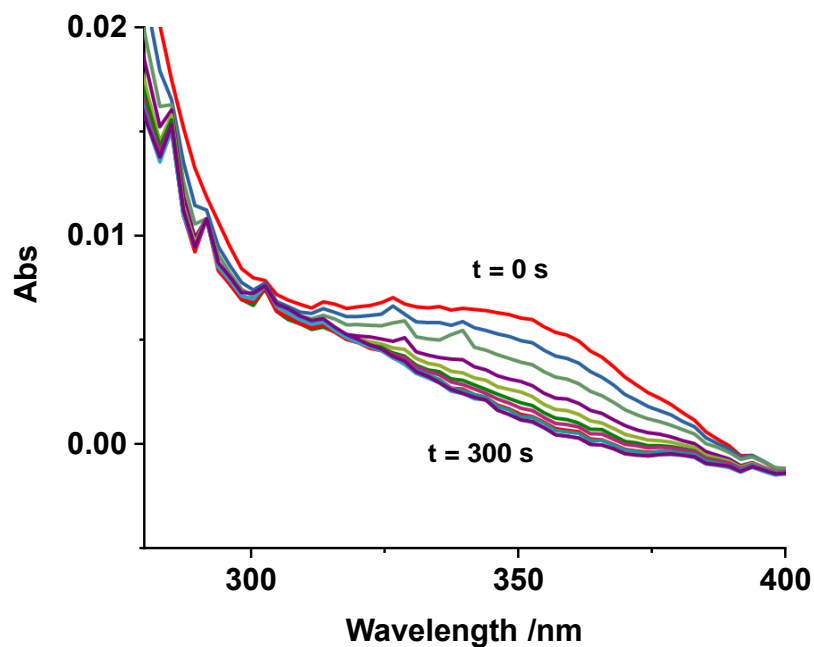


Figure 63: $10\ \mu\text{M}$ **187** plus 1 mM GSH in $\text{H}_2\text{O}/\text{MeCN}$ (50:50) buffered to pH 7.5 with 100 mM tris. Reaction time: 300 s. Spectra: 10. Sample period: 1 ms. Samples per spectrum: 3000.

188 was used in solution A in **procedure for collection of full UV/vis spectra**. The reaction with glutathione was monitored over 300 seconds.

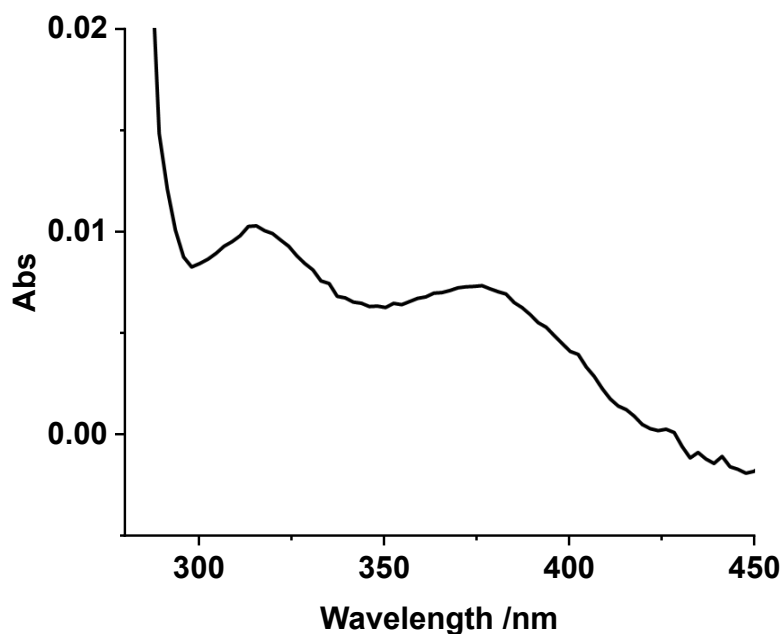


Figure 64: 10 μM **188** in $\text{H}_2\text{O}/\text{MeCN}$ (50:50) buffered to pH 7.5 with 100 mM tris. Spectra: 1. Sample period: 1 ms. Samples per spectrum: 1000.

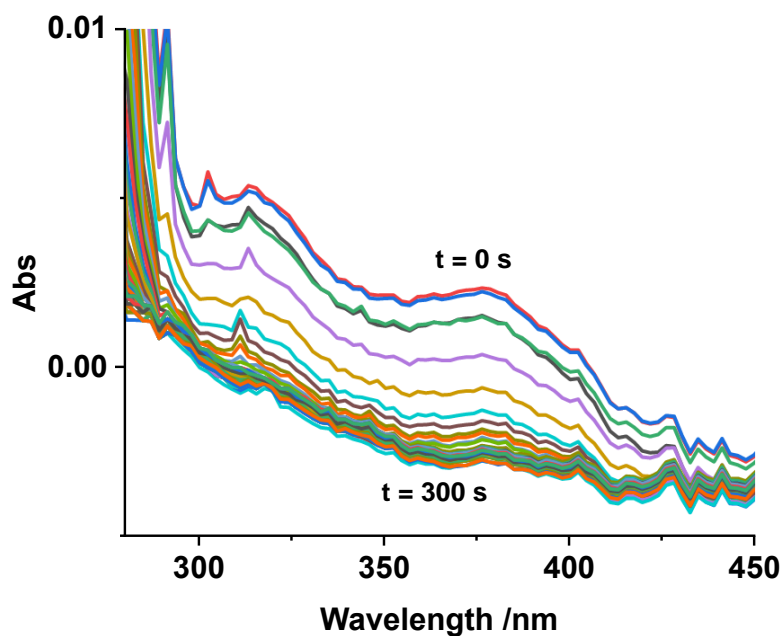


Figure 65: 10 μM **188** plus 1 mM GSH in $\text{H}_2\text{O}/\text{MeCN}$ (50:50) buffered to pH 7.5 with 100 mM tris. Reaction time: 300 s. Spectra: 20. Sample period: 1 ms. Samples per spectrum: 3000.

200 was used in solution A in **procedure for collection of full UV/vis spectra**. The reaction with glutathione was monitored over 1 second and 300 seconds.

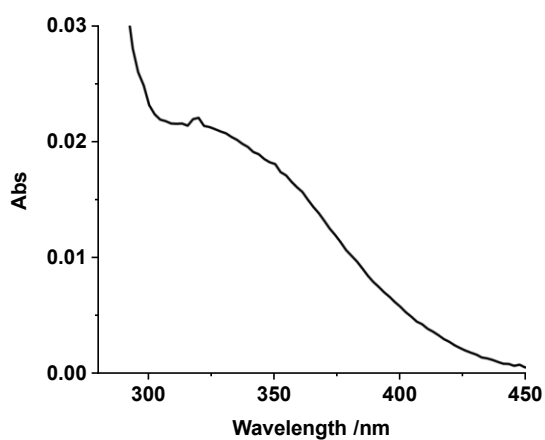


Figure 66: $10\ \mu\text{M}$ **200** in $\text{H}_2\text{O}/\text{MeCN}$ (50:50) buffered to pH 7.5 with 100 mM tris. Spectra: 1. Sample period: 1 ms. Samples per spectrum: 1000.

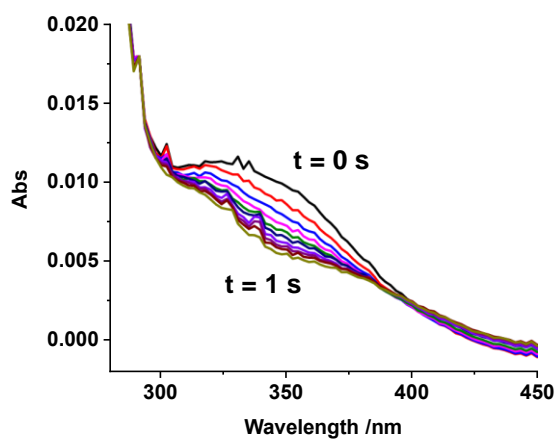


Figure 67: $10\ \mu\text{M}$ **200** plus 1 mM GSH in $\text{H}_2\text{O}/\text{MeCN}$ (50:50) buffered to pH 7.5 with 100 mM tris. Reaction time: 1 s. Spectra: 10. Sample period: 1 ms. Samples per spectrum: 100.

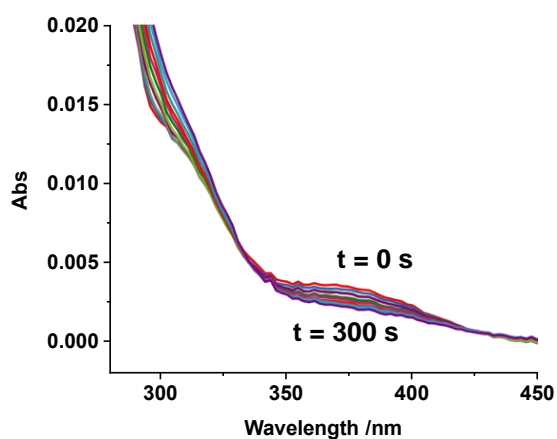
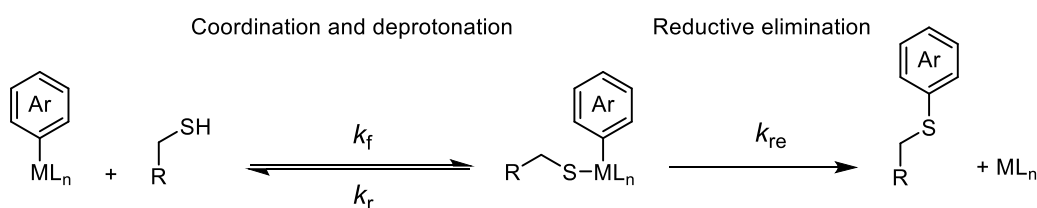


Figure 68: $10\ \mu\text{M}$ **200** plus 1 mM GSH in $\text{H}_2\text{O}/\text{MeCN}$ (50:50) buffered to pH 7.5 with 100 mM tris. Reaction time: 300 s. Spectra: 100. Sample period: 1 ms. Samples per spectrum: 3000.

5.7.4.2. Collection of Single Wavelength Absorbance Measurements

Procedure for collection of single wavelength measurements: Using the SX-20 fitted with the Absorbance Photomultiplier, absorbance was monitored over time for the reaction of a given bioconjugation reagent (Solution A: 10 μM bioconjugation reagent, $\text{H}_2\text{O}/\text{MeCN}$ 50:50, 100 μM tris, pH 7.5) with an excess of glutathione (Solution B: 1 – 15 mM glutathione, $\text{H}_2\text{O}/\text{MeCN}$ 50:50, 100 μM tris, pH 7.5). Bioconjugation reaction spectra were referenced to Solution B at each differing concentration. Single wavelength measurements were fitted according to $e^{-k_{\text{obs}}t}$ to obtain k_{obs} at given glutathione concentrations.

The model bioconjugation mechanism used for kinetic analysis was as follows:



Scheme 80: General mechanism for arylation of glutathione with organometallic complexes.

Measuring k_{re} :

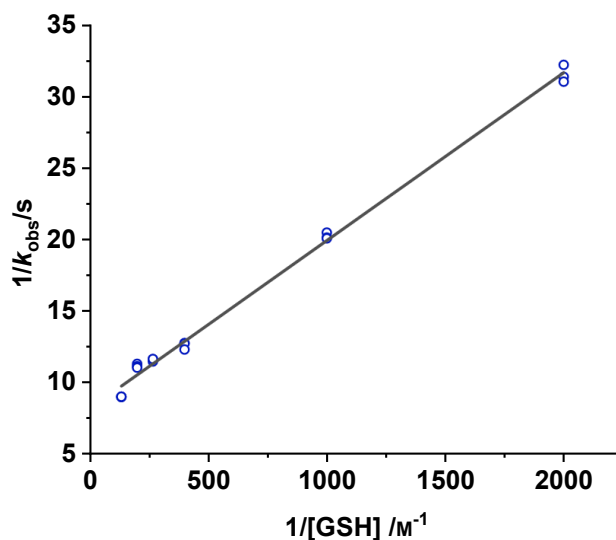
For bioconjugation reagents that did not display a linear relationship between k_{obs} and $[\text{glutathione}]$ (48), assuming the initial equilibrium is rapid, $k_f + k_r \gg k_{re}$, it follows that:

$$\frac{1}{k_{\text{obs}}} = \frac{1}{k_{re}} + \frac{1}{k_{re}K[\text{Glutathione}]}$$

Equation 2: Equation relating the observed first order rate constant with the concentration of glutathione in pre-equilibrium conditions.

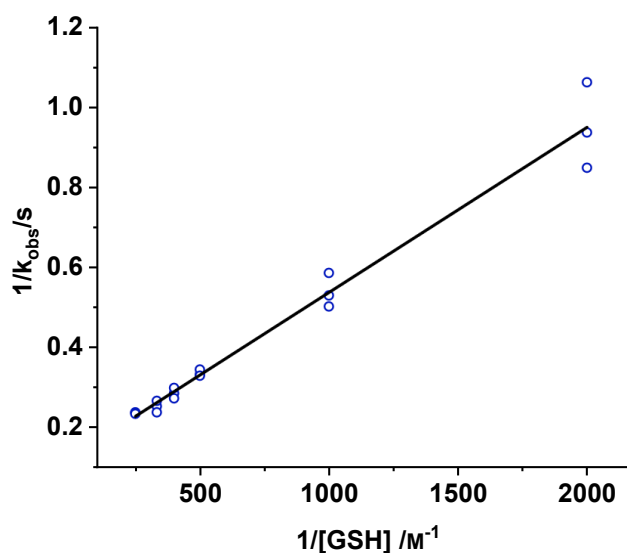
Where k_{obs} is the rate constant measured using stopped-flow.

191 was used in solution A in **procedure for collection of single wavelength measurements**. Absorbance at 257 nm was monitored up to 120 s to obtain k_{obs} at reaction concentrations of glutathione ranging from 0.50 – 15 mM. Data plotted according to Equation 2.



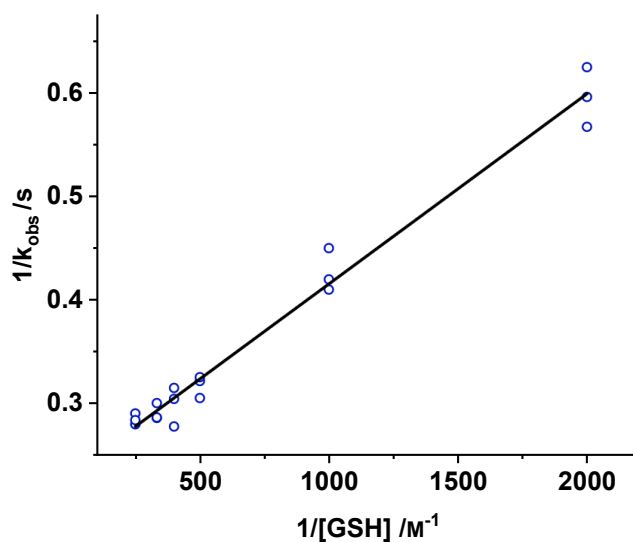
Graph 11: Plot of $1/k_{\text{obs}}$ against $1/[\text{glutathione}]$ for **191**. $K = 701 \pm 27 \text{ M}^{-1}$, k_{obs} measured over 120 s. $k_{\text{re}} = 0.122 \pm 0.0027 \text{ s}^{-1}$.

42 was used in solution A in **procedure for collection of single wavelength measurements**. Absorbance at 330 nm was monitored up to 3 s to obtain k_{obs} at reaction concentrations of glutathione ranging from 0.50 – 4.0 mM. Data plotted according to Equation 2.



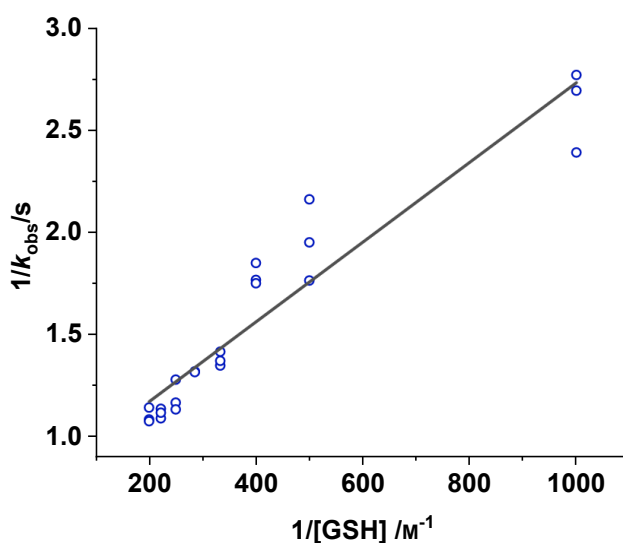
Graph 12: Plot of $1/k_{\text{obs}}$ against $1/[\text{glutathione}]$ for **42**. k_{obs} measured over 3 s. $K = 306 \pm 50 \text{ M}^{-1}$, $k_{\text{re}} = 7.92 \pm 0.98 \text{ s}^{-1}$.

181 was used in solution A in **procedure for collection of single wavelength measurements**. Absorbance at 330 nm was monitored up to 3 s to obtain k_{obs} at reaction concentrations of glutathione ranging from 0.50 – 4.0 mM. Data plotted according to Equation 2.



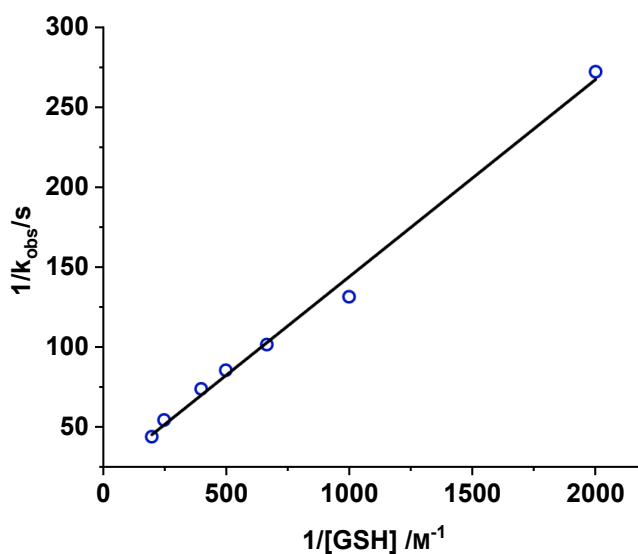
Graph 13: Plot of $1/k_{\text{obs}}$ against $1/[\text{glutathione}]$ for **181**. k_{obs} measured over 3 s. $K = 1260 \pm 78 \text{ M}^{-1}$, $k_{\text{re}} = 4.32 \pm 0.98 \text{ s}^{-1}$.

180 was used in solution A in **procedure for collection of single wavelength measurements**. Absorbance at 330 nm was monitored up to 3 s to obtain k_{obs} at reaction concentrations of glutathione ranging from 1.0 – 5.0 mM. Data plotted according to Equation 2.



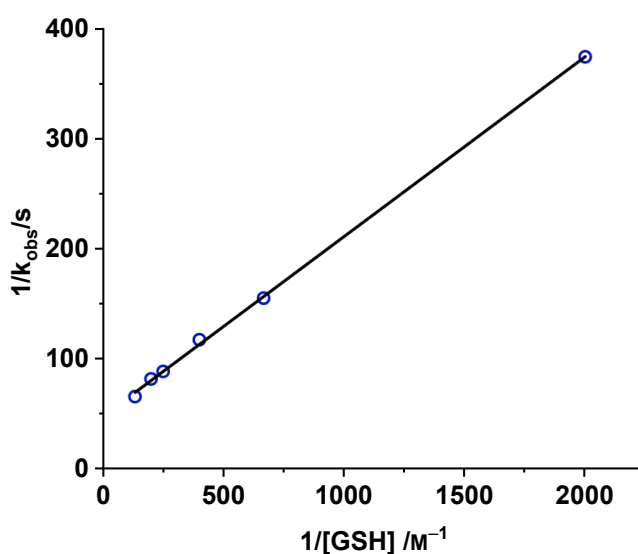
Graph 14: Plot of $1/k_{\text{obs}}$ against $1/[\text{glutathione}]$ for **180**. k_{obs} measured over 3 s. $K = 401 \pm 55 \text{ M}^{-1}$, $k_{\text{re}} = 1.28 \pm 0.084 \text{ s}^{-1}$.

183 was used in solution A in **procedure for collection of single wavelength measurements**. Absorbance at 330 nm was monitored up to 300 s to obtain k_{obs} at reaction concentrations of glutathione ranging from 0.50 – 5.0 mM. Data plotted according to Equation 2.



Graph 15: Plot of $1/k_{\text{obs}}$ against $1/[\text{glutathione}]$ for **183**. k_{obs} measured over 300 s. $K = 172 \pm 38 \text{ M}^{-1}$, $k_{\text{re}} = 0.0473 \pm 0.0088 \text{ s}^{-1}$.

187 was used in solution A in **procedure for collection of single wavelength measurements**. Absorbance at 330 nm was monitored up to 300 s to obtain k_{obs} at reaction concentrations of glutathione ranging from 0.50 – 7.5 mM. Data plotted according to Equation 2.



Graph 16: Plot of $1/k_{\text{obs}}$ against $1/[\text{glutathione}]$ for **187**. k_{obs} measured over 300 s. $K = 290 \pm 14 \text{ M}^{-1}$, $k_{\text{re}} = 0.0208 \pm 0.00074 \text{ s}^{-1}$.

Measuring k_f and k_r :

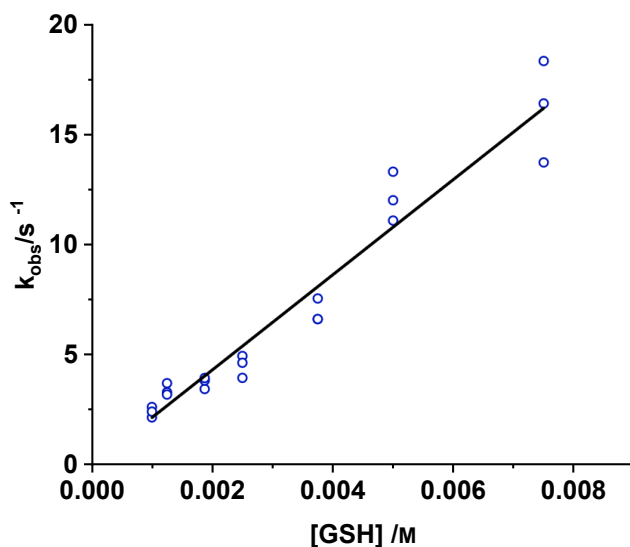
For bioconjugation reagents with a rapid pre-equilibrium, the absorbance at a given wavelength was measured over a shorter period to obtain the observed first order rate constant, k_{obs} , which is related to the equilibrium rate constant, k_{eq} , and the concentration of glutathione as follows:

$$k_{obs} = [\text{Glutathione}]k_{eq}$$

Equation 3: Equation relating the observed first order rate constant to the concentration of glutathione and the equilibrium rate constant.

Where $k_{eq} = k_f + k_r$, and $K = \frac{k_f}{k_r}$, allowing k_f and k_r to be calculated.

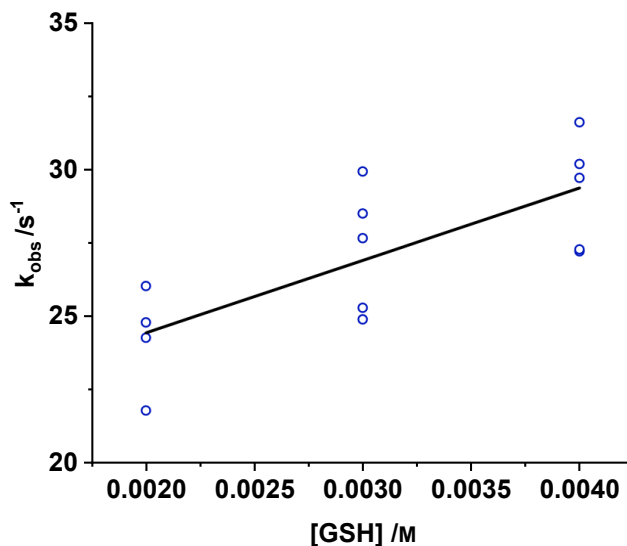
191 was used in solution A in **procedure for collection of single wavelength measurements**. Absorbance at 257 nm was monitored up to 3 s to obtain k_{obs} at reaction concentrations of glutathione ranging from 1.0 – 7.5 mM. Data plotted according to Equation 3.



Graph 17: Plot of k_{obs} against [glutathione] for **191**. k_{obs} measured over 0.2 s. $k_f = 2160 \pm 260 \text{ M}^{-1}\text{s}^{-1}$, $k_r = 3.08 \pm 0.26 \text{ s}^{-1}$.

42 was used in solution A in **procedure for collection of single wavelength measurements**.

Absorbance at 330 nm was monitored up to 0.2 s to obtain k_{obs} at reaction concentrations of glutathione ranging from 2.0 – 4.0 mM. Data plotted according to Equation 3.

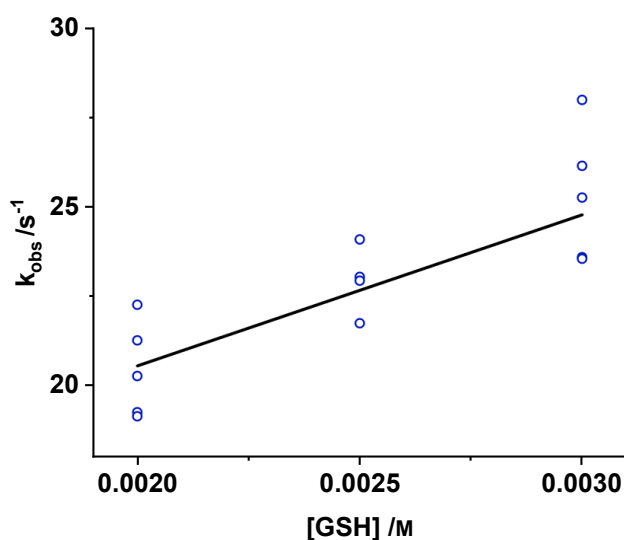


Graph 18: Plot of k_{obs} against [glutathione] for **42**. k_{obs} measured over 0.2 s. $k_f = 2460 \pm 1300 \text{ M}^{-1}\text{s}^{-1}$, $k_r = 8.33 \pm 2.8 \text{ s}^{-1}$.

181 was used in solution A in **procedure for collection of single wavelength measurements**.

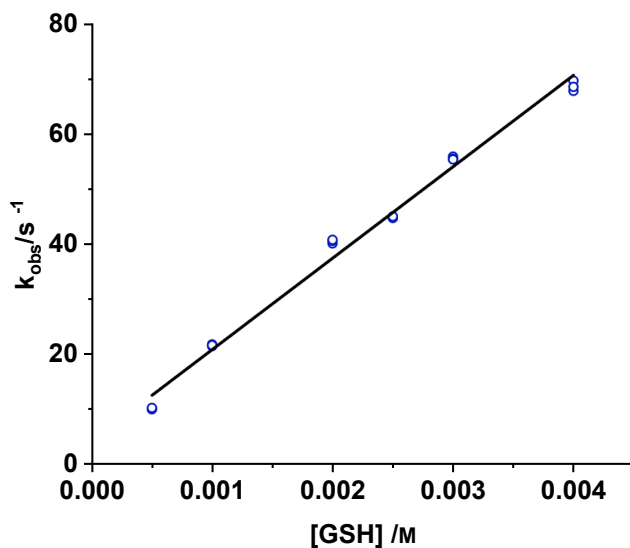
Absorbance at 330 nm was monitored up to 0.2 s to obtain k_{obs} at reaction concentrations of glutathione ranging from 2.0 – 4.0 mM. Data plotted according to Equation

3.



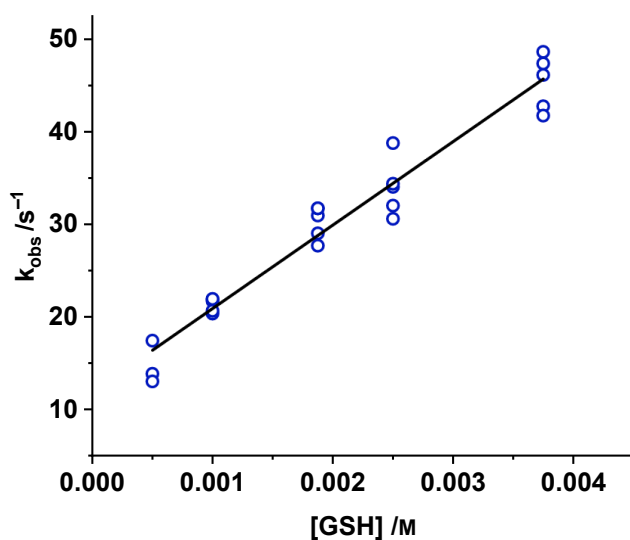
Graph 19: Plot of k_{obs} against [glutathione] for **181**. k_{obs} measured over 0.2 s. $k_f = 4220 \pm 1100 \text{ M}^{-1}\text{s}^{-1}$, $k_r = 2.99 \pm 0.65 \text{ s}^{-1}$.

180 was used in solution A in **procedure for collection of single wavelength measurements**. Absorbance at 330 nm was monitored up to 0.2 s to obtain k_{obs} at reaction concentrations of glutathione ranging from 2.0 – 4.0 mM. Data plotted according to Equation 3.



Graph 20: Plot of k_{obs} against [glutathione] for **180**. k_{obs} measured over 0.2 s. $k_f = 16600 \pm 4900 \text{ M}^{-1}\text{s}^{-1}$, $k_r = 41.3 \pm 6.7 \text{ s}^{-1}$.

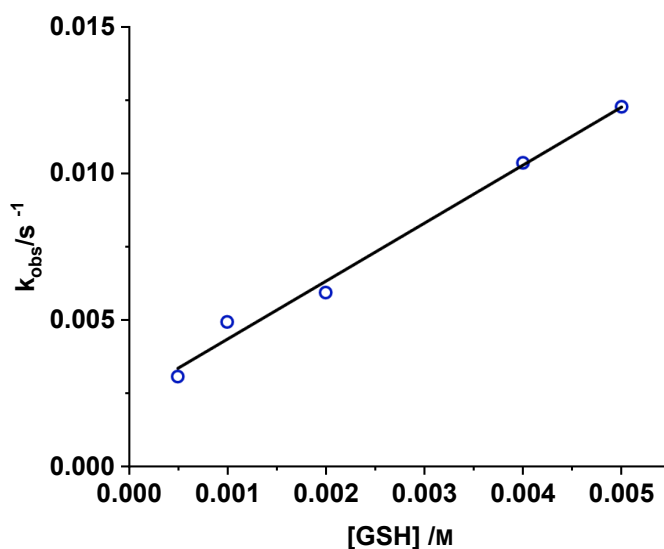
187 was used in solution A in **procedure for collection of single wavelength measurements**. Absorbance at 330 nm was monitored up to 0.2 s to obtain k_{obs} at reaction concentrations of glutathione ranging from 2.0 – 4.0 mM. Data plotted according to Equation 3.



Graph 21: Plot of k_{obs} against [glutathione] for **187**. k_{obs} measured over 0.2 s. $k_f = 16600 \pm 4900 \text{ M}^{-1}\text{s}^{-1}$, $k_r = 41.3 \pm 6.7 \text{ s}^{-1}$.

Kinetics of 188:

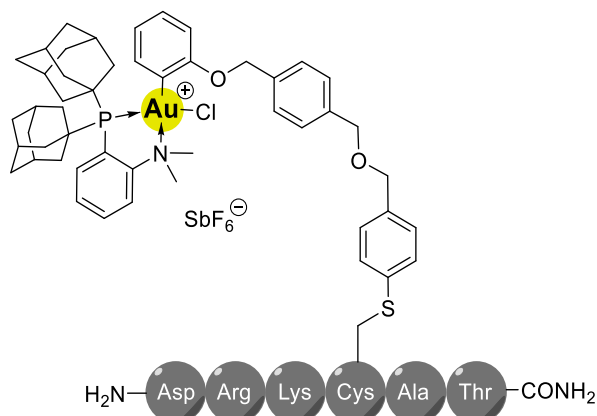
The kinetics of **188** displayed a second order relationship. **188** was used in solution A in **procedure for collection of single wavelength measurements**. Absorbance at 330 nm was monitored up to 300 s to obtain k_{obs} at reaction concentrations of glutathione ranging from 0.5 – 5.0 mM. Data plotted according to $k_{obs} = k_2[glutathione]$, where k_2 is the second order rate constant for the reaction.



Graph 22: Plot of k_{obs} against [glutathione] for **188**. k_{obs} measured over 300 s. $k_2 = 1.97 \pm 0.11 M^{-1} s^{-1}$.

5.7.5. Biomolecule Cross-Coupling[‡]

201



200 (100 μ L, 1.0 mM in MeCN, 1.0 equiv.) was combined with H-DRKCAT-NH₂ (100 μ L, 1.0 mM in 200 mM pH 8.0 tris buffer, 1.0 equiv.) in a 1.5 mL Eppendorf tube. After vortexing, the mixture was held at 35°C for 15 min and then centrifuged (10 seconds, 2000 \times g). The supernatant was removed, which contained **201** as a stock solution (0.50 mM in 200 mM pH 8.0 tris buffer/MeCN 50:50) and was used for subsequent bioconjugation reaction(s).

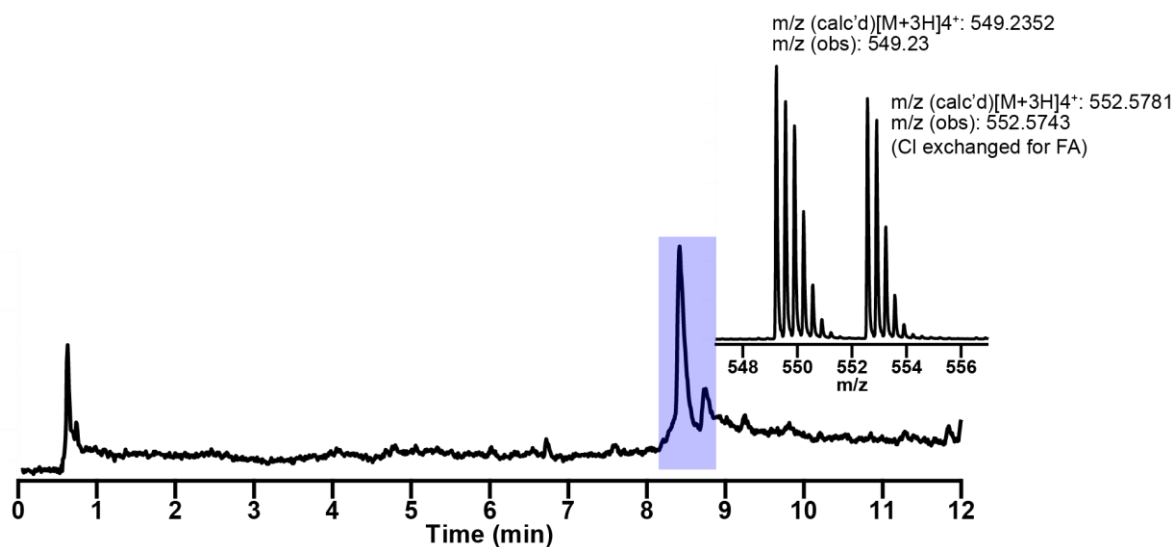
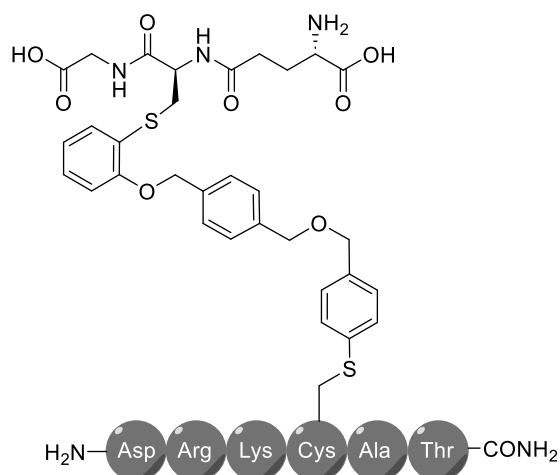


Figure 69: LC-MS TIC of the **201** stock solution. Peak highlighted in blue. The signal at 552.5743 m/z corresponds to exchange of a Cl for a formic acid moiety.

[‡] Experiments performed and analysed by Dr Evan Doud (UCLA).

202



201 (200 μL , 0.50 mM in 200 mM pH 8.0 tris buffer /MeCN 50:50) was combined with glutathione (100 μL , 1.0 mM in 200 mM pH 8.0 tris buffer, 1.0 equiv.) in a 1.5 mL Eppendorf tube. After vortexing, the mixture was held at 35°C for 30 min and then centrifuged (10 s, 2000 \times g). An aliquot (10 μL) of the supernatant was removed and diluted with 0.1% TFA in H₂O/MeCN (50:50, 90 μL) and analysed using LC-MS **method A**.

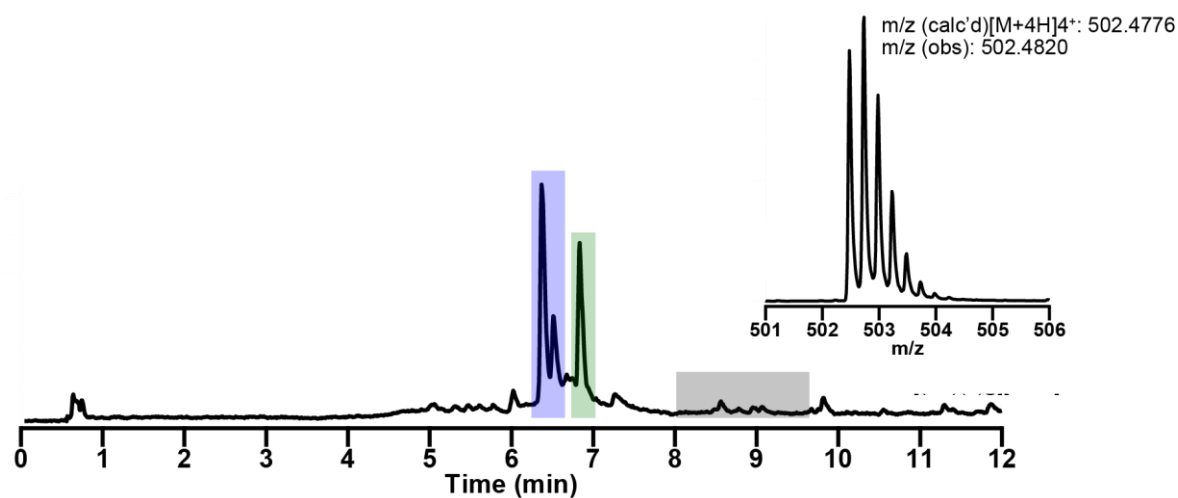


Figure 70: LC-MS TIC of **202**, peak highlighted in blue. Peak highlighted in green corresponds to glutathione dimer, and grey corresponds to unreacted **202**.

6. References

- 1 E. J. Wood, *Biochem. Mol. Biol. Educ.*, 2008, **36**, 319–320.
- 2 A. M. Scott, J. D. Wolchok and L. J. Old, *Nat. Rev. Cancer*, 2012, **12**, 278–287.
- 3 J. A. Francisco, C. G. Cerveny, D. L. Meyer, B. J. Mixan, K. Klussman, D. F. Chace, S. X. Rejniak, K. A. Gordon, R. DeBlanc, B. E. Toki, C. L. Law, S. O. Doronina, C. B. Siegall, P. D. Senter and A. F. Wahl, *Blood*, 2003, **102**, 1458–1465.
- 4 R. Lonsdale and R. A. Ward, *Chem. Soc. Rev.*, 2018, **47**, 3816–3830.
- 5 L. Xue, I. A. Karpenko, J. Hiblot and K. Johnsson, *Nat. Chem. Biol.*, 2015, **11**, 917–923.
- 6 I. Cobo, M. Li, B. S. Sumerlin and S. Perrier, *Nat. Mater.*, 2015, **14**, 143–149.
- 7 J.-F. Lutz and Z. Zarafshani, *Adv. Drug Deliv. Rev.*, 2008, **60**, 958–970.
- 8 B. A. Kairdolf, X. Qian and S. Nie, *Anal. Chem.*, 2017, **89**, 1015–1031.
- 9 O. Boutoureira and G. J. L. Bernardes, *Chem. Rev.*, 2015, **115**, 2174–2195.
- 10 M. Haque, N. Forte and J. R. Baker, *Chem. Commun.*, 2021, **57**, 10689–10702.
- 11 G. W. Anderson, J. E. Zimmerman and F. M. Callahan, *J. Am. Chem. Soc.*, 1963, **85**, 3039–3039.
- 12 G. W. Anderson, J. E. Zimmerman and F. M. Callahan, *J. Am. Chem. Soc.*, 1964, **86**, 1839–1842.
- 13 G. W. Anderson, *Metab. - Clin. Exp.*, 1964, **13**, 1026–1031.
- 14 T. Nakamura, Y. Kawai, N. Kitamoto, T. Osawa and Y. Kato, *Chem. Res. Toxicol.*, 2009, **22**, 536–542.
- 15 A. Narayanan and L. H. Jones, *Chem. Sci.*, 2015, **6**, 2650–2659.
- 16 I. Dovgan, S. Ursuegui, S. Erb, C. Michel, S. Kolodych, S. Cianférani and A. Wagner, *Bioconjug. Chem.*, 2017, **28**, 1452–1457.
- 17 P. M. S. D. Cal, J. B. Vicente, E. Pires, A. V. Coelho, L. F. Veiros, C. Cordeiro and P. M. P. Gois, *J. Am. Chem. Soc.*, 2012, **134**, 10299–10305.
- 18 L. Hao, Q. Zhou, Y. Piao, Z. Zhou, J. Tang and Y. Shen, *J. Controlled Release*, 2021, **330**, 362–371.
- 19 C. D. Spicer and B. G. Davis, *Nat. Commun.*, 2014, **5**, 4740.
- 20 J. E. Moore and W. H. Ward, *J. Am. Chem. Soc.*, 1956, **78**, 2414–2418.
- 21 J. M. J. M. Ravasco, H. Faustino, A. Trindade and P. M. P. Gois, *Chem. – Eur. J.*, 2019, **25**, 43–59.
- 22 F. R. N. Gurd, in *Methods in Enzymology*, Academic Press, 1972, vol. 25, pp. 424–438.
- 23 K. Renault, J. W. Fredy, P.-Y. Renard and C. Sabot, *Bioconjug. Chem.*, 2018, **29**, 2497–2513.
- 24 C.-W. Lin and A. Y. Ting, *J. Am. Chem. Soc.*, 2006, **128**, 4542–4543.
- 25 J. W. Wollack, J. M. Silverman, C. J. Petzold, J. D. Mougous and M. D. Distefano, *ChemBioChem*, 2009, **10**, 2934–2943.
- 26 M. Fernández-Suárez, H. Baruah, L. Martínez-Hernández, K. T. Xie, J. M. Baskin, C. R. Bertozzi and A. Y. Ting, *Nat. Biotechnol.*, 2007, **25**, 1483–1487.
- 27 M. W. Popp, J. M. Antos, G. M. Grotenbreg, E. Spooner and H. L. Ploegh, *Nat. Chem. Biol.*, 2007, **3**, 707–708.

- 28 C. C. Liu and P. G. Schultz, *Annu. Rev. Biochem.*, 2010, **79**, 413–444.
- 29 J. E. Hein and V. V. Fokin, *Chem. Soc. Rev.*, 2010, **39**, 1302–1315.
- 30 H. C. Kolb, M. G. Finn and K. B. Sharpless, *Angew. Chem. Int. Ed.*, 2001, **40**, 2004–2021.
- 31 C. S. McKay and M. G. Finn, *Chem. Biol.*, 2014, **21**, 1075–1101.
- 32 D. C. Kennedy, C. S. McKay, M. C. B. Legault, D. C. Danielson, J. A. Blake, A. F. Pegoraro, A. Stolow, Z. Mester and J. P. Pezacki, *J. Am. Chem. Soc.*, 2011, **133**, 17993–18001.
- 33 C. C. C. Johansson Seechurn, M. O. Kitching, T. J. Colacot and V. Snieckus, *Angew. Chem. Int. Ed.*, 2012, **51**, 5062–5085.
- 34 P. Devendar, R.-Y. Qu, W.-M. Kang, B. He and G.-F. Yang, *J. Agric. Food Chem.*, 2018, **66**, 8914–8934.
- 35 D. G. Brown and J. Boström, *J. Med. Chem.*, 2016, **59**, 4443–4458.
- 36 X. Chen, K. M. Engle, D.-H. Wang and J.-Q. Yu, *Angew. Chem. Int. Ed.*, 2009, **48**, 5094–5115.
- 37 J. A. Leitch, Y. Bhonoah and C. G. Frost, *ACS Catal.*, 2017, **7**, 5618–5627.
- 38 A. H. Sandtorv, *Adv. Synth. Catal.*, 2015, **357**, 2403–2435.
- 39 J. F. Hartwig, *Nature*, 2008, **455**, 314–322.
- 40 L. D. Boger and J. S. Panek, *Tetrahedron Lett.*, 1984, **25**, 3175–3178.
- 41 B. T. Ingoglia, C. C. Wagen and S. L. Buchwald, *Tetrahedron*, 2019, **75**, 4199–4211.
- 42 H. Zhang, P. Ruiz-Castillo and S. L. Buchwald, *Org. Lett.*, 2018, **20**, 1580–1583.
- 43 J. Xu, R. Y. Liu, C. S. Yeung and S. L. Buchwald, *ACS Catal.*, 2019, **9**, 6461–6466.
- 44 J. M. Chalker, C. S. C. Wood and B. G. Davis, *J. Am. Chem. Soc.*, 2009, **131**, 16346–16347.
- 45 N. Li, R. K. V. Lim, S. Edwardraja and Q. Lin, *J. Am. Chem. Soc.*, 2011, **133**, 15316–15319.
- 46 J. Willwacher, R. Raj, S. Mohammed and B. G. Davis, *J. Am. Chem. Soc.*, 2016, **138**, 8678–8681.
- 47 J. Flint, E. Taylor, M. Yang, D. N. Bolam, L. E. Tailford, C. Martinez-Fleites, E. J. Dodson, B. G. Davis, H. J. Gilbert and G. J. Davies, *Nat. Struct. Mol. Biol.*, 2005, **12**, 608–614.
- 48 D. Sehnal, S. Bittrich, M. Deshpande, R. Svobodová, K. Berka, V. Bazgier, S. Velankar, S. K. Burley, J. Koča and A. S. Rose, *Nucleic Acids Res.*, 2021, **49**, W431–W437.
- 49 R. A. A. Al-Shuaeeb, S. Kolodych, O. Koniev, S. Delacroix, S. Erb, S. Nicolaÿ, J. C. Cintrat, J. D. Brion, S. Cianféroni, M. Alami, A. Wagner and S. Messaoudi, *Chem. - Eur. J.*, 2016, **22**, 11365–11370.
- 50 A. Bruneau, M. Roche, A. Hamze, J. D. Brion, M. Alami and S. Messaoudi, *Chem. - Eur. J.*, 2015, **21**, 8375–8379.
- 51 N. Probst, R. Lartia, O. Théry, M. Alami, E. Defrancq and S. Messaoudi, *Chem. - Eur. J.*, 2018, **24**, 1795–1800.
- 52 D. Montoir, M. Amoura, Z. E. A. Ababsa, T. M. Vishwanatha, E. Yen-Pon, V. Robert, M. Beltramo, V. Piller, M. Alami, V. Aucagne and S. Messaoudi, *Chem. Sci.*, 2018, **9**, 8753–8759.

- 53 S. Humpert, M. A. Omrane, E. A. Urusova, L. Gremer, D. Willbold, H. Endepols, R. N. Krasikova, B. Neumaier and B. D. Zlatopolskiy, *Chem. Commun.*, 2021, **57**, 3547–3550.
- 54 P. Yang, X. Wang, B. Li, Y. Yang, J. Yue, Y. Suo, H. Tong, G. He, X. Lu and G. Chen, *Chem. Sci.*, 2021, **12**, 5804–5810.
- 55 P. Yang, C. Zhang, B. Li, G. He and G. Chen, *Asian J. Org. Chem.*, 2021, **10**, 2888–2891.
- 56 J. Ohata, M. B. Minus, M. E. Abernathy and Z. T. Ball, *J. Am. Chem. Soc.*, 2016, **138**, 7472–7475.
- 57 Y. Jin, M. A. Lewis, N. H. Gokhale, E. C. Long and J. A. Cowan, *J. Am. Chem. Soc.*, 2007, **129**, 8353–8361.
- 58 L. W. Donaldson, N. R. Skrynnikov, W.-Y. Choy, D. R. Muhandiram, B. Sarkar, J. D. Forman-Kay and L. E. Kay, *J. Am. Chem. Soc.*, 2001, **123**, 9843–9847.
- 59 K. P. Wilson, B. A. Malcolm and B. W. Matthews, *J. Biol. Chem.*, 1992, **267**, 10842–10849.
- 60 J. Ohata, Y. Zeng, L. Segatori and Z. T. Ball, *Angew. Chem. Int. Ed.*, 2018, **57**, 4015–4019.
- 61 M. K. Miller, H. Wang, K. Hanaya, O. Zhang, A. Berlaga and Z. T. Ball, *Chem. Sci.*, 2020, **11**, 10501–10505.
- 62 S. Z. Tasker, E. A. Standley and T. F. Jamison, *Nature*, 2014, **509**, 299–309.
- 63 G. Dave and R. Xiu, *Arch. Environ. Contam. Toxicol.*, 1991, **21**, 126–134.
- 64 K. Hanaya, J. Ohata, M. K. Miller, A. E. Mangubat-Medina, M. J. Swierczynski, D. C. Yang, R. M. Rosenthal, B. V. Popp and Z. T. Ball, *Chem. Commun.*, 2019, **55**, 2841–2844.
- 65 M. Prudent and H. H. Girault, *Metallomics*, 2009, **1**, 157–165.
- 66 K. Hanaya, M. K. Miller and Z. T. Ball, *Org. Lett.*, 2019, **21**, 2445–2448.
- 67 M. J. Swierczynski and Z. T. Ball, *Bioconjug. Chem.*, 2020, **31**, 2494–2498.
- 68 M. K. Miller, M. J. Swierczynski, Y. Ding and Z. T. Ball, *Org. Lett.*, 2021, **23**, 5334–5338.
- 69 M. J. Swierczynski, Y. Ding and Z. T. Ball, *Bioconjug. Chem.*, 2022, **33**, 2307–2313.
- 70 S. D. Tilley and M. B. Francis, *J. Am. Chem. Soc.*, 2006, **128**, 1080–1081.
- 71 R. L. Simmons, R. T. Yu and A. G. Myers, *J. Am. Chem. Soc.*, 2011, **133**, 15870–15873.
- 72 G. Cheng, R. K. V. Lim, N. Li and Q. Lin, *Chem. Commun.*, 2013, **49**, 6809–6811.
- 73 G. Cheng, R. K. V. Lim, C. P. Ramil and Q. Lin, *Chem. Commun.*, 2014, **50**, 11679–11682.
- 74 E. V. Vinogradova, C. Zhang, A. M. Spokoyny, B. L. Pentelute and S. L. Buchwald, *Nature*, 2015, **526**, 687–691.
- 75 E. Alvaro and J. F. Hartwig, *J. Am. Chem. Soc.*, 2009, **131**, 7858–7868.
- 76 A. J. Rojas, C. Zhang, E. V. Vinogradova, N. H. Buchwald, J. Reilly, B. L. Pentelute and S. L. Buchwald, *Chem. Sci.*, 2017, **8**, 4257–4263.
- 77 W. Zhao, H. G. Lee, S. L. Buchwald and J. M. Hooker, *J. Am. Chem. Soc.*, 2017, **139**, 7152–7155.
- 78 A. J. Rojas, B. L. Pentelute and S. L. Buchwald, *Org. Lett.*, 2017, **19**, 4263–4266.

- 79 H. G. Lee, G. Lautrette, B. L. Pentelute and S. L. Buchwald, *Angew. Chem. - Int. Ed.*, 2017, **56**, 3177–3181.
- 80 K. Kubota, P. Dai, B. L. Pentelute and S. L. Buchwald, *J. Am. Chem. Soc.*, 2018, **140**, 3128–3133.
- 81 H. H. Dhanjee, I. Buslov, I. W. Windsor, R. T. Raines, B. L. Pentelute and S. L. Buchwald, *J. Am. Chem. Soc.*, 2020, **142**, 21237–21242.
- 82 H. H. Dhanjee, A. Saebi, I. Buslov, A. R. Loftis, S. L. Buchwald and B. L. Pentelute, *J. Am. Chem. Soc.*, 2020, **142**, 9124–9129.
- 83 M. A. Starovasnik, A. C. Braisted and J. A. Wells, *Proc. Natl. Acad. Sci.*, 1997, **94**, 10080–10085.
- 84 J. Santoro, C. González, M. Bruix, J. L. Neira, J. L. Nieto, J. Herranz and M. Rico, *J. Mol. Biol.*, 1993, **229**, 722–734.
- 85 M. Gazvoda, H. Dhanjee, J. Rodriguez, J. Brown, C. Farquhar, N. Truex, A. Loas, S. Buchwald, B. Pentelute and B. Pentelute, *J Am Chem Soc*, 2022, **144**, 7852–7860.
- 86 J. Rodriguez, H. H. Dhanjee, B. L. Pentelute and S. L. Buchwald, *J. Am. Chem. Soc.*, 2022, **144**, 11706–11712.
- 87 A. J. Rojas, J. M. Wolfe, H. H. Dhanjee, I. Buslov, N. L. Truex, R. Y. Liu, W. Masefski, B. L. Pentelute and S. L. Buchwald, *Chem. Sci.*, 2022, **13**, 11891–11895.
- 88 C. Petosa, R. J. Collier, K. R. Klimpel, S. H. Leppla and R. C. Liddington, *Nature*, 1997, **385**, 833–838.
- 89 P. Stockmann, M. Gozzi, R. Kuhnert, M. B. Sárosi and E. Hey-Hawkins, *Chem. Soc. Rev.*, 2019, **48**, 3497–3512.
- 90 J. Rodriguez, H. H. Dhanjee and S. L. Buchwald, *Org. Lett.*, 2021, **23**, 777–780.
- 91 K. K. Y. Kung, H. M. Ko, J. F. Cui, H. C. Chong, Y. C. Leung and M. K. Wong, *Chem. Commun.*, 2014, **50**, 11899–11902.
- 92 J.-J. Zhang, R. W.-Y. Sun and C.-M. Che, *Chem. Commun.*, 2012, **48**, 3388–3390.
- 93 J.-J. Zhang, K.-M. Ng, C.-N. Lok, R. W.-Y. Sun and C.-M. Che, *Chem. Commun.*, 2013, **49**, 5153–5155.
- 94 M. N. Wenzel, R. Bonsignore, S. R. Thomas, D. Bourissou, G. Barone and A. Casini, *Chem. – Eur. J.*, 2019, **25**, 7628–7634.
- 95 S. Gukathasan, S. Parkin, E. P. Black and S. G. Awuah, *Inorg. Chem.*, 2021, **60**, 14582–14593.
- 96 M. S. Messina, J. M. Stauber, M. A. Waddington, A. L. Rheingold, H. D. Maynard and A. M. Spokoyny, *J. Am. Chem. Soc.*, 2018, **140**, 7065–7069.
- 97 S.-L. Zhang and J.-J. Dong, *Org. Biomol. Chem.*, 2019, **17**, 1245–1253.
- 98 J. M. Stauber, A. L. Rheingold and A. M. Spokoyny, *Inorg. Chem.*, 2021, **60**, 5054–5062.
- 99 H. R. Montgomery, M. S. Messina, E. A. Doud, A. M. Spokoyny and H. D. Maynard, *Bioconjug. Chem.*, 2022, **33**, 1536–1542.
- 100 G. E. Mudd, S. J. Stanway, D. R. Witty, A. Thomas, S. Baldo, A. D. Bond, P. Beswick and A. Highton, *Bioconjug. Chem.*, 2022, **33**, 1441–1445.
- 101 M. A. Waddington, X. Zheng, J. M. Stauber, E. Hakim Mouly, H. R. Montgomery, L. M. A. Saleh, P. Král and A. M. Spokoyny, *J. Am. Chem. Soc.*, 2021, **143**, 8661–8668.

- 102 X. Lin, E. Haimov, B. Redko and A. Vigalok, *Angew. Chem. Int. Ed.*, 2022, **61**, e202205368.
- 103 W. R. Moser, A. W. Wang and N. K. Kildahl, *J. Am. Chem. Soc.*, 1988, **110**, 2816–2820.
- 104 T. I. Wallow, F. E. Goodson and B. M. Novak, *Organometallics*, 1996, **15**, 3708–3716.
- 105 S. Verbeeck, C. Meyers, P. Franck, A. Jutand and B. U. W. Maes, *Chem. – Eur. J.*, 2010, **16**, 12831–12837.
- 106 B. T. Ingoglia and S. L. Buchwald, *Org. Lett.*, 2017, **19**, 2853–2856.
- 107 J. M. Dennis, N. A. White, R. Y. Liu and S. L. Buchwald, *J. Am. Chem. Soc.*, 2018, **140**, 4721–4725.
- 108 S. D. McCann, E. C. Reichert, P. L. Arrechea and S. L. Buchwald, *J. Am. Chem. Soc.*, 2020, **142**, 15027–15037.
- 109 M. R. Uehling, R. P. King, S. W. Krska, T. Cernak and S. L. Buchwald, *Science*, 2019, **363**, 405–408.
- 110 R. P. King, S. W. Krska and S. L. Buchwald, *Org. Lett.*, 2021, **23**, 7927–7932.
- 111 J. P. Kleiman and Michael. Dubeck, *J. Am. Chem. Soc.*, 1963, **85**, 1544–1545.
- 112 T. Rogge, N. Kaplaneris, N. Chatani, J. Kim, S. Chang, B. Punji, L. L. Schafer, D. G. Musaev, J. Wencel-Delord, C. A. Roberts, R. Sarpong, Z. E. Wilson, M. A. Brimble, M. J. Johansson and L. Ackermann, *Nat. Rev. Methods Primer*, 2021, **1**, 1–31.
- 113 J. Dupont, C. S. Consorti and J. Spencer, *Chem. Rev.*, 2005, **105**, 2527–2572.
- 114 A. C. Cope and R. W. Siekman, *J. Am. Chem. Soc.*, 1965, **87**, 3272–3273.
- 115 A. C. Cope and E. C. Friedrich, *J. Am. Chem. Soc.*, 1968, **90**, 909–913.
- 116 T. Boschi, R. Pietropaolo and U. Belluco, *J. Chem. Soc. Inorg. Phys. Theor.*, 1970, 531–535.
- 117 T. Itoh and T. Mase, *Org. Lett.*, 2004, **6**, 4587–4590.
- 118 P. J. Milner, T. J. Maimone, M. Su, J. Chen, P. Müller and S. L. Buchwald, *J. Am. Chem. Soc.*, 2012, **134**, 19922–19934.
- 119 N. C. Bruno, M. T. Tudge and S. L. Buchwald, *Chem. Sci.*, 2013, **4**, 916–920.
- 120 N. B. Cech and C. G. Enke, *Mass Spectrom. Rev.*, 2001, **20**, 362–387.
- 121 Liang. Tang and Paul. Kebarle, *Anal. Chem.*, 1993, **65**, 3654–3668.
- 122 D. A. Abaye, F. S. Pullen and B. V. Nielsen, *Rapid Commun. Mass Spectrom.*, 2011, **25**, 1107–1116.
- 123 A. Kasahara, *Bull. Chem. Soc. Jpn.*, 1968, **41**, 1272.
- 124 H. Horino and N. Inoue, *Tetrahedron Lett.*, 1979, **20**, 2403–2406.
- 125 T. Pugliese, N. Godbert, I. Aiello, M. Ghedini and M. La Deda, *Inorg. Chem. Commun.*, 2006, **9**, 93–95.
- 126 Y.-J. Kim, X. Chang, J.-T. Han, M. S. Lim and S. W. Lee, *Dalton Trans.*, 2004, 3699–3708.
- 127 A. D. Ryabov, I. K. Sakodinskaya and A. K. Yatsimirsky, *J. Chem. Soc. Dalton Trans.*, 1985, 2629–2638.
- 128 S. Tollari, F. Demartin, S. Cenini, G. Palmisano and P. Raimondi, *J. Organomet. Chem.*, 1997, **527**, 93–102.

- 129 S. B. Atla, A. A. Kelkar, V. G. Puranik, W. Bensch and R. V. Chaudhari, *J. Organomet. Chem.*, 2009, **694**, 683–690.
- 130 V. V. Dunina, O. A. Zalevskaya and V. M. Potapov, *Russ. Chem. Rev.*, 1988, **57**, 250–269.
- 131 T. Wang, A. Pfisterer, S. L. Kuan, Y. Wu, O. Dumele, M. Lamla, K. Müllen and T. Weil, *Chem. Sci.*, 2013, **4**, 1889–1894.
- 132 J. A. Siepen, E.-J. Keevil, D. Knight and S. J. Hubbard, *J. Proteome Res.*, 2007, **6**, 399–408.
- 133 A. D. Ryabov, V. A. Polyakov and A. K. Yatsimirsky, *Inorganica Chim. Acta*, 1984, **91**, 59–65.
- 134 A. D. Ryabov, *Chem. Rev.*, 1990, **90**, 403–424.
- 135 V. V. Dunina, O. A. Zalevskaya and V. M. Potapov, *Zhurnal Obshchei Khimii*, **54**, 389–397.
- 136 Y. Fuchita and H. Tsuchiya, *Inorganica Chim. Acta*, 1993, **209**, 229–230.
- 137 Y. Fuchita and H. Tsuchiya, *Polyhedron*, 1993, **12**, 2079–2080.
- 138 J. Vicente, I. Saura-Llamas and P. G. Jones, *J. Chem. Soc. Dalton Trans.*, 1993, 3619–3624.
- 139 A. Avshu, R. D. O’Sullivan, A. W. Parkins, N. W. Alcock and R. M. Countryman, *J. Chem. Soc. Dalton Trans.*, 1983, 1619–1624.
- 140 J. Vicente and I. Saura-Llamas, *Comments Inorg. Chem.*, 2007, **28**, 39–72.
- 141 Y. Fuchita, K. Yoshinaga, Y. Ikeda and J. Kinoshita-Kawashima, *J. Chem. Soc. Dalton Trans.*, 1997, 2495–2500.
- 142 J. Vicente, I. Saura-Llamas and D. Bautista, *Organometallics*, 2005, **24**, 6001–6004.
- 143 J. Vicente, I. Saura-Llamas, J.-A. García-López, B. Calmuschi-Cula and D. Bautista, *Organometallics*, 2007, **26**, 2768–2776.
- 144 M.-J. Oliva-Madrid, J.-A. García-López, I. Saura-Llamas, D. Bautista and J. Vicente, *Organometallics*, 2012, **31**, 3647–3660.
- 145 J. Vicente, I. Saura-Llamas, J.-A. García-López and D. Bautista, *Organometallics*, 2009, **28**, 448–464.
- 146 B. E. I. Ramakers, J. C. M. van Hest and D. W. P. M. Löwik, *Chem. Soc. Rev.*, 2014, **43**, 2743–2756.
- 147 D. J. Craik, D. P. Fairlie, S. Liras and D. Price, *Chem. Biol. Drug Des.*, 2013, **81**, 136–147.
- 148 M. Góngora-Benítez, J. Tulla-Puche and F. Albericio, *Chem. Rev.*, 2014, **114**, 901–926.
- 149 L. Mendive-Tapia, S. Preciado, J. García, R. Ramón, N. Kielland, F. Albericio and R. Lavilla, *Nat. Commun.*, 2015, **6**, 1–9.
- 150 Y. Tan, H. Wu, T. Wei and X. Li, *J. Am. Chem. Soc.*, 2020, **142**, 20288–20298.
- 151 J. Vicente, I. Saura-Llamas, M.-J. Oliva-Madrid, J.-A. García-López and D. Bautista, *Organometallics*, 2011, **30**, 4624–4631.
- 152 A. Mahindra, N. Bagra and R. Jain, *J. Org. Chem.*, 2013, **78**, 10954–10959.
- 153 I. S. Golovanov, A. V. Leonov, V. K. Lesnikov, E. V. Pospelov, K. V. Frolov, A. A. Korlyukov, Y. V. Nelyubina, V. V. Novikov and A. Y. Sukhorukov, *Dalton Trans.*, 2022, **51**, 4284–4296.

- 154C. Bechtler and C. Lamers, *RSC Med. Chem.*, 2021, **12**, 1325–1351.
- 155F.-J. Chen and J. Gao, *Chem. – Eur. J.*, 2022, **28**, e202201843.
- 156M. J. Matos, C. D. Navo, T. Hakala, X. Ferhati, A. Guerreiro, D. Hartmann, B. Bernardim, K. L. Saar, I. Compañón, F. Corzana, T. P. J. Knowles, G. Jiménez-Osés and G. J. L. Bernardes, *Angew. Chem. Int. Ed.*, 2019, **58**, 6640–6644.
- 157D. Abegg, R. Frei, L. Cerato, D. Prasad Hari, C. Wang, J. Waser and A. Adibekian, *Angew. Chem. Int. Ed.*, 2015, **54**, 10852–10857.
- 158D. Abegg, M. Tomanik, N. Qiu, D. Pechalrieu, A. Shuster, B. Commare, A. Togni, S. B. Herzon and A. Adibekian, *J. Am. Chem. Soc.*, 2021, **143**, 20332–20342.
- 159B. Bernardim, M. J. Matos, X. Ferhati, I. Compañón, A. Guerreiro, P. Akkapeddi, A. C. B. Burtoloso, G. Jiménez-Osés, F. Corzana and G. J. L. Bernardes, *Nat. Protoc.*, 2019, **14**, 86–99.
- 160J. Yu, X. Yang, Y. Sun and Z. Yin, *Angew. Chem. Int. Ed.*, 2018, **57**, 11598–11602.
- 161J. Yu, X. Yang, Y. Sun and Z. Yin, *Angew. Chem.*, 2018, **130**, 11772–11776.
- 162F.-J. Chen, M. Zheng, V. Nobile and J. Gao, *Chem. – Eur. J.*, 2022, **28**, e202200058.
- 163N. J. Smith, K. Rohlfing, L. A. Sawicki, P. M. Kharkar, S. J. Boyd, A. M. Kloxin and J. M. Fox, *Org. Biomol. Chem.*, 2018, **16**, 2164–2169.
- 164H. F. Motiwala, Y.-H. Kuo, B. L. Stinger, B. A. Palfey and B. R. Martin, *J. Am. Chem. Soc.*, 2020, **142**, 1801–1810.
- 165B.-Q. Shen, K. Xu, L. Liu, H. Raab, S. Bhakta, M. Kenrick, K. L. Parsons-Reponte, J. Tien, S.-F. Yu, E. Mai, D. Li, J. Tibbitts, J. Baudys, O. M. Saad, S. J. Scales, P. J. McDonald, P. E. Hass, C. Eigenbrot, T. Nguyen, W. A. Solis, R. N. Fuji, K. M. Flagella, D. Patel, S. D. Spencer, L. A. Khawli, A. Ebens, W. L. Wong, R. Vandlen, S. Kaur, M. X. Sliwkowski, R. H. Scheller, P. Polakis and J. R. Junutula, *Nat. Biotechnol.*, 2012, **30**, 184–189.
- 166G. Gorin, P. A. Martic and G. Doughty, *Arch. Biochem. Biophys.*, 1966, **115**, 593–597.
- 167M. Joost, A. Amgoune and D. Bourissou, *Angew. Chem. Int. Ed.*, 2015, **54**, 15022–15045.
- 168J. F. Hartwig, *Inorg. Chem.*, 2007, **46**, 1936–1947.
- 169D. Baranano and J. F. Hartwig, *J. Am. Chem. Soc.*, 1995, **117**, 2937–2938.
- 170A. M. Spokoyny, Y. Zou, J. J. Ling, H. Yu, Y. S. Lin and B. L. Pentelute, *J. Am. Chem. Soc.*, 2013, **135**, 5946–5949.
- 171C. Zhang, E. V. Vinogradova, A. M. Spokoyny, S. L. Buchwald and B. L. Pentelute, *Angew. Chem. - Int. Ed.*, 2019, **58**, 4810–4839.
- 172R. J. Christie, R. Fleming, B. Bezabeh, R. Woods, S. Mao, J. Harper, A. Joseph, Q. Wang, Z.-Q. Xu, H. Wu, C. Gao and N. Dimasi, *J. Controlled Release*, 2015, **220**, 660–670.
- 173A. Bandyopadhyay, S. Cambray and J. Gao, *Chem. Sci.*, 2016, **7**, 4589–4593.
- 174S. Cambray and J. Gao, *Acc. Chem. Res.*, 2018, **51**, 2198–2206.
- 175B. Chance, *Rev. Sci. Instrum.*, 1951, **22**, 619–627.
- 176B. Chance and V. Legallais, *Rev. Sci. Instrum.*, 1951, **22**, 627–634.
- 177E. Friedmann, *Biochim. Biophys. Acta*, 1952, **9**, 65–75.

- 178 B. G. Cox, D. M. A. Grieve and A. E. A. Porter, *J. Chem. Soc. Perkin Trans. 2*, 1975, 1512–1515.
- 179 I. Dovgan, O. Koniev, S. Kolodych and A. Wagner, *Bioconjug. Chem.*, 2019, **30**, 2483–2501.
- 180 S. Zhang, C. Yan, D. G. Millar, Q. Yang, J. M. Heather, A. Langenbucher, L. T. Morton, S. Sepulveda, E. Alpert, L. R. Whelton, D. T. Zarrella, M. Guo, E. Minogue, M. S. Lawrence, B. R. Rueda, D. R. Spriggs, W. Lu, D. M. Langenau and M. Cobbold, *Cancer Res.*, 2022, **82**, 773–784.
- 181 T. MacCulloch, A. Buchberger and N. Stephanopoulos, *Org. Biomol. Chem.*, 2019, **17**, 1668–1682.
- 182 G. Cai, Y. Fu, Y. Li, X. Wan and Z. Shi, *J. Am. Chem. Soc.*, 2007, **129**, 7666–7673.
- 183 G. Cai, Y. Fu, Y. Li, X. Wan and Z. Shi, *J. Am. Chem. Soc.*, 2007, **129**, 7666–7673.
- 184 V. A. Stepanova, V. V. Dunina and I. P. Smoliakova, *Organometallics*, 2009, **28**, 6546–6558.
- 185 R. Giri, J. K. Lam and J.-Q. Yu, *J. Am. Chem. Soc.*, 2010, **132**, 686–693.
- 186 S. Nakai, T. Yatabe, K. Suzuki, Y. Sasano, Y. Iwabuchi, J. Hasegawa, N. Mizuno and K. Yamaguchi, *Angew. Chem. Int. Ed.*, 2019, **58**, 16651–16659.
- 187 L. Henry, N. Delsuc, C. Laugel, F. Lambert, C. Sandt, S. Hostachy, A. S. Bernard, H. C. Bertrand, L. Grimaud, A. Baillet-Guffroy and C. Policar, *Bioconjug. Chem.*, 2018, **29**, 987–991.
- 188 A. Spaeth, A. Graeler, T. Maisch and K. Plaetzer, *Eur. J. Med. Chem.*, 2018, **159**, 423–440.
- 189 H. Li, P. Zhang, L. P. Smaga, R. A. Hoffman and J. Chan, *J. Am. Chem. Soc.*, 2015, **137**, 15628–15631.
- 190 M. Yu, J. K. H. Wong, C. Tang, P. Turner, M. H. Todd and P. J. Rutledge, *Beilstein J. Org. Chem.*, 2015, **11**, 37–41.
- 191 M. Hogan, B. Gleeson and M. Tacke, *Organometallics*, 2010, **29**, 1032–1040.
- 192 R. Feng, J. Yao, Z. Liang, Z. Liu and Y. Zhang, *J. Org. Chem.*, 2013, **78**, 3688–3696.
- 193 C. T. Mbofana, E. Chong, J. Lawniczak and M. S. Sanford, *Org. Lett.*, 2016, **18**, 4258–4261.
- 194 D. Y. Ong, Z. Yen, A. Yoshii, J. Revillo Imbernon, R. Takita and S. Chiba, *Angew. Chem. Int. Ed.*, 2019, **58**, 4992–4997.
- 195 D. Chamorro-Arenas, U. Osorio-Nieto, L. Quintero, L. Hernández-García and F. Sartillo-Piscil, *J. Org. Chem.*, 2018, **83**, 15333–15346.
- 196 S. A. Spring, S. Goggins and C. G. Frost, *Org. Biomol. Chem.*, 2017, **15**, 7122–7126.
- 197 V. N. Tsarev, Y. Morioka, J. Caner, Q. Wang, R. Ushimaru, A. Kudo, H. Naka and S. Saito, *Org. Lett.*, 2015, **17**, 2530–2533.
- 198 G. A. Price, A. K. Brisdon, S. Randall, E. Lewis, D. M. Whittaker, R. G. Pritchard, C. A. Muryn, K. R. Flower and P. Quayle, *J. Organomet. Chem.*, 2017, **846**, 251–262.
- 199 N. L. Bell, C. Xu, J. W. B. Fyfe, J. C. Vantourout, J. Brals, S. Chabbra, B. E. Bode, D. B. Cordes, A. M. Z. Slawin, T. M. McGuire and A. J. B. Watson, *Angew. Chem. Int. Ed.*, 2021, **60**, 7935–7940.
- 200 J. Vicente, I. Saura-Llamas and D. Bautista, *Organometallics*, 2005, **24**, 6001–6004.

- 201 R. J. Lundgren, A. Sapping-Kumankumah and M. Stradiotto, *Chem. – Eur. J.*, 2010, **16**, 1983–1991.
- 202 K. D. Hesp and M. Stradiotto, *J. Am. Chem. Soc.*, 2010, **132**, 18026–18029.
- 203 J. M. Stauber, E. A. Qian, Y. Han, A. L. Rheingold, P. Král, D. Fujita and A. M. Spokoyny, *J. Am. Chem. Soc.*, 2020, **142**, 327–334.
- 204 A. Zeineddine, L. Estévez, S. Mallet-Ladeira, K. Miqueu, A. Amgoune and D. Bourissou, *Nat. Commun.*, 2017, **8**, 565.
- 205 D. Drew, J. R. Doyle and A. G. Shaver, in *Inorganic Syntheses*, John Wiley & Sons, Ltd, 1990, pp. 346–349.
- 206 M. D. Heredia, M. Puiatti, R. A. Rossi and M. E. Budén, *Org. Biomol. Chem.*, 2021, **20**, 228–239.
- 207 Y. Han, F. Albericio and G. Barany, *J. Org. Chem.*, 1997, **62**, 4307–4312.